

A critical evaluation of the mass transfer and fouling behaviour in forward osmosis with integrated flow-reversal

by

Marielle Hurter

Thesis presented in partial fulfilment
of the requirements for the degree

of

**MASTER OF ENGINEERING
(CHEMICAL ENGINEERING)**



in the Faculty of Engineering
at Stellenbosch University

Supervisor

Professor A.J. Burger

April 2019

Declaration

By submitting this thesis electronically, I declare that the entirety of the work contained therein is my own, original work, that I am the sole author thereof (save to the extent explicitly otherwise stated), that reproduction and publication thereof by Stellenbosch University will not infringe any third-party rights and that I have not previously in its entirety or in part submitted it for obtaining any qualification.

Date: April 2019

Copyright © 2019 Stellenbosch University

All rights reserved

Plagiarism Declaration

1. Plagiarism is the use of ideas, material and other intellectual property of another's work and to present it as one's own.
2. I agree that plagiarism is a punishable offence because it constitutes theft.
3. I also understand that direct translations are plagiarism.
4. Accordingly, all quotations and contributions from any source whatsoever (including the internet) have been cited fully. I understand that the reproduction of text without quotation marks (even when the source is cited) is plagiarism.
5. I declare that the work contained in this assignment, except where otherwise stated, is my original work and that I have not previously (in its entirety or in part) submitted it for grading in this module/assignment or another module/assignment.

Initials and surname: M. Hurter

Date: April 2019

Abstract

Forward osmosis (FO) is a membrane-based technology that can be operated at relatively low mechanical pressures and may be utilised in processes where water needs to be added or removed from process streams. Options for its potential application are diverse and it could, for example, be used in the regulation of water content in fruit juices, or in the augmentation of clean water to high-TDS cooling water circuits.

Similar to reverse osmosis (RO) processes, scale formation by sparingly soluble salts can limit the maximum allowed recovery of water, while flux profiles, salt rejection characteristics and cross-flow velocity (CFV) play key roles in the overall behaviour of the system. However, FO systems are more amenable to the utilisation of osmotic backwashing than RO systems.

Therefore, this study endeavoured to critically evaluate the mass transfer and fouling behaviour of FO membranes at different operating conditions, including the intermittent switching of the flow path (i.e. intermittently reversing the flux).

To support this study, a bench scale FO setup was designed, constructed and commissioned. Subsequent laboratory work entailed:

- Evaluate and assess the bench scale setup by comparing the theoretical and measured recovery, based on the measured water flux.
- Evaluate the effects of changes in the CFV on the mass transfer of water and solutes over the membrane, while using a feed solution with TDS well below $100 \text{ mg}\cdot\text{L}^{-1}$.
- Determine the effects of the operational configuration on the mass transfer over the membrane.
- Investigate the process realities and limitations of intermittent flow path switching on reducing scale formation.

Two operational modes were considered, viz. with the membrane active layer (1) facing the feed solution (AL-FS) or (2) facing the draw solution (AL-DS), with CFVs ranging from $13 \text{ cm}\cdot\text{s}^{-1}$ to $52 \text{ cm}\cdot\text{s}^{-1}$. Within this CFV range, the water fluxes attained in the AL-FS configuration were on average 40% lower than those in the AL-DS configuration.

In the AL-FS configuration, the flux increased from $11.2 \text{ L}\cdot\text{m}^{-2}\cdot\text{h}^{-1}$ to $20 \text{ L}\cdot\text{m}^{-2}\cdot\text{h}^{-1}$ when the CFV was increased from $13 \text{ cm}\cdot\text{s}^{-1}$ to $37 \text{ cm}\cdot\text{s}^{-1}$. However, a further increase in CFV above $37 \text{ cm}\cdot\text{s}^{-1}$ did not result in higher fluxes and the limiting flux of $20 \text{ L}\cdot\text{m}^{-2}\cdot\text{h}^{-1}$ was reached. This is ascribed to the potential increase in dilutive internal concentration polarisation in the support layer of the membrane, thereby limiting the effective driving force (effective osmotic pressure difference) over the membrane.

In the AL-DS configuration, this limiting flux was not reached within the defined CFV range. However, it was found that operation in the AL-DS configuration tended to a limiting flux of $20 \text{ L}\cdot\text{m}^{-2}\cdot\text{h}^{-1}$ when

operating at draw solution concentrations above 50 000 mg·L⁻¹ TDS. This is considered to be partly the result of an increased reverse solute flux (RSF) along with dilutive external concentration polarisation on the active layer side of the membrane.

During operation with intermittent flow path switching when recovering water from a 1.9 super-saturated gypsum feed solution, *ca* 15 minutes were required to purge the flow channels of the respective residual solutions in the specific laboratory system under investigation. Operation at a CFV of *ca* 28 cm·s⁻¹ then proved to enable the most rapid alleviation of internal concentration polarisation (ICP) in the AL-FS configuration (or mostly RSF in the AL-DS configuration). Under the most stable conditions in the AL-FS configuration, the operational flux dropped from 12 L·m⁻²·h⁻¹ to *ca* 9 L·m⁻²·h⁻¹ over a period of only 12 hours. In other words, flux declines of *ca* 38% were observed over a period of 12 hours when operating in the AL-DS configuration at 15-minute switch-intervals every two hours. This indicated the formation of gypsum scale in the support layer and highlighted the detrimental effects of the support layer in a scaling environment.

Key words: Forward osmosis, cross-flow velocity, intermittent flow path switching, mass transfer, gypsum scaling, flux, recovery, reverse salt flux/diffusion, concentration polarisation

Uittreksel

Voorentoe osmose (FO) is 'n membraan-gebaseerde tegnologie wat bedryf kan word teen relatiewe lae meganiese druk en kan gebruik word in prosesse waar water bygevoeg of verwyder moet word van die prosesstroom. Opsies vir potensiële toepassings is divers en kan, byvoorbeeld, gebruik word in die regulasie van waterinhoud in vrugtesappe, of in die aanvulling van skoon water by hoë TDS verkoeling water kringlope.

Soortgelyk aan tru-osmose (RO) prosesse, kan skilfer formasie deur spaarsaam oplosbare soute die maksimum toegelate herwinning van water beperk, terwyl fluks profiele, sout verwerping karakteristieke en kruisvloei snelheid (CFV) sleutel rolle in die algehele gedrag van die stelsel speel. FO stelsels is egter meer inskiklik vir die gebruik van osmotiese terugspoeling as RO stelsels.

Daarom het hierdie studie gepoog om die massa-oordrag en bevuiling gedrag van FO-membrane by verskillende bedryfskondisies, insluitend die afwisselende omruiling van die stroomlyn (i.e. afwisselende omkering van die fluks), krities te evalueer.

Om hierdie studie te ondersteun is 'n banktoets skaal FO-opstel ontwerp, opgerig en in bedryf gestel. Opvolgende laboratorium werk het behels:

- Evalueer en assessee die banktoets skaal deur die teoretiese en gemete herwinning, gebaseer op die gemete waterfluks, te evalueer.
- Evalueer die effek van veranderinge in die CFV op die massa-oordrag van water en opgeloste stowwe oor die membraan, terwyl 'n voeroplossing met TDS ver onder 100 mg.L⁻¹, gebruik word.
- Bepaal die effek van die operasionele konfigurasie op die massa-oordrag oor die membraan.
- Ondersoek die proses realiteite en beperkinge van afwisselende stroomlyn omruiling op die vermindering van skilfer formasie.

Twee operasionele metodes is oorweeg, viz. met die membraan aktiewe laag (1) gerig na die voeroplossing (AL-FS) of (2) gerig na die trekoplossing (AL-DS), met CFVs binne bestek van 13 cm.s⁻¹ tot 52 cm.s⁻¹. Binne hierdie CFV-bestek, was die waterflukse bereik op gemiddeld 40% laer in die AL-FS-konfigurasie as dié in die AL-DS-konfigurasie.

In die AL-FS-konfigurasie, het die fluks vermeerder van 11.2 L.m⁻².h⁻¹ tot 20 L.m⁻².h⁻¹ wanneer die CFV verhoog is van 13 cm.s⁻¹ tot 27 cm.s⁻¹. 'n Verdere verhoging in CFV bo 37 cm.s⁻¹ het nie hoër flukse tot gevolg gehad nie en die beperkende fluks van 20 L.m⁻².h⁻¹ is bereik. Dit word toegeskryf aan die potensiële verhoging in verwaterde interne konsentrasie polarisasie in die ondersteuningslaag van die membraan, wat sodoende die effektiewe dryfkrag (effektiewe osmotiese drukverskil) oor die membraan beperk.

In die AL-DS-konfigurasie, was hierdie beperkende fluks nie bereik binne die gedefinieerde CFV-bestek nie. Dit is egter bevind dat bedryf in die AL-DS-konfigurasie 'n neiging tot 'n beperkende fluks van $20 \text{ L}\cdot\text{m}^{-2}\cdot\text{h}^{-1}$ gehad het as trekoplossingkonsentrasies bo $50\,000 \text{ mg}\cdot\text{L}^{-1}$ TDS was. Dit word beskou om deels die resultaat van 'n verhoogde omgekeerde opgeloste stof fluks (RSF) saam met verwaterde eksterne konsentrasie polarisasie op die aktiewe laag kant van die membraan te wees.

Gedurende bedryf met afwisselende stroomlynruiling toe water herwin is van 'n 1.9 superversadigde gipsvoeroplossing, is *ca* 15 minute nodig om die vloeikanale van die onderskeidelike oorblywende oplossings in die laboratoriumstelsel spesifiek tot dié ondersoek, te suiwer. Bedryf by 'n CFV van *ca* $28 \text{ cm}\cdot\text{s}^{-1}$ is toe bewys om die spoedigste vermindering van interne konsentrasie polarisasie (ICP) in die AL-FS-konfigurasie (of meestal RSF in die AL-DS-konfigurasie), in staat te stel. Onder die mees stabiele kondisies in die AL-FS-konfigurasie, het die operasionele fluks geval van $12 \text{ L}\cdot\text{m}^{-2}\cdot\text{h}^{-1}$ tot *ca* $9 \text{ L}\cdot\text{m}^{-2}\cdot\text{h}^{-1}$ oor 'n periode van slegs 12 ure. Met ander woorde, fluks afnames van *ca* 38% is waargeneem oor 'n periode van 12 ure by bedryf in die AL-DS-konfigurasie met 15 minute omruilintervalle elke twee ure. Dit dui formasie van gipsskilfer in die ondersteuningslaag aan en beklemtoon die nadelige effek van die ondersteuningslaag in 'n verskalingsomgewing.

Sleutelwoorde: *Voorentoe osmose, kruisvloei snelheid, afwisselende stroomlynruiling, massa-oordrag, gips verskaling, fluks, herwinning, omgekeerde soutfluks/diffusie, konsentrasie polarisasie*

Table of Contents

ABSTRACT	V
UITTREKSEL	VII
TABLE OF CONTENTS	IX
ACKNOWLEDGEMENTS	XI
LIST OF FIGURES & TABLES	XV
NOMENCLATURE	XXIII
GLOSSARY	XXVII
1. INTRODUCTION AND PROJECT RATIONALE	1
1.1. Desalination & Membrane-Based Processes	2
1.1.1. Technology Background	3
1.1.2. Flux and Fouling in Forward Osmosis	4
1.2. Motivation and Aim of Project.....	6
1.3. Research Objectives	7
1.4. Thesis Outline	7
2. LITERATURE REVIEW	9
2.1. Fundamental Principles of FO.....	9
2.1.1. Driving Force: Osmotic Pressure	9
2.1.2. Basic Terms & Definitions.....	12
2.1.3. Mass Transport Phenomena in FO	15
2.2. Membrane Fouling in FO.....	27
2.2.1. General aspects of membrane fouling in FO	28
2.2.2. Factors Affecting Fouling in FO.....	30
2.3. Physical Fouling Control Measures	41
2.3.1. Membrane Flushing.....	41
2.3.2. Osmotic Backwashing.....	41
2.4. Literature Review Summary	46
3. LABORATORY-SCALE SETUP DESIGN	51
3.1. Problem Definition	51
3.1.1. Problem Scope	51
3.1.2. Technical Review	51
3.1.3. Design Requirements.....	52
3.2. Design Description.....	53
3.2.1. Overview	53
3.2.2. Detailed Description.....	59
3.2.3. Operation	63
3.3. Evaluation.....	66
3.3.1. Overview	66
3.3.2. Data Acquisition	69
3.3.3. Flux	69
3.3.4. Recovery	71
3.3.5. Cross-Flow Velocity	71
3.3.6. Rejection.....	71
3.4. Prototype	73
3.5. Testing and Results	74
3.6. Assessment	84
4. MATERIALS AND METHODS	85

4.1.	Experimental Problem Statement.....	85
4.2.	Overall Approach.....	85
4.3.	Materials	87
4.3.1.	Chemicals	87
4.3.2.	FO Membrane.....	92
4.4.	Experimental Procedures	93
4.4.1.	Phase 1: Validation Tests.....	94
4.4.2.	Phase 2: Intermittent Flow-Path Switching	95
4.4.3.	Phase 3: Practical Implementation	96
4.5.	Analytical Methods.....	96
4.5.1.	Calcium Ions (Ca ²⁺)	97
4.5.2.	Sodium Ions (Na ⁺)	97
5.	RESULTS AND DISCUSSION	99
5.1.	System Validation & Characterisation.....	99
5.2.	Intermittent Flow-Path Switching	120
5.3.	Practical Implementation	128
5.4.	Evaluating Intermittent Flow-Path Switching.....	132
5.4.1.	Relevance to a Scaling Solution	132
5.4.2.	Product Water Contamination & Cost Trade-Off	134
6.	CONCLUSIONS & RECOMMENDATIONS.....	137
6.1.	Conclusions.....	137
6.1.1.	Bench-Scale Setup	137
6.1.2.	Validation and Characterisation Tests.....	137
6.1.3.	Intermittent Flow-Path Switching.....	138
6.1.4.	Practical Implementation.....	138
6.2.	Recommendations	139
7.	REFERENCES	141
A.	DESIGN	149
A.1.	In-line Flow Meter Design	149
A.2.	Hydraulic Design: Membrane Housing Blocks.....	151
A.3.	Drawing: Membrane Housing Design.....	152
B.	SAMPLE CALCULATIONS.....	153
B.1.	Supersaturation Concentrations.....	153
B.2.	Experimental Data Sample Calculations.....	155
C.	OPERATIONAL PROCEDURES.....	158
C.1.	Operational Procedure.....	158
C.1.1.	Special Safety Considerations.....	158
C.1.2.	Process Risks & Precautionary Measures	159
C.2.	Pre-start-up Checklist	159
C.2.1.	Process Start-Up Procedure	159
C.2.2.	Process Measurements.....	160
C.2.3.	Process Shut-Down Procedure	160
C.3.	Preparation of Various Solutions	160
C.3.1.	Sodium Chloride Draw Solution	160
C.3.2.	Sodium Sulphate	160
C.3.3.	Calcium Chloride	160
C.4.	System Operation.....	161

Acknowledgements

"You get one life, it is actually your duty to live it as fully as possible. Live with intent. Live boldly." – Will Traynor

(Me Before You – Jojo Moyes)

- Professor A.J. Burger. It was a privilege to learn from you. Thank you for *everything* you have taught me. The culmination of what you've taught me not only shaped me into an engineer, but also gave me valuable insight into how I approach this magical and mysterious thing we get to call *life*. Thank you for your guidance, encouragement and support, and especially for believing in me in times when I did not believe in myself.
- The Workshop – Mr Jos Weerdenburg, Mr Anton Cordier, Mr Brent Gideons and Mr Bevan Koopman. Thank you for everything.
- The Analytical Laboratory. Thank you for all your advice on laboratory practices and for the analyses.
- The administrative staff – Tannie Juliana and Francis. Thank you for all the admin you handled for me regarding purchases.
- Jandré Lamprecht & Heinrich Bock. Thank you for your help with the electrical side of this project. Your friendship is very close to my heart.
- Fellow Postgraduate Students. Thank you for creating a fun and friendly environment. A special mention should be made to the Three Musketeers (Jano van Rensburg & Riccardo Swanepoel). Thank you for always reminding me that every cloud has a silver lining, or maybe not quite.
- Susan King, your friendship was the serendipity of my Masters. Thank you for your companionship in the forward osmosis journey. Also a big thank you to my support group (Anke, Philisa, Carlie and Susan.)
- Mieke de Jager, Cara Broeksma, Nicola Smith, Ilze Swart and Marleza du Toit. Thank you for always checking in and reminding me to stay sane in spite of the many challenges faced.
- PROXA Colleagues – Nathalie Fernandes, Adél Wilson, Léander Steynberg, Alana Human and Adam Keuler.
- Christoff Botha & Wimpie Greyvenstein. Your support means the world to me. Thank you for being like brothers to me and for 7 years of unconditional friendship. I love you from the bottom of my heart. –
- Marno Roselt and the entire Roselt family (Oom Sirol, Tannie Marthie, Sirolene, Manie and Skylah). You were the surprise I did not see coming. Thank you for supporting me through the final stages of this project. *(Sometimes you can't make it on your own. – U2)*
- My parents, Serf & Alsan Hurter. Thank you for always pushing me beyond the limits I set for myself. Thank you for being my best friends and thank you for your unconditional love and support.
- Grace. This study was completed through Grace alone. I am and will always continue to be a *lover of the Light*.

"Harde werk & Genade dans altyd saam!" – Bouwer Bosch

Dedicated to my Grandfather – Richard Hermann Peckham

List of Figures & Tables

Figure 1-1. Permeation direction in osmotically driven membrane processes (OMDPs) for (a) pressure assisted osmosis (PAO) where a hydraulic pressure is applied to the feed solution, (b) normal forward osmosis (FO) with the absence of an externally applied hydraulic pressure, (c) pressure retarded osmosis (PRO) where a hydraulic pressure is applied to the draw solution and (d) RO where the permeation direction is the reverse of normal FO due to the hydraulic pressure applied to the brine/DS.....	3
Figure 1-2. (a) Conventional FO process where the product stream is a diluted draw solution stream and (b) extracting high quality water while at the same time regenerating the draw solution via a conventional RO process.....	4
Figure 2-1. Qualitative representation of the osmotic pressure profile in a (a) co-current system, and (b) counter-current system (adapted from [36]).....	11
Figure 2-2. Basic FO configuration for defining basic FO terminology and parameters.....	12
Figure 2-3. Diffusion of electrolytes. The ions have the same charge and are present in the system at the same concentrations. The cations, which are the larger ions, move inherently slower than the smaller anions. However, due to the electroneutrality of the system, both ions have the same net motion and hence the same permeation flux (redrawn and adapted from [16]).....	18
Figure 2-4. Intrinsic relationship between fouling, CP and RSF and how each factor influences the other. Redrawn from [48].....	21
Figure 2-5. The phenomenon of CP within membrane systems in terms of the (a) ideal case where no concentration gradients are formed on either side of the membrane and (b) actual case where the solute concentrations vary significantly from the bulk fluid on either side, to the boundary layer on either side of the membrane.....	22
Figure 2-6. Illustration of the effective osmotic pressure for the effective driving force of the process and how the concentration gradients affect the system driving force. (a) The ideal case where the driving force is the absolute difference between the osmotic pressure of the adjacent solutions, (b) AL-DS where dilutive ECP and concentrative ICP is dominant and (c) AL-FS where concentrative ECP and dilutive ICP is dominant. Redrawn from [26].	23
Figure 2-7. Experimental data generated for (a) NaCl DS varied from 0.125–1.0 M and deionized feed water operating in AL-FS, (b) 0.5 M NaCl DS with the feed solution varying from 0.0625–0.375 M NaCl operating in AL-DS and (c) a 0.5 M NaCl DS with a feed solution varying from 0.0625–0.375 M NaCl operating in AL-FS. Experimental conditions: CFV and temperature of both the DS and the FS were at $30 \text{ cm}\cdot\text{s}^{-1}$ and $22.5 \pm 1.5 \text{ }^\circ\text{C}$, respectively. Data obtained from [25].....	24
Figure 2-8. Basic fouling mechanism in membrane processes. (a) Foulant interaction with the membrane leads to the accumulation of foulants on the surface of the membrane. The deposition of foulants on the membrane surface enhances foulant interaction with other constituent foulants in the feed water. (b) The hydraulic resistance created by the foulant layer on the membrane surface reduces net driving force for permeation and leads to increased concentration polarisation.	27
Figure 2-9. Visual illustration of the fast influences of membrane fouling on flux behavior according to the osmotic-resistance filtration model. (Modified and redrawn from [48].)	28

Figure 2-10. Visual representation of external and internal fouling in FO processes. (a) When the active layer faces the FS containing the foulants, only external fouling is present in the system. (b) When the system is operated so that the FS faces the porous support layer of the membrane, internal fouling occurs. (Redrawn and modified from [48].)..... 30

Figure 2-11. Variations in the diffusion coefficients of Na⁺ and Cl⁻ respectively for (a) variations in NaCl solution concentration and (b) the solution temperature. Modelled in *OLI Stream Analyser*. 32

Figure 2-12. Osmotic pressures generated by the most common inorganic salts as draw solutes at various concentrations. MgCl₂ generates the highest osmotic pressure at low concentrations (mol·L⁻¹), with MgSO₄ generating the lowest osmotic pressure at higher solute concentrations (mol·L⁻¹) (data obtained from [17].)..... 33

Figure 2-13. The process of crystallisation of calcium containing minerals [87]. 38

Figure 2-14. Variability of gypsum solubility at various operating temperatures where the solubility of gypsum decreases with an increase in temperature. (a) [88]; (b) [89]; (c) [90]; (d) [91]. 39

Figure 2-15. Osmotic backwashing principle: (A) normal forward osmosis operation (permeate flows from feed side to draw solution side) and (B) osmotic backwashing (permeate from draw side to feed side (redrawn from [21])). 42

Figure 3-1. Process Flow Diagram (PFD) of the designed and built setup..... 58

Figure 3-2. Categorisation of sub-design components of the FO bench-scale setup. 59

Figure 3-3. Membrane housing and internal component assembly..... 60

Figure 3-4. Schematic diagram of the flowrate measurement column used to measure the inlet and the outlet flowrates continuously. The outlet flow meters are on the left and the inlet flow meters are on the right. For dimensions see Appendix A.1. 61

Figure 3-5. PLC programme operation..... 62

Figure 3-6. Intrinsic relationship between the mechanical and process design parameters both dictating the system performance indicators. 67

Figure 3-7. The inter-relationships between the primary mechanical and process design parameters and the system performance indicators to characterise the operation of the bench-scale setup. A_m is the membrane cross sectional area, h_{ch} is the channel height, w_{ch} is the channel width, Q_F is the inlet flow rate, A_m is the membrane active area, l_{ch} is the channel length, v_{in} is the inlet flow velocity, CFV is the cross-flow velocity, ϕ is the spacer porosity, J_w is the water flux, R is recovery, Q_P is the permeate flow rate, π is the osmotic pressure, Q_B is the brine flow rate, T is the temperature, C is the concentration and R_g is the Universal Gas Constant. 68

Figure 3-8. Photographs showing the final commissioned setup, specifically indicating (a) the variable height grip of the inlet flow meter as well as the two 200 L feed tanks (b) the six housing blocks forming the FO train, as well as (c) the (1) pumps, (2) filters, and (3) outlet flow meters..... 73

Figure 3-9. The impact of different CFVs on the water recovery of the system at three constant fluxes of 35 L·m⁻²·h⁻¹, 25 L·m⁻²·h⁻¹ and 10 L·m⁻²·h⁻¹. The mechanical design was fixed and membrane area used for these calculations was fixed at 0.1344 m². The cross-sectional area was also assumed to be constant at 0.17 cm², which again assumed a uniform membrane flow-path area. 76

Figure 3-10. The theoretical recovery and actual recovery attained at a CFV of 19 cm·s ⁻¹ and a variable system area.	77
Figure 3-11. Variance in water recovery as experimentally determined, theoretically calculated and the recovery at which the system was designed to operate.	78
Figure 3-12. Experimental, calculated (actual) and designed CFV of the system.	79
Figure 3-13. Indicates how deviations in the channel depth translate to deviations in the calculation of the system CFV.	80
Figure 3-14. Translation of variations in the spacer porosity to the system CFV for variations in the channel depth. The channel height for the system modelled by Siddiqui et al. [115] was not reported.	80
Figure 3-15. Inlet CFV variations within the system for the FS and the DS with the addition of membrane area (flow- path length), thereby increasing the overall recovery and water extraction capacity of the system. The total system area is 0.1344 m ²	81
Figure 3-16. Pressure differential as per the suction side of the pump as a function of the hydraulic liquid height inside the respective tank from the inlet of the pump. This is due to the expanding cavity on the suction side of the pump.	83
Figure 3-17. Water flux and recovery results from switching the operational flow path from the AL-FS configuration to the AL-DS configuration, at an inlet CFV of 19 cm·s ⁻¹	84
Figure 4-1. General approach process followed for the execution of the experimental work.	86
Figure 4-2. Osmotic pressure (bar) curves (generated in <i>OLI Stream Analyser</i>) for three of the most common inorganic solutes used for generating high osmotic pressures as draw solution solutes at 20°C.	87
Figure 4-3. Ion diffusivity curves (generated in <i>OLI Stream Analyser</i>) for three of the most common inorganic solutes (Na ⁺ in NaCl, Mg ²⁺ in MgCl ₂ and SO ₄ ²⁻ in Na ₂ SO ₄), used for generating high osmotic pressures as draw solution solutes at 20°C.	89
Figure 4-4. Calcium concentration corresponding to the various saturation indices as modelled in Minteq and Phreeqc.	90
Figure 4-5. Jar tests to investigate how gypsum precipitation will affect conductivity measurements. Experiments were conducted at a temperature of 20°C.	91
Figure 4-6. SEM images for the (a) cross section between the support layer (top) and the active layer (bottom) indicating the porosity of the support layer, (b) tortuosity of the support layer whereas (c) surface of the active layer and (d) surface of the support layer.	93
Figure 4-7. Typical Ca ²⁺ concentrations for various degrees of supersaturation in gypsum solution.	97
Figure 5-1. Experimental runs done in triplicate to determine the baseline flux curve at a CFV of 13 cm·s ⁻¹ in the AL-FS configuration. The standard operating conditions were the same, with the FS being deionised water and the DS being a 0.5 M NaCl solution. Data normalised to a temperature of 20°C and a driving force of 27 bar.	101

Figure 5-2. Experimental runs done in duplicate to determine the baseline flux curve at a CFV of 13 $\text{cm}\cdot\text{s}^{-1}$ in the AL-DS configuration. The standard operating conditions were the same, with the FS being deionised water and the DS being a 0.5 M NaCl solution. Data normalised to a temperature of 20°C and a driving force of 27 bar.	101
Figure 5-3. Experimental runs done in triplicate to determine the baseline flux curve at a CFV of 28 $\text{cm}\cdot\text{s}^{-1}$ in the AL-FS configuration. The standard operating conditions were the same, with the FS being deionised water and the DS being a 0.5 M NaCl solution. Data normalised to a temperature of 20°C and a driving force of 27 bar.	102
Figure 5-4. Experimental runs done in duplicate to determine the baseline flux curve at a CFV of 28 $\text{cm}\cdot\text{s}^{-1}$ in the AL-DS configuration. The standard operating conditions were the same, with the FS being deionised water and the DS being a 0.5 M NaCl solution. Data normalised to a temperature of 20°C and a driving force of 27 bar.	102
Figure 5-5. Experimental runs done in triplicate to determine the baseline flux curve at a CFV of 52 $\text{cm}\cdot\text{s}^{-1}$ in the AL-FS configuration. The standard operating conditions were the same, with the FS being deionised water and the DS being a 0.5 M NaCl solution. Data normalised to a temperature of 20°C and a driving force of 27 bar.	103
Figure 5-6. Experimental runs done in duplicate to determine the baseline flux curve at a CFV of 52 $\text{cm}\cdot\text{s}^{-1}$ in the AL-DS configuration. The standard operating conditions were the same, with the FS being deionised water and the DS being a 0.5 M NaCl solution. Data normalised to a temperature of 20°C and a driving force of 27 bar.	103
Figure 5-7. Variance in flux at different CFVs ranging from 13 – 52 $\text{cm}\cdot\text{s}^{-1}$ when operating in the AL-FS configuration. The FS is deionized water and the DS is a 29 220 $\text{mg}\cdot\text{L}^{-1}$ TDS NaCl solution. Data is normalised to 20°C and a driving force of 27 bar.....	106
Figure 5-8. Variance in flux at different CFVs ranging from 13 – 15 $\text{cm}\cdot\text{s}^{-1}$ when operating in the AL-DS configuration. The FS is deionized water and the DS is a 29 220 $\text{mg}\cdot\text{L}^{-1}$ TDS NaCl solution. Data is normalised to 20°C and a driving force of 27 bar.....	106
Figure 5-9. The experimentally-measured recovery along with the assumed operating CFV, compared to the calculated recovery and corrected CFV, as per the experimentally-measured water flux for the AL-FS operating configuration.....	108
Figure 5-10. The experimentally-measured recovery along with the assumed operating CFV, compared to the calculated recovery and corrected CFV, as per the experimentally-measured water flux for the AL-DS operating configuration.	108
Figure 5-11. Fluid contact time with the membrane as a function of the operating CFV.....	109
Figure 5-12. Effect of the DS dilution on decreasing the driving force of the process. The initial DS concentration was 29 220 $\text{mg}\cdot\text{L}^{-1}$ and decreased to 23 835 $\text{mg}\cdot\text{L}^{-1}$ along the length of the process train. Data obtained at a CFV of 19 $\text{cm}\cdot\text{s}^{-1}$	111
Figure 5-13. Dilution factors of the DS at the respective operating CFVs for the AL-FS and the AL-DS configuration.	112
Figure 5-14. Effect of the boundary layer thickness (20, 30 and 50 μm) on the Peclet number for flux data attained in the AL-FS configuration, at various operating CFVs.	115

Figure 5-15. Relationship between flux and variable process driving force (variable transmembrane osmotic pressures) at a constant CFV of $37 \text{ cm}\cdot\text{s}^{-1}$ and a FS of deionised water.	116
Figure 5-16. Reverse salt diffusion as a function of cross-flow velocity when the membrane AL is facing the FS and the DS. DS concentration was kept constant at 0.5 M, and normalised temperatures for both solutions were kept constant at 20°C	118
Figure 5-17. Continuous operational mode switching starting in the AL-DS configuration, switching to the AL-FS configuration at $t = 1250$ min and switching back to the AL-DS configuration at $t = 3125$ min. The operating conditions were $13 \text{ cm}\cdot\text{s}^{-1}$, deionised water as the FS, and 0.5 M NaCl DS, with the temperature maintained at 24°C	123
Figure 5-18. Continuous operational mode switching starting in the AL-DS configuration, switching to the AL-FS configuration at $t = 370$ min and switching back to the AL-DS configuration at $t = 1777$ min. The operating conditions were $28 \text{ cm}\cdot\text{s}^{-1}$, deionised water as the FS, and 0.5 M NaCl DS, with the temperature maintained at 24°C	123
Figure 5-19. Continuous operational mode switching starting in the AL-DS configuration, switching to the AL-FS configuration at $t = 250$ min and switching back to the AL-DS configuration at $t = 3235$ min. The operating conditions were $52 \text{ cm}\cdot\text{s}^{-1}$, deionised water as the FS, and 0.5 M NaCl DS, with the temperature maintained at 24°C	124
Figure 5-20. Normalised flux declines for a NaCl at an osmotic pressure of 3 bar and a gypsum scaling solution (containing) at an SSF of 0.95, at a CFV of $28 \text{ cm}\cdot\text{s}^{-1}$, with a normalised solution temperature at 20°C , and a DS concentration of 0.6 M NaCl, operating in the AL-FS configuration. The effective osmotic driving force between the two solutions is 24 bar.	130
Figure 5-21. Normalised flux declines for a MgCl_2 at an osmotic pressure of 2 bar and a gypsum scaling solution (containing) at a SI of 0.95, at a CFV of $28 \text{ cm}\cdot\text{s}^{-1}$, with a normalised solution temperature at 20°C , and a DS concentration of 0.6 M NaCl, operating in the AL-FS configuration. The effective osmotic driving force between the two solutions is 24 bar.....	130
Figure 5-22. Normalised fluxes for three feed solutions and varying the calcium saturation factor by SSF of 0.95, 1.3 and 3 at a CFV of $28 \text{ cm}\cdot\text{s}^{-1}$, normalised solution temperatures of 20°C , and operating in the AL-FS configuration with a DS concentration of 0.6 M NaCl.....	131
Figure 5-23. Normalised flux for a feed solution containing ($1191.78 \text{ mg}\cdot\text{L}^{-1} \text{ Ca}^{2+}$), translating to an SSF of 1.9 at a CFV of $28 \text{ cm}\cdot\text{s}^{-1}$, and normalised solution temperatures of 20°C for both the AL-FS and the AL-DS operational configuration, with a 0.6 M NaCl DS.	131
Figure 5-24. Water flux decline profile for a 1.9 SSF gypsum solution for accelerated fouling. Six flushing cycles with in-situ FS and DS switching at 15 minutes each at a CFV of $28 \text{ cm}\cdot\text{s}^{-1}$. Accelerated fouling conditions: Feed solution was $1.9 \times \text{Ca}^{2+}$ gypsum solution; NaCl DS maintained at 0.6 M; the CFV of both the feed and the draw solution at $28 \text{ cm}\cdot\text{s}^{-1}$ (corresponding to $\pm 200 \text{ mL}\cdot\text{min}^{-1}$).	133
Figure A-1. Line drawing of the Perspex outlet inline flow meters.....	149
Figure A-2. Line drawing of the PVC inlet inline flow meters.....	150
Figure A-3. Mechanical line drawing of the membrane housing block design.....	152
Table 2-1. Various parameters and the corresponding effects these parameters have on rejections attained [40].	14

Table 2-2. Experimental fluxes and salt rejections for typical TFC FO membranes operated with the active layer facing the feed solution [41].	15
Table 2-3. Diffusion coefficients of the most common ions forming inorganic salts in FO processes at 25°C [42].	18
Table 2-4. Summary of the basic types of CP within the membrane system (adapted and redrawn from [11]).	23
Table 2-5. Various draw solutions solutes used in FO processes along with the osmotic pressure generated at the respective concentrations and typical fluxes attained. (Redrawn from [49]).	35
Table 2-6. Typical Ca^{2+} and SO_4^{2-} concentrations and corresponding induction times for crystal formations.	39
Table 2-7. The effect of excess (free) sulphate concentrations on the induction time of gypsum crystallisation at different supersaturation ratios. (Redrawn from [94]).	40
Table 2-8. Characteristics of membrane fouling in terms of foulant type, membrane orientation and backwashing efficiency [21].	43
Table 2-9. The effects of increasing the cross-flow velocity on mitigating fouling in various studies.	44
Table 2-10. Standardisation test conditions reported in recent publications pertaining to FO (adapted from [23]).	48
Table 2-11. Standard operating conditions for the testing of FO membrane in the AL-FS and AL-DS configurations [23].	48
Table 2-12. Flux performances and corresponding operating conditions of some of the most common draw solutes utilised (redrawn from [49]).	49
Table 2-13. Experimental conditions and performances of typical gypsum scaling experimental runs for TFC-FO membranes.	50
Table 3-1. Membrane housing block design for the feed channel.	56
Table 3-2. Membrane housing block design for the DS channel.	57
Table 3-3. Volume and errors associated with each designed flow measurement column.	62
Table 3-4. Valve sequencing, operating times and set points for each operational mode. (X = closed, O = open).	63
Table 3-5. Design requirements along with the respective target values and the test method that will be used to evaluate the design requirement.	69
Table 3-6. Experimental conditions for the evaluation of the bench-scale setup.	69
Table 3-7. K-Factors for various desalination water types at 25°C [44].	71
Table 3-8. Equipment list and description of the bench scale FO setup and apparatus.	74

Table 3-9. Summary of calculation procedure to validate system operating parameters.	75
Table 3-10. Block-by-block analysis of the FS inlet and outlet CFV, and the corresponding CFV for the DS inlet and outlet channels for counter-current operation, with the corresponding membrane area and the per block addition to the system of the attained water recovery.	82
Table 4-1. Chemicals, chemical suppliers and purity of chemicals used for the FS and the DS.	89
Table 4-2. Initial and final Ca ²⁺ concentration at a 20% recovery, assuming no RSF in the system. ...	91
Table 4-3. Gypsum feed solution make-up at an SSF of 1.6 and 1.9 comprising CaCl ₂ ·H ₂ O and Na ₂ SO ₄	92
Table 4-4. CSM spiral wound FO-8040 membrane characteristics.	92
Table 4-5. Experimental design to investigate the effect of CFV and membrane orientation on membrane performance parameters such as flux, recovery and solute rejections. Secondary parameters that are evaluated are CP moduli and RSF.	95
Table 4-6. Experimental design for investigation of the intermittent osmotic backwashing.	96
Table 4-7. Experimental design for the investigation of continuous osmotic backwashing for a typical industrial effluent stream.	96
Table 5-1. Standard operating conditions to which measured data were normalised.	100
Table 5-2. Average water fluxes, recoveries and draw solute rejections attained for 0.5M NaCl DS and deionised water as the FS, with data normalised to 20°C and a driving force of 27 bar.	104
Table 5-3. Evaluation of ECP by calculating the Peclet number and the CP moduli at the actual operating CFV in the AL-FS configuration, with an assumed boundary layer thickness of 20µm.	114
Table 5-4. Evaluation of ECP by calculating the Peclet number and the CP moduli at the actual operating CFV in the AL-DS configuration, with an assumed boundary layer thickness of 20µm.	115
Table 5-5. The effects of ICP are demonstrated with red food colouring when operating with the active layer facing the feed solution (AL-FS) and the active layer facing the draw solution (AL-DS). With the AL facing the DS, ICP occurs within the SL with the FS (the red solution). These photographs were taken for 52 cm·s ⁻¹ CFV on both sides, with a 0.5 M DS, and a deionised water FS, both at 24°C.	125
Table 5-6. Properties of Vitec [®] 7000, a commercially used antiscalant.	134
Table 5-7. Cost comparison between continuous osmotic backwashing and the dosing of Vitec [®] 7000 for impeding the effects of gypsum scaling on the membrane surface.	135
Table A-1. Hydraulic characterisation of the flow channels in each housing block.	151
Table B-1. Molecular weights of species used to synthesise a saturated gypsum feed solution.	153
Table B-2. Data measurements from the baseline test in the AL-FS configuration at a CFV of 19 cm·s ⁻¹	155

Nomenclature

Subscripts

Symbol	Description
<i>AL</i>	Active layer
<i>a</i>	Actual Conditions
<i>B</i>	Brine
<i>b</i>	Bulk solution
<i>ch</i>	channel
<i>D</i>	Draw Solution
<i>DS</i>	Draw Solution
<i>eff</i>	Effective
<i>F</i>	Feed
<i>F</i>	Feed Solution
<i>FS</i>	Feed Solution
<i>m</i>	Membrane
<i>o</i>	Membrane interface
<i>0</i>	Normalised Conditions
<i>s</i>	Solute
<i>solvent</i>	Solvent
<i>i</i>	Species
<i>SL</i>	Support layer
<i>T</i>	Temperature
<i>w</i>	Water

Superscripts

Symbol	Description
*	Standard operating conditions

Abbreviations

Abbreviation	Description
AAS	Atomic absorption spectroscopy
AL	Membrane active layer
AL-DS	Active layer of the membrane facing the draw solution (high salinity solution)
AL-FS	Active layer of the membrane facing the feed solution (low salinity solution)
CECP	Concentrative external concentration polarisation
CFV	Cross-Flow Velocity
CICP	Concentrative internal concentration polarisation
CIP	Cleaning in place
CP	Concentration polarisation
CTA	Cellulose Triacetate
DECP	Dilutive external concentration polarisation
DI	Deionised water
DICP	Dilutive internal concentration polarisation
DS	Draw solution
EC	Electrical conductivity
ECP	External concentration polarisation
FF	Flow factor
FO	Forward osmosis
FR	Flow Ratio
FS	Feed solution
ICP	Internal concentration polarisation
OMDPs	Osmotically driven membrane processes
PAO	Pressure assisted osmosis
Pe	Peclet Number
PLC	Programmable Logic Computer
POA	Pressure assisted osmosis
PRO	Pressure retarded osmosis
PRO	Pressure retarded osmosis
RO	Reverse osmosis
RPM	Rotations per minute
RSD	Reverse solute diffusion
RSF	Reverse solute flux
SEM	Scanning Electron Microscope
SI	Saturation Index
SL	Membrane support layer
SMBS	Sodium Metabisulphate
SS	Supersaturation
SSF	Supersaturation Factor
TDS	Total dissolved solids
TFC	Thin-Film Composite Membrane
UOM	Unit of Measurement
ZLD	Zero liquid discharge

List of Greek Symbols

Definition	Description
μ	Chemical potential
γ	Activity coefficient
π	Osmotic pressure
δ	Laminar mass transfer boundary layer
ϕ	Spacer porosity / Flow restriction factor
ε	Support layer porosity
τ	Support layer tortuosity

List of Roman Symbols

Definition	Description
C	Concentration
D	Diffusion coefficient
Q	Flow rate
J	Flux
h	height
l	length
k	Mass transfer coefficient
E	Membrane enrichment factor
P	Membrane permeability coefficient
l	Membrane thickness
x	Molar fraction
M	Molarity
n	Moles
P	Pressure
R	Recovery
B	Solute permeability
B	Solute permeability coefficient
T	Temperature
V	Volume
v	Velocity
w	width

Physical Constants

Symbol	Description	Value
R	Universal gas constant	$8.314 \text{ J}\cdot(\text{mol}\cdot\text{K})^{-1}$

Glossary

Term	Definition
Atomic Absorption Spectroscopy	An analytical method analysing for ions via atomic absorption spectroscopy.
Average Cross-Flow Velocity	Average operational CFV of the process train either of the feed solution or on the draw solution side.
Backwash	Reverse the flow of water across or through the medium designed to remove the collected foreign material from the membrane surface.
Boundary Layer	A thin layer adhering to the membrane either on the feed water side or on the draw solution side. The water velocities deviate significantly less than those in the bulk flow.
Brine Solution	A concentrate stream containing total dissolved solids at a concentration that is greater than 36 000 ppm.
Bulk Solution Osmotic Pressure	The osmotic pressure of the bulk solution, not forming part of the mass-transfer boundary layer.
Cake Enhanced Concentration Polarisation	A phenomenon which occurs when salts diffuse from the draw solution to the feed side of the membrane and accumulate in the fouling layer.
Cellulose Triacetate Membrane	A polymeric substance used in the manufacturing of semipermeable membranes.
CIP	Cleaning in place.
Concentrate	The output stream of the feed solution that contains water and solutes rejected by the membrane. This is the stream where constituents in the feed water stream are concentrated. It is also known as the reject, retentate or residual stream.
Concentration Polarisation	The increase of the solute concentration over the bulk solution which occurs in the thin boundary layer on the feed and draw solution sides at the membrane surface, resulting in a deviation in the effective driving force across the membrane.
Continuous Osmotic Backwashing	See flow path switching
Desalination	The process in which minerals are removed from water sources.
Dissolved Solids	See solute.
Draw Solution	An engineered solution of a high concentration used to induce an osmotic pressure gradient relative to the feed water to ensure the net flow of water through the membrane from the feed solution to the draw solution thus effectively separating the feed water from the feed solutes.

Term	Definition
Feed Solution	Influent or the source water that requires treatment via the membrane process. The low salinity solution.
Flow Path Switching / Integrated flow reversal	The instantaneous switch of the feed water relative to the membrane orientation. Usually switching from the feed water facing the active layer to the feed water facing the support layer of the membrane.
Flux	Membrane throughput usually expressed in volume of permeate per unit time per unit area.
Forward Osmosis	The spontaneous flow/permeation of water from a less concentrated solution to a more concentrated solution through a semipermeable membrane until chemical potential equilibrium is achieved.
Fouling	The reduction of flux due to the build-up of solids on the surface or within the pores of the membrane which results in changed performance of the element.
Gypsum	$\text{CaSO}_4 \cdot 2\text{H}_2\text{O}$, a common scalant found in industrial water effluents.
Hydraulic	A branch of science that deals with practical applications (such as transmission of energy or the effects of flow) of liquid in motion.
Hydrodynamic	A branch of physics that deals with the motion of fluids and the forces acting on solid bodies immersed in fluids and in motion relative to them.
ICP	An analytical method analysis for ions via inductively coupled plasma.
Ion	An electrified portion of matter either by atomic or molecular dimensions.
Ionic Strength	Measure of the overall electrolytic potential of a solution. The strength of a solution is based on both the concentrations and valences of the ions present.
Mass Transfer	Mass transfer can be described as the movement of mass from one location – be it steam, phase fraction or component – to another location.
Mass Transfer Coefficient	Mass or volume transfer through a membrane based on the driving force across the membrane.
Measured Parameters	Inlet and outlet flow rates, inlet pressures, inlet and outlet solution conductivities.
Mechanical Pressure	The gauge hydraulic pressure at which the feed solution and the draw solution enters the process train.
Membrane	A highly engineered thin semipermeable film which serves as a barrier permitting the passage ions and particles up to a certain size, shape or electro-chemical character.

Term	Definition
Membrane-Liquid Interface	The interface where the membrane is directly in contact with the fluid, typically the mass-transfer boundary region.
Operating Pressure	The gauge hydraulic pressure at which the respective solutions enter the process train.
Operational Parameters	Water flux, water recovery and solute rejections.
Osmotic Backwashing	The instantaneous switch of the permeate direction in an attempt to dislodge the foulant layers formed on the membrane surface.
Osmotic Pressure	A measurement of the potential energy difference between the solutions on either sides of the semipermeable membrane due to the difference in dissolved species of each solution.
Osmotically Driven Membrane Processes	Pressure retarded osmosis, pressure assisted osmosis and forward osmosis.
Performance Indicators	See operational parameters.
Permeability	The capacity of a membrane to allow water or solutes to pass through.
Pressure Assisted Osmosis	Pressure assisted osmosis pressurises the feed solution to enhance water permeation through synergistic osmotic and hydraulic driving forces.
Pressure Retarded Osmosis	The utilisation of the osmotic pressure difference between two source waters of different salinities to perform work and hence produce energy. Osmotic pressure is provided by the saline water that draws fresh water through the semipermeable membrane and the diluted draw solution, now with a greater volume and pressure moved through the turbine to provide electricity.
Primary Mechanical Parameters	Mechanical parameters identified which influence the performance indicators.
Primary Process Parameters	Process parameters identified which influence the performance indicators.
Process Train	The entire FO process encompassing all of the housing blocks.
Recovery	The ratio of product quantity over the feed quantity, represented as a fraction or as a percentile.
Reverse Osmosis	A separation process by which water passes through a porous membrane in the opposite direction of natural osmosis when subjected to a hydrostatic pressure greater than the osmotic pressure of the feed solution.
Reverse Solute Diffusion	See reverse solute flux.
Reverse Solute Flux	Amount of dissolved salt passing through the membrane from the draw solution in moles per day per square unit of membrane area.

Term	Definition
Salinity	The concentration of the inorganic ions in the water.
Saturation Index (SI)	An index particularly showing whether a water source will tend to dissolve or precipitate a particular mineral such as gypsum. When its value is negative the mineral will remain in its dissolved form, when its value is positive the mineral may precipitate and when the index is zero the water and the mineral is said to be at chemical equilibrium.
Scaling	The precipitation of inorganic salts on the feed side of the membrane.
Solids Rejection	The ability of the membrane to hinder the diffusion of certain elements passing through the membrane. Rejection is expressed as one minus the ratio of the brine outlet to the draw solution inlet concentration.
Solute	A liquid mixture containing inorganic salts homogeneously distributed in dissolved in water.
Solution	A mixture of inorganic salts dissolved in water.
Solution-diffusion Model	Mass transfer through a membrane by diffusion. The general approach is to assume that the chemical potential of the feed and permeate fluids are in equilibrium with the adjacent membrane surface.
Solvent	A liquid medium carrying dissolved substances or solutes, typically water.
Spacer	The mesh-like fabric or other material through which permeate flows after passing through the flat sheet membrane. Spacers are placed on both sides of the membrane to promote turbulence on the membrane surface as well as robust support to the membrane.
Supersaturation	A state in which the inorganic salts dissolved in solution reaches a level at which the solubility product is exceeded and causes salt crystals to precipitate out of the solution.
Supersaturation Factor (SSF)	The factor by which the Ca^{2+} ions is present above saturation in a solution.
Thin Film Composite Membrane	A membrane having two or more layers with different physical or chemical properties. A membrane manufactured by forming a thin desalinating barrier layer on a porous carrier membrane.
Total Dissolved Solids (TDS)	Total dissolved solids usually expressed as mg/l or ppm.
Transmembrane Pressure	The net driving force across the membrane. The osmotic pressure of the feed and draw solutions sides less the mechanical pressure on each side.
Zeta Potential	The electrical potential at the surface of shear of the membrane.

Chapter 1

Introduction and Project Rationale

“One thing is clear: we need a fundamental rethink of our water sector and water’s place in the economy. Our current drought is expected to be a taste of the future, so we need to learn quickly and adapt. Demand for water is increasing, a growing economy needs reliable, safe water supplies. Those needs will be met in an increasingly uncertain, volatile and warmer climate.”

Christine Colvin – Freshwater Senior Manager: WWF-SA

Osmotically driven membrane processes (ODMPs) find application in water treatment, desalination and power generation industries, along with applications in the dewatering of aqueous solutions. These methods specifically utilise the osmotic pressure difference between two solutions, the low salinity feed solution (FS), and the concentrated (high salinity) draw solution (DS), to induce mass transfer across the membrane. Forward osmosis (FO) is one such technology where water flows from a low salinity FS to a high salinity DS due to the osmotic pressure difference between the solutions. FO has attracted growing attention worldwide, due to the great promise this technology shows in the industries of (1) desalination, (2) wastewater treatment and (3) liquid food processing [1].

A decline in the efficient operability of the FO process is observed when inorganic salts, comprised of low solubility minerals, precipitate on the membrane surface [2]. This is caused by the supersaturation of certain salts in the FS when water is removed. The feed stream is thus concentrated beyond the solubility limit of the salts in solution. The supersaturation of solutions results in scale formation on the membrane surface. Scale formation on a membrane surface is detrimental to water flux and such fouling can be permanent. The scaling mechanisms on FO membranes are in many ways similar to that observed on reverse osmosis (RO) membranes. The difference in transport phenomena such as concentration polarisation (CP), specifically internal CP [3–5], as well as reverse solute diffusion (RSD) [5–9] of the draw solutes, introduces additional scaling mechanisms specific to FO membranes. Many studies have been conducted to understand these mechanisms [5,8,10–12].

To understand the scaling mechanisms in FO systems, the specific FO system and membranes need to be characterised in terms of the various operating conditions. These are mainly but not limited to (1) temperature, (2) draw solution type and concentration, (3) cross-flow velocity (CFV) and (4) the operational mode.

Several earlier investigations have characterised the effects of operational temperature, the available DSs and the respective concentrations of solutes [13–17]. Various improvements in the development

of membranes and DSs have also been recorded. Recent improvements in the FO membrane morphology migrated towards the use of asymmetric membranes, thereby providing two possible operational configurations, either with the FS facing the active layer (AL) or facing the support layer (SL).

Until recently however, few studies focussed on the transport effects in FO systems brought about by varying the CFV and by changing the operational configuration (e.g. intermittent switching of the flow-path). Therefore, this study was motivated in pursuit of an improved understanding of related effects and the following brief discussion is offered in support of this motivation.

1.1. Desalination & Membrane-Based Processes

Membrane filtration used for desalination refers to processes which can effectively reject dissolved ionic compounds in water. Typically, these compounds are <1 nm in size. FO membranes fall under the same category as RO membranes in terms of their rejection capacity of the dissolved ionic compounds. Although RO and FO membranes can both effectively reject the same ionic compounds, the respective waters which these processes are typically applied to, are markedly different.

There are three main variations of OMDPs which have gained much interest in the international research community. These processes are visually presented in Figure 1-1, and compared to the operation of a RO process. The inherent difference between a RO and an FO process is the driving force. In RO processes the applied hydraulic pressure needs to be higher than that of the osmotic pressure of the feed water. In FO processes the osmotic pressure needs to be higher than that of the applied hydraulic pressure to pump fluid through the system. This inherent difference in driving force brings about the permeation of water in opposite directions as illustrated in Figure 1-1.

The process of osmosis and the variations thereof has considerable potential across a wide variety of applications, including (1) emergency drinks, (2) power generation, (3) enhanced oil recovery, (4) water treatment, (5) fluid concentration, (6) thermal desalination feed water softening, (7) water substitution (8) and desalination [18]. One of the main areas of interest for the application of FO lies in zero-liquid discharge (ZLD) processes.

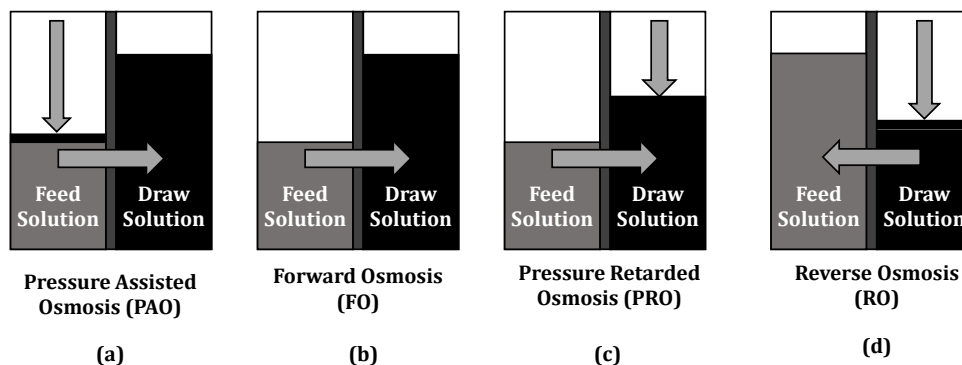


Figure 1-1. Permeation direction in osmotically driven membrane processes (OMDPs) for (a) pressure assisted osmosis (PAO) where a hydraulic pressure is applied to the feed solution, (b) normal forward osmosis (FO) with the absence of an externally applied hydraulic pressure, (c) pressure retarded osmosis (PRO) where a hydraulic pressure is applied to the draw solution and (d) RO where the permeation direction is the reverse of normal FO due to the hydraulic pressure applied to the brine/DS.

1.1.1. Technology Background

The unique ability of RO membranes to reject inorganic compounds effectively, while allowing the permeation of clean water through the semi-permeable membrane, has led to widespread utilisation in the treatment and the reclamation of high salinity inland water sources, seawater desalination and wastewater streams [19]. For the implementation of RO membranes to be economically feasible, sufficiently high recoveries need to be attained. This results in an increased brine concentration which in turn makes low cost brine disposal challenging. Membrane fouling in RO systems is a notorious problem that results in flux decline and increased transmembrane pressures. Some of the key issues pertaining to membrane processes, in particular the RO process, are (1) high energy consumptions relative to other membrane processes, (2) high capital costs and (3) membrane fouling [19].

Effective and environmentally safe brine disposal methods have become an increased hindrance for desalination processes. Brine concentrations of $65\,000\text{ mg}\cdot\text{L}^{-1}$ total dissolved solids (TDS) are attained at a recovery of 45% in typical seawater desalination processes. Industrial brine streams can have brine concentrations of as high as $>80\,000\text{ mg}\cdot\text{L}^{-1}$ TDS, depending on the water recovery and the concentration factor within the RO membrane system. Re-treating these streams with RO membranes becomes uneconomical, due to the high energy requirement to overcome the osmotic pressure of the brine stream. In some cases, the hydraulic pressure required to overcome the osmotic pressure is beyond the operating limits of typical RO processes. Therefore the magnitude of waters, especially industrial effluent streams, are often too saline and high in foulants to be effectively treated with RO membranes [20].

Studies have shown that the fouling propensity in FO membranes are potentially less severe than for RO membranes, due to the difference in fouling mechanisms and factors affecting fouling in these two processes [21,22]. The added advantage of FO is the operational flexibility with regard to the applied process, due to the low operational hydraulic pressures of FO systems and its ability to treat high TDS

streams effectively. FO has gained much traction for the application to process waters beyond the operational limits of conventional RO processes. As per Figure 1-2, the product stream in FO processes is a diluted DS stream. By using a DS solute with a low fouling propensity, the extracted water from the FO process can easily be separated from the DS via an appropriately designed RO system.

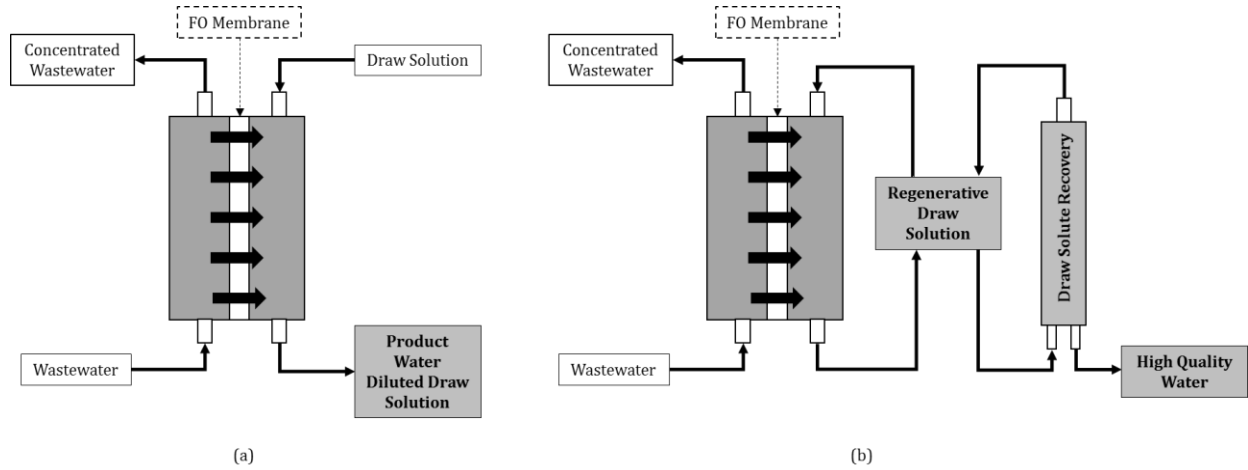


Figure 1-2. (a) Conventional FO process where the product stream is a diluted draw solution stream and (b) extracting high quality water while at the same time regenerating the draw solution via a conventional RO process.

1.1.2. Flux and Fouling in Forward Osmosis

One of the main drivers for FO technology is the relatively low mechanical pressure and hydraulic energy requirements during operation, which in turn results in lower capital costs of pumps and other high-pressure membrane accessories.

Water flux during OMDPs through a semipermeable membrane can be described by Equation (1.1), where P_w is defined as the water permeability coefficient, along with π_D and π_F that are described as the osmotic pressures of the DS and the FS, respectively [23].

$$J_w = P_w(\pi_D - \pi_F) \quad (1.1)$$

The main assumptions made with regard to Equation (1.1), is that the system is well stirred and that the existence of boundary layers within the system is negligible. In reality this assumption is not valid, as concentration gradients forming on each side of the membrane are one of the dominating factors limiting effective operation of FO systems in conjunction with reverse solute leakage from the DS. Therefore, a more appropriate model was presented by McCutcheon et al. [4,24] to describe the water flux across a dense, symmetric membrane as per Equation (1.2):

$$J_w = P_w[\pi_{D,b} \exp\left(\frac{-J_w}{k_D}\right) - \pi_{F,b} \exp\left(\frac{J_w}{k_F}\right)] \quad (1.2)$$

where $\pi_{D,b}$ and $\pi_{F,b}$ represent the bulk osmotic pressure for the DS and the FS respectively, and k_D and k_F represent the mass transfer coefficients on the DS and FS sides. This derived flux model

incorporates the effects of CP, which accounts for the boundary layer phenomenon on both sides of the membrane [23]. With FS solutes being rejected on the FS side of the membrane, water permeation from the FS to the DS side results in a dilution effect on the DS membrane interface. This decreases the effective process driving force. With the development and further enhancement of FO membranes, the membrane morphology changed from being a symmetric membrane to an asymmetric membrane. A thick, non-selective porous support layer is cast upon the thin selective layer to provide mechanical support. Because the effective osmotic driving force is only established on the membrane interface, the asymmetric membrane results in one of the boundary layers now forming within the porous support layer, thereby causing internal concentration polarisation (ICP).

Accounting for this change has given rise to the development of a mass transfer coefficient term, which incorporates the morphology of the porous support layer as described by Equation (1.3):

$$k_{eff} = \frac{D_s \varepsilon}{\tau \delta} = \frac{D_s \varepsilon}{\tau t} \quad (1.3)$$

where D_s is the solute diffusivity, δ is the thickness of the boundary layer, and ε , τ and t are the porosity, tortuosity and thickness of the porous support layer of the membrane respectively [4,24,25]. In the AL-FS operation k_{eff} replaces k_F and in the AL-DS operation it replaces k_D . Equations (1.1) to (1.3) infer the importance of both the operating conditions and the membrane properties, and how these properties can substantially influence the performance of OMDPs. Results from a recent study showed that the water flux ranged from 6.5–8.3 L·m⁻²·h⁻¹, and that reverse solute flux (RSF) ranged from 45–54 mmol·m⁻²·h⁻¹, when the flow velocity ranged from 4–110 cm·s⁻¹ on the FS and the DS side respectively [23,26].

The immediate detection of fouling on the membrane surface can ensure the longevity of the membrane and aid in restoring the membrane performance [27]. Non-invasive and visual online methods can aid in detecting the early stages of membrane fouling in real time by monitoring the flux decline, solute rejection and different operating parameters (temperature, feed, total dissolved solids (TDS), permeate flow and recovery) [27].

For efficient operation, FO processes require membrane cleaning to alleviate the detrimental fouling effects of CP and reverse solute diffusion (RSD) in the system. Some of the cleaning strategies employed to date include (1) increasing the CFV across the membrane and (2) introducing air bubbles in the feed stream [21].

Another cleaning strategy, namely backwashing, is a common principle employed in membrane processes. Backwashing has been employed mainly in processes such as microfiltration (MF) and ultrafiltration (UF) [21]. The principle of osmotic backwashing in FO processes involves the instantaneous switching of the permeate direction [21]. This is achieved by replacing the DS with deionised water, thereby reversing the direction of water permeation. Several studies have investigated osmotic backwashing as a non-invasive cleaning method for FO membranes [21,27,28].

These studies have shown that the reversal of the permeate flux caused a dislodgement of the external foulant layer from the membrane surface. Osmotic backwashing employed in conjunction with high CFVs significantly restored the original water flux.

The orientation of the membrane also plays an important role in membrane scaling in FO processes [4,7,9,10–12]. Generally it is recommended that the AL faces the feed solution (AL-FS) to avoid severe scaling within the membrane SL [4,9]. Literature suggests that better rejection of feed solutes is attained in the AL-FS orientation [31,32]. In contrast, when the AL faces the DS, AL-DS, greater water fluxes and better mechanical stability are achieved [33]. Severe ICP of the feed solutes in the support layer occurs in the AL-DS orientation.

1.2. Motivation and Aim of Project

Many industrial wastewaters (brines) contain very high levels of inorganic salts, particularly calcium, sulphate and carbonate ions [34]. Treating these waters for reuse purposes by means of membrane-based processes leads to detrimental scaling issues on the membrane surfaces [35]. When membrane systems are operated at high recoveries, sparingly soluble salts reach levels of supersaturation. Consequently, this causes the sparingly soluble salts to crystallise spontaneously and precipitate at or near the surface of the membrane. The most common crystal configurations of calcium and carbonate ions are gypsum ($\text{CaSO}_4 \cdot 2\text{H}_2\text{O}$) and calcite (CaCO_3), which are two potential major scalants in membrane processes [34]. Scaling by the precipitation of calcite crystals can be inhibited by means of adjusting the pH of the feed solution. Gypsum, however, is not as sensitive to pH adjustments and therefore gypsum scaling is a major challenge during the purification and reuse of industrial wastewaters [34,35].

Osmotically driven membrane processes (OMDPs) have been proposed as an effective method to treat impaired water streams for reuse purposes, when operated at cost-effective water recoveries. FO is a low-pressure membrane treatment method, which has demonstrated potential in the treatment of industrial wastewater streams [3–5]. As with any membrane-based water treatment method utilised in industrial processes, scaling on the membrane surface is a major operational hindrance. However, due to the low-pressure operation of FO systems, the mechanism by which fouling occurs is different to industrially established RO systems [3–6]. Furthermore, physical cleaning methods such as the reversal of the permeate direction in FO systems by the principle of osmotic backwashing, have been demonstrated to be effective in flux recovery applications [21].

Against this background, this study endeavoured to expand our understanding of FO operation, with the **primary aim** to critically evaluate and characterise the mass transfer and membrane fouling behaviour, specifically considering:

- the effects of cross-flow velocity (CFV),
- the effects of operational configuration (whether the AL is facing the FS or the DS),
- the effects of intermittent switching of the flow path, as a combination of flushing and osmotic backwashing, and

- the practical realities related to flow-path switching when treating feed water saturated with gypsum.

1.3. Research Objectives

The objectives of this study were fourfold:

1. Design build and commission a bench-scale FO system.
2. Conduct validation tests to evaluate performance parameters such as (1) water fluxes, (2) water recoveries and (3) solute rejections attained at CFVs ranging from 9–35 cm·s⁻¹, in both the AL-FS and the AL-DS operational mode.
3. Experimentally investigate routine osmotic backwashing in terms of (1) stabilisation times and (2) optimum CFV, by switching the operational mode instantaneously through reversal of the water permeation direction.
4. Extrapolate findings of routine osmotic backwashing to establish (1) the efficiency of flux recovery and (2) the commercial impact due to product water losses during stabilisation times.

1.4. Thesis Outline

Chapter 2 of this thesis consists of an in-depth literature study. It starts by investigating the mass transport phenomena inherent to FO processes, followed by the characterisation of fouling on FO membranes and typical factors which affect fouling. Chapter 2 is concluded by presenting physical fouling control techniques. **Chapter 3** is a design chapter providing an overview of the design and construction of the laboratory-scale setup used in this study. **Chapter 4** explains the experimental approach followed in this study including various apparatuses used, experimental procedures performed, as well as the analytical methods utilised. Results obtained from the experiments outlined in Chapter 4 are presented in **Chapter 5**. Final thesis conclusions are presented in **Chapter 6**, with recommendations for future work. Complementary information is presented in **Appendix A-C**.

Chapter 2

Literature Review

Despite the many advantages that OMDPs have to offer, the performance of these processes is significantly hindered by membrane fouling. Fouling is caused by the deposition of suspended particles or colloids, organic macromolecules, sparingly soluble inorganic salts (membrane scaling), microorganisms, or a mixture of all these. Membrane fouling does not only lead to rapid flux declines, decreased water recoveries and permeate qualities, but impacts the process operational costs and the membrane operational lifetime. To fundamentally understand the mechanisms underpinning membrane fouling, the system needs to be characterised hydrodynamically. The aim of this review is to investigate the factors affecting the hydrodynamic conditions of an FO system.

2.1. Fundamental Principles of FO

In this section the fundamental principles governing the operation of FO systems are elaborated on. Firstly, the driving force of a FO process is expanded on following mass transport phenomena central to FO. A brief discussion of the basic terms and definitions relevant to FO processes are given, and furthermore, critical design parameters and operational challenges are highlighted.

2.1.1. Driving Force: Osmotic Pressure

The driving force in OMDPs is the osmotic pressure differential between two adjacent solutions. In OMDPs water diffuses from a solution with a lower osmotic pressure through a semi-permeable membrane, to a solution having a higher osmotic pressure. When equilibrium is attained, the rate of diffusion of a specific component (be it water, or salt ions) through the membrane is the same in both directions.

An FO process is not only a separation process but can also be approached from the viewpoint of being a mixing process [36]. Water molecules that diffuse through the membrane, mix with the high salinity DS and reduce the chemical potential of the DS. The spontaneity with which the FO process operates, implies that entropy is generated, which is in accordance with the Second Law of Thermodynamics. Then, according to the Second Law of Thermodynamics, the chemical potential of two adjacent solutions tends to equilibrate in an isolated system [15,36].

2.1.1.1. Origin of the Osmotic Pressure Equation

The osmotic pressure difference is driven by the chemical potential difference of the solutes and solvents on either side of the membrane. The equation to calculate the osmotic pressure was developed by Van't Hoff [37] and is a mathematical expression which quantifies the driving force of each solution in OMDPs. This expression is given in Equation (2.1).

$$\pi = i \frac{n_{solute} RT}{V} \quad (2.1)$$

where π = osmotic pressure (Pa)
 R = universal gas constant ($\text{Pa}\cdot\text{m}^3\cdot\text{mol}^{-1}\cdot\text{K}^{-1}$)
 T = temperature (K)
 i = Van't Hoff factor (dimensionless)
 M = the concentration of constituent *solute* in the water sample ($\text{mol}\cdot\text{m}^{-3}$)

The flow configuration of the system also plays a significant role in the profile of the osmotic pressure along the FO process train. Evidently, the low salinity feed solution will have a lower osmotic pressure than the feed solution (brine) exiting the process train. This is due to the concentration gradient of the feed solution forming along the FO process train. The water volume decreases on the feed side of the solution which is caused by water diffusing from the FS to the DS. The osmotic pressure of the draw solution is decreased along the process train, due to the dilutive effects of water permeation.

The difference in the osmotic pressure across the membrane gives an estimation of the driving force for the process of osmosis. It is important that the concentration of the DS should always be high enough to ensure that osmotic equilibrium is not reached within the system. The osmotic pressure differential in FO processes is a dynamic quantity continually changing along the length of the process train.

2.1.1.2. Osmotic Equilibrium

The osmotic equilibrium of a system is a physical limit of fundamental importance in FO processes. When the osmotic pressures of the FS and DS are the same, the system is said to have reached osmotic equilibrium, and water flux will cease. This is a fundamental thermodynamic physical constraint of FO processes. The osmotic equilibrium of a FO process limits the total volume of water which can be extracted from the feed solution. The constraint of the osmotic dilution also influences the final solute concentrations in the FS and DS respectively. The exiting concentrations play a pronounced role in determining downstream processing of the product water, whether it be for DS regeneration or the intended use of the product stream.

To ensure a significant driving force along the process train, the feed solution exiting the process (with the higher osmotic pressure) should flow adjacent to the DS containing the highest osmotic pressure (the inlet of the DS). This is achieved by operating in the counter-current configuration. Figure 2-1 is

a qualitative illustration of this principle, with Figure 2-1(a) and Figure 2-1(b) qualitatively representing the osmotic pressure profiles for co-current and counter-current flow FO systems [38].

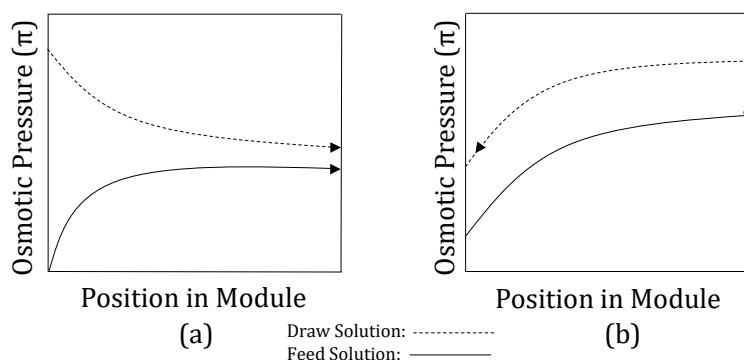


Figure 2-1. Qualitative representation of the osmotic pressure profile in a (a) co-current system, and (b) counter-current system (adapted from [36]).

As per Figure 2-1, a near constant driving force is achieved when operating in the counter-current mode as opposed to the co-current mode where the effective driving force decreases along the process train. In a study conducted by Phuntsho et al. [38] the significance of osmotic equilibrium in FO processes was investigated by modelling a FO process under co-current and counter-current crossflow directions, using established models [38,39]. Various operational parameters were investigated:

- (1) flow conditions within the membrane module;
- (2) feed and draw solution properties; and
- (3) membrane active area.

It was concluded that the crossflow direction plays a significant role in the determination of the point at which osmotic equilibrium occurs. It was found that operation in counter-current mode offered the following advantages as opposed to operation in co-current mode:

- (1) a more gradual decrease in the water flux along the length of the channel was observed;
- (2) on average higher water fluxes were attained;
- (3) the membrane module could operate at higher feed recovery rates;
- (4) a higher dilution factor of the final DS was attained; and
- (5) higher water extraction capabilities of the DSs were observed.

Benavides et al. [39] developed a model to describe the module-level performance of FO systems for co-current and counter-current FO systems where the thermodynamic limit is the osmotic equilibrium of the system. Analysis of the model showed that the flow ratio *viz.* the ratio of the inlet flow rate of the DS to the inlet flowrate of the FS – is an important parameter, especially in counter-current operation. A critical value of 1 for the flow ratio was identified which maximised the recovery rate of the system [39]. It should also be noted that, for the system to tend to osmotic equilibrium, an

infinite membrane area would be required. According to this study then, the recovery of the water from the FS is maximised when the flow rate of the FS and the DS are equal.

Solution properties such as the (1) osmotic pressure, (2) solution density, (3) solution viscosity and (4) solute diffusion coefficient have pronounced effects on the mass transfer occurring within the FO membrane system. Section 2.1.2 investigates the mass transport phenomena in FO systems in conjunction with the effects of the thermodynamic properties on the efficient operation of FO systems. Superimposed upon the osmotic pressure differential of two adjacent solutions are the diffusion of electrolytes across membranes.

2.1.2. Basic Terms & Definitions

Basic terms relevant to the FO process are defined and expanded on below. These terms include: (1) osmotic pressure, (2) water flux, (3) recovery, (4) concentration factor and (5) solute rejection. These terms are defined slightly differently as is typically done for RO systems, as process parameters can be defined either by evaluating the parameters in terms of the DS, or in terms of the FS. Relevant terms and definitions are defined following the counter-current process description as per Figure 2-2.

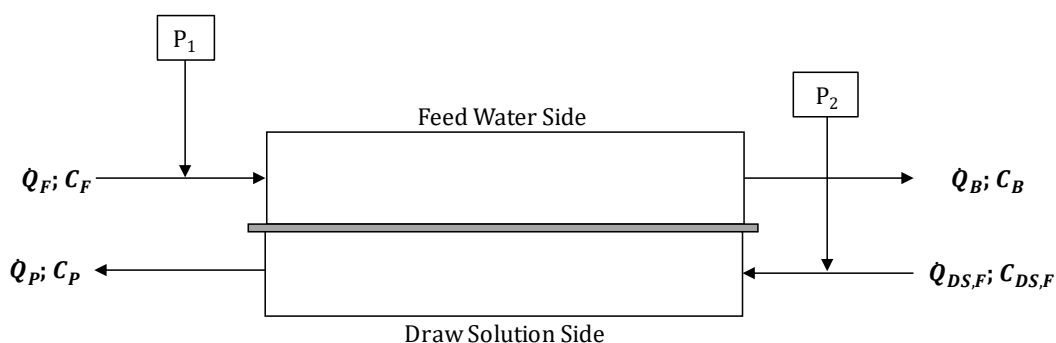


Figure 2-2. Basic FO configuration for defining basic FO terminology and parameters.

2.1.2.1. Osmotic Pressure

The osmotic pressure of a solution is a function of the concentration of the dissolved ions in the solution, as well as the solution temperature, and can be calculated via Equation (2.2):

$$\pi = iRT \sum M \quad (2.2)$$

where π = osmotic pressure (Pa)

R = universal gas constant ($\text{Pa}\cdot\text{m}^3\cdot\text{mol}^{-1}\cdot\text{K}^{-1}$)

T = temperature (K)

i = Van't Hoff factor (dimensionless)

M = the concentration of constituent i in the water sample ($\text{mol}\cdot\text{m}^{-3}$)

2.1.2.2. Flux

Flux is defined as the volumetric flow rate of a fluid through a given area of the membrane. In FO applications the area is the membrane-active area and the fluid is water [40]. Water flux in FO is defined as per Equation (2.3):

$$J_w = P_w(\Delta\pi - \Delta P) \quad (2.3)$$

where J_w = water flux ($L \cdot m^{-2} \cdot h^{-1}$)
 P_w = water permeability coefficient ($L \cdot m^{-2} \cdot h^{-1} \cdot Pa^{-1}$)
 $\Delta\pi$ = osmotic pressure across the membrane (Pa)
 ΔP = pressure difference across the membrane (Pa)

2.1.2.3. Recovery

Water recovery is the term used to quantify the amount of product water retrieved from the FO process. Recovery is the term used to describe the volume percentage of the influent water which exits in the membrane system as permeate [40]. The recovery attained by a membrane system can be calculated using Equation (2.4):

$$R = \left(\frac{Q_F - Q_B}{Q_F} \right) \times 100 \quad (2.4)$$

where R = recovery as a percentage (%)
 Q_B = volumetric flow rate of brine exiting the process ($L \cdot h^{-1}$)
 Q_F = volumetric feed water inlet flow rate ($L \cdot h^{-1}$)

2.1.2.4. Concentration Factor

The concentration factor is used as a tool to estimate the degree to which the low-salinity feed solution is concentrated along the process train. To evaluate the degree to which the feed solution is concentrated along the process path, Equation (2.5) can be used:

$$CF = \frac{C_B}{C_F} \quad (2.5)$$

where C_B = concentration of the exiting brine solution ($mg \cdot L^{-1}$) on the feed side
 C_F = concentration of the entering feed solution ($mg \cdot L^{-1}$) on the feed side

2.1.2.5. Solute Rejection & Solute Passage

Rejection is the term used to describe what percentage of the influent species the membrane retains [40]. For example: if 98% rejection is attained it means that 98% of the solutes in the feed solution will be retained (rejected) by the membrane and it also means that 2% of the influent solutes will pass through the membrane to the permeate stream; this is known as salt or solute passage [40]. The rejection of a given solute can be calculated via Equation (2.6):

CHAPTER 2: Literature Review

$$\% \text{ Rejection} = 1 - \left[\frac{C_B - C_F}{C_{DS,F}} \right] \times 100 \quad (2.6)$$

where C_F = concentration of the entering feed solution ($\text{mg}\cdot\text{L}^{-1}$) on the feed side

C_B = concentration of the exiting brine solution ($\text{mg}\cdot\text{L}^{-1}$) on the feed side

$C_{DS,F}$ = concentration of DS inlet ($\text{mg}\cdot\text{L}^{-1}$)

Many factors influence the degree to which solutes are rejected in a FO system. These factors and the effect of each are listed in Table 2-1. Interestingly enough, all of the factors are proportional to the rejection property of the membrane, except the polarity of the ion, which has inverse effects on the rejections attained by the membrane.

Table 2-1. Various parameters and the corresponding effects these parameters have on rejections attained [40].

Parameter	Increase/Decrease	Rejection (Increase/Decrease)
Ion Valence	↑	↑
Molecular Weight	↑	↑
Polarity	↑	↓
Hydration Degree	↑	↑
Molecular Branching/Molecular Size	↑	↑

In a study conducted by Wang et al. [53], the typical performance and cleaning strategies for six thin-film composite (TFC) FO membranes were investigated. The performance parameters are listed in Table 2-2 and give valuable insight into the typical order of magnitude of the performance parameters in FO systems. The difference in the membrane performance parameters also emphasises the extent to which the intrinsic morphological parameters influence membrane performance indicators, such as flux and rejection.

Table 2-2. Experimental fluxes and salt rejections for typical TFC FO membranes operated with the active layer facing the feed solution [41].

Membrane	Feed Concentration (M)	DS Concentration (M)	$\Delta\pi$ (atm)	Experimental FO Flux ($L \cdot m^{-2} \cdot h^{-1}$)	Salt Rejection (%)
TFC-FO-1	DI	1.5 M NaCl	75.1	19.51	97.1
TFC-FO-2	DI	1.5 M NaCl	75.1	16.81	98.4
TFC-FO-3	DI	1.5 M NaCl	75.1	17.57	97.5
TFC-FO-4	DI	1.5 M NaCl	75.1	17.95	97.2
TFC-FO-5	DI	1.5 M NaCl	75.1	18.93	97.3
TFC-FO-6	DI	1.5 M NaCl	75.1	18.17	97.1

2.1.3. Mass Transport Phenomena in FO

The most important property of membranes is their ability to control the rate of permeation of various species within the system [34], due to their designed capacity and selectivity. Two models are mainly used to describe permeation through membrane systems: (1) the pore-flow model and (2) the solution-diffusion model. The pore flow model attributes the transport of permeants by the pressure-driven convective flow through the tiny membrane pores. Via this model separation is achieved due to the permeates being filtered from the pores through which other permeates selectively move [34]. Effectively, the membrane is modelled as a sieve via the pore flow model.

The solution-diffusion model describes permeation as the movement and dissolution of permeates in the membrane material whereby the permeates move down a concentration gradient [34]. Solute and solvent particles diffuse through the membrane system in an attempt to equilibrate the system. FO membranes are highly hydrophilic, hence promoting the transport of water across the membrane. In reality, no membrane material is perfect, thus the diffusion of solute particles also occurs.

The semipermeable membranes typically used in FO systems are either cellulose triacetate (CTA) or thin film composite (TFC) polyamide membranes. These membranes are designed to allow for the free-flowing permeation of water from the FS to the DS whilst retaining most of the dissolved ions on either side of the membrane. Concentration polarisation (CP) and reverse solute diffusion (RSD) are two main transport consequences of the solution-diffusion model. However, to understand these mechanisms on a fundamental basis, the underlying thermodynamic principles governing the solution-diffusion model require attention. This section seeks to delve into the underlying thermodynamic principles governing CP and RSD, after which the fundamental mechanisms of CP and RSD will be elaborated on.

Considering the chemical potentials of the two adjacent solutions, many factors come into play and require careful attention. One of these factors are the rate of diffusion through the membrane system. Any mass flux, whether it be water or solutes, occurring in membrane systems may include both convection in conjunction with diffusion [42]. In turn this affects solute rejections attained within the FO system. In the derivation of the solution diffusion model two main assumptions are made:

CHAPTER 2: Literature Review

- (1) The first assumption governing the transport through membranes is that the fluids on either side of the membrane are in equilibrium with the interface of the membrane material. Implicit to this assumption is that the rates of adsorption to and desorption from the membrane interface are higher than the rate of diffusion through the membrane [34].
- (2) It is assumed that the pressure throughout the membrane is uniform and that the chemical potential gradient across the membrane can be represented as a concentration difference.

Detailed derivations of the solution diffusion model can be viewed in Cussler et al. and Seader et al. [42,43]. The basic flux across the membrane can be described as the transport across a thin film. The flux attained by the membrane is proportional to the concentration difference across the membrane as described by Equation (2.7), which is also based on the solution-diffusion model.

$$J_w = \frac{D}{l}(C_{10} - C_{1l}) \quad (2.7)$$

where J_w = water flux ($\text{mol}\cdot\text{m}^{-2}\cdot\text{h}^{-1}$)
 D = diffusion coefficient ($\text{m}^2\cdot\text{h}^{-1}$)
 l = membrane thickness (m)
 C_{10} = draw solution side concentration ($\text{mol}\cdot\text{m}^{-3}$)
 C_{1l} = feed solution side concentration ($\text{mol}\cdot\text{m}^{-3}$)

There are three key points relevant to Equation (2.7) [42]:

- (1) The separation attained by membrane-based processes are inherently based on the rate of transport of solutes and water which implies that the degree of separation is dependent on diffusion.
- (2) Membrane separation is strongly influenced by the partition of the solute between the membrane and the adjacent solution. That is, the concentration of the solute and the solvent may differ significantly from the concentration of these respective fluids directly adjacent to the membrane and to the concentrations in the bulk of the solutions.
- (3) The membrane itself can be viewed as one of several resistances in series for water permeation. However, as membrane technology advanced the thickness of the membrane has been minimised significantly, hence implying that the resistance via the membrane is lower than it used to be.

The diffusion of strong electrolytes plays a role in the transport mechanisms in FO systems. Many factors within membrane systems dictate the rate at which diffusion occur, such as: (1) solute-solute interactions, (2) solute-solvent interactions and (3) interactions with the membrane through which selective diffusion occur.

2.1.3.1. Solute-Solute Interactions

The diffusion of strong electrolytes, such as sodium chloride, can accurately be described by a single diffusion coefficient. Sodium chloride ionises completely in water; hence the sodium and chloride ions diffuse at the same rate. The diffusion rate of the large cation (sodium ion) dictates the diffusion rate of the smaller anion (chloride ion). The sodium and chloride ions are tied together electrostatically, hence the rate of diffusion will be the same, to maintain electroneutrality within the system. However, as there is a significant difference in the size of the cation and anion, the kinetic energy exhibited by the anion (chloride ion) is greater than that of the cation (sodium ion) (see Table 2-3). This phenomenon is demonstrated visually by Figure 2-3.

To evaluate fundamental membrane parameters such as solute rejections, the degree of diffusion needs to be quantified within the system. The measurement and approximation of the various diffusion coefficients of ions in solution is challenging, partly because the diffusion coefficients for the anions and cations within the system differ and is dictated by the faster diffusing ion, but mainly because typical feed waters contain associating solutes which further complicates the accurate quantification of the diffusion numbers [42]. For derivations of these diffusion coefficients, see Cussler [42]. A brief summary of the diffusion numbers for commonly used ions in FO processes are presented in Table 2-3.

For electrolyte solutions the electrical resistance and its reciprocal, the electrical conductance, can give an accurate measurement of the number of ions in solution. In order to quantitatively evaluate the solute transport via diffusion across membranes, the evaluation of the electrical conductance of the respective solutions is of importance. The conductivity of solutions vary with concentration, especially at very high dilutions [42]. Typical DS concentrations are in the range of 0.5–5 M, depending on the osmotic pressure requirement, and typically contain strong electrolytes such as calcium chloride (CaCl_2) and sodium chloride (NaCl). For strong electrolytes these variations are chemically and practically negligible [42]. In general terms, the diffusivity of the ions decreases with an increase in the molecular weight of the solute, the charge, as well as the hydrated radius [16].

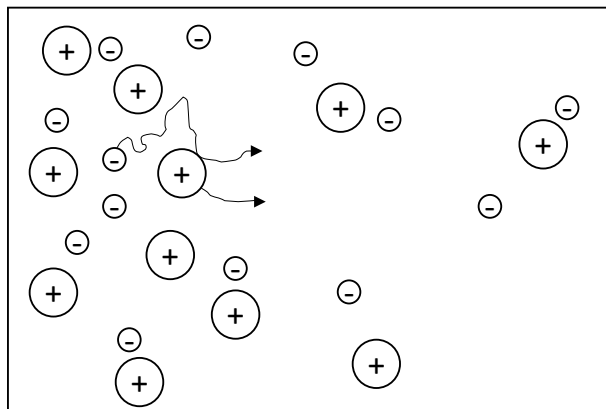


Figure 2-3. Diffusion of electrolytes. The ions have the same charge and are present in the system at the same concentrations. The cations, which are the larger ions, move inherently slower than the smaller anions. However, due to the electroneutrality of the system, both ions have the same net motion and hence the same permeation flux (redrawn and adapted from [16]).

It has been shown that conductivity measurements can provide an indication of ionic movements and mass transfer within the system. This will greatly simplify the quantification of ionic transport across membranes; however, derivations have shown that conductance is dominated by the ion with the larger diffusion coefficient, hence the faster ion. Conversely, diffusion is mainly influenced by the ion with the smaller diffusion coefficient, hence the slower ion [42]. This implies that conductance and diffusion represent different averages of the solute mobility coefficients in similar molecular processes. Furthermore, this also implies that the information quantitatively supplied by diffusion and conductivity will not be completely equivalent unless both associating ions have the same mobility [42].

Table 2-3. Diffusion coefficients of the most common ions forming inorganic salts in FO processes at 25°C [42].

Cation _i	$D_i \times 10^{-5} \text{ (cm}^2\cdot\text{s}^{-1}\text{)}$	Anion _i	$D_i \times 10^{-5} \text{ (cm}^2\cdot\text{s}^{-1}\text{)}$
H ⁺	9.31	OH ⁻	5.28
Na ⁺	1.33	Cl ⁻	2.03
Ca ²⁺	0.79	CH ₃ COO ⁻	1.09
Mg ²⁺	0.71	SO ₄ ²⁻	1.06
		CO ₃ ²⁻	0.92

For the purposes of this investigation it is valid to assume that the conductivity measurements would give an accurate enough representation of the solute mobility over the membrane. However, in order to evaluate the system as a whole in terms of mass transport and the effects thereof (RSD and CP), system mass balances are required. Calculations of the respective TDS values via the approximation of a conductivity constant then becomes inaccurate and can lead to inaccuracies of as high as 30%

[44]. However, when evaluating the rejection property of the membrane these inaccuracies become relative and will effectively cancel out.

2.1.3.2. Solute-Solvent Interactions

Solute-solvent interactions also influence the rate of transport of solutes across the membrane. Typically, this phenomenon manifests as hydration of the ions in solution. When water and the solvent combine to form a new species, which is actually diffusing across the membrane, it is typically termed hydration. Mathematically the ionic radius of hydrated species is larger than that of non-hydrated species, thereby leading to increased hydrated-solute rejections [42]. It is however inevitable that all solutes will be hydrated; hence the effects of hydrates are not exclusive to particular solutes.

2.1.3.3. Membrane Interactions

The permeation of electrolytes from the DS into FS and from the FS into the DS requires transport across three distinct regions [45]:

- (1) the external boundary layer;
- (2) the dense AL; and
- (3) the porous SL.

Transport of these electrolytes in the support layer as well as the boundary layer are dictated by both diffusion as well as water permeation through the membrane. However, only diffusion controls electrolyte transport through the AL of the membrane – as per the solution-diffusion transport mechanism [45].

The AL is the selective transport barrier, therefore, the performance of FO systems is greatly determined by the inherent characteristics of the AL. The AL is typically designed to be exclusively selective towards water, thus very hydrophilic. Water molecules can thus freely diffuse through the AL whilst solutes and pollutants are rejected from passing and remain within the FS [46]. Water flux is a result of diffusion of the water molecules across the membrane, where two factors affect the velocity of the water transport across the membrane: (1) the magnitude of the driving force and (2) the selectivity of the FO membrane to water molecules [46]. Water flux can thus be calculated using Equation (2.8):

$$J_w = P_w \Delta \pi \quad (2.8)$$

where J_w = Water flux, ($\text{L}\cdot\text{m}^{-2}\cdot\text{h}^{-1}$)

P_w = Pure water permeability coefficient, ($\text{L}\cdot\text{m}^{-2}\cdot\text{h}^{-1}\cdot\text{bar}^{-1}$)

$\Delta \pi$ = Delta osmotic pressure, (bar)

The diffusion of solutes through the membrane is dictated by the concentration difference of the solutes across the membrane. Solute transport across the membrane can be calculated via Equation (2.9), which is also an indicator for the solute selectivity of the membrane [46]:

$$J_s = B\Delta C \quad (2.9)$$

where J_s = Solute flux, ($\text{g}\cdot\text{m}^{-2}\cdot\text{h}^{-1}$)
 B = Solute permeability, ($\text{L}\cdot\text{m}^{-2}\cdot\text{h}^{-1}$)
 ΔC = Concentration difference between the FS and DS, ($\text{g}\cdot\text{L}^{-1}$)

Solutes in FO systems can diffuse in two directions, based on the concentration gradient within the system: (1) forward feed and (2) reverse solute diffusions (RSDs). The solute permeability parameter (B) should thus be minimised to reject unwanted salts and pollutants permeating from the FS to the DS and vice versa [46].

The SL of the membrane is used to provide mechanical support for the AL. It tends to be thicker, more porous and more tortuous [46]. For this reason there is a diffusion hindrance of the draw solute across the SL of the membrane leading to ICP, resulting in reduced membrane performance [46]. Quantifying this transport phenomenon is thus important for efficient FO membrane performance. The structural parameter (S) of the membrane can act as a guidance parameter to describe the characteristics of the SL [46]. The structural parameter of the membrane is a function of (1) the SL thickness, (2) tortuosity and (3) the porosity of the membrane [46].

FO membranes can be operated in two configurations depending on which side of the membrane is facing which solution. Typically, in FO the AL of the membrane faces the FS and the DS faces the SL. When operating the membrane in PRO mode the active layer faces the DS. These two notations will be referred to by stating which solution the active layer of the membrane faces: AL-FS and AL-DS. Since the morphology of the two respective sides of the membrane are markedly different, the occurrence of RSD and CP at each side of the membrane also differ distinctly.

ICP affects the rates of water permeation and RSD within the membrane SL. On the other hand, water permeation and RSD will affect the extent to which external concentration polarisation (ECP) and ICP occur within the system [24–29]. There is an intrinsic relationship between (1) RSD, (2) CP and (3) fouling. These relationships are detailed in Figure 2-4 .

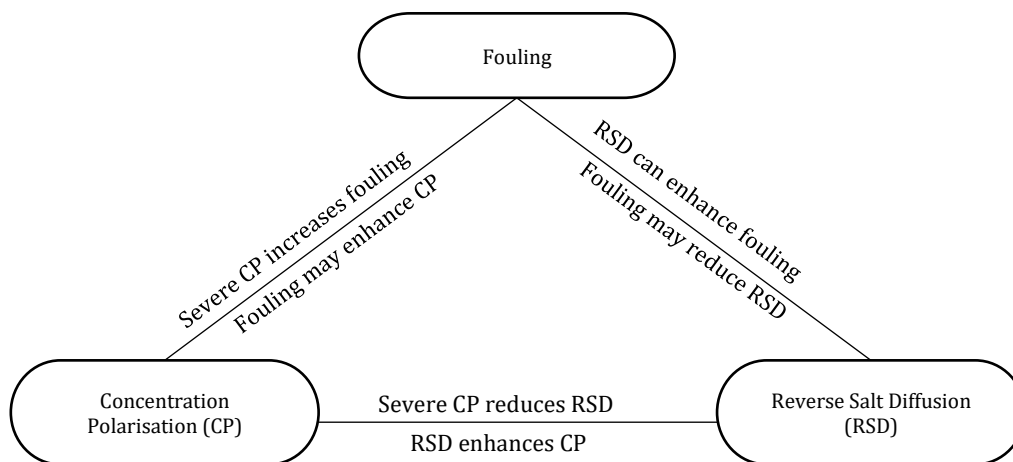


Figure 2-4. Intrinsic relationship between fouling, CP and RSD and how each factor influences the other. Redrawn from [48].

In this subsection RSD and CP will be critically evaluated to investigate the effect of these transport phenomena on fouling in FO processes, and to develop effective fouling control strategies.

2.1.3.4. Reverse Solute Flux

Small amounts of dissolved solutes diffuse through and across the FO membrane from the DS to the FS and *vice versa* [5,6,9,26]. The reverse solute diffusion from the DS into the FS has costly effects on the operation of an FO system, as it leads to the loss in draw solutes, thereby decreasing the system driving force. This raises process operational costs as the replenishment of draw solutes are required to maintain a constant osmotic gradient for the system [9]. Moreover, the accumulation of draw solutes in the FS can detrimentally change the solution chemistry, which may lead to enhanced fouling within the feed solution [47]. Understanding and accurately quantifying the reverse diffusion of solutes is of great importance to quantify membrane rejections attained.

In theory it can be assumed that the semipermeable membrane allows only for water permeation. However, in reality solutes still diffuse from the DS stream through the semipermeable membrane to the FS in order to equilibrate the system. This is due to the high solute concentration on the DS side and the effective concentration difference between the feed solution and the draw solution.

2.1.3.5. Concentration Polarisation

CP is the term used to describe the phenomenon that the solute concentration at or near the membrane surface significantly differs from the concentration of the solute in the bulk solution [48]. When analysing important operation performance parameters of membrane-based processes, CP is an important factor to consider. CP diminishes the driving force for water permeation during membrane processes. The fact that the driving force in FO processes is essentially a concentration gradient, makes CP a detrimental process occurrence [49]. Figure 2-5 visually represents the ideal case of concentration gradients throughout the membrane system and the actual case where steep concentration gradients are formed on either side of the membrane.

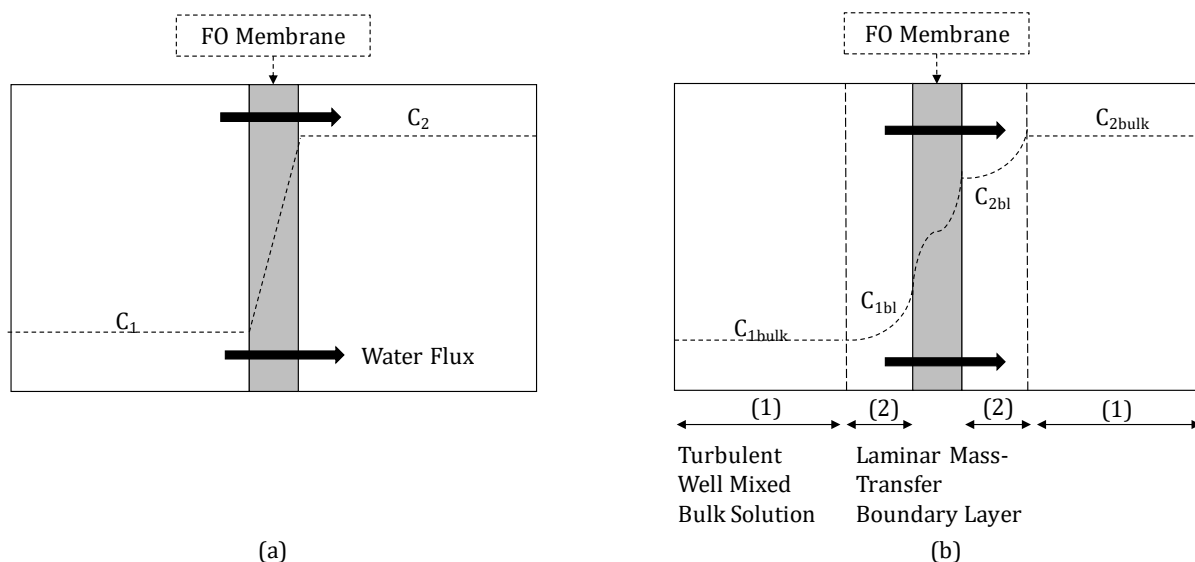


Figure 2-5. The phenomenon of CP within membrane systems in terms of the (a) ideal case where no concentration gradients are formed on either side of the membrane and (b) actual case where the solute concentrations vary significantly from the bulk fluid on either side, to the boundary layer on either side of the membrane.

As per Figure 2-5 a concentrative effect is observed on the FS side, due to the accumulation of solute particles on the membrane surface. This is caused by the water permeation drag through the membrane. On the DS side a dilutive effect is observed. Hence, the concentration of the DS solute decreases on the surface of the membrane. The effective driving force across the FO membrane is then decreased which reduces the effectiveness of the FO membrane operation.

CP can either manifest as (1) ICP or (2) ECP. ECP occurs near the surface of the membrane on both sides. The effects of ECP can easily be alleviated by adjusting the hydrodynamic flow conditions of the system [48] to increase the turbulence on the membrane surface. ICP occurs within the porous support layer of the membrane. ICP is the unstirred layer that hinders solvent diffusion from the FS to the DS [48]. Of the two forms of CP, ICP plays the more dominant role in hindering the effective operation of FO systems.

In FO separation processes, four cases of CP exist and require description: (1) concentrative ECP (CECP), (2) dilutive ECP (DECP), (3) concentrative ICP (CICP) and (4) dilutive ICP (DICP) [49]. In FO separation, water permeates through the AL of the membrane, which is highly selective to water permeation, until the difference in the chemical potential becomes equilibrated to the point where the osmotic pressure of the FS and the DS is equal. As water flux continues, the FS is concentrated and the draw solution is diluted. Hence, ICP is an unavoidable occurrence within the FO system.

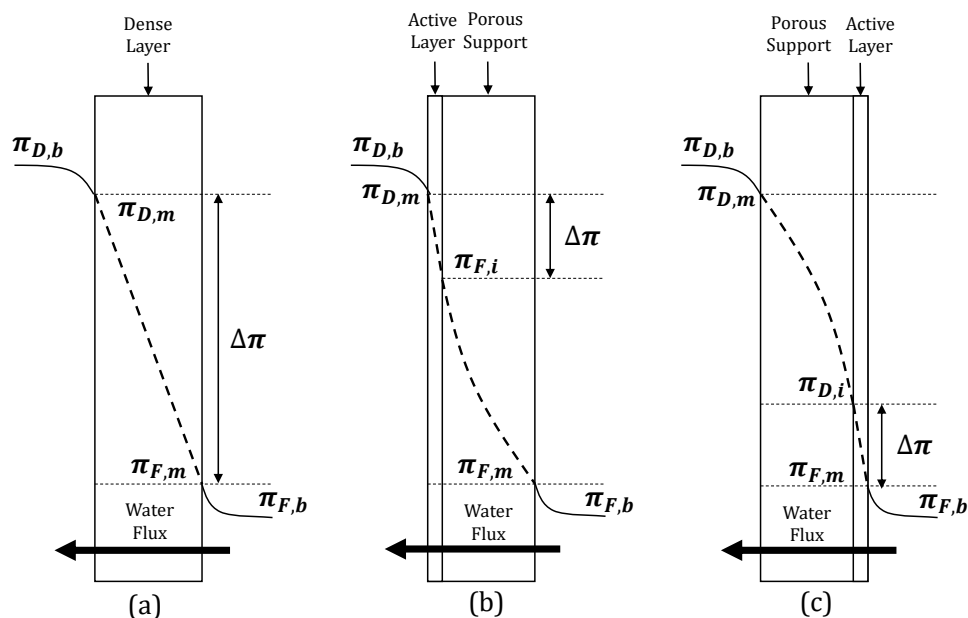


Figure 2-6. Illustration of the effective osmotic pressure for the effective driving force of the process and how the concentration gradients affect the system driving force. (a) The ideal case where the driving force is the absolute difference between the osmotic pressure of the adjacent solutions, (b) AL-DS where dilutive ECP and concentrative ICP is dominant and (c) AL-FS where concentrative ECP and dilutive ICP is dominant. Redrawn from [26].

When the AL is facing the draw solution (AL-DS), dilutive ECP is paired with concentrative ICP as denoted by Figure 2-6(b). Dilutive ICP is paired with concentrative ECP when the AL is facing the feed solution (AL-FS), as in Figure 2-6(c). ICP is exclusive to FO. ICP occurs mainly within the SL of the membrane and is defined as the differing solute concentrations at the transverse boundaries of the SL. The result is the reduction in the osmotic pressure gradient across the AL of the membrane which is manifested as a reduction in water flux. A basic summary of the different types of CP is presented in Table 2-4.

Table 2-4. Summary of the basic types of CP within the membrane system (adapted and redrawn from [11]).

Category	Location	Type	Membrane Orientation
External concentration polarisation (ECP)	Surface of the membrane active layer	Concentrative ECP	AL-FS
		Dilutive ECP	AL-DS
Internal concentration polarisation (ICP)	Membrane support layer	Concentrative ICP	AL-DS
		Dilutive ICP	AL-FS

CHAPTER 2: Literature Review

Studies [4,5,25] conducted, identified ICP as a key performance-limiting phenomenon, occurring in FO processes that are capable of reducing water fluxes up to 80%. Due to the location where ICP manifests within the membrane, the decline of water flux cannot be mitigated by altering the system hydrodynamic conditions [25].

In Figure 2-7 experimental data [25] depicts the effects of ICP on flux, depending on the mode of operation – AL-FS or AL-DS.

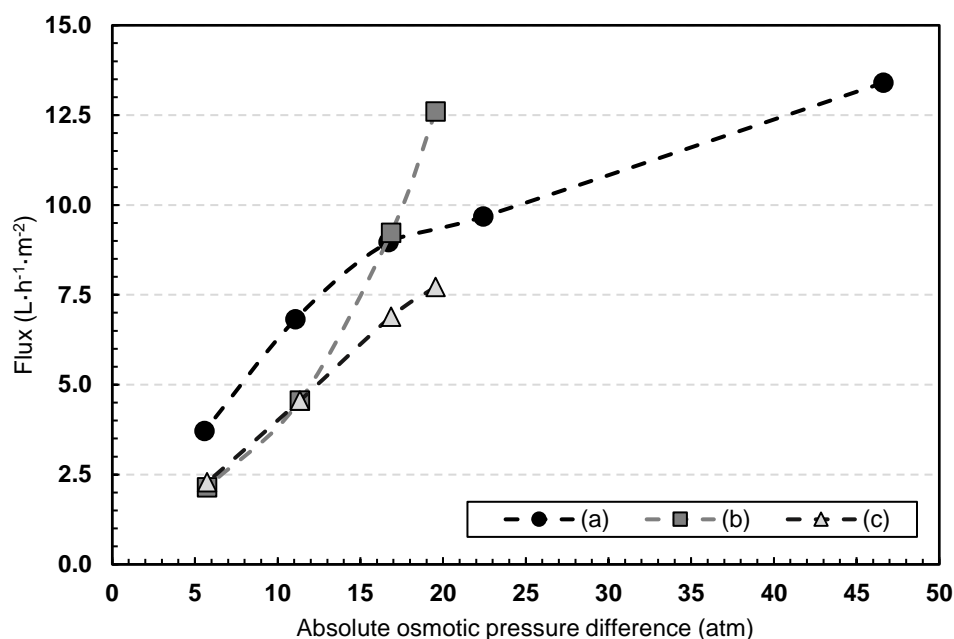


Figure 2-7. Experimental data generated for (a) NaCl DS varied from 0.125–1.0 M and deionized feed water operating in AL-FS, (b) 0.5 M NaCl DS with the feed solution varying from 0.0625–0.375 M NaCl operating in AL-DS and (c) a 0.5 M NaCl DS with a feed solution varying from 0.0625–0.375 M NaCl operating in AL-FS. Experimental conditions: CFV and temperature of both the DS and the FS were at 30 cm·s⁻¹ and 22.5 ± 1.5 °C, respectively. Data obtained from [25].

When the DS is placed against the SL (AL-FS), dilutive ICP is observed. Varying the concentration of the FS produces a linear relationship between the osmotic pressure and the flux, as observed in Figure 2-7 (c). In contrast to this variation, in the FS concentration, the concentration of the DS resulted in a non-linear trend, Figure 2-7 (a). When the DS is placed against the active layer (AL-DS) as in Figure 2-7 (b), concentrative ICP occurs. A non-linear relationship between the bulk osmotic pressure difference and the flux exists. The higher the osmotic pressure difference, the higher the measured water flux. In summary, higher water fluxes are observed when the DS faces the active layer (AL); due to the fact that in order to maintain a significant driving force, the FS will contain far less solutes, which decreases the concentrative ICP effects [25]. It can thus be concluded that dilutive ICP has a more significant effect on flux than concentrative ICP.

When the system is operated in AL-DS and the feed water is deionised water, ICP is negligible as the DS faces the active layer of the membrane and not the porous support structure of the membrane. From Figure 2-7 it is evident that CP arises when the DS is placed against the active layer and the FS

(containing a significant concentration of solutes) is placed against the porous SL. The water flux crossing from the support layer through the AL, causes the solutes against the interior surface of the AL to become more concentrated, resulting in a decreased driving force for water permeation adjacent to the membrane surface. This effect is counteracted by the back-diffusion away from the AL. However, at steady state conditions, the concentration at the interface of the AL and SL is higher than that of the bulk feed solution resulting in concentrative ICP. This is then where the assumption inherent to the adsorption and desorption of the ions to the membrane of the diffusion model becomes prevalent.

The increase or decrease in the concentration of the permeating species at the interface of the membrane, compared to the concentration of the species in the bulk solution, determines the extent of CP. Equation (2.11) shows the calculation of the CP modulus – a useful measure of the extent of the CP occurring within the membrane system. When the modulus is equal to unity, the concentration of the permeating species is the same as in the bulk solution and CP is negligible [34]. As the modulus deviates further from unity, the extent of CP becomes pronounced in the system. The CP modulus of the system provides significant information depending whether the modulus is smaller or larger than unity:

- (1) The CP modulus is smaller than unity when the permeating minor component is enriched within the permeate, where in this case, the component becomes depleted within the laminar mass transfer boundary layer [6].
- (2) The CP modulus is larger than one when the permeating minor component is depleted within the permeate; therefore, the component is enriched within the laminar mass transfer boundary layer [6].

The CP modulus is a function of the Peclet number. The Peclet number is presented in Equation (2.10). The Peclet number can be used as an indication of the diffusion and convection effects within the system. The Peclet number is a function of (1) the water flux measured, (2) the thickness of the laminar mass-transfer boundary layer and (3) the diffusion coefficient of the species being rejected by the membrane [34]. A Peclet number less than unity implies that the convective flow of the permeating species is more dominant than the diffusion of the species being rejected by the membrane.

$$Pe = \frac{J_w \delta}{D_i} \quad (2.10)$$

where J_w = Water volumetric flux, ($\text{m} \cdot \text{s}^{-1}$)

δ = Laminar mass transfer boundary layer thickness, (m)

D_i = Solute specie diffusion coefficient, ($\text{m}^2 \cdot \text{s}^{-1}$)

In FO systems the evaluation of the Peclet number can be evaluated from two sides of the membrane: the AL and the SL, respectively. For direction of water permeation, it is important to bear in mind the thickness of the mass-transfer boundary layer. When the system is operated in AL-DS, the thickness of the mass-transfer boundary layer will increase to account for the thicker support layer. In FO

CHAPTER 2: Literature Review

systems the DS can be viewed as a carrier fluid for the permeating species (pure water). However, the DS ions influence the estimation of the Peclet number as DS solutes are not completely rejected by the membrane. Hence, in FO systems, two Peclet numbers require calculation to estimate whether diffusion of solutes or convection of water (permeate) is dominant. This provides a quantitative measurement of the extent of RSD within the system [25].

$$\frac{c_{io}}{c_{ib}} = \frac{\exp\left(\frac{J_w \delta}{D_i}\right)}{1 + E_0[\exp\left(\frac{J_w \delta}{D_i}\right) - 1]} \quad (2.11)$$

where J_w = Water volumetric flux, ($\text{m}\cdot\text{s}^{-1}$)
 δ = Laminar mass transfer boundary layer thickness, (m)
 D_i = Solute specie diffusion coefficient, ($\text{m}^2\cdot\text{s}^{-1}$)
 E_0 = Membrane enrichment factor, dimensionless
 c_{io} = Membrane surface concentration of solute, ($\text{mg}\cdot\text{L}^{-1}$)
 c_{ib} = Bulk solute concentration, ($\text{mg}\cdot\text{L}^{-1}$)

For a detailed derivation of Equation (2.11) see Baker [34]. The enrichment factor in Equation (2.11) is a function of the selectivity of the membrane. For typical RO systems this factor is less than unity, since the membrane is hydrophilic and water is the permeating species. The same holds true for FO systems. The enrichment factor can be roughly estimated by evaluating the solute rejections attained by the membrane. For typical RO systems this factor is equal to 0.01, corresponding to solute rejections of 99.9% [34].

More recently, in a study conducted by Field et al. [50], the occurrence of boundary layers within a FO system was studied. Adaptations to the CP modulus were included in the derived model to incorporate the two solutions flowing adjacent to each other with the FS being concentrated and the DS being diluted. It was shown that in an FO system, a maximum Peclet number can be calculated based on the phenomenon of RSF.

In a study conducted by Wang et al. [51], ICP and ECP were quantitatively evaluated by assessing the osmotic pressure drop across the membranes under different operating conditions but in normal FO operation (AL-FS). Significant results of this study showed that as the concentration of the DS was increased from 0.25 M to 1.5 M, the proportion of CP consisting of ICP rose from 33% to 51%, and for the ECP portion from 12% to 31% [32]. These results are significant as it indicated the predominance of ICP in FO systems and that the effects of ECP are pronounced enough that it cannot be ignored as a factor that decreases the driving force across the system. For a comprehensive review into the many approaches that can be followed to model the various forms of CP, refer to [4,25,48].

2.2. Membrane Fouling in FO

Membrane fouling is considered the main cause of flux decline and decreased permeate quality. The design of membrane systems is mainly dictated by fouling control. The cause and the prevention of fouling in membrane systems depend on the characterisation of the feed water. Sources of membrane fouling can be divided into four major categories, depending on the source of the feed water being treated: (1) scale, (2) silt, (3) organic fouling and (4) biofouling [34].

The majority of industrial wastewaters contain very high levels of inorganic salts, particularly calcium, sulphate and carbonate ions [34]. Treating these waters for reuse purposes by means of membrane-based processes, leads to detrimental scaling issues on the membrane surfaces [35]. When membrane systems are operated at high recoveries, sparingly soluble salts reach levels of supersaturation. Consequently, this causes the sparingly soluble salts to crystallise spontaneously and precipitate at or near the surface of the membrane [34,35].

Figure 2-8 demonstrates the basic fouling mechanism of membrane processes. It is evident that the membrane surface chemistry plays a significant role in the onset of membrane fouling. Therefore, in this sub-section, the general aspects of membrane fouling are elaborated on, and specific mention is made of the hydrodynamic and operational factors influencing fouling.

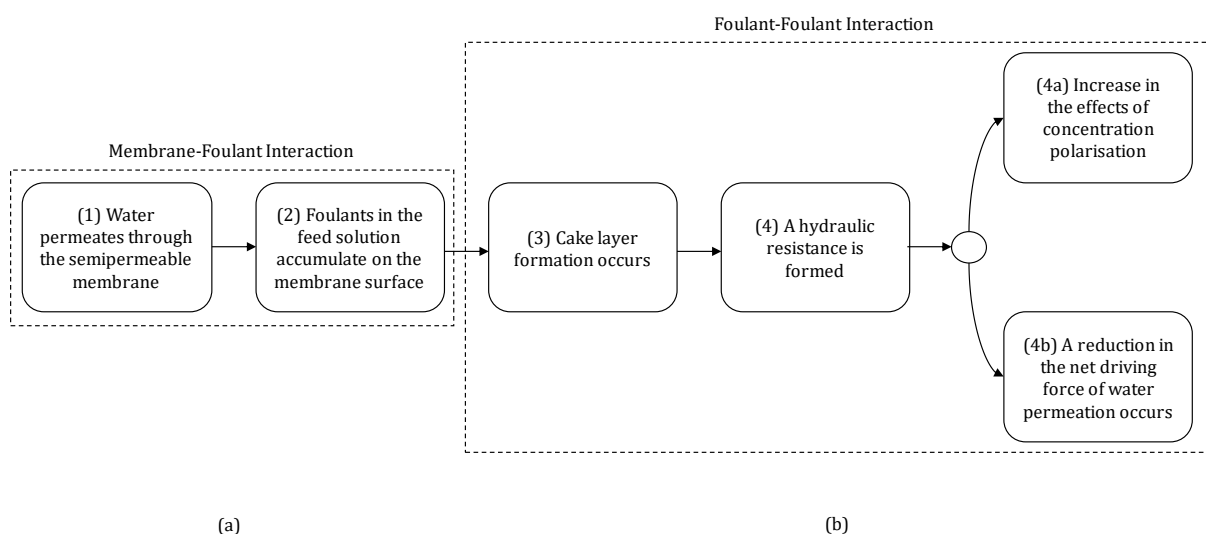


Figure 2-8. Basic fouling mechanism in membrane processes. (a) Foulant interaction with the membrane leads to the accumulation of foulants on the surface of the membrane. The deposition of foulants on the membrane surface enhances foulant interaction with other constituent foulants in the feed water. (b) The hydraulic resistance created by the foulant layer on the membrane surface reduces net driving force for permeation and leads to increased concentration polarisation.

2.2.1. General aspects of membrane fouling in FO

The general aspects of fouling in FO systems have been documented extensively in literature. For more in-depth explanations refer to [27,36,48,52,53]. This discussion follows a structure similar to the one presented in the review paper of She et al. [48]. Aspects specific to this project are detailed below.

2.2.1.1. Fouling Mechanisms

As stated previously, water fluxes attained in membrane systems can be affected by (1) CP, (2) RSD and (3) foulant deposition. In this section the influence of foulant deposition on water flux attained will be elaborated on [48]. Figure 2-9 illustrates the various effects of foulant deposition visually.

- (1) **Addition of extra hydraulic resistance.** Water permeation is decreased due to the foulant cake-layer formed. The addition of the hydraulic resistance caused by the deposition of the foulants decreases water flux even at the same effective osmotic driving force [48].
- (2) **Induction of fouling-enhanced CP.** The cake layer formed can hinder the diffusion of solutes in the unstirred/less turbulent region near the surface of the membrane back to the bulk solution, thereby increasing the effects of CP [48].
- (3) **Altering the rejection property of the membrane.** The membrane rejection property can be altered via foulant deposition by sealing the membrane pores/defects, thereby not allowing solute diffusion. This could lead to increased membrane rejections and a reduction in reverse solute diffusion from the DS to the FS. In principle this would seem as an advantageous phenomenon, however, data produced from such a membrane is unreliable as the exact sealing conditions cannot be recreated and would differ from one experimental run to the other [48].

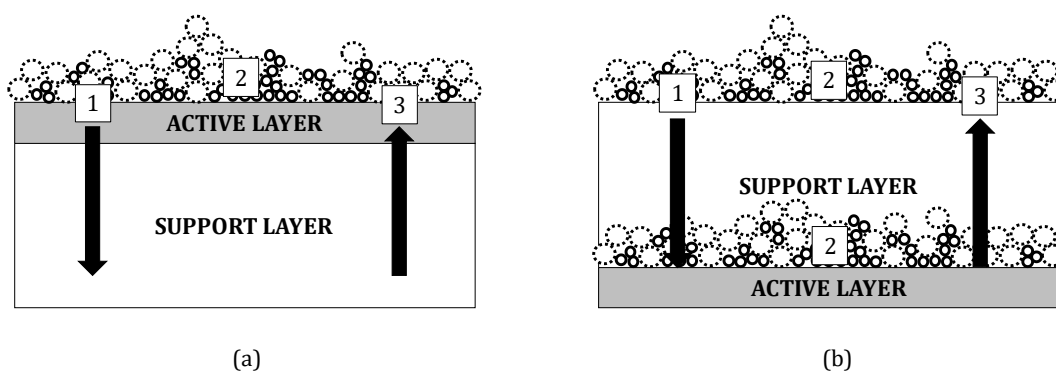


Figure 2-9. Visual illustration of the fast influences of membrane fouling on flux behavior according to the osmotic-resistance filtration model. (Modified and redrawn from [48].)

2.2.1.2. External and Internal Fouling

Various studies conducted to investigate membrane fouling have stated that fouling can take place at different locations around and within the membrane [10,29,33,54]. As stated in Section 2.1, FO membranes typically contain an AL and an SL. Depending on which side faces which solution (either

the feed water or the engineered DS), fouling can occur at different locations, either inside the porous support layer or on the membrane surface. Hence, membrane fouling in FO systems can be classified either by, or a combination of: (1) external fouling or (2) internal fouling.

External fouling is the deposition and accumulation of foulants on the surface of the membrane when the AL of the membrane is facing the FS. A cake-layer of foulants forms on the surface of the membrane enhancing the hydraulic resistance across the membrane. External fouling is relatively easy to remove when compared to internal fouling, as external fouling can be reduced by adapting the operational hydrodynamic conditions of the feed flow system to and on the membrane.

Reducing the effects of internal fouling on the membrane system proves to be a more tedious task. Internal fouling manifests inside the porous support structure of the membrane when the AL of the membrane faces the DS. Several configurations of internal fouling can occur either simultaneously or individually. As depicted by Figure 2-10, the following five scenarios could possibly occur depending on the molecular size of the foulants in the feed water [48]:

- (1) If the foulants in the feed water have a relatively small molecular size, the foulants can enter into the porous support layer of the membrane via feed water convection. Two scenarios occur: (1) the foulant will adsorb on the walls of the porous SL and move down in the channel and be retained to deposit on the backside of the AL surface, subsequently (2) other foulants which enter the same channel will attach to the deposited foulants on the backside of the AL. Eventually pore clogging will occur.
- (2) The conditions described in (1) causes the foulants to accumulate in the pore channel which causes severe pore clogging.
- (3) When the foulants in the feed water have a larger molecular size, the foulant is too large to enter the pore channel of the support layer, hence, external fouling occurs on the surface of the support layer.
- (4) & (5) If the feed water contains a mixture of membrane foulants, a combination of internal and external fouling can occur, which affects the membrane performance detrimentally.

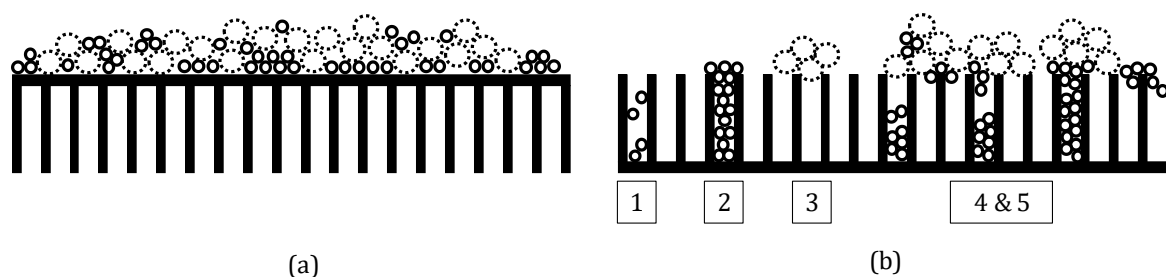


Figure 2-10. Visual representation of external and internal fouling in FO processes. (a) When the active layer faces the FS containing the foulants, only external fouling is present in the system. (b) When the system is operated so that the FS faces the porous support layer of the membrane, internal fouling occurs. (Redrawn and modified from [48].)

Researchers [21,28,55] suggest FO membranes to be operated with the AL facing the FS to minimise the extent of fouling. However, when the AL faces the FS, severe ICP occurs within the porous support layer of the membrane. Osmotic backwashing has been developed as a successful physical cleaning method to dislodge and remove foulants from the channels in the porous support layer, by reversing the permeate direction. Limited studies have been conducted on membrane fouling within the porous support layer of the membrane [56].

2.2.2. Factors Affecting Fouling in FO

Many factors affect fouling in OMDPs. These factors can be listed in five groups as detailed and elaborated by She et al. [48]: (1) operating conditions, (2) feed water characteristics, (3) DS composition, (4) membrane properties and (5) the orientation of the membrane. Inherent to low pressure OMDPs is the selection of the DS and the orientation of membrane, while the other factors also play pronounced roles in pressure-driven membrane processes [52,57].

2.2.2.1. Operating Conditions

The effects of adapting various hydrodynamic conditions have been studied and include: (1) operating at an increased cross-flow velocity (CFV), (2) utilising a spacer on the feed side of the membrane, (3) the induction of pulsated flow and (4) employing air scouring. The optimisation of these hydrodynamic conditions increases the turbulence on the membrane surface, thereby dislodging and removing the formed foulant cake-layer and may also be advantageous in alleviating the effects of ECP.

Various operating conditions such as spacer configurations and CFVs of the membrane system, dictate the membrane performance parameters such as water fluxes and recoveries attained. These performance parameters in turn influence if and to what extent fouling occurs within the system. She et al. [48] report that more severe fouling occurs at higher water fluxes and at lower CFVs. This statement was considered with due caution, as it is not clear whether the two factors were considered independently or jointly. Various studies have been conducted to assess fouling with a variety of feed waters containing macro-molecules, inorganic colloids, scalants and microorganisms [5,9,10,29,33,58]. From these studies it was consistently observed that high initial water fluxes exacerbate membrane fouling. This observation can be attributed to (1) larger water volumes

permeating the membrane, hence more foulant brought in contact with the membrane surface per unit time, (2) more severe CP and (3) increased hydrodynamic drag forces of the foulants towards the membrane surface. However, to study this statement and the validity thereof, the relationship between flux and CFV should be quantified.

To investigate the hydrodynamic drag forces toward the membrane, the intrinsic relationship between flux, recovery and inlet flow rate requires characterisation.

Standard operating conditions were deduced in a study by Cath et al. [23]. The modal CFV for FO operation, as per the findings in this study, is $25 \text{ cm}\cdot\text{s}^{-1}$, with CFV above this value being characterised as high, and below this value characterised as low. In FO applications, lower CFVs may result in higher CP effects [27]. Studies [59] suggested that operating at lower CFVs can minimise reverse solute leakage, however, water fluxes will be reduced, which will lead to an increase in ECP and hence, membrane fouling [27]. Furthermore, research studies by Cath et al., Loeb and McCutcheon et al. [59–61] found that ECP can be affected by both the flows of the FS as well as the DS, which result in maximum water fluxes attained when the CFVs of the FS and DS were the same, hence the system flow ratio was one. Other studies [27,62] found no change in water fluxes under different flow regimes.

Using a spacer to increase the turbulence on the membrane surface has proved to decrease ECP as well as external fouling. However, in a study conducted by Wang et al. [58] (in the presence of a spacer), it was found that the foulant particles had a strong tendency to preferentially deposit near the hydrodynamic dead zones [48,58], which are the spaces between the spacer filaments. The findings of this study were corroborated via optical coherence tomography as done by Goa et al. [63].

CFVs affects CP as well as the mass transfer occurring near the membrane surface. Various studies [11,35,64–66] have been conducted to study the influence of increased CFVs on minimising ECP when the system is operated in the AL-FS configuration. In membrane systems, scaling ions are transported towards the membrane due to the convective flow of water permeating through the membrane. Operating the system at increased CFVs, increases the hydrodynamic shear and turbulence at the membrane interfaces, sweeping the scaling ions back to the bulk solution [52]. It is, however, evident that for specific membrane systems, the effect of CFV on flux becomes negligible above a certain minimum CFV. Factors limiting this phenomenon are not discussed in the abovementioned study; therefore, it should be noted that increasing the hydrodynamic shear on the surface of the membrane only becomes evident at a certain CFV range. This range was defined to be the CFVs where the velocity of the bulk fluid is larger than the velocity of water permeating through the membrane.

The operating temperature of the FS and DS, respectively, also affects the intensity of fouling in the system. In a study conducted by Zhao et al. [13] it was observed that inorganic scaling became more severe when the working temperature of the brackish water desalination was increased. Typical operational temperatures that were investigated ranged from $25^\circ - 45^\circ\text{C}$. This observation was ascribed to the increased water permeation drag force at an increased initial water fluxes, as well as increased concentration factors (increased feed water recoveries).

CHAPTER 2: Literature Review

The operating temperature of the two solutions flowing adjacent to each other also have pronounced effects on the driving force of the FO process. An increase in the solution temperature increases the effective osmotic pressure of the solution, which could lead to an overall increase or an overall decrease in the effective driving force of the system. Various studies have investigated the effect that transmembrane temperature has on the effective driving force of the FO process [13,14]. It was observed throughout all the studies that the salt permeability increased with an increase in the operating temperature of the FO process. Figure 2-11 details the intrinsic relationship between the diffusion coefficient and the concentration of a sodium chloride solution at different temperatures.

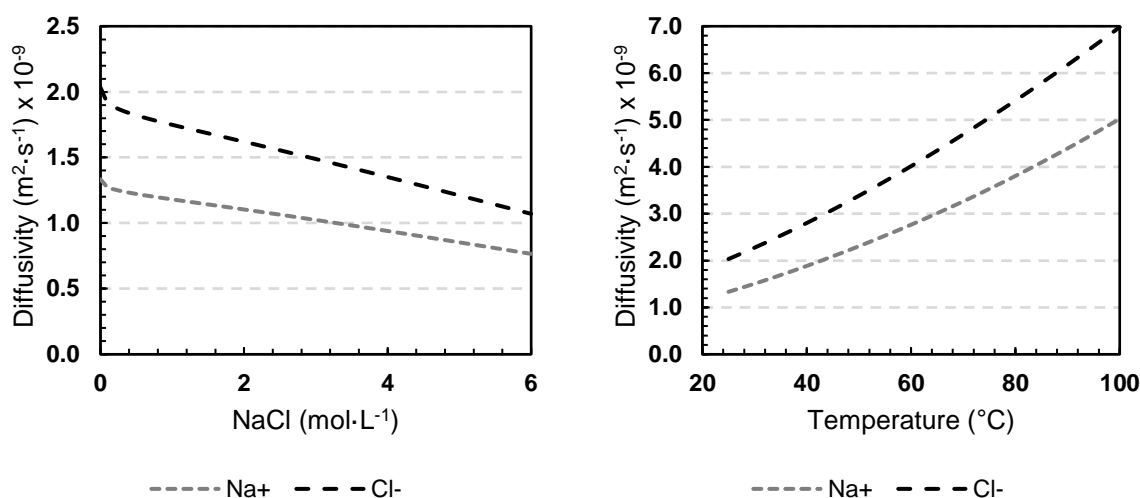


Figure 2-11. Variations in the diffusion coefficients of Na⁺ and Cl⁻ respectively for (a) variations in NaCl solution concentration and (b) the solution temperature. Modelled in *OLI Stream Analyser*.

Figure 2-11(a) demonstrates the variation in the diffusion coefficient of NaCl at various solute concentrations and (b) temperatures. The trends observed indicate that the diffusion coefficient of both Na⁺ and Cl⁻ vary significantly with temperature (a 74% increase in the diffusion coefficient of Na⁺ is observed when the temperature increases from 25°C to 100°C) and are not significantly influenced by the concentration of ions in solution (a decrease of 42% in the diffusion coefficient of Na⁺ when the solution concentration increases from 0.01 to 6 M). The membrane selectivity also has a pronounced effect on the passage of ions. The hydrophobicity or hydrophilicity of the membrane also influences salt passage.

2.2.2.2. Draw Solution Composition

The DS provides the osmotic driving force for the FO process. The choice of DS thus plays a cardinal role in the performance and the viability of the FO process. An ideal draw solution should, *inter alia*, have the following characteristics:

- (1) Generate high water flux
- (2) Low fouling potential
- (3) Low RSF
- (4) Low or no toxicity to microorganisms

(5) Low cost and ease of regeneration.

The fundamental criterion for selecting the applicable DS is that the osmotic pressure of the DS should be higher than that of the FS. These DSs include: (1) organic solutes, (2) inorganic salts, (3) thermolytic salts, (4) polyelectrolytes, (5) surfactants, (6) nanoparticles and (7) ionic liquids. Each of these draw solutes have inherent strengths and limitations, depending on the specific application.

In the development of FO technology, the selection of the appropriate and application-specific DS is considered a critical component. Two significant concerns associated with DSs are (1) the draw solute leakage to the feed water side in the FO process and (2) the intensive energy consumption associated with the regeneration of the draw solute [67]. Figure 2-12 visually presents the osmotic pressures which can be attained by different concentrations, ranging from 0.2 to 1.2 M, of inorganic draw solutes dissolved in a pure water solution at 25°C.

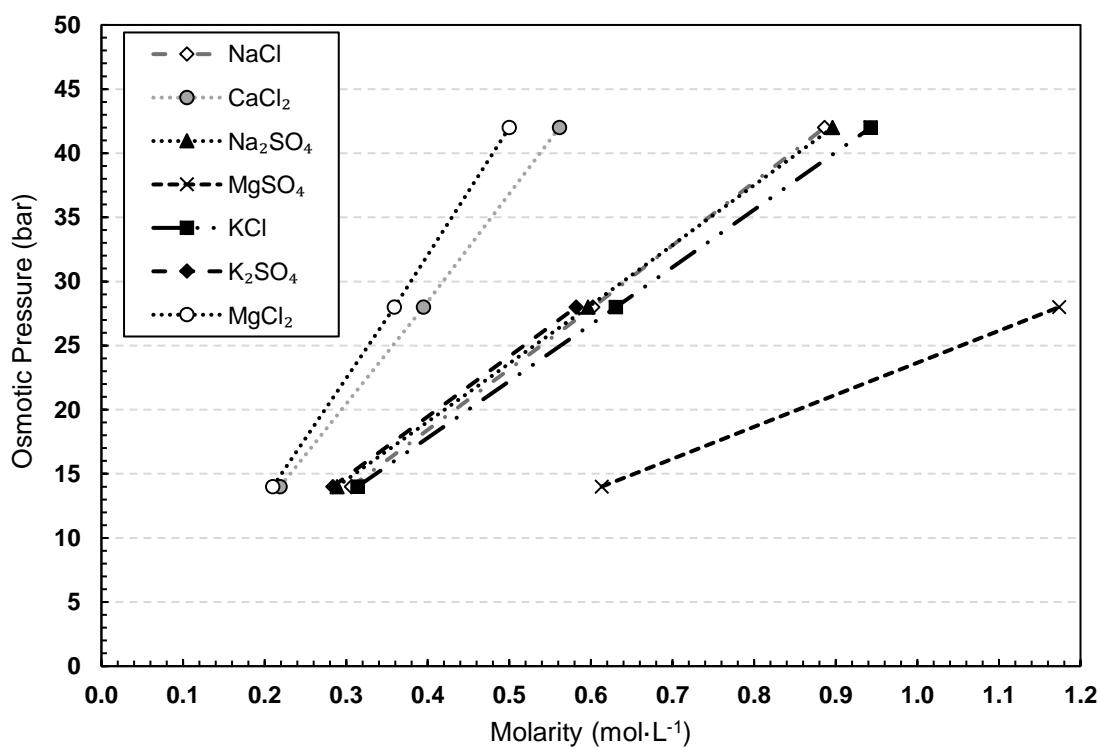


Figure 2-12. Osmotic pressures generated by the most common inorganic salts as draw solutes at various concentrations. MgCl₂ generates the highest osmotic pressure at low concentrations (mol·L⁻¹), with MgSO₄ generating the lowest osmotic pressure at higher solute concentrations (mol·L⁻¹) (data obtained from [17].)

It is evident from Figure 2-12 that MgCl₂ and CaCl₂ generate the highest osmotic pressure at low solute concentrations with the former generating the overall highest osmotic pressure. In the generation of a suitable osmotic pressure, the valence number of the cation and the specific anion it formed a bond with, play an intricate role.

CHAPTER 2: Literature Review

The use of monovalent and divalent cations as inorganic draw solutes also plays a pronounced role in that the membrane effectively rejects the diffusion of these solutes to the FSs. In general terms the diffusivity of ions through the membrane decreases with: (1) increasing molecular weight, (2) increasing ionic charge and (3) the hydrated radius of the ion [68]. The detrimental effects that ICP have on attaining sufficient water fluxes, are exacerbated when solutes with low diffusivities through the membrane are used. These ions include Mg^{2+} , Ca^{2+} , SO_4^{2-} and certain organic salts [16]. Typically, these solutes get entrapped in the SL of the membrane. Instead of diffusing through the membrane, the effects of ICP are increased.

The detrimental effects from RSF can be lowered by using inorganic DSs such as $MgCl_2$, $MgSO_4$ and trisodium citrate when compared to NaCl at the same osmotic pressures. This is attributed to the lower diffusivities through the membrane of divalent ions [16], as opposed to the slightly higher diffusivities observed when using only monovalent ions as solutes in the DS [17,26,69]. A trade-off then exists as to which transport phenomena will prevail – ICP or RSF.

The criteria for optimal DS selection have been discussed earlier; however, in light of the significant role that the ionic charge of the chosen solute play in the selection of the optimal DS, the criteria for optimum DS selection can be adapted as follows [16]:

- (1) Attain high water fluxes as induced by the monovalent NaCl; or
- (2) have low RSFs as observed with divalent inorganic and organic salts.

Various studies [6,16,26,45,70,71] have been conducted to investigate the use of a mixture of monovalent and divalent ions as draw solutes. The study conducted by Coday et al. [70] investigated the use of synthetic seawater containing low concentrations of divalent salts. Results indicate that the addition of low concentrations of divalent ions in the NaCl DS, reduced RSF by 55% and 22% for CTA and TFC membranes, respectively. The RSF of the chloride ions decreased by 25% and 27% when compared to a DS containing only NaCl. Interestingly, the initial fluxes observed in these studies utilising only NaCl as DS, yielded the same water fluxes [70].

The mechanisms associated with utilising mixed DSs containing mono and divalent ions were studied by Hancock et al. [26,45] and Phillip et al. [6]. These studies investigated the coupled transport of various ions across a FO membrane. Important findings of these studies demonstrated the following:

- (1) Negatively and positively charged ions diffuse through the membrane at equal molar rates in order to maintain electroneutrality within the system.
- (2) The driving force for ionic transport across the membrane is governed by solution diffusion mechanisms and not electrostatic interactions¹.

¹ Migration of ions from one side of the membrane to the other side of the membrane is dictated by diffusion only and not by the attractive and repulsive forces (Van der Waals forces) between the ions. Hence, the electrostatic interaction between the ions (i.e. interactions between the ions due to the charge) does not dictate the rate of diffusion.

- (3) The transport of oppositely charged ions is affected by the diffusivity and mobility of the counter ion. In essence the more diffusive chloride ion binds with the less diffusive sodium ion, and diffuse through the membrane to maintain electroneutrality.

When Mg^{2+} is in solution with Cl^- and Na^+ ions, the transport of Cl^- ions across the membranes are retarded due to the lower diffusivity of Mg^{2+} , compared to Cl^- and Na^+ [16]. Another study has shown that although Na^+ and Cl^- ions diffuse across the membrane, the transport of other ions (if present in the draw solution) of a certain charge is higher, due to the charged functional groups on the active side of the membrane. In conclusion, the study found that the RSF of cations increased with increasing membrane electronegativity [16,72]. Therefore, it is pertinent that the role of the membrane charge and surface chemistry can have a pronounced role in how the FO process operates. For a more comprehensive overview of the typical draw solutions utilised, the recovery methods and advantages and disadvantages of each, see Shon et al. [49]. A brief summary of DSs used along with the osmotic pressures generated and the fluxes attained are presented in Table 2-5.

Table 2-5. Various draw solutions solutes used in FO processes along with the osmotic pressure generated at the respective concentrations and typical fluxes attained. (Redrawn from [49]).

Draw Solute(s)	Concentration	Osmotic Pressure (atm)	Molecular Weight	Feed Solution	Water Flux ($L \cdot m^{-2} \cdot h^{-1}$)
NaCl	0.60 M	28	58.5 $g \cdot mol^{-1}$	DI Water	9.6
MgCl ₂	0.36 M	28	95 $g \cdot mol^{-1}$	DI Water	8.4
KCl	2 M	89.3	74.6 $g \cdot mol^{-1}$	DI Water	22.6
NH ₄ HCO ₃	0.67 M	28	79 $g \cdot mol^{-1}$	DI Water	7.3
Sucrose	1 M	26.7	324.3 $g \cdot mol^{-1}$	DI Water	12.9
PAA-Na 1200	0.72 g/mL	44	1200 Da	DI Water	22
PEG-(COOH) ₂ -MNPs 250	0.065 M	73	-	DI Water	13
1,2,3 - Trimethylimidazolium iodide	1 M	50	238 $g \cdot mol^{-1}$	DI Water	13
Sodium Formate	0.68 M	28	68 $g \cdot mol^{-1}$	DI Water	9.4
Polyglycol Copolymer	30 - 70%	40 - 95	>500 Da	3.5% NaCl	>= 4
Sodium hexa - carboxylatophenoxy phosphazene	0.067 M	-	1089 $g \cdot mol^{-1}$	DI Water	6

2.2.2.3. Membrane Properties

The two most common membrane materials used in the FO industry are CTA membranes and polyamide TFC membranes. Studies [35,73] have suggested that gypsum scaling in membranes are controlled by both surface/heterogeneous crystallisation, as well as the deposition of crystals that form in the bulk of the solution. In this study the impact of membrane materials on the scaling mechanism on FO systems will not be considered. It is, however, important and relevant to gain a

mechanistic understanding of how the membrane surface morphology affects surface crystallisation, and how the feed solution interacts with the AL and the SL of the membrane.

Membranes designed for OMDPs should: (1) reject dissolved solutes, (2) produce high permeate water fluxes, (3) be compatible with a variety of DSs and (4) be able to withstand the mechanical stresses generated by the array of system operating conditions [7]. The membrane morphologies of FO membranes are significantly different to the membranes utilised in RO applications. This is due to the fact that FO membranes do not have to withstand high hydraulic pressures. Hence, the SL in RO and FO membranes are different.

Xie et al. [73] characterised the membrane surface chemistry of typical CTA and TFC membranes used in FO operation. The difference in functional groups on the respective membrane surfaces indicated that there are differences in the membrane surface charges [73]. The surface charges of the membranes were determined by investigating the zeta potential of the respective membranes.

Zeta potential measurements indicated that the surface of a typical TFC membrane is more negatively charged than a CTA membrane at an operating pH of 6.8. The highly negatively charged surface of the TFC membrane can be attributed to the dissociation of free and uncross-linked carboxylic acid functional groups on the polyamide active skin layer of the membrane [73]. In contrast with this phenomenon, the predominant functional group on a CTA membrane is hydroxyl, which can only be deprotonated at a high pH. Previous investigations have shown that CTA membranes are only marginally negatively charged and that it can be attributed to preferential adsorptions of anions such as chloride and hydroxide on the membrane surface [74,75].

Xie et al. [73] reported that the presence of carboxylic groups on the membrane surface lead to calcium bridging between the membrane itself and other organic foulants, which consequently lead to the increase of organic fouling [73]. Limited investigations have been conducted to investigate the fouling behaviour of CTA and TFC FO membranes with different surface chemistries. More severe gypsum scaling was observed with the operation of a TFC membrane when compared to a CTA membrane [35,76], because of the stronger adhesion forces measured by atomic force measurement (AFM). In contrast to these findings, negligible differences in water fluxes were observed between a TFC and a CTA membrane during silica scaling. Hence, it can be concluded that the foulant and its interaction with the functional groups on the membrane surface plays a pronounced role in observed flux declines in FO systems. The adhesion force measurement via AFM showed stronger hydrogen bonding between silica and a CTA membrane, which is abundant with hydroxyl groups [76].

2.2.2.4. Membrane Orientation

The orientation in which the membrane is operated affects the performance of a FO membrane. The influence of membrane orientation is through the combined effects of surface properties, hydrodynamic conditions and CP. Various research groups have documented that the membrane is less prone to fouling when operated with the AL facing the feed solution (AL-FS) [1,5,58,77–79]. This observation was attributed to the following reasons [48]:

- (1) the active layer has a smoother surface, which reduces the possibility of foulant deposition;
- (2) there is no cross flow within the support layer. This reduces the acceleration of foulant deposition within the support layer;
- (3) foulants cannot be retained in the active layer, hence the foulant retention and entrapment within the support layer is reduced; and
- (4) ICP is reduced and pore clogging is eliminated.

It is unclear from the publications whether DS ion retainment within the support layer was considered by conducting system mass balances. Researchers have also observed that CECP in the membrane system, when operated in AL-FS orientation, is more reversible by surface flushing while DICP in the membrane system, when operated in AL-DS, exhibited a lower cleaning efficiency [2,11,76,80,81].

Interestingly enough, despite the enhanced flux recovery after fouling and reduced fouling tendency that the membrane exhibits when operated in AL-FS, the ICP occurring in this orientation in the SL from the DS ions, are so pronounced that a lower initial flux is achieved when compared to the AL-DS orientation [4,5,25]. Unfortunately, from the publications it is unclear whether a system mass balance was conducted, thus this phenomenon should be considered with due caution. For increased FS osmotic pressures (increased concentrations) the effects and driving force differences brought about by ICP becomes marginally small and the fluxes in both configurations converge [1,3,82–85].

2.2.2.5. Feed Water Scaling Potential

The extent and the rate of fouling is strongly dependent on the type, properties and the concentrations of the foulants in the feed water. The feed water chemistry such as the ionic strength, pH and the divalent ionic concentration, also play a pronounced role in the fouling behaviour of the membrane. This is because the feed water chemistry can influence the physiochemical properties of the foulants as well as the foulant-foulant interactions and the foulant-membrane interactions [48].

Scaling is caused by the precipitation of salts in the feed water on the surface of the membrane. In theory, as pure water permeates through the membrane to dilute the DS, the concentration of the salt ions in the feed water increases. The end/last part of the membrane will then be affected the most adversely by the high concentration feed water, and it will essentially be scaled to the greatest extent. This is because the salt ions in the feed water reach their solubility limit and the feed water becomes supersaturated. Salt then precipitates on the membrane surface to form scale. The tendency of a particular feed water to scale a membrane, can be predetermined by analysing the feed water, and by determining the expected brine-concentration factor over the length of the membrane module, at the predetermined recovery. The crystallisation process of calcium containing minerals is qualitatively detailed in Figure 2-13.

The salts that most commonly form scale on the membrane surface are (1) calcium carbonate, (2) calcium sulphate, (3) silica complexes, (4) barium sulphates, (5) strontium sulphates and (6) calcium

CHAPTER 2: Literature Review

fluorides [34]. Studies [35,73,86] have demonstrated the significant impact of membrane surface topology and chemistry on the mechanism of surface crystallisation.

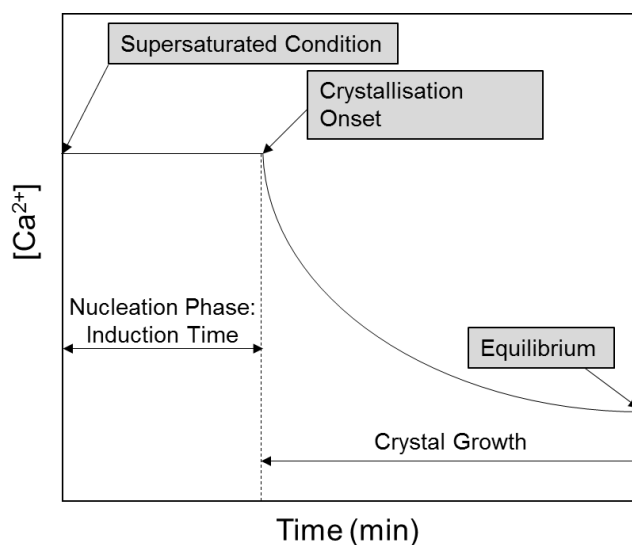


Figure 2-13. The process of crystallisation of calcium containing minerals [87].

The magnitude of industrial effluent streams contains high concentrations of calcium and sulphate, thereby giving rise to inevitable gypsum scaling when the water is treated via membrane processes. The solubility of gypsum is not sensitive to pH adjustments which further complicates the management of gypsum scaling.

Factors such as the solution temperature along with the presence of sodium chloride in the system affects the solubility of gypsum in a solution. The solubility concentration of gypsum at 25°C and at equimolar concentrations of Ca^{2+} and SO_4^{2-} is $0.015 \text{ mol}\cdot\text{L}^{-1}$. This translates to a Ca^{2+} concentration of $627 \text{ mg}\cdot\text{L}^{-1}$ and a SO_4^{2-} concentration of $1503 \text{ mg}\cdot\text{L}^{-1}$. The variability of gypsum solubility with temperature is detailed in Figure 2-14.

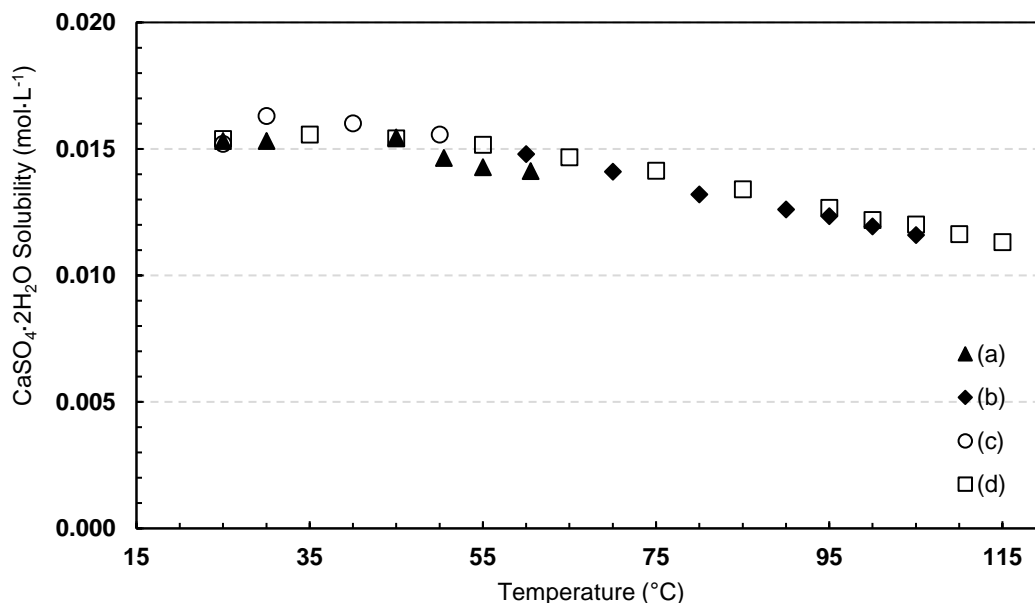


Figure 2-14. Variability of gypsum solubility at various operating temperatures where the solubility of gypsum decreases with an increase in temperature. (a) [88]; (b) [89]; (c) [90]; (d) [91].

In a study conducted by Rahman [92] the induction times of various concentrations of calcium sulphate solutions were monitored. A RO reject brine stream attained at a recovery of 70%, contained 866 mg·L⁻¹ TDS Ca²⁺ ions and 2100 mg·L⁻¹ TDS SO₄²⁻. This translated to a molarity of 0.022 mol·L⁻¹ of Ca²⁺ indicating that gypsum was 1.4 times above its saturation limits. Calcium chloride and sodium sulphate solutions were mixed to prepare various calcium sulphate solutions. The induction times of the various solutions were then monitored via conductivity measurements. These results are listed in Table 2-6 along with typical induction times for gypsum at a lower range of supersaturation.

Table 2-6. Typical Ca²⁺ and SO₄²⁻ concentrations and corresponding induction times for crystal formations.

CaSO ₄ ·2H ₂ O Supersaturation	[Ca ²⁺] mg·L ⁻¹	[SO ₄ ²⁻] mg·L ⁻¹	Induction Time (min)	Initial Conductivity (mS·cm ⁻¹)	Final Conductivity (mS·cm ⁻¹)	Reference
1	627	1503				[93]
1.4*	866	2100				[92]
2	1254	3006	106			[93]
3	1881	4510	25			[93]
4	2509	6013	7			[93]
4.2*	2598	6300	19	13.3	12	[92]
5.6*	3464	8400	3	16.8	14.6	[92]
7*	4330	10500	2	19	16.5	[92]
8.4*	5196	12600	1	21.5	18.5	[92]

*SO₄²⁻ in excess

As reported in Table 2-6, in some studies the ratio of Ca²⁺ ions to SO₄²⁻ ions are not equimolar. Excess SO₄²⁻ concentrations can impact the induction times. In a study conducted by Abdel-Aal et al. [94]

CHAPTER 2: Literature Review

gypsum crystallisation experiments were conducted at increasing excess (free) SO_4^{2-} concentrations. It was observed that the induction time for gypsum crystallisation decreased significantly. The results from these experiments are documented in Table 2-7. It was reported that a higher supersaturation ratio translated to higher concentrations of Ca^{2+} ions to SO_4^{2-} ions in solution. The shortened distance separating these ions caused higher inter-ionic attractions which enhanced the formation of gypsum crystals. This rendered the induction time to be shorter [94].

Table 2-7. The effect of excess (free) sulphate concentrations on the induction time of gypsum crystallisation at different supersaturation ratios. (Redrawn from [94]).

$\text{CaSO}_4 \cdot 2\text{H}_2\text{O}$ Supersaturation	Excess (Free) Sulphate (%)	Induction Time (min)
1.301	1.5	66.7
1.301	2.5	45.0
1.301	3.5	13.3
1.880	1.5	11.7
1.880	2.5	3.6
1.880	3.5	1.5

2.3. Physical Fouling Control Measures

A thorough understanding of the roots and causes of membrane fouling, as detailed in Section 2.2, is especially useful for developing and implementing the applicable fouling control measures. In this section, various fouling control strategies will be discussed. This section is divided into two sub-sections addressing, firstly, how to remove fouling and clean the membrane system and, secondly, implementing strategies to ensure that membrane fouling is reduced in the longer term.

Physical cleaning methods have been extensively studied for OMDPs, the main reason being the non-invasiveness with which the restoration of fluxes can be attained [2,20,21,27,28,80,95], as opposed to chemical cleaning. Two physical cleaning methods mainly employed in OMDPs are (1) membrane flushing and (2) osmotic backwashing [2,80]. Membrane surface flushing with deionised water relies on the enhanced shear force (enhanced CFVs) along the membrane surface, to remove the deposited foulant layer [48,57]. Osmotic backwashing entails reversing the direction of water permeation and using the permeation drag force to remove and detach the external foulant layer from the membrane surface.

2.3.1. Membrane Flushing

In a study conducted by Mi et al. [80] a systematic investigation was conducted to evaluate the effectiveness of membrane surface flushing based on the recovery of water flux. It was observed that membrane fouling was more reversible via membrane surface flushing in FO systems compared to RO systems. This is attributed to the absence of high external hydraulic pressures that contributes to compaction of the external fouling layer [80]. Flux recoveries as high as 98% from the original fluxes were attained, by employing membrane surface flushing at high CFVs and for extended cleaning durations [48].

Despite the high cleaning efficiencies observed for membrane surface flushing, this physical cleaning method requires that some of the product water be used (i.e. clean water) for flushing, which reduces the actual water recoveries [48]. When the system is operated in AL-DS mode the shear force via enhanced cross flow may diminish due to the SL. It was proposed and investigated that osmotic backwashing is an effective alternative to physically clean the support layer of the membrane [2,55].

2.3.2. Osmotic Backwashing

Backwashing is a common principle employed in membrane systems. Hydraulic backwashing has mainly been employed in processes such as microfiltration (MF) and ultrafiltration (UF), but not to processes such as nanofiltration (NF) and RO, as these processes have asymmetric membrane structures with very small pores [7]. However, in FO systems, osmotic backwashing yielded promising results for the removal of foulants in the porous support layer of the membrane². The principle of

² Hydraulic backwashing can be advantageous when osmotic backwashing cannot work well enough [48]. However, it should be noted that typical FO membranes are not fabricated with the thick support layers of its counterparts in the RO industry, hence FO membranes cannot withstand excessive hydraulic pressures.

CHAPTER 2: Literature Review

osmotic backwashing in FO processes involves the instantaneous switch of the permeate direction [7]. The principle of osmotic backwashing is visually shown in Figure 2-15.

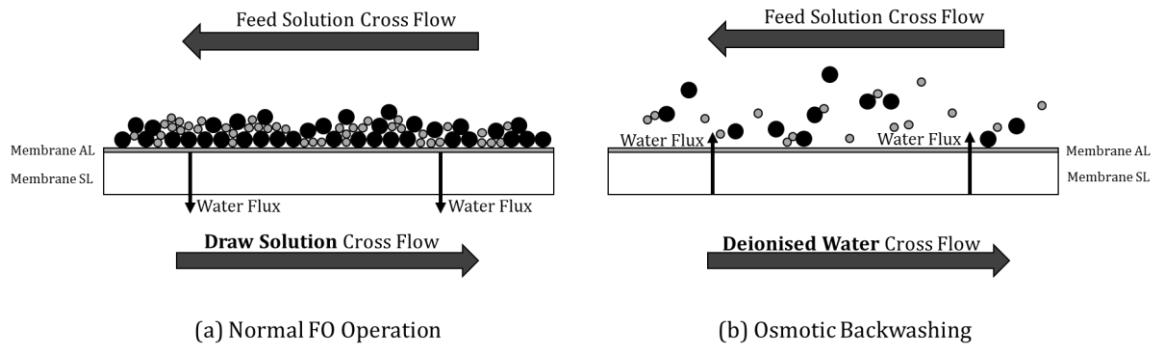


Figure 2-15. Osmotic backwashing principle: (A) normal forward osmosis operation (permeate flows from feed side to draw solution side) and (B) osmotic backwashing (permeate from draw side to feed side (redrawn from [21])).

In a study conducted by Kim et al. [21] the principle of osmotic backwashing was employed for a time interval of 30 minutes, as per Figure 2-15. In Figure 2-15(a) the permeate flows from the feed side of the membrane, through the semipermeable membrane, to the DS side of the membrane. Foulants in the FS are deposited on the membrane surface [21]. As the FO operation continues, the DS is diluted which decreases the osmotic pressure across the membrane and ultimately decreases the operational driving force. A decrease in the operational driving force leads to a decrease in the permeate flux, due to the increase in the hydraulic pressure and the decrease in the effective osmotic pressure across the semipermeable membrane [21].

In Figure 2-15(b) the principle of osmotic backwashing employed for membrane cleaning is depicted. During the process of osmotic backwashing, the DS is replaced with deionised water. When the deionised water flows opposite to the original feed solution, an osmotic pressure gradient is formed in the opposite direction, which causes the permeate to flow from the deionised water to the FS. This causes the foulant layer on the membrane surface of the feed side to possibly detach from the opposite permeate flow and is consequently removed from the membrane surface by the CFV [21].

In the osmotic backwashing investigation by Kim, Lee & Hong [21] it was found that the effectiveness of osmotic backwashing is highly dependent on the type of foulant present in the feed water solution. Two types of foulants were investigated: (1) organic foulants (alginate and humic acids) and (2) inorganic foulants (i.e. SiO_2 particles). Osmotic backwashing was able to restore some of the flux effectively, however, flux recovery was never completely restored [21]. The study conducted was done under extreme fouling conditions, as the feed solution contained an above average foulant concentration. The study concluded that osmotic backwashing as a membrane cleaning strategy could be a promising method to clean fouled membranes [21]. It was also concluded that the efficiency of the osmotic backwashing can be increased by carefully optimising the duration and the interval [21].

A brief summary of the main results found in this study are detailed in Table 2-8.

Table 2-8. Characteristics of membrane fouling in terms of foulant type, membrane orientation and backwashing efficiency [21].

Foulants	Foulant Characteristic	Membrane Orientation	Flux Declines Observed	Backwashing Efficiency	Cause
Alginate	Hydrophilic	AL-FS	Mild	High	Less chemically interacted
		AL-DS	Mild	High	Less chemically interacted
Humic Acid	Hydrophobic	AL-FS	Mild	Low	Chemically interacted
		AL-DS	Severe	Low	Chemically interacted, attachment to pore inside
Silica	20 nm	AL-FS	Mild	Low	Shear force
		AL-DS	Severe	Medium	Entrapped inside pore
	100 nm	AL-FS	Severe	Medium	A-CEOP: Small diffusion coefficient
		AL-DS	Severe	Medium	A-CEOP: Small diffusion coefficient

A similar and more recent study was conducted by Blandin et al. [28]. After significant flux decreases were observed, high CFV osmotic backwashing was employed as a cleaning strategy for the membrane. This study also investigated the impact of the osmotic backwashing duration as well as employing osmotic backwashing at high CFVs. It was found that the foulant cake was only partially removed by employing osmotic backwashing at high CFVs.

Employing osmotic backwashing for a duration of 15 minutes showed promising results to address hydraulic enhanced fouling, when compared to only employing high CFVs for membrane cleaning. However, only using backwashing for membrane cleaning is not sufficient to remove the foulant cake layer occurring in FO operation at high permeation fluxes [28]. As such, it was demonstrated that the foulant cake layer is more difficult to remove when FO is operated under high permeation flux. Therefore, an extended osmotic backwashing period of 1 hour was allowed, which resulted in 85% of the original flux being recovered. It was also found that full flux recovery could be attained if the osmotic backwashing was implemented at high CFVs [28].

This indicated that intensive cleaning is required since only the combination of long-term reverse flux (osmotic backwashing) and hydrodynamic shear (increased CFVs) allowed the separation of the

CHAPTER 2: Literature Review

foulant cake layer from the membrane surface [28]. It can be concluded from this study that operating the cleaning of osmotic backwashing at high CFVs, is more efficient than the consecutive two-step osmotic backwashing protocol: (1) implementing osmotic backwashing and (2) only after implementing high CFVs. This is because the external foulant layer is simultaneously loosened from the membrane surface, due to the (1) reverse flux and (2) the dislodging of the foulant layer because of the high CFV [28]. Table 2-9 summarises studies conducted to investigate the effects of increased CFV as a membrane-cleaning method.

Table 2-9. The effects of increasing the cross-flow velocity on mitigating fouling in various studies.

Foulants	Solution pH	CFV (cm·s ⁻¹)	Duration	Cleaning Efficiency	Reference
Seawater prefiltered by a 10 mm capsule filter	8.2	4.2–16.7	Fouling run	Flux decline reduced	[66]
1 g/L of 139 nm silica	4 and 9	8.5–25.6	Not reported	Fully reversible, up to 80% flux restoration	[96]
75 mg/L of algininate SRNOM and BSA	6.5–7.5 feed, and 7.5–8.5 draw solution	10.7–32.1	Fouling run	Flux decline reduced	[96]
200 mg/L alginate + 0.5 mM CaCl ₂	5.8	8.5–21	15 minutes	Fully reversible	[80]
Gypsum Scaling	7.5	8.5–21 with air bubbles	20 minutes	Fully reversible	[12]
Combined gypsum-alginate scaling ³	7.5	8.5–21 with air bubbles	20 minutes	75% reversible	[12]

On the other end of the spectrum, Vallandares Linares et al. [97] studied the effectiveness of osmotic backwashing which provided conflicting results with regards to other research groups. The research conducted was on the cleaning efficiency of several methods to remove natural organic matter (NOM): fouling from the AL of a FO membrane that was submerged in municipal secondary wastewater effluents. The hypotheses presented for the ineffective osmotic backwashing were: (1) the replacement of the FS and the DS with 4% NaCl and deionised water, may have caused an interaction with the salt in the cleaning solution with the foulants, which could have enhanced membrane pore

³ Although a gypsum scaling reversal of approximately 75% was quantified, it was unclear if the authors estimated the reversal based on the baseline flux before scaling ions were introduced in the feed water, or the flux before any scaling took place. This has implications for the driving force of the process, which affects the original flux and hence the extent of flux recovery of the system.

blockage, and (2) the accumulation of salts in the fouling layer reduced the effective osmotic pressure-gradient across the membrane, thus the driving force was reduced, causing a decline in the water flux.

From the above studies, as well as those summarised in Table 2-9, it is evident that there are no hard or fast rule as to when increased hydrodynamic shear conditions will effectively restore the system flux – rather its efficiency is dependent on the types of foulants in the feed water.

2.4. Literature Review Summary

A systematic hydraulic study was conducted to evaluate the specific aspects that may influence the operation of varying the CFV and the operating configuration. These parameters were evaluated by monitoring performance indicators which include water flux, water recovery, solute rejections and RSF, all of which can be affected by the CFV and the operational configuration. Key points drawn from the above literature review are summarised below:

(1) Fundamental Principles of FO

- The driving force of a typical FO process is mainly quantified via the osmotic pressure differential across the membrane which can be calculated using the established Van't Hoff Equation. Mainly two factors influence the driving force of an FO process: (1) the solute concentration in either solution and (2) the solution temperature.
- Solute-solute interactions on either side of the membrane can be quantified via (1) quantification of the diffusion coefficient or (2) measuring the solution conductivity.
- Conductivity measurements can cause discrepancies in the quantification of solute mobility across the membrane of up to 30%. This was deemed to be a relative error in the estimation of RSF and evaluating the membrane rejection.
- Two transport phenomena are inevitable for FO processes: CP and RSD. Both inherently act as fouling promoters within the system.
- The CP moduli is a mathematical quantification tool that is typically used for evaluating the effects of CP.
- The contribution of the convective flow within the system can be quantified via the Peclet number, whereby the contribution of RSF within the system can be quantified.

(2) Fouling in FO

- Fouling can be characterised as internal or external fouling and may increase the hydraulic resistance, which leads to the induction of fouling-enhanced CP and can ultimately alter the rejection property of the membrane.

Factors affecting fouling in FO systems include: (1) the operating conditions, (2) the DS composition, (3) membrane properties, (4) membrane orientation and (5) the feed water chemistry. Limited and contradictory results were obtained for the operating CFV and the membrane orientation. Conflicting results regarding the effect of CFV on the attained fluxes revealed, that clarification and accurate characterisation of the hydrodynamic effects of CFVs on the system required investigation.

- There is an intrinsic relationship between flux, recovery and CFV velocity in FO systems which can be directly translated to the extent of fouling in the system, and hence the extent to which fouling control strategies can be employed in membrane systems.

- Generally, the membrane is less prone to fouling when operated in the AL-FS configuration. This is attributed to the smoother surface and absence of a porous support layer which reduces foulant retention and no CICP.
- However, lower initial fluxes are delivered when operating in the AL-FS configuration as opposed to the AL-DS configuration due to DICP.

Factors such as the effects regarding operating temperature, spacer inclusion, and DS composition have been studied extensively. The following findings are relevant to this study:

- Operating at an increased temperature provides the advantage of a higher solution osmotic pressure; however, the diffusion coefficients of the solutes also increase, thereby increasing the RSF occurring in the system. Optimum temperatures are 20°–25°C for comparative reasons for literature results.
- Spacer inclusion increases the hydrodynamic shear on the membrane surface; however, the dead zones in between the spacer filaments act as seeding points for membrane scaling. Commercial FO membranes are fabricated with the inclusion of a spacer on the FS and DS sides; therefore, it should be included in investigations which aim to be extrapolated to pilot and industrial scale plants.
- The most commonly used DS solutes are NaCl and MgCl₂. The osmotic pressure of a MgCl₂ solution is significantly higher than that of NaCl. However, NaCl is commonly employed for its cost-effectiveness and its higher diffusivity and viscosity, thereby decreasing the detrimental effects of ECP, but increasing the RSF in the system. NaCl does not comprise scaling promoting ions, thereby making it more advantageous and decreasing the detrimental effects of RSF. Typical fluxes attained for various DS solutes are detailed in Table 2-12.

(3) Fouling Control Measures

Mainly two physical cleaning methods/fouling control methods are implemented in FO systems. Osmotic backwashing proved to be more effective when compared to system flushing in terms of (1) flux recovery and (2) alleviating ICP within the support layer. Reversing the direction of water permeation when employing osmotic backwashing is generally achieved by replacing the DS with deionised water. However, the same principle can be employed when continuously switching the FS and DS with respect to the membrane orientation, thereby operating in the AL-FS configuration and then employing osmotic backwashing by operating in the AL-DS configuration.

(4) Standard Operating Conditions

Literature revealed that a host of setups testing various membranes are utilised, each operating at various operating conditions. The various operating conditions tested are listed in Table 2-10. Typically, the most commonly used draw solute is NaCl at a concentration of 0.5 to 1.5 M. Typical operating temperatures vary between 20°– 25°C. Deionised water is the most commonly used feed water for membrane standardisation.

CHAPTER 2: Literature Review

Table 2-10. Standardisation test conditions reported in recent publications pertaining to FO (adapted from [23]).

Draw Solution Solute	Draw Solution Concentration	Feed Water	Operating Temperature	Reference
NaCl	1.5 M	Deionised Water	23±1	[98]
NaCl	0.5–5 M	Deionised Water	22±0.5	[99]
NaCl	0.5–1 M	NaCl (10 – 80 mM)	25	[85]
NaCl	0.5	Deionised Water	23	[100]
MgCl ₂	0.5–3.5M	Deionised Water	23	[101]
NaCl	0.5, 2 M	100 ppm NaCl	23	[102]
MgCl ₂	0.5–4 M	Deionised Water	23	[103]
MgSO ₄	150 g/L	35 g/L NaCl	20	[104]
NaCl	3 M	Deionised Water	20	[105]
NaCl	1–2.5 M	Deionised Water/3.5% NaCl	22±0.5	[106]
NaCl	0.5,2 M	100 ppm NaCl	23	[107]
MgCl ₂	0.5–3 M	Deionised Water/10 mM NaCl	23	[108]
NaCl	1.5 M	Deionised Water	25±0.5	[7]
NH ₄ HCO ₃	1.5 M	Deionised Water	25±0.5	[7]
MgCl ₂	5 M	Deionised Water	23	[109]
NaCl	0.5 M	Deionised Water	25	[110]

In order to compare the operability of various setups and membranes, standard protocols need to be followed. In a study conducted by Cath et al. [23] a standard methodology was developed for the testing of ODMPs. The base case conditions determined by this study are presented in Table 2-11.

Table 2-11. Standard operating conditions for the testing of FO membrane in the AL-FS and AL-DS configurations [23].

Experimental Condition	UOM	Value	Notes
FS and DS Temperature	°C	20	
DS Concentration	M	1	58.44 g·L ⁻¹ NaCl
FS Concentration	M	0	Deionised Water
FS and DS pH	-	Unadjusted	As close to neutral as possible
FS and DS CFV	cm·s ⁻¹	25	No spacer inclusion and co-current flow
FS and DS Pressures	bar	<0.2	Keep as low as possible and similar on both sides of the membrane

The experimental conditions for typical gypsum scaling experiments are detailed in Table 2-13. A variety of DSs were used along with varying CFVs. Some experiments were also conducted in the AL-DS configuration as opposed to the standard AL-FS configuration. This translated to variant degrees of flux declines, due to the varying extents of gypsum scaling in the system.

Table 2-12. Flux performances and corresponding operating conditions of some of the most common draw solutes utilised (redrawn from [49]).

Draw Solute(s)	Concentration	Osmotic Pressure (atm)	Molecular Weight	Feed Solution	Water Flux (L·m ⁻² ·h ⁻¹)
NaCl	0.60 M	28	58.5 g·mol ⁻¹	DI Water	9.6
MgCl ₂	0.36 M	28	95 g·mol ⁻¹	DI Water	8.4
KCl	2 M	89.3	74.6 g·mol ⁻¹	DI Water	22.6
NH ₄ HCO ₃	0.67 M	28	79 g·mol ⁻¹	DI Water	7.3
Sucrose	1 M	26.7	324.3 g·mol ⁻¹	DI Water	12.9
PAA-Na 1200	0.72 g·mL ⁻¹	44	1200 Da	DI Water	22
PEG-(COOH) ₂ -MNPs 250	0.065 M	73	None	DI Water	13
1,2,3 - Trimethylimidazolium iodide	1 M	50	238 g·mol ⁻¹	DI Water	13
Sodium Formate	0.68 M	28	68 g·mol ⁻¹	DI Water	9.4
Polyglycol Copolymer	30 - 70%	40 - 95	>500 Da	3.5% NaCl	>= 4
Sodium hexa - carboxylatophenoxy phosphazene	0.067 M	None	1089 g·mol ⁻¹	DI Water	6

CHAPTER 2: Literature Review

Table 2-13. Experimental conditions and performances of typical gypsum scaling experimental runs for TFC-FO membranes.

Research Group	Operational Mode	Supersaturation	Feed Composition			Draw Solution Concentration (M)	Experimental Duration (h)	Cross-Flow Velocity (cm·s ⁻¹)	Initial Water Flux (L·m ⁻² ·h ⁻¹)	Flux Decline (%)	Reference
			Na ₂ SO ₄ (mM)	NaCl (mM)	CaCl ₂ (mM)						
Xie & Gray (2016)	AL-FS	1.3	20	19	35	NaCl (2.5 M)	25	8.5	25	65%	[73]
Mi & Elimelech (2010)	AL-FS	1.3	20	19	35	NaCl (4 M)	25–35	8.5	7	85%	[80]
Mi & Elimelech (2010)	AL-DS	1.3	20	19	35	NaCl (4 M)	25–35	8.5	28	82%	[80]
Wang et al. (2016)	AL-DS	1.4	21.6	10	72	NaCl (0.5 M)	2	9	16	±10%	[51]
Liu & Mi (2012)	AL-FS	1.3	20	20	35	NaCl (4 M)	50	21	17	80%	[12]
	AL-DS	Baseline	0	163	0	NaCl (2 M)	8	7	15	-	
Zhang et al. (2014)	AL-DS	0.8	37.9	68	13.7	NaCl (2 M)	8	7	15	20%	
	AL-DS	1.5	57.6	30	20.9	NaCl (2 M)	8	7	15	40%	[33]
	AL-DS	2	72	26.1	10	NaCl (2 M)	8	7	15	53%	
	AL-DS	2.3	73.2	0	28.7	NaCl (2 M)	8	7	15	50%	

Chapter 3

Laboratory-Scale Setup Design

In order to improve the efficiency of industrial plants, the finer mechanical and process aspects need to be fully understood. On a bench-scale level, it is of importance that the fundamental hydrodynamic principles of FO be well understood, as well as how various mechanical parameters can influence the efficient operation of a FO membrane. In this study a bench-scale FO system was designed and constructed. The primary aims of this chapter then were to (1) define the design problem by identifying the design requirements, (2) give a detailed description of the design and (3) evaluate the design requirements as defined by the design problem.

3.1. Problem Definition

In this section the construction of a FO membrane system is elaborated on. This is done by defining the problem scope and identifying the design requirements to provide a sensible solution.

3.1.1. Problem Scope

The treatment of high TDS brine streams has become increasingly challenging, due to the lack of effective and environmental-friendly disposal techniques. As such, ZLD processes have gained much attention, due to the minimisation of liquid waste streams. FO is a technology which finds application in ZLD processes, because it can treat waters with highly concentrated waste streams at low hydraulic pressures. However, due to the high TDS values of the streams requiring treatment, fouling is said to be a major hindrance further in the development of FO membrane-based processes. As such, the underlying mass transport phenomena exacerbating membrane fouling, is still not well understood and requires investigation to propose appropriate cleaning strategies.

3.1.2. Technical Review

Disposal of brine streams is highly significant both from an economical and environmental viewpoint. Improper surface disposal to groundwater sources could have far-reaching consequences for downstream processing units. The pollution of groundwater sources partly stems from the introduction of a highly saline stream, along with harmful chemicals [111]. Typical brine disposal methods include: (1) pumping into specially designed evaporation ponds (2) deep well injection, (3) disposal into surface water bodies, (4) disposal into pipelines of municipal sewers and (5) secondary treatment [111].

CHAPTER 3: Laboratory-Scale Setup Design

Over the past 40 years FO has been proposed by researchers as an effective method for desalinating water and to reduce the waste concentrate produced by desalination plants [112]. In an investigation by Tang and Ng [113] a water recovery of 38.5% was achieved by treating feed water similar in concentration to brine streams (1 to 2 M or 58.5 to 117 g·L⁻¹ TDS). Water extraction from the DS was achieved by implementing a RO system at a recovery of 45%, which resulted in an overall system recovery of *ca* 66% to 76%. It was however reported that mineral scaling deposits were found on the inner wall of the FO membrane cell, which indicated the presence of scaling within the system. A flux decline of 8.2 L·m⁻²·h⁻¹ to 6.9 L·m⁻²·h⁻¹ was reported over a period of 18 hours.

A similar study was conducted by Martinetti et al., where overall water recoveries of as high as 90% were achieved [114]. It was however reported, that the system was severely limited by salt precipitation on the membrane surface which was reduced by the addition of scale inhibitors. These studies indicated that FO is effective in treating highly saline streams and achieving high overall system recoveries when combining an FO and a RO system. It is also clear that fouling on the membrane surface limits the efficient operation of the system. Furthermore, the development and implementation of an online physical cleaning method would greatly assist in prolonging operational times between CIPs, when the system would be required to go offline.

3.1.3. Design Requirements

Taken into account the above background, and in conjunction with the findings from the literature study, the following design requirements for the bench-scale setup were identified:

- Achieve CFVs of 9 to 35 cm·s⁻¹;
- Measure the respective inlet flow rates of the FS and the DS accurately and continuously, along with the respective outlet flow rates, without having to stop the operation;
- Automate the flow configuration of the system by intermittently changing from the AL-FS configuration to the AL-DS configuration;
- Purge the system from residual solutions before continuing normal operation after switching the operating configuration;
- Maintain constant temperature control;
- Maintain a flux range of 5 - 20 L·m⁻²·h⁻¹ at a median CFV of 19 cm·s⁻¹ in the normal AL-FS configuration, without the presence of scaling ions in the FS;
- Finally, based on the design of the housing blocks, attain a median recovery of 20% according to the above operating conditions.

3.2. Design Description

In this section, a technical breakdown of the design will be given. An overview of the bench-scale setup along with the design bases are given. Following the overview, is a technical breakdown of the main design parts of the bench-scale setup. Finally, the operation of the designed setup is described.

3.2.1. Overview

The proposed solution seeks to develop an efficient and non-invasive physical cleaning method to minimise membrane fouling, which is still a hindrance in the further development of FO processes. The proposed cleaning method entails the intermittent flow reversal, hence intermittently switching from the AL-FS configuration to the AL-DS configuration. As a result, the direction of water permeation is reversed, thereby dislodging external foulants from the membrane surface.

System operational downtime can significantly contribute to operational costs. To minimise system downtime, requires the implementation of this cleaning strategy to be integrated and automated with the system. For example: When severe flux declines are observed in the AL-FS configuration, the system should, via instruction, automatically switch to the AL-DS configuration for a said period of time, to dislodge the external foulant layer and restore the operational flux without going offline. However, when switching between configurations, each channel needs to be flushed to remove residual solution. Most importantly is that the solutions exiting the system during the flushing cycle, should not be pumped to the exiting tanks, but rather to the waste tanks. Additionally, the user must be able to evaluate membrane performance indicators (water flux and recovery along with solute rejection) continuously, to be able to investigate the effectiveness of switching the operational configuration online, on an intermittent basis.

3.2.1.1. Process Design

The design bases were based on the (1) desirable water flux and (2) the membrane dimensions. As such, a flux of $20 \text{ L}\cdot\text{m}^{-2}\cdot\text{h}^{-1}$ and membrane dimensions of $280 \times 80 \text{ mm}$ were used to design the system, and with a channel width of 0.25 mm . The inlet flow conditions to the membrane train was manipulated to achieve an overall recovery of 20% at a CFV of $19 \text{ cm}\cdot\text{s}^{-1}$. The design was done for both channels, taking into account that the CFV will decrease on the FS side and increase on the DS side, due to the water mass transfer over the membrane.

The process design is detailed in Table 3-1 and Table 3-2. A once-through system was designed, hence without DS recycle. This was done to mitigate cross-contamination of solutes via RSF. The system was designed for six membrane housing blocks, each with a dimension of $280 \times 80 \times 0.25 \text{ mm}$ and hence an overall membrane active area of 1344 cm^2 . Six housing blocks were used to attain a water recovery of 20% in the system. By using the design bases, the area of the membrane was maximised to achieve an overall recovery of 20% at a CFV of $19 \pm 2 \text{ cm}\cdot\text{s}^{-1}$, as is evident from the design.

In Section 2.1.1.2 the differences along with the advantages of operation in counter-current as opposed to co-current mode, were explored. To ensure that a significant driving force is maintained

CHAPTER 3: Laboratory-Scale Setup Design

over the membrane train, it was decided to design a counter-current system with a flow ratio of 1, regarding the inlet FS flow rate and the inlet flow rate of the DS.

Another important design manipulated variable was the flow factor (FF) achieved. The FF was defined as the ratio between the outlet flow rate of the membrane system and the flux flow rate through the membrane. It was indicated in the Literature Review (Section 2.2.2.1) that the detrimental effects of CP are minimised when the FF is sufficiently high (i.e. >1) compared to the CFV. Hence, there is an optimum ratio between the flux velocity and the CFV, where CP is minimised. This exact ratio is yet to be determined.

The FS channel was designed for a FF of ~4 and the DS channel for ~9. As water permeates along the membrane flow path, the outlet flow rate of the DS will increase. Subsequently, the outlet flow rate of the FS will decrease. This results in the CFV changing along the membrane flow path. This influences the FF of the system as the FF is also dependent on the CFV of the system. That is why the system was designed according to an overestimation of 400% for the FF, to ensure that at lower and higher CFVs the effects of CP would still be minimised.

3.2.1.2. Process Description

The designed process is illustrated in Figure 3-1 with a process flow diagram (PFD). A counter-currently operated FO process was designed with the inclusion of automating the switch from the AL-FS operational configuration to the AL-DS operational configuration, and *vice versa*. TK - 102, equipped with a heater and a thermostat, is filled with the respective feed solution. The feed solution is then pumped through a strainer with a peristaltic pump to the inlet of the FO membrane train. The feed flow rate is measured with the inline inlet flow meter (FM - 102) and checked with a rotameter (F - 102) before entering the FO process train.

TK - 101, also equipped with a heater and a thermostat, is filled with the DS at the applicable concentration. The DS is filtered through a carbon-filter as well as a 10 µm cartridge-filter. The DS flow rate is measured by the inline flow meter (FM - 101) and checked with a rotameter (F - 101).

The electrical panel is equipped with a Phoenix Nanoline Programmable Logic Computer (PLC). Once the AL-FS configuration is selected and the timer has been actuated, the solenoid valves will be actuated or impeded accordingly. For the AL-FS configuration the DS will enter the FO train (FO - 106) by VA - 106 and exit the process train (FO - 101) by VA - 101. Counter-currently to the DS, the FS will enter the FO train (FO - 101) by VA-104, and exit the FO train (FO - 106) by VA - 107. For the AL-DS configuration the DS will enter the FO train (FO - 106) by VA - 108, and exit the FO train (FO - 101) by VA-103. Counter-currently, the FS will enter the FO process train (FO - 101) by VA - 102, and exit the FO train (FO - 106) by VA - 105. The PLC is programmed for the duration of each configuration to be manipulated, along with the flushing time between configurations.

The outlet flow rate of the DS is measured by FM - 104. When the system is operated in the flushing cycle, the outlet solution will be pumped to TK - 105, conversely, when in operation, the DS will be

pumped to the outlet tank TK – 106. The same holds true for the FS where the outlet FS flow rate is measured via FM – 103. Residual solution is pumped to TK – 103 when operating in the flushing mode, and TK – 104 when in operation.

CHAPTER 3: Laboratory-Scale Setup Design

Table 3-1. Membrane housing block design for the feed channel.

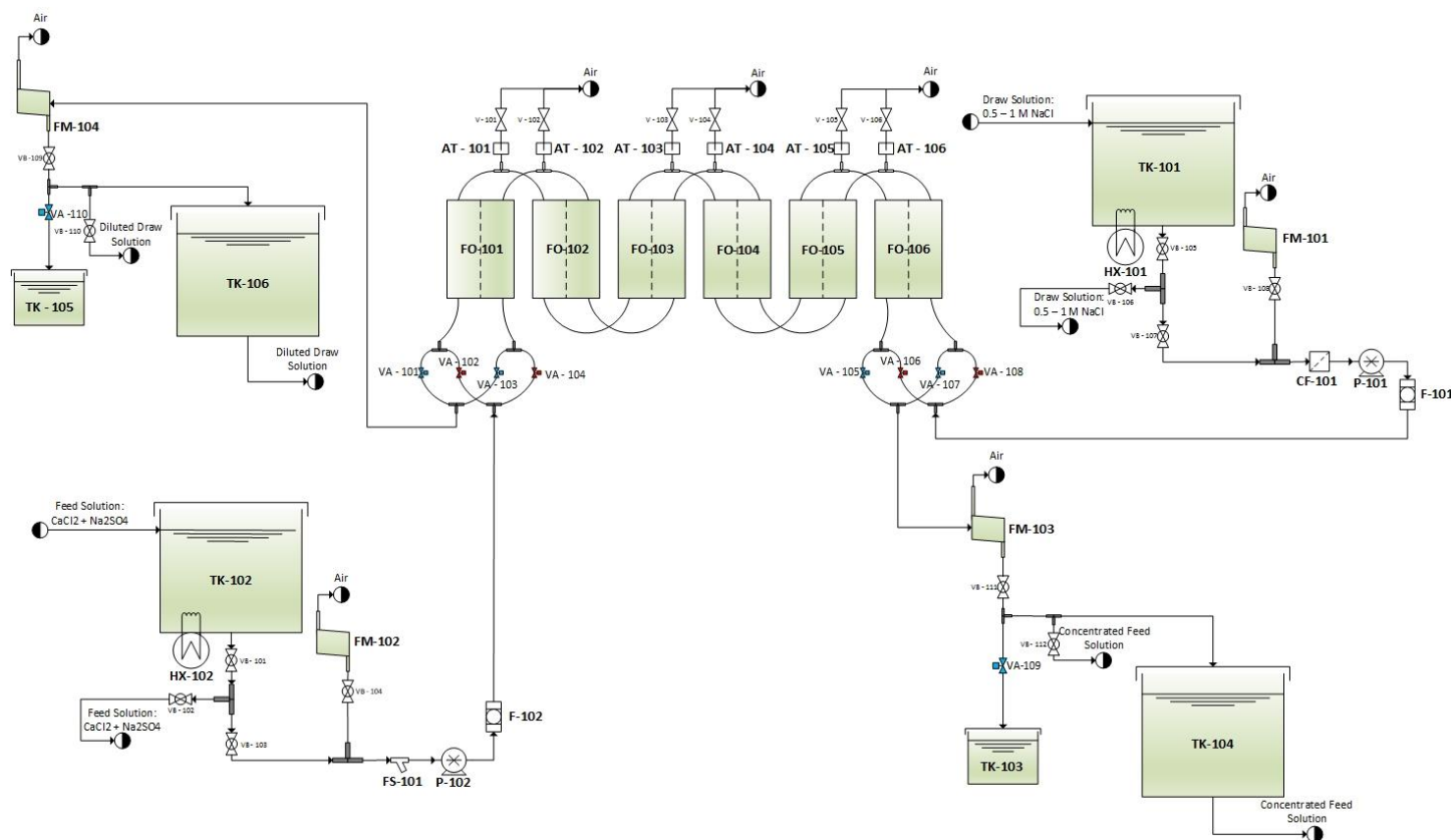
		Feed Solution						COMPLETE SYSTEM
Fixed Variables		Block 1	Block 2	Block 3	Block 4	Block 5	Block 6	
Entry Flow (F_i)	$L \cdot \text{min}^{-1}$	0.210	0.202	0.194	0.187	0.179	0.172	0.210^a
Flux	$L \cdot \text{m}^{-2} \cdot \text{h}^{-1}$	21.25	20.75	20.25	19.75	19.25	18.75	20.00^b
Membrane Block Dimensions								
Length	cm	28.00	28.00	28.00	28.00	28.00	28.00	168.00^c
Width	cm	8.00	8.00	8.00	8.00	8.00	8.00	8.00
Depth	cm	0.025	0.025	0.025	0.025	0.025	0.025	0.025
Manipulated Variables								
Membrane Active Area	cm^2	224.00	224.00	224.00	224.00	224.00	224.00	1344.00^d
Spacer Volume/Channel Volume		0.15	0.15	0.15	0.15	0.15	0.15	
Spacer Porosity		0.85	0.85	0.85	0.85	0.85	0.85	
Membrane Cross Sectional Area	cm^2	0.17	0.17	0.17	0.17	0.17	0.17	
Flux Flow	$L \cdot \text{min}^{-1}$	0.01	0.01	0.01	0.01	0.01	0.01	0.04^e
Outlet Flow (F_o)	$L \cdot \text{min}^{-1}$	0.20	0.19	0.19	0.18	0.17	0.17	0.17
Recovery Over Block	%	3.78	3.83	3.89	3.95	4.01	4.07	23.52^f
Entry Cross-Flow Velocity to Block 1	$\text{cm} \cdot \text{s}^{-1}$	20.42	19.65	18.90	18.16	17.45	16.75	20.42
Outlet Cross-Flow Velocity from Block 6	$\text{cm} \cdot \text{s}^{-1}$	19.65	18.90	18.16	17.45	16.75	16.07	16.07
Flow Factor: Outlet Flow/Flux Flow	Ratio	25.47	25.08	24.70	24.33	23.96	23.60	3.69

^aEntry flow to housing block 1.^bAverage flux over six housing blocks^cSum of lengths of six housing blocks^dSum of total membrane area (complete system)^e $20 L \cdot \text{m}^{-2} \cdot \text{h}^{-1} \times 0.1344 \text{ m}^2 \div 60 \text{ min} = 0.04 L \cdot \text{min}^{-1}$ ^fSum of recovery over individual housing blocks

Table 3-2. Membrane housing block design for the DS channel.

		Draw Solution						COMPLETE SYSTEM
Fixed Variables		Block 1	Block 2	Block 3	Block 4	Block 5	Block 6	
DS Concentration: Molarity	mol·L ⁻¹	0.5						
Entry Flow (D _i)	L·min ⁻¹	0.210	0.218	0.226	0.233	0.241	0.248	0.210
Manipulated Variables								
Osmotic Pressure DS	bar	27						
Membrane Active Area	cm ²	224.00	224.00	224.00	224.00	224.00	224.00	1344.00
Spacer Volume/Channel Volume		0.15	0.15	0.15	0.15	0.15	0.15	
Spacer Porosity		0.85	0.85	0.85	0.85	0.85	0.85	
Membrane Cross Sectional Area	cm ²	0.17	0.17	0.17	0.17	0.17	0.17	
Flux Flow	L·min ⁻¹	0.01	0.01	0.01	0.01	0.01	0.01	0.04
Outlet Flow (D _o)	L·min ⁻¹	0.22	0.23	0.23	0.24	0.25	0.41	0.41
Entry Cross-Flow Velocity to Block 1	cm·s ⁻¹	20.42	21.20	21.95	22.69	23.40	24.10	20.42
Outlet Cross-Flow Velocity from Block 6	cm·s ⁻¹	21.20	21.95	22.69	23.40	24.10	24.78	24.78
Flow Factor: Outlet Flow/Flux Flow	Ratio	27.47	29.13	30.85	32.63	34.48	59.00	9.22

CHAPTER 3: Laboratory-Scale Setup Design



FM-104	TK-105	TK-106	TK-102	HX-102	FM-102	FS-101	P-102	F-102	FO-101	FO-102	FO-103	FO-104	FO-105	FO-106
Manual Flow Meter Column	Flush Tank	Spent Draw Solution Reservoir	Feed Solution Inlet Tank	Feed Solution Submersible Tank Heater	Manual Flow Meter Column	Feed Inlet Strainer	Feed Inlet Positive Displacement Pump	Feed Inlet Rotameter	FO Cell 1	FO Cell 2	FO Cell 3	FO Cell 4	FO Cell 5	FO Cell 6
AT-101	AT-102	AT-103	AT-104	AT-105	AT-106	FM-103	TK-103	TK-101	HX-101	TK-104	FM-101	CF-101	P-101	F-101
Air Trap	Air Trap	Air Trap	Air Trap	Air Trap	Air Trap	Manual Flow Meter Column	Flush Tank	Draw Solution Inlet Tank	Draw Solution Submersible Tank Heater	Spent Feed Solution Reservoir	Manual Flow Meter Column	Carbon Filter	Draw Solution Inlet Positive Displacement Pump	Draw Solution Inlet Rotameter

Figure 3-1. Process Flow Diagram (PFD) of the designed and built setup.

3.2.2. Detailed Description

The bench-scale setup comprised sub-design components which were arranged in three categories: (1) mechanical design, (2) electronic design and (3) process design. The sub-design components and the subsequent category to which it belongs are detailed in Figure 3-2. The mechanical design was finalised first, the electronic PLC programming and testing followed, and finally the setup was evaluated, based on the process design requirements identified and defined.

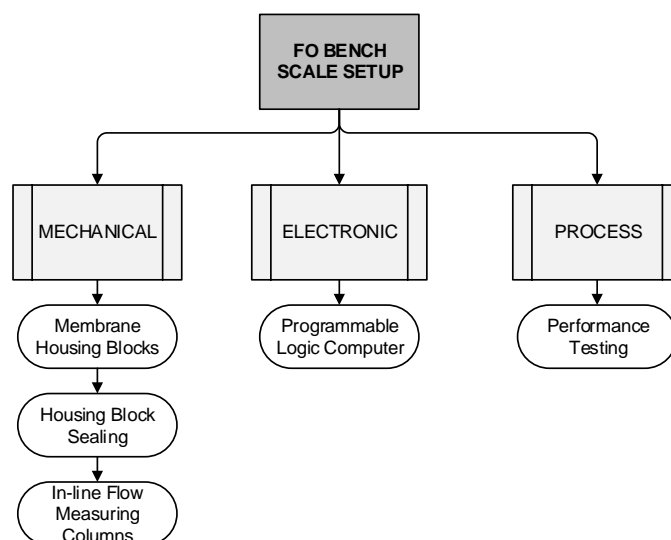


Figure 3-2. Categorisation of sub-design components of the FO bench-scale setup.

3.2.2.1. Membrane Housing

The membrane housing design was finalised first. The design and construction of the six housing blocks comprised part of the mechanical design of the system. Polyvinyl chloride (PVC) was used as the material of construction for the housing blocks. Perspex sight glasses were installed in order to view the membrane whilst the system was in operation. The housing blocks along with the internal components are detailed in Figure 3-3. The dimensions of the housing blocks were 340 mm × 140 mm × 25 mm, to fit a membrane coupon with the dimensions of 300 mm × 100 mm with an active area of 280 mm × 80 mm. The 40 mm loss in the membrane area was to ensure sealing of the gasket and to prohibit fluid leaking from one channel to the other around the membrane. The housing blocks along with the internal components were screwed together with 8 mm screws and torqued to 20 N·m to ensure that membrane deformation will not occur and to ensure uniformity throughout. A detailed line drawing of the housing block design features in Appendix A.3 along with the hydraulic characterisation in Appendix A.2.

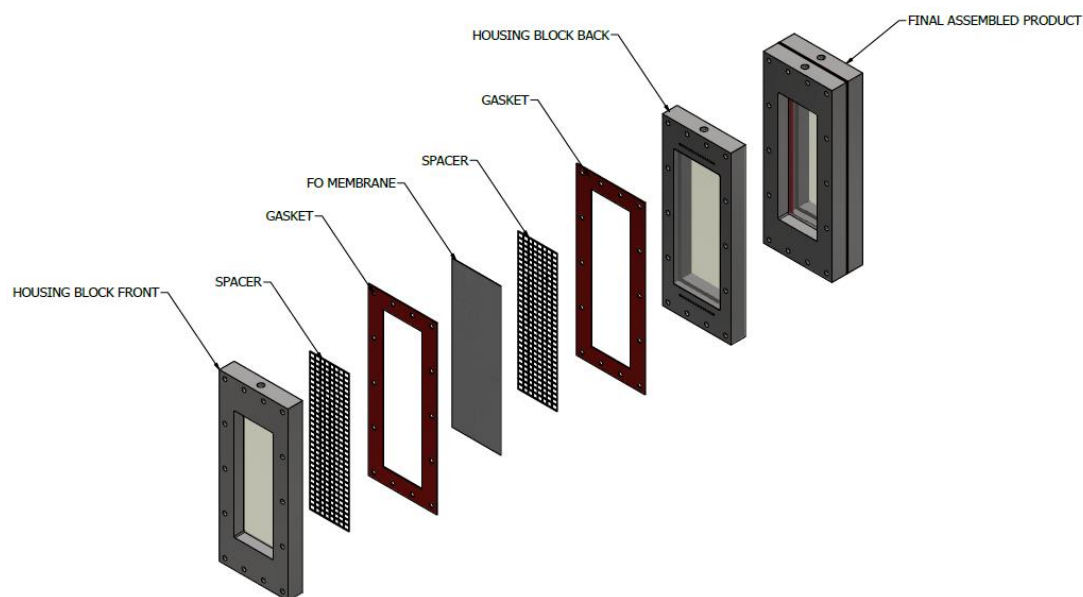


Figure 3-3. Membrane housing and internal component assembly.

3.2.2.2. Sealing

As detailed in Figure 3-3, the housing blocks were assembled with gaskets as the sealing mechanism. Mainly two options for the sealing of the housing blocks were investigated: (1) O-ring sealing and (2) gasket sealing. The sealing mechanism typically used in FO setups is two O-rings pinched on-top of each other, preventing water from leaking from the membrane housing. However, after a prolonged period of operation, it was found that the O-ring pinched and damaged the membrane itself. The extent of the damage caused to the membrane could not be quantified; however, it was observed that solute rejections decreased dramatically (20% in a 30-minute operational period) the more the O-ring pinched and punctured the corners of the membrane.

To ensure sealing of the membrane housing, two blocks were screwed together with 8 mm screws. These screws were tightened with a torque wrench at exactly the same torque, to ensure that the membrane does not tear or fold between the housing blocks. It was decided rather to use a 1.5 mm thick silicone rubber gasket on either side of the membrane to seal the housing blocks.

3.2.2.3. In-line Flow Measuring Columns

One of the key design requirements is the continuous and in-line measurements of the respective flow rates in and out of the FO membrane train. The objective of these in-line measuring columns was to measure the respective flow rates in and out of the FO process train, while the system is in operation and to ensure that measurements are taken accurately. The columns were designed to accurately measure flow rates in the range from 97 to 382 mL·min⁻¹.

The measurement device detailed in Figure 3-4 was developed and constructed to measure the respective inlet and outlet flow rates of the FS and the DS. Subsequent line drawings along with visual 3D drawings of the measuring columns are presented in Figure 3-4.

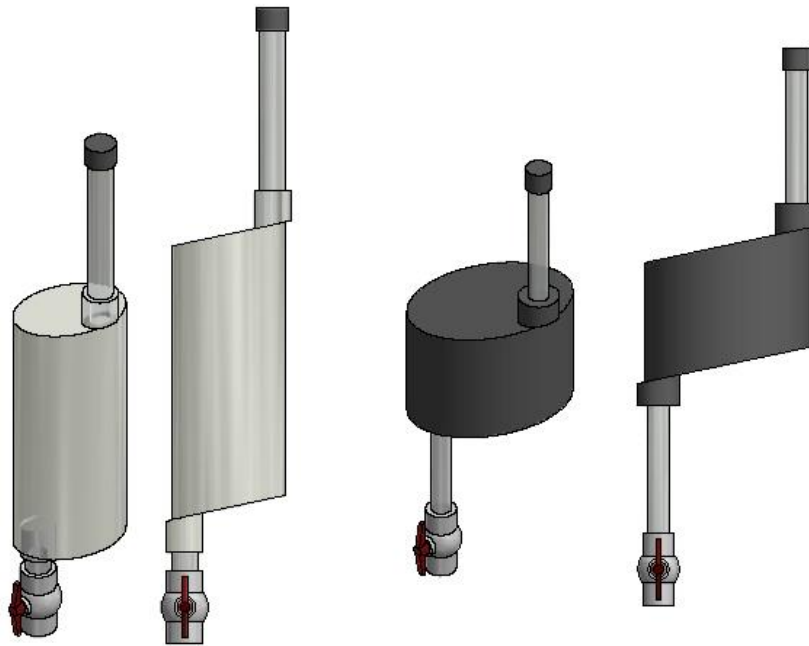


Figure 3-4. Schematic diagram of the flowrate measurement column used to measure the inlet and the outlet flowrates continuously. The outlet flow meters are on the left and the inlet flow meters are on the right. For dimensions see Appendix A.1.

The column on the left was the outlet measuring columns, which were used to measure the outlet flow rates by filling the column with the respective solution to a predetermined volume, whilst measuring the time with a stopwatch. The columns on the right were used to measure the feed flow rate by filling the column with a predetermined volume of feed water, whilst noting the time it takes for the column to run empty. The flow meter was designed in terms of (1) hold-up volume, (2) fluid-rise rate and (3) the diameter of the calibrated tube, where readings will be taken from. The design detail of these columns in terms of dimensions can be viewed in Appendix A.1. These columns were placed before the suction side of the pump, thereby indicating the specific inlet flow rate per pump. The following design notes are related to the flow meters:

- The top and bottom parts of the meters were designed with an angle of 12° to ensure no liquid hold-up inside the column and no entrapped air (which may vary between readings) at the top of the column.
- Manual ball valves were installed at the bottom of the respective meter columns, in order to take periodic measurements on a manual basis.
- The adhesion forces for water droplets on the sides of the columns were minimal, due to the chosen material of construction – Perspex for the outlet columns and PVC for the inlet columns.

CHAPTER 3: Laboratory-Scale Setup Design

The calibrated volume, as well as the measurement error associated with each reading taken, are presented in Table 3-3. The error incorporates (1) the personal bias when activating the stopwatch, (2) reading errors associated with the meniscus and (3) variations in the flow rate which will cause the columns to fill up or run dry at different rates.

Table 3-3. Volume and errors associated with each designed flow measurement column.

Parameter	UOM	Inlet Columns		Outlet Columns	
		Feed Solution	Draw Solution	Feed Solution	Draw Solution
Volume	mL	1 854	1 888	2 035	2 300
Error	mL	0.330	1.220	0.647	0.830
Error Percentage	%	0.02	0.06	0.03	0.04

3.2.2.4. Programmable Logic Computer (PLC) Programme

In order to investigate the operational configuration of the membrane by switching the flow paths of the FS and the DS, a PLC was programmed to actuate and impede 220V solenoid valves. Hence, the system operates in two configurations. The basic control philosophy followed in programming the PLC is detailed in Figure 3-5. All the solenoid valves installed in the setup are normally closed.

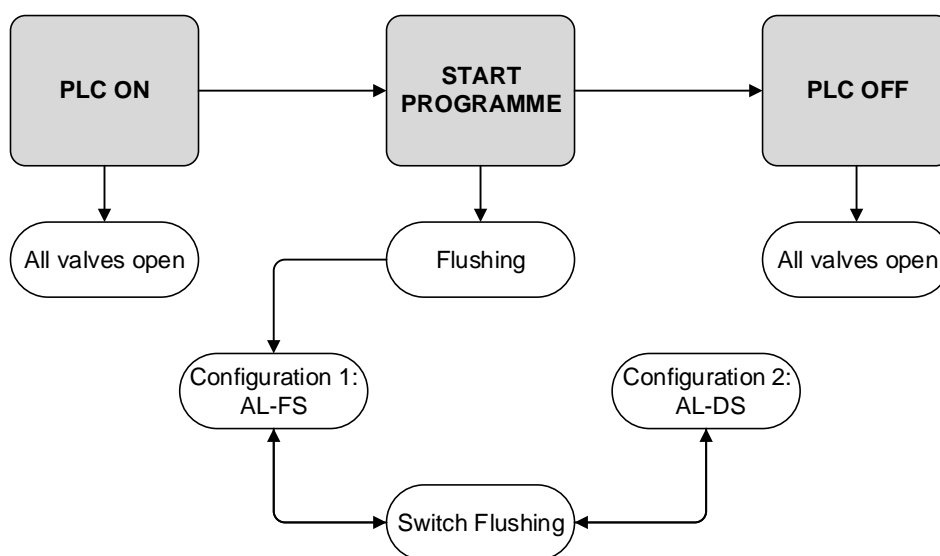


Figure 3-5. PLC programme operation.

The detailed control philosophy along with the valve sequencing are detailed in Table 3-4. The typical operational times and the timer set points are highlighted, along with the valve sequence for each operational mode.

Table 3-4. Valve sequencing, operating times and set points for each operational mode. (X = closed, O = open).

Step	Mode	Typical Operating Time	Set Point	Valve Tag Numbers									
				VA - 101	VA - 102	VA - 103	VA - 104	VA - 105	VA - 106	VA - 107	VA - 108	VA - 109	VA - 110
A	PLC - Switched On	-	-	0	0	0	0	0	0	0	0	0	0
B	Valve Transition Switch	5 seconds	5 sec	X - O	O - X	O - X	X - O	O - X	X - O	X - O	X - O	O - X	O
	Flushing: Configuration 2 - 1	0 - 15 min	15 min	0	X	X	0	X	0	0	X	0	0
C	Valve Transition Configuration 1: AL-FS	5 seconds	5 sec	0	X	X	0	X	0	0	X	O - X	O - X
		0 - ∞	4 h	0	X	X	0	X	0	0	X	X	X
D	Valve Transition Switch	5 seconds	5 sec	O - X	X - O	X - O	O - X	X - O	O - X	O - X	X - O	X - O	X - O
	Flushing: Configuration 1 - 2	0 - 15 min	15 min	X	0	0	X	0	X	X	0	0	0
E	Valve Transition Configuration 2: AL-DS	5 seconds	5 sec	X	0	0	X	0	X	X	0	O - X	O - X
		0 - ∞	4 h	X	0	0	X	0	X	X	0	X	X

As is detailed in Table 3-4, all the solenoid valves are actuated when the setup is switched on. The control philosophy begins with a flushing cycle whereby the solutions from the housing blocks are discarded, to ensure that all residue solutions are purged from the system. Following the flushing cycle is the normal operation in the AL-FS operational mode, termed Configuration 1. Another flushing cycle is actuated when the timer of Configuration 1 has run out. The AL-DS operational (termed Configuration 2) mode is then actuated, followed by the initial flushing cycle when the Configuration 2 timer has run out. When the PLC is switched off and the programme is stopped, all of the valves are actuated to be open. Only after the power supply to the setup electrical box is cut, will the valves close. This was done to prevent pressure build-up in the system as the pumps are positive displacement pumps. Pressure build-up in the system will subsequently cause pipe leakages at connection points in the system. Details pertaining to each operation will be elaborated on below.

3.2.3. Operation

The basic setup operation is detailed below.

3.2.3.1. Configuration 1 (Active Layer - Feed Solution)

In Configuration 1 the AL of the FO membrane faces the FS, with the DS flowing counter-currently on the support side of the membrane. The start-up procedure starts by pumping the FS and DS to the FO process train via Configuration 1. The inlet flow rates are measured via FM - 101 and FM - 102. This

CHAPTER 3: Laboratory-Scale Setup Design

is done by filling the column to the predetermined volume and recording the time it takes for the column to be pumped empty.

A strainer is installed after the flow meter on the FS side, to remove any larger agglomerates which may have been present in the feed tank. The feed solution enters the FO process train via VA – 102. After the inlet flow rate measurement of the DS, the solution passes through a 10 μ m cartridge filter as well as a carbon filter, and enters the FO process train via VA – 108. Two mercury manometers are installed before the inlet points, on either side of the FO train, to record the inlet pressure to the process. The two solutions flow counter-currently to each other, through six membrane housing units. Where a solution flows upward in the membrane block, air traps are installed (AT-101 – 106) to reduce air accumulation within the blocks, as well as on the membrane surface. The FS exits the FO process train via VA – 105 and the draw solution exits via VA – 103.

Before the FS and the DS reach TK – 104 and TK – 106, the flowrate is measured via FM – 103 and FM – 104. The ball valve attached at the bottom (VB – 109 and VB – 111) is closed. The time it takes for each solution to reach a predetermined volume in the tubes in FM – 103 and FM – 104, is recorded manually. Once the volume/time measurement is made, the FS and DS continuously flow to TK – 104 and TK – 106, respectively.

3.2.3.2. Flushing

Before operating in Configuration 2 mode, the residual FS and DS still present in the FO process train are flushed. This is done by switching the flow of the FS and the DS. Thus, the residual FS is evidently flushed from the system with the DS, and the residual DS is flushed with the FS. Residual solutions are pumped to TK – 103 and TK – 105, respectively, by actuating VA – 109 and VA – 110. The flushing time as well as the operational time per configuration is a system variable. The FS outlet conductivity was measured continuously to determine when residual solutions were purged from the system and normal operation was achieved.

3.2.3.3. Configuration 2 (Active Layer – Draw Solution)

Once all of the residual solutions in the FO process train is displaced to TK – 103 and TK – 105, normal operation in Configuration 2 mode can commence via the same operation as Configuration 1. Configuration 2 follows a similar process flow than Configuration 1, with the main variable being the direction of water permeation. The FS enters the FO process train via VA – 104 and the DS enters via VA – 106.

Before the FS and the DS reach TK – 104 and TK – 106, the flowrate/flux is measured via FM – 103 and FM – 104. The ball valve attached at the bottom (VB – 109 and VB – 111) is closed. The time it takes for each solution to reach a predetermined volume in the tubes in FM – 103 and FM – 104, is recorded manually. Once the volume/time measurement is made, the FS and DS continuously flow to TK – 104 and TK – 106 via VA – 109 and VA – 110, respectively. When switching from Configuration 1 to

Configuration 2, the respective residual solutions must once again be displaced by the opposite solution to the residual flushing tanks (TK - 103 and TK - 105).

3.3. Evaluation

The designed bench-scale setup was evaluated based on an experimental basis. In the overview of this subsection, the most important parameters influencing the design on a process and mechanical basis are highlighted. Furthermore, the relationship between these variables and the effects these variables have on the process performance indicators such as water flux, water recovery, and solute rejections, are highlighted.

3.3.1. Overview

The basic definitions for evaluating the system performance indicators are detailed in Chapter 2. The mechanical design of the housing blocks along with the flow rates attained in the system, influence the performance indicators. To date no projection software have been developed to predict the performance of FO membranes. Therefore, to evaluate the system performance accurately, mathematical expressions were developed to define the relationship between the system performance indicators and the designed mechanical parameters along with the process parameters.

3.3.1.1. Primary Mechanical Parameters

The hydrodynamic advantages of the addition of a spacer in the flow channels were listed in Section 2.2.2.1. Mainly, the inclusion of a spacer in the respective channels enhances the hydrodynamic turbulence on the membrane surface, thereby alleviating the effects of CP, especially ECP. Addition of the spacer is thus inherent to the membrane housing regarding whether additional membrane support is required or not.

The porosity of channel spacers in FO systems influences the hydrodynamics of the operability of FO membranes. There are mainly three techniques with which the volume and hence the porosity of spacers can be quantified. These techniques are: (1) volume displacement, (2) weight and density and (3) computed tomography. The filament thickness and width of the spacer can be quantified by means of stereomicroscopic images. The number of filament strands can be counted by using this same technique. Detailed methods of spacer volume quantification are listed in [101].

In a study conducted by Siddiqui et al. [115], deviation in the estimations of the spacer porosity of up to 6% related to miscalculations of the CFV of up to 6.4%, and 43% for the channel pressure drop. Therefore, to accurately quantify the effects of hydrodynamic changes the system has for the performance parameters, certain mechanical aspects such as the spacer geometry needs to be accurately quantified. The equations governing the spacer porosity and the channel CFV are given in Equation (3.1) and (3.2) respectively [115].

$$\emptyset = 1 - \frac{V_{spacer}}{V_{channel}} = 1 - \frac{V_{spacer}}{w_{ch} \times h_{ch} \times l_{ch}} \quad (3.1)$$

V_{spacer} and $V_{channel}$ is the volume of the spacer and the flow channel, respectively. The flow channel volume is calculated via the channel width (w), height (h) and length (l). For this system a spacer

porosity of 0.85 was assumed [115]. Quantifying the channel porosity via the addition of the spacer, directly influences CFV, as per Equation (3.2).

$$CFV = \frac{Q_F}{A} = \frac{Q_F}{w_{ch} \times h_{ch} \times \emptyset} \quad (3.2)$$

CFV is the cross-flow velocity and Q_F is the feed flow rate to the flow channel. From Equation (3.1) and (3.2) it is clear that (1) the porosity of spacer-filled channels is dependent on the designed channel dimensions and (2) the CFV is indirectly proportional to the spacer porosity.

3.3.1.2. Design Parameters Relationship

The performance of FO systems is dictated by the mechanical as well as the process design parameters. Figure 3-6 highlights the primary mechanical and process parameters considered for meeting the set design requirements.

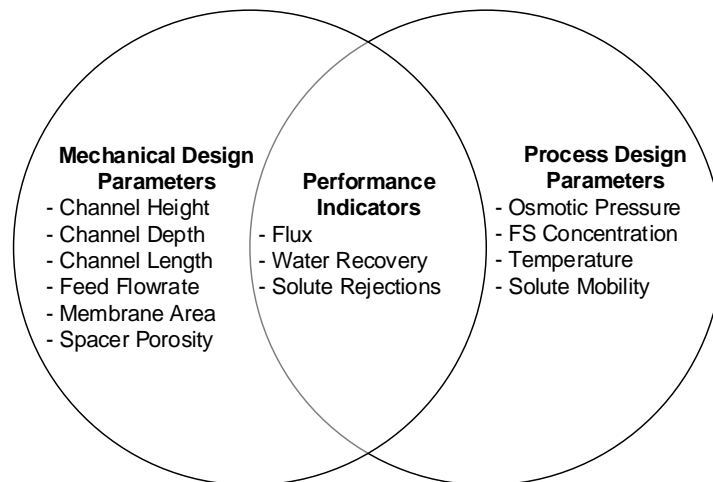


Figure 3-6. Intrinsic relationship between the mechanical and process design parameters both dictating the system performance indicators.

To characterise the system performance, subsequent mathematical expressions were derived. The system was characterised mathematically by identifying the mechanical and process primary variables required to meet the design requirements of the bench-scale setup. The primary variables identified in Figure 3-6 were used to derive secondary variables via basic expression manipulation. The aim of deriving these expressions is to find the relationship between the mechanical and process parameters, to evaluate its effects on the system performance indicators, and hence to be able to characterise the system. The inter-relationships between the mechanical and process parameters along with the process indicators are detailed in Figure 3-7.

CHAPTER 3: Laboratory-Scale Setup Design

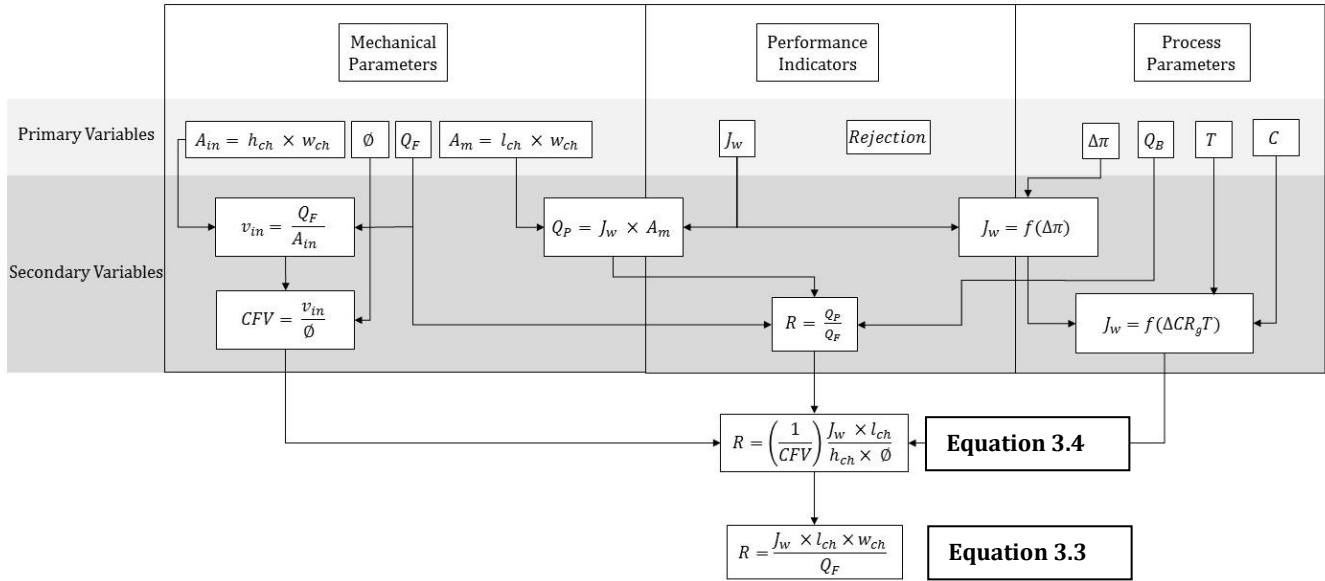


Figure 3-7. The inter-relationships between the primary mechanical and process design parameters and the system performance indicators to characterise the operation of the bench-scale setup. A_{in} is the membrane cross sectional area, h_{ch} is the channel height, w_{ch} is the channel width, Q_F is the inlet flow rate, A_m is the membrane active area, l_{ch} is the channel length, v_{in} is the inlet flow velocity, CFV is the cross-flow velocity, ϕ is the spacer porosity, J_w is the water flux, R is recovery, Q_P is the permeate flow rate, π is the osmotic pressure, Q_B is the brine flow rate, T is the temperature, C is the concentration and R_g is the Universal Gas Constant.

As is indicated there is an intrinsic relationship between the system mechanical and process parameters along with the system performance indicators. The recovery of the system can be theoretically estimated via measuring the water flux by a set of predetermined conditions. The relationship between water flux and recovery is detailed in Equation (3.3).

$$R = \frac{J_w \times A_m}{Q_F} = \frac{J_w \times l_{ch} \times w_{ch}}{Q_F} \quad (3.3)$$

Once the *correct* recovery is calculated via Equation (3.3) incorporating the measurement errors associated with the in-line flow measurement columns, the actual CFV with which the system operated, can be calculated by using Equation (3.4). It was indicated that the system CFV is a function of the housing block mechanical design. Via the manipulation of Equation (3.4) the relationship between water flux, recovery, and CFV can be quantified. The robustness of the system mechanical design can be evaluated via these equations.

$$R = \left(\frac{1}{CFV}\right) \frac{J_w \times l_{ch}}{h_{ch} \times \phi} \quad (3.4)$$

Against the above background for setup evaluation, the design requirements identified along with the respective target value ranges and test methods, are detailed Table 3-5.

Table 3-5. Design requirements along with the respective target values and the test method that will be used to evaluate the design requirement.

Design Requirement	Target Value	Test Method
Vary CFVs	9 – 35 cm·s ⁻¹	VSD on pump to vary inlet flow rate
Evaluate flow rates	-	Mass balance verification
Automate flow configurations	-	Conductivity measurement
Purge residual solutions	±15 minutes	Conductivity measurements
Temperature control	20 - 25°C	Thermometer
Water flux at 19 cm·s ⁻¹	5 – 20 L·m ⁻² ·h ⁻¹	Verify by calculation
Water recovery at 19 cm·s ⁻¹	Median value of 20%	Verify by calculation

3.3.1.3. Evaluation Method

After the appropriate leak-tests and commissioning procedures, an experimental run was conducted. The conditions for this experimental run are listed in Table 3-6.

Table 3-6. Experimental conditions for the evaluation of the bench-scale setup.

Experimental Conditions	UOM	Value
Entry CFV	cm·s ⁻¹	19
Flow Ratio	-	1
Entry Flow Rate	mL·min ⁻¹	210
Water Recovery	%	20
Water Flux	L·m ⁻² ·h ⁻¹	20
Operational Mode	-	AI-FS
NaCl DS	M / mg·L ⁻¹	0.5 / 29 220
Temperature	°C	24±1.5

3.3.2. Data Acquisition

The robustness and errors associated with the primary mechanical aspects of the setup were identified along with subsequent errors measurements. Whilst then in operation, the following measurements needed to be taken to achieve the objectives set out by this study:

- (1) Inlet and outlet flow rate of the FS;
- (2) Inlet and outlet flow rate of the DS;
- (3) Conductivity measurements for the inlet and outlet streams; and
- (4) Monitoring and recording of the inlet pressures to the two flow channels.

The formulae used to convert the measurements above to the performance parameters of the system, are detailed below. Sample calculations pertaining to a typical data set are given in Appendix B.2.

3.3.3. Flux

As detailed in Chapter 3, a flux measurement device was developed in which the flux of the system could periodically be evaluated by operating the system in a continuous manner. This was done by measuring the inlet and outlet flow rates of the respective solutions. The flux was calculated with the mathematical expression in Equation (3.5).

CHAPTER 3: Laboratory-Scale Setup Design

$$J_w = \frac{\Delta\dot{Q}}{A_m} = \frac{\dot{Q}_{F,i} - \dot{Q}_B}{A_m} = \frac{\dot{Q}_P - \dot{Q}_{DS,F}}{A_m} \quad (3.5)$$

where J_w = Water flux, $L \cdot m^{-2} \cdot h^{-1}$

\dot{Q}_i = Inlet flow rate, $L \cdot h^{-1}$

\dot{Q}_o = Outlet flow rate, $L \cdot h^{-1}$

A_m = Membrane active area, m^2

To account for any system variations, the measured data were normalised to standard operating conditions in order to compare data-sets. Data normalisation was required to enable true and correct comparison of measured fluxes. Normalisation considered temperature and osmotic pressure, for the following reasons:

- (1) The South African summer climate is hot; therefore, tank solution temperatures sometimes exceeded the controlled 24°C and reached temperatures of up to 30°C.
- (2) The designed system was a once-through system, which means that no solution was recycled to the respective FS and DS tanks. This was done to evaluate RSF as accurately as possible, thereby eliminating the possibility that solutes mix inside the feed tanks, due to RSF and give inaccurate conductivity measurements. As feed volumes of up to 200 L were required, small deviations in solution make-up concentrations could arise. Therefore, the osmotic pressure difference was normalised for data comparison purposes.
- (3) Water fluxes attained in FO were normalised to equivalent fluxes at 20°C. Due to changes in the viscosity of water with temperature, a correction factor for the changes in water viscosity requires incorporation in the calculation of the measured water fluxes. For low-pressure membrane systems, it is common practice to normalise flux data to 20°C. Equation (3.6) is a correlation which normalises the water flux measured at a given temperature to 20°C. The terms in brackets are correlations of water viscosity with temperature [117].

$$J_{w,20^\circ C} = J_{w,T} [1.784 - (0.0575 \cdot T) + (0.001 \cdot T^2) - (10^{-5} \cdot T^3)] \quad (3.6)$$

where $J_{w,20^\circ C}$ = Water flux at 20°C, $L \cdot m^{-2} \cdot h^{-1}$

$J_{w,T}$ = Water flux measured, $L \cdot m^{-2} \cdot h^{-1}$

T = Temperature, °C

To account for variations in the driving force between experimental runs, an additional term was added to Equation (3.6). The driving force in an FO system is mainly dependent on two terms: (1) osmotic pressure and (2) mechanical pressure. A factor was derived from Equations (1.1)–(1.3) to account for driving force variations due to (1) pressure fluctuations and (2) inconsistent DS make-up, due to the large required volume. The correction factors added for flux normalisation are presented in Equation (3.7).

$$J_{w,0} = J_{w,a} \cdot (1.784 - (0.0575T) + (0.001T^2) - (10^{-5}T^3)) \cdot \frac{(\Delta\pi - \Delta P)_0}{(\Delta\pi - \Delta P)_a} \quad (3.7)$$

These normalisation correlations were derived specifically for this study. The following limitations apply to the abovementioned normalisation correlations:

- (1) The effects of CP were not included and were not accounted for.
- (2) DS solute specific parameters, such as diffusivity, were not included.
- (3) The effects of RSF on the driving force were not included.

For the scope of this study the normalisation correlations derived above, were considered satisfactory.

3.3.4. Recovery

Water recovery was also calculated from the measured flow rates, with the detailed mathematical expression given in Equation (2.4). The recovery of the system was evaluated based on the flux measured. Experimental error was quantified by evaluating the difference in the measured recovery (Equation (2.4)) and the calculated recovery, based on the measured flux – Equation (3.3).

3.3.5. Cross-Flow Velocity

The CFV over the membrane was calculated with Equation (3.2). The assumptions made while using Equation (3.2) were: (1) the channel height, h_{ch} , was equal to 3 mm and (2) the flow restriction factor in the channel due to the spacer porosity, was equal to 0.85. Based then on the recovery of the system, the actual operational CFV of the system was calculated via manipulation of Equation (3.4). As indicated in the evaluation of the setup, correcting of the CFV, points out the uncertainties in the mechanical design.

3.3.6. Rejection

Rejection and RSF were calculated via the conductivity measurements. Conductivity measurements were taken to evaluate solute migration across the membrane. There is an intrinsic relationship between conductivity measurements and TDS. The conductivity probe was calibrated on a weekly basis. The conductivity probe was from Eutech ®. Conductivity measurements were converted to TDS values via the multiplication with a K-Factor. The K-Factors correlating with the specific conductance of the respective water samples are listed in Table 3-7.

Table 3-7. K-Factors for various desalination water types at 25°C [44].

Water Sample	Typical EC ₂₅ (µS·cm ⁻¹)	K-Factor
Distillate	1 – 10	0.50
RO Permeate	300 – 800	0.55
Saline Waters	800 – 45 000	0.64
Seawater	45 000 – 60 000	0.70
Reject Brines	65 000 – 80 000	0.75

CHAPTER 3: Laboratory-Scale Setup Design

After the conversion of conductivity measurements to TDS, the rejection of the membrane could be quantified via Equation (2.6).

3.4. Prototype



Figure 3-8. Photographs showing the final commissioned setup, specifically indicating (a) the variable height grip of the inlet flow meter as well as the two 200 L feed tanks (b) the six housing blocks forming the FO train, as well as (c) the (1) pumps, (2) filters, and (3) outlet flow meters.

Details of the FO setup and specific apparatus shown in Figure 3-8 are given in Table 3-8.

CHAPTER 3: Laboratory-Scale Setup Design

Table 3-8. Equipment list and description of the bench scale FO setup and apparatus.

Equipment	Description	Operating Conditions
FS feed tank with submersible heater (1)	Plastic feed tank with a 300 W explosion proof glass heater and thermostat	Total volume of 0.2 m ³ with the heater operating between 20–35°C.
FS inlet mercury manometer (2)	Measure inlet pressure of the FS to the respective channel	Highest pressure 0.3 bar
FS inlet flow rate meter (3)	Variable height inlet flow meter	Typical flow rates 97–382 mL·min ⁻¹
FS pump (4)	Watson Marlow 503S pump, equipped with 8mm marprene tubing.	Maximum RPM 400
DS feed tank with submersible heater (5)	Plastic feed tank with a 300 W explosion proof glass heater and thermostat	Total volume of 0.2 m ³ with the heater operating between 20–35°C.
DS inlet flow rate meter (6)	Variable height inlet flow meter	Typical flow rates 97–382 mL·min ⁻¹
DS 10 µm filter (7)	Filter to remove any particulate matter from the DS.	-
DS carbon filter (8)	Carbon filter to remove any organic content from the DS.	-
DS pump (9)	Watson Marlow 503S pump, equipped with 8mm marprene tubing.	Maximum RPM 400
DS outlet flow rate meter (10)	Outlet flow meter	-
Membrane housing blocks (11)	Six housing blocks made from PVC with perspex sight glasses on either side.	Dimensions 340 mm × 140 mm
FS outlet flow rate meter (12)	Outlet flow meter	-
DS inlet flow rotameter (13)	Basic rotameter with Teflon float	Maximum range 0.1–1 L·min ⁻¹
Electrical box (14)	Phoenix Nanoline PLC with 7 timers	-
Solenoid valves (15)	220 V washing machine valves	-
Outlet sample ports (16)	-	-

3.5. Testing and Results

The system design was evaluated based on experimentation. All of the design requirements were incorporated in a single experimental run. The robustness of the design could be evaluated, based on the derived mathematical equations relating the performance indicators to the system mechanical and process parameters.

3.5.1.1. Recovery to Evaluate Cross-Flow Velocity (CFV)

The recovery attained is the main performance indicator, relating the primary mechanical parameters to the primary process parameters. There are three ways to analyse for the recovery of the system: (1) experimentally determined recovery with flow rate differences, (2) via Equation (3.3) where the recovery is only a function of flux, and (3) via Equation (3.4) which highlights the relationship between recovery, CFV and water flux. The methods for calculating and evaluating the recovery are detailed in Table 3-9.

Table 3-9. Summary of calculation procedure to validate system operating parameters.

Recovery: Calculation Method	Equation Number in Document	Equation Used	Manipulation of Equation
Designed		-	See Table 3-1 and Table 3-2
Theoretical 1	(3.3)	$R = \frac{J_w \times l_{ch} \times w_{ch}}{Q_F}$	See Experimental
Theoretical 2 ^a	(3.4) ^c	$R = \left(\frac{1}{CFV}\right) \frac{J_w \times l_{ch}}{h_{ch} \times \emptyset}$	$CFV = \left(\frac{1}{R}\right) \frac{J_w \times l_{ch}}{h_{ch} \times \emptyset}$
Experimental ^b	(2.4)	$R = \left(\frac{Q_F - Q_B}{Q_F}\right) \times 100$	$R = \frac{Q_F - Q_B}{Q_F} = \frac{\left(\frac{Q_F - Q_B}{A_m}\right) \times A_m}{Q_F} = \frac{J_w \times A_m}{Q_F}$

^aTheoretical Equation 2 can be used to evaluate the CFV of the system by using the recovery calculated in Theoretical 1.

^bVia manipulation, the experimentally determined recovery should be the same as the recovery calculated in Theoretical 1. The errors or uncertainties can be introduced when evaluating the recovery from the FS side or from the DS side. This difference can be attributed to measuring errors as stipulated in Table 3-3.

^cCalculation of the CFV of the system using Theoretical 2 [Equation (3.4)] is referred to as the **actual** CFV.

The water recovery of the system is a function of the water flux attained. This is highlighted by the three methods whereby recovery can be evaluated. The system was designed to attain a flux of $20 \text{ L}\cdot\text{m}^{-2}\cdot\text{h}^{-1}$ at a CFV of $19 \text{ cm}\cdot\text{s}^{-1}$. The water flux attained is a function of the driving force differential across the membrane, and the permeability coefficient of the membrane. This is detailed in Equation (1.1). The driving force differential can be manipulated in order to manipulate the flux attained; however, the water permeability coefficient (P_w) is a parameter which is intrinsic to the membrane itself. Water flux dictates recovery, which in turn is a function of the mechanical and process design parameters of the system. Based on this, the driving force was kept constant in the evaluation, and hence the water fluxes measured were used in the theoretical evaluation of the recovery and the CFV of the system.

The only process condition which can influence the variability in water recovery is the CFV, when assumed that the driving force (osmotic differential) is kept constant. This is highlighted by Equation (3.4) that is a function of the system CFV and the flux. The influence of these parameters can be quantified when assumed that the mechanical design of the system is fixed.

Figure 3-9 illustrates the relationship between water recovery and CFV at a constant flux for a fixed system mechanical design.

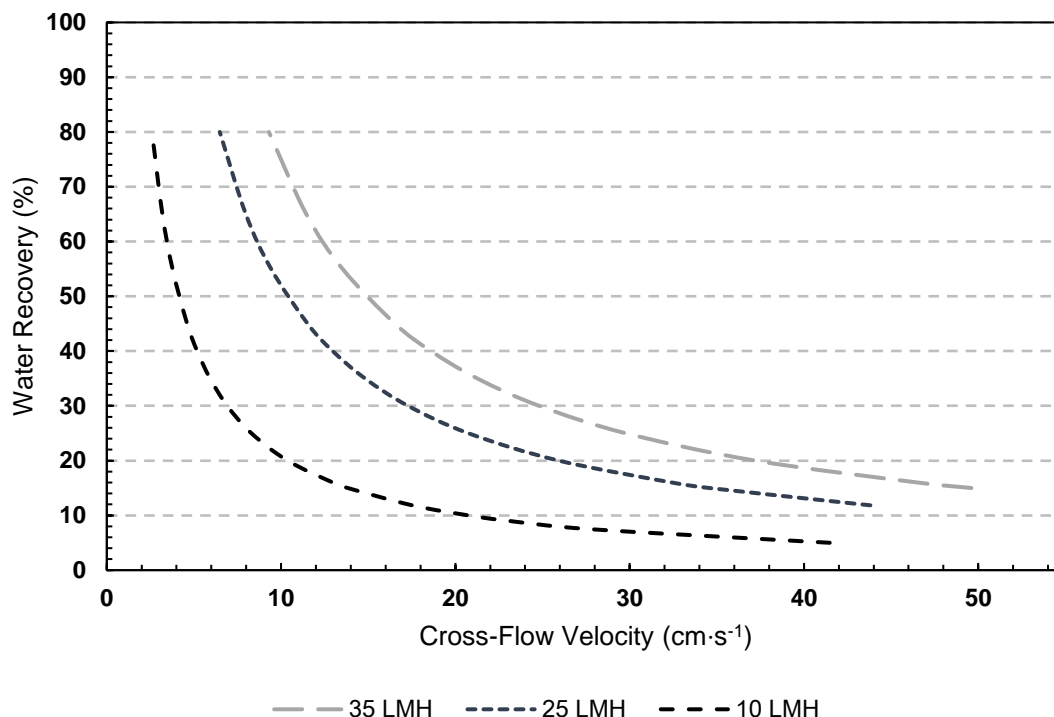


Figure 3-9. The impact of different CFVs on the water recovery of the system at three constant fluxes of $35 \text{ L}\cdot\text{m}^{-2}\cdot\text{h}^{-1}$, $25 \text{ L}\cdot\text{m}^{-2}\cdot\text{h}^{-1}$ and $10 \text{ L}\cdot\text{m}^{-2}\cdot\text{h}^{-1}$. The mechanical design was fixed and membrane area used for these calculations was fixed at 0.1344 m^2 . The cross-sectional area was also assumed to be constant at 0.17 cm^2 , which again assumed a uniform membrane flow-path area.

Figure 3-9 highlights that the system recovery is maximised when the CFV is decreased – assuming a constant system flux. The recovery increases as the CFV decreases. It is also evident that there is a minimum CFV at which the system can operate when the flux is constant. This is due to the hyperbolic relationship between water recovery and CFV. The vertical asymptote is at zero CFV and the horizontal asymptote lies at 0% recovery. Therefore, the CFV needs to be infinitely high to recover no water from the system and infinitesimally small to attain a 100% water recovery. Also, as per Equation (3.4), the lower the flux, the lower the operating CFV to attain the same water recovery. The recovery of the system can also be altered by operating the system at a constant CFV and changing the operational flux. This is a more representative scenario for actual FO membrane systems. Mass transport phenomena such as CP and RSF are prevalent in FO systems, thereby constantly altering the water flux and hence the system recovery. This, in turn, illustrates the relationship between the primary mechanical and process parameters of the system.

Six housing blocks were used in order to attain the designed system recovery. This was done because recovery is a function of the membrane flow-path length (l_{ch}). The actual recovery attained per housing block (membrane area) and the theoretical modelled recovery are visually compared in Figure 3-10.

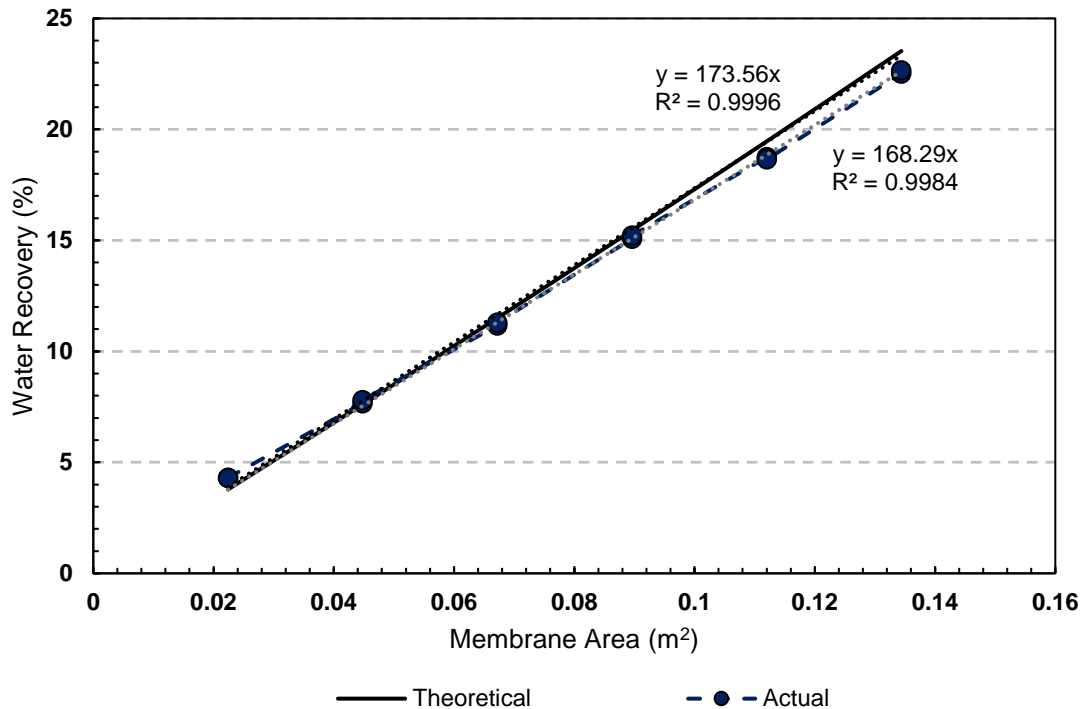


Figure 3-10. The theoretical recovery and actual recovery attained at a CFV of 19 cm·s⁻¹ and a variable system area.

Figure 3-10 indicates that the gradient of the actual data differs, when compared to the theoretical relationship. The designed theoretical system overestimated the system recovery at the operating conditions by approximately 3.04%. The actual flux measured was the flux that was used in the theoretical evaluation of the recovery. Therefore, the 3.04% difference in the recovery along the length of the membrane system can only be ascribed to uncertainties in the primary mechanical parameters, theoretically calculated for the system, along with error made when measuring the respective flow rates with the in-line flow measuring columns to determine the recovery. This was investigated more closely by evaluating the theoretical recovery of the system, based on Equations (3.3) and (3.4), and by comparing the theoretical recovery with the actual recovery.

The recovery of the system was evaluated based on the (1) actual experimental recovery attained, (2) the theoretical recovery calculated by using the measured experimental flux and (3) the theoretical recovery calculated based on the calculated CFV of the system (assuming that the channel height is 3 mm), and the measured flux. Figure 3-11 indicates the variance in water recovery, depending on the equation used. The Actual and Theoretical 1 [Equation (3.3)] deviates within 2±1% from the designed recovery. With the incorporation of the CFV term in the calculation of the recovery, as per Theoretical 2 [Equation (3.4)], the calculated recovery deviates by 10% from the experimentally

CHAPTER 3: Laboratory-Scale Setup Design

determined recovery. This indicated that the CFV at which the system was set up to operate was not accurate.

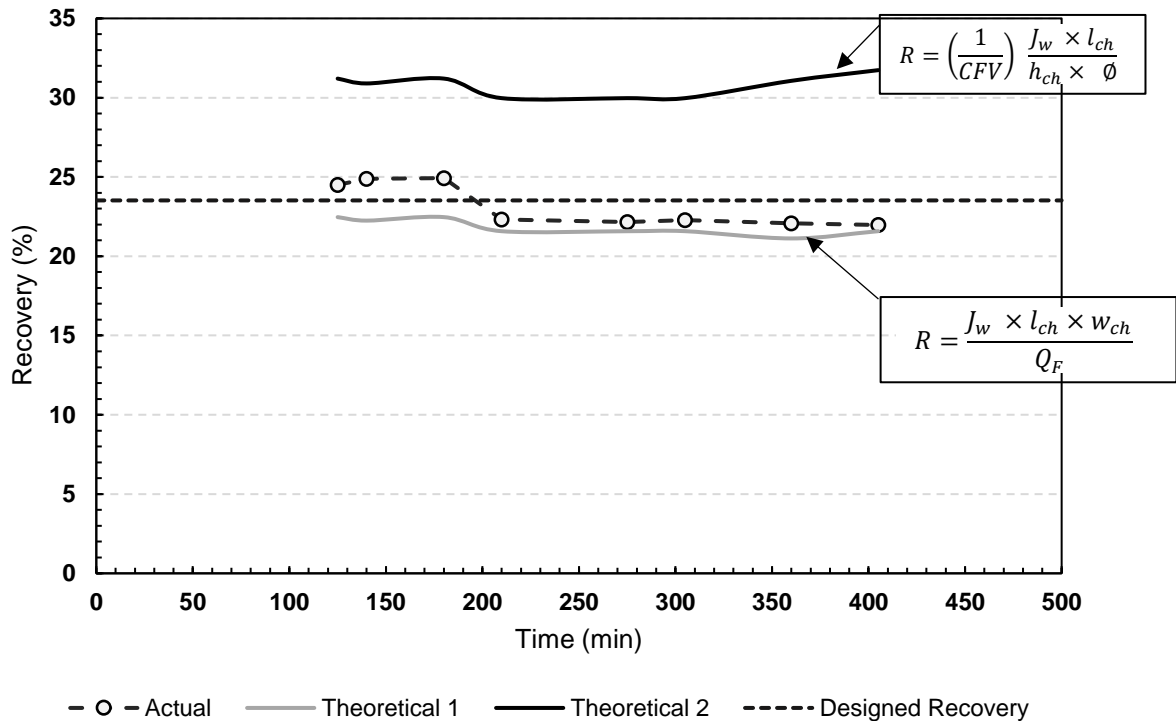


Figure 3-11. Variance in water recovery as experimentally determined, theoretically calculated and the recovery at which the system was designed to operate.

Based on the ~10% deviation in the calculated water recovery, with Equation (3.4), brought about by incorporating the CFV, the recoveries calculated with Equation (3.3) were used to determine what the CFV within the system actually was. The results from this investigation are presented in Figure 3-12.

From Figure 3-12 it is clear that the assumed CFV at which the system operates, is significantly lower than the actual operating CFV of the system. The CFV of the system is a function of the mechanical parameters as indicated by Equation (3.2). The inlet flow rate (Q_F) can be evaluated accurately via the in-line flow meters. The channel width (w_{ch}) of the housing block is also a parameter which can be accurately evaluated by measuring the membrane width prior to installation. The mechanical uncertainty is thus introduced via the channel height (h_{ch}) and the channel porosity or flow restriction factor. Factors which may influence the channel height is the (1) torque at which the membranes are tightened and (2) gasket deformation over time.

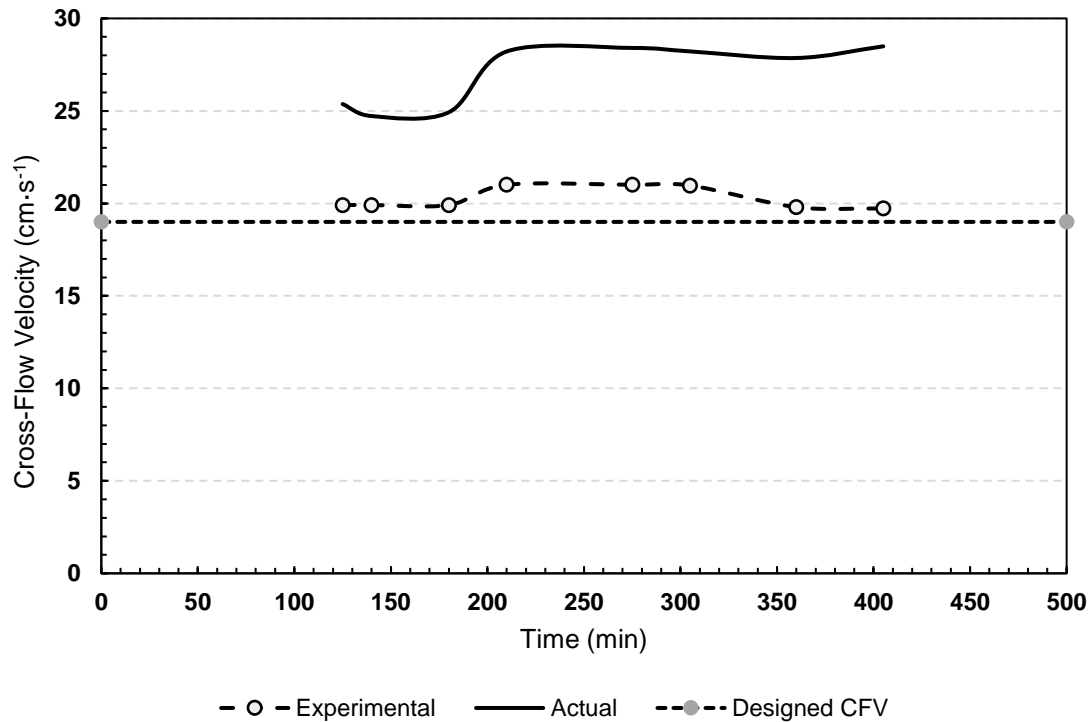


Figure 3-12. Experimental, calculated (actual) and designed CFV of the system.

3.5.1.2. Effect of Primary Mechanical Parameters

It was indicated in the above evaluation of the water recovery, that the uncertainties in the mechanical design of the system can translate to errors as large as 10% in water recovery, when the CFV is calculated incorrectly. Two primary mechanical parameters are a function of the CFV: (1) channel height and (2) spacer porosity, or the flow restriction factor of the channel.

Figure 3-13 highlights the relationship between the channel depth and the calculated CFV of the system. If the channel depth is underestimated, the calculated CFV will be overestimated by at least 1.5 times. This inverse relationship is highlighted by Equation (3.2).

Figure 3-14 clearly indicates, that the narrower the channel height, the higher the CFVs which can be attained within the flow channel. This is in accordance with Equation (3.2), which mathematically describes the inverse relationship between the channel depth and the operating CFV. The effect of spacer porosity is highlighted by Figure 3-14. The more porous the spacer, the larger the cross-sectional channel volume, which decreases the channel CFV. The porosity used for the spacer in this study was 0.85. Therefore, the volume occupation of the spacer was assumed to be 15% of the total channel volume.

CHAPTER 3: Laboratory-Scale Setup Design

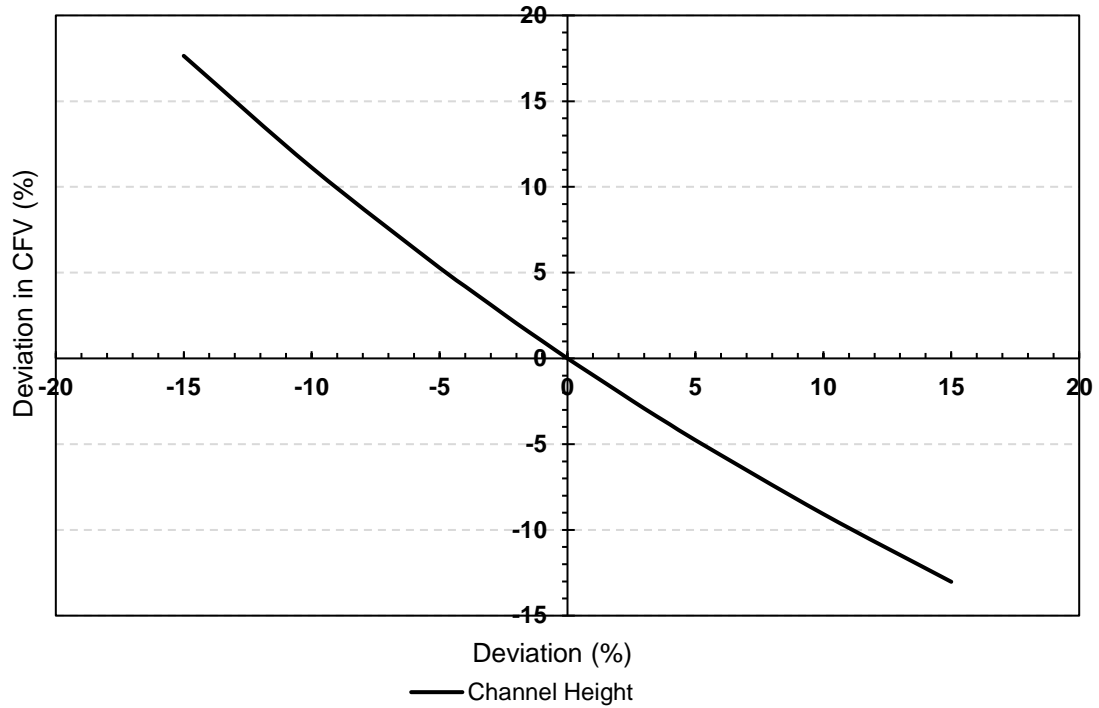


Figure 3-13. Indicates how deviations in the channel depth translate to deviations in the calculation of the system CFV.

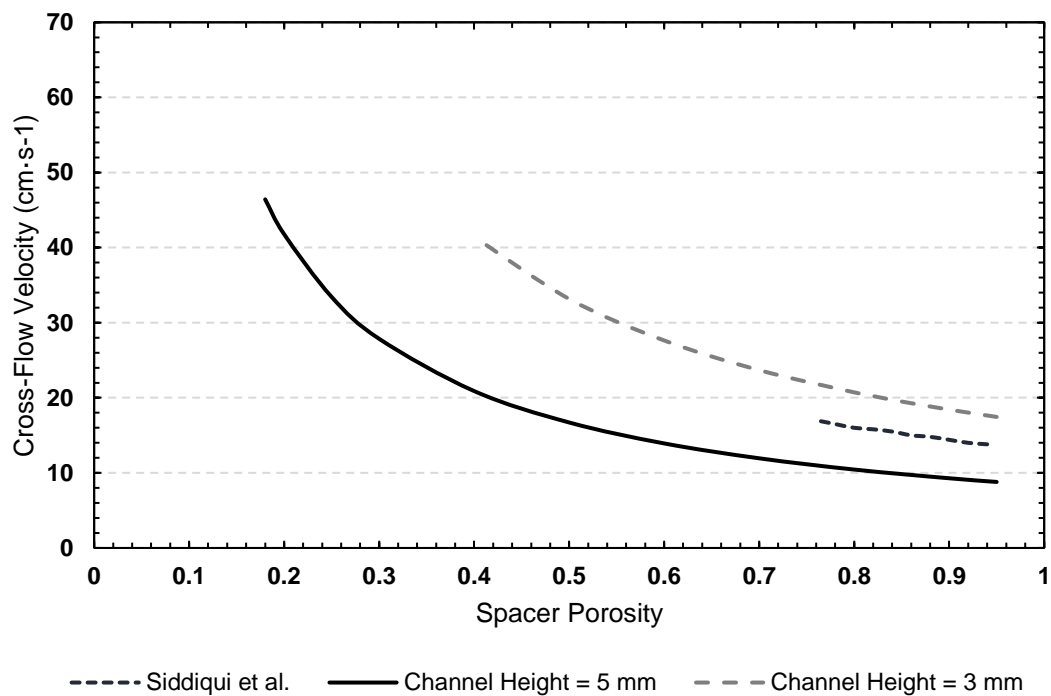


Figure 3-14. Translation of variations in the spacer porosity to the system CFV for variations in the channel depth. The channel height for the system modelled by Siddiqui et al. [115] was not reported.

3.5.1.3. Variation in CFV

The effect of the channel height and the spacer porosity on the calculation of the CFV have been quantified. The effects of miscalculating the CFV on the evaluation of the water recovery, have also been demonstrated. With each of these evaluations it was assumed that the operating CFV of the system represented the average operating CFV, but this was found to be inaccurate. Due to the mass transfer of water from the FS to the DS, the water volume in the FS channel will decrease, and subsequently the water volume in the DS channel will increase. This is translated to variances in the flow rate at each point along the membrane flow length. These variances in the flow rate, due to the mass transfer of water, manifest as changes in the CFV along the membrane flow-path length.

This is visually presented in Figure 3-15. The flow ratio for experimental evaluation of the system was equal to unity, thereby implying that the inlet CFV of the FS and the DS is equal. The setup was operated in the counter-current configuration. In Section 2.1.1.2 the advantages of operating in the counter-current configuration are highlighted. In Figure 3-15 it is clear that the inlet CFVs of the system are equal. The increase in the DS CFV from $19 \text{ cm}\cdot\text{s}^{-1}$ to $23 \text{ cm}\cdot\text{s}^{-1}$, and the decrease in the FS CFV from $19 \text{ cm}\cdot\text{s}^{-1}$ to $14 \text{ cm}\cdot\text{s}^{-1}$ is indicated in Figure 3-15.

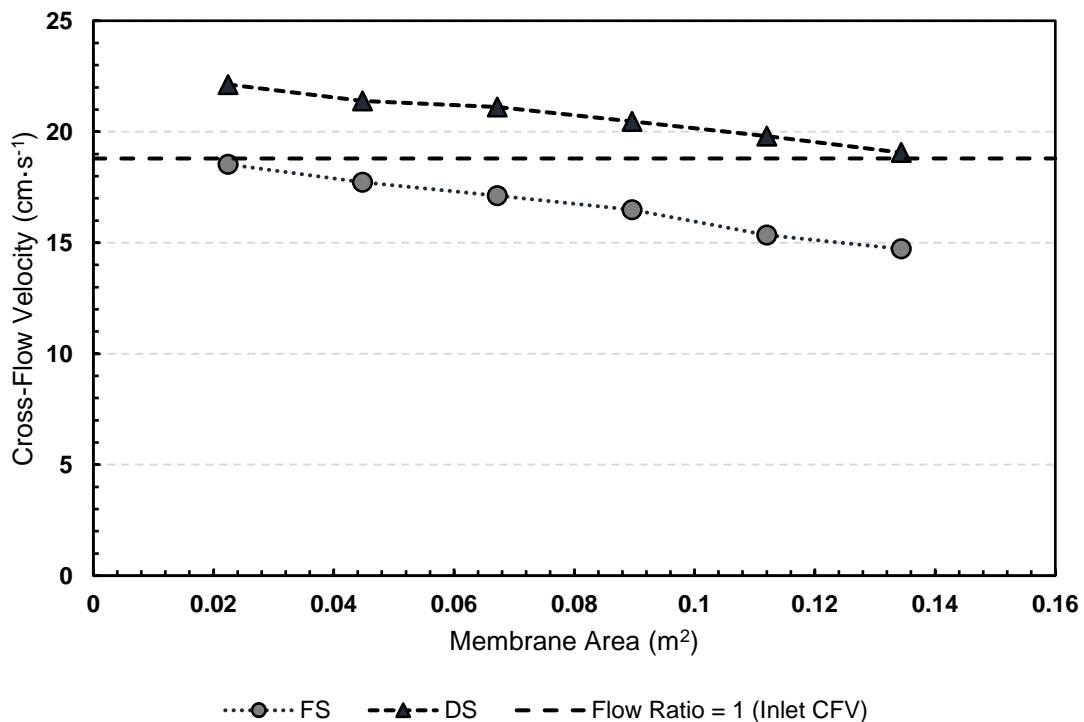


Figure 3-15. Inlet CFV variations within the system for the FS and the DS with the addition of membrane area (flow-path length), thereby increasing the overall recovery and water extraction capacity of the system. The total system area is 0.1344 m^2 .

Equation (3.4) can thus be adapted to Equation (3.8), as Figure 3-15 illustrates that the CFV is a function of the membrane flow-path channel length (l_{ch}).

CHAPTER 3: Laboratory-Scale Setup Design

$$R = \left(\frac{1}{\int_{l_{ch,1}}^{l_{ch,2}} CFV dl_{ch}} \right) \frac{J_w \times l_{ch}}{h_{ch} \times \emptyset} \quad (3.8)$$

The inlet and outlet CFV of each block, along with the experimentally determined recovery, are detailed in Table 3-10.

Table 3-10. Block-by-block analysis of the FS inlet and outlet CFV, and the corresponding CFV for the DS inlet and outlet channels for counter-current operation, with the corresponding membrane area and the per block addition to the system of the attained water recovery.

	Feed Solution		Draw Solution		Membrane Area (m ²)	Water Recovery (%)
	Inlet CFV (cm·s ⁻¹)	Outlet CFV (cm·s ⁻¹)	Inlet CFV (cm·s ⁻¹)	Outlet CFV (cm·s ⁻¹)		
Block 1	18.53	17.73	22.13	22.85	0.0224	4.30
Block 2	17.73	17.12	21.39	22.13	0.0448	7.73
Block 3	17.12	16.48	21.11	21.39	0.0672	11.23
Block 4	16.48	15.35	20.47	21.11	0.0896	15.15
Block 5	15.35	14.72	19.8	20.47	0.112	18.70
Block 6	14.72	14.05	19.06	19.8	0.1344	22.59

3.5.1.4. In-line Flow Measurement

A major effect of positive displacement pump performance is the loss in flow due to slip. The expanding cavity on the inlet side of a positive displacement pump creates a low-pressure area that fills with fluid. This cavity can be filled with fluid from the inlet line during normal performance. However, if slip occurs, the cavity will also be partly filled with fluid flowing back through the pump clearances from the outlet side.

This is visually presented in Figure 3-16 which indicates how the pressure on the suction side of the pump varies with the liquid (hydraulic) height inside the tank. The higher the pressure on the suction side, the greater the pump slip, which then translates to major errors in the inlet flow rate measurements. Figure 3-16 proved the importance of correcting the method of measuring the inlet flow rates to the FO train. The problem was addressed by adding a shifting grip to the inlet flow meters so that measurements may be taken on exactly the same height as the liquid level in the tank, instead of on a fixed height.

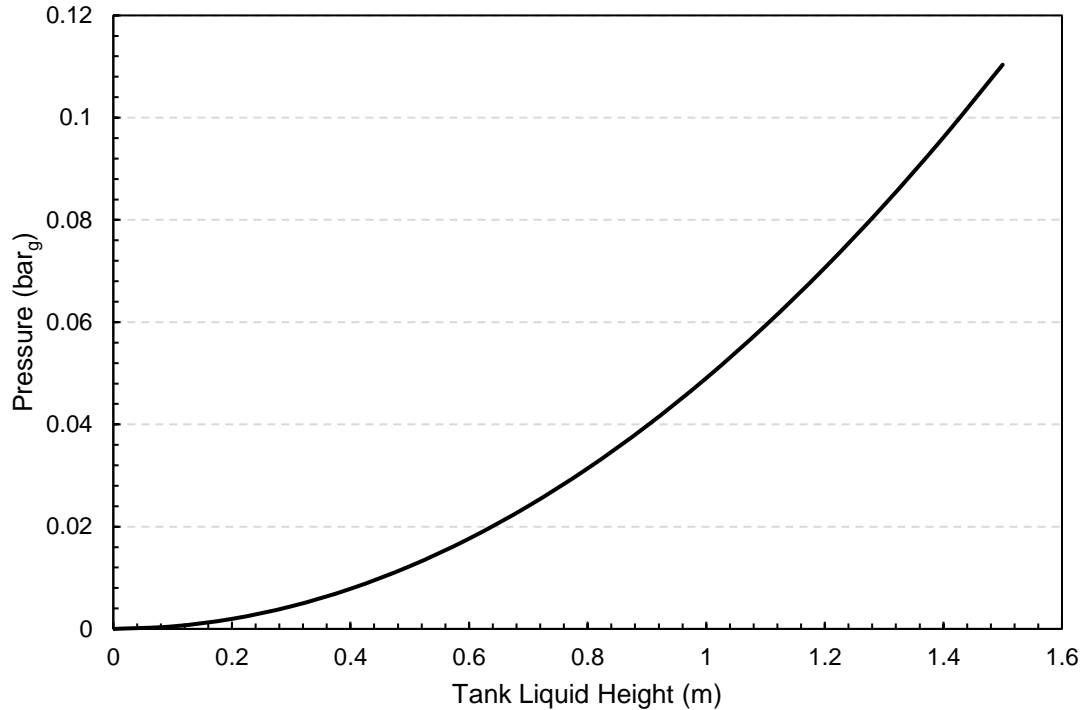


Figure 3-16. Pressure differential as per the suction side of the pump as a function of the hydraulic liquid height inside the respective tank from the inlet of the pump. This is due to the expanding cavity on the suction side of the pump.

3.5.1.5. Flow-Path Switching

One of the design requirements was to automate the intermittent flow path switching from the one operational configuration to the other. Figure 3-17 highlights the change in performance indicators, such as water flux and recovery, when switching the flow-path from the AL-FS to the AL-DS configuration. The mass balance of the system was also validated by evaluating the water flux from the FS (water mass transfer loss) and the DS (water mass transfer gain). Due to the error associated with the flow rate measurement, the flux values will not be completely the same. For this system a mass balance deviation of up to 5% was found to be acceptable.

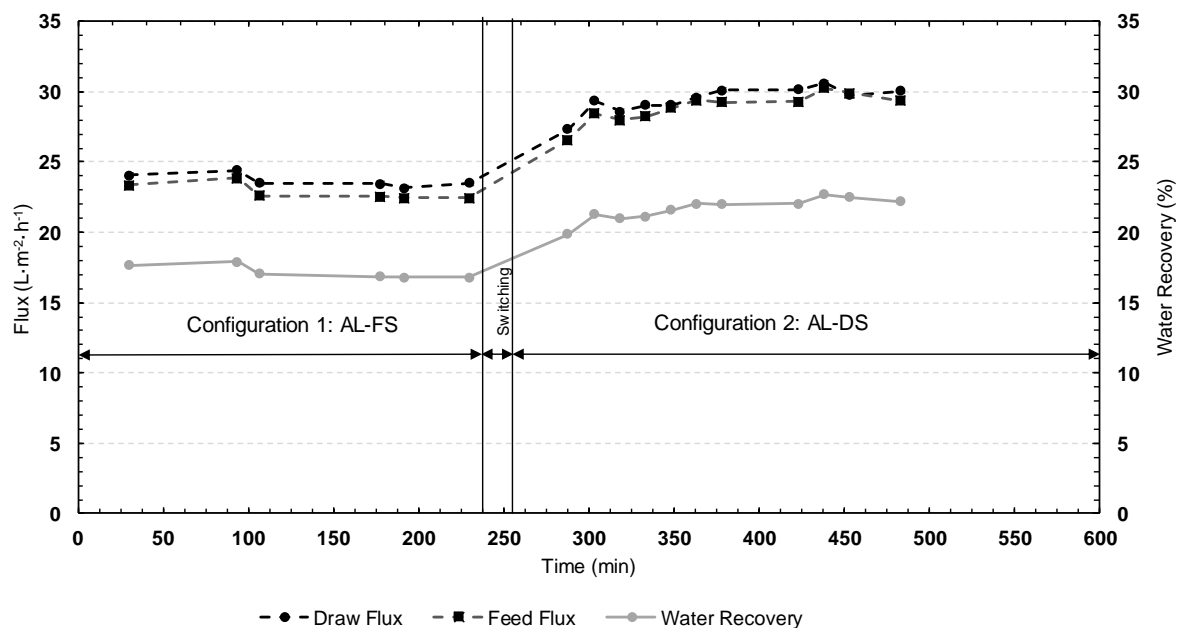


Figure 3-17. Water flux and recovery results from switching the operational flow path from the AL-FS configuration to the AL-DS configuration, at an inlet CFV of $19 \text{ cm}\cdot\text{s}^{-1}$.

3.6. Assessment

The design and prototype of the bench-scale setup will be evaluated, based on the identified design requirements.

Seven design requirements were identified for the design and operation of the bench-scale setup. The evaluation of the flow rates, automations of the flow configurations, and the purge of residual solutions were evaluated in the commissioning phase. It was found that these design requirements were met successfully.

The robustness of the system was investigated by conducting an experimental run. By varying the inlet flow to the housing blocks, the assumed CFV at which the system operates, could be varied. The fluxes attained along with the water recoveries, were at the target values of the design requirements, $20 \text{ L}\cdot\text{m}^{-2}\cdot\text{h}^{-1}$ and a recovery of 20% respectively. The CFV at which the system was designed, was found to be lower than the actual operational CFV of the system. Upon investigation it was found that mechanical parameters such as the channel height and the spacer porosity or flow restriction factor, were estimated inaccurately, which gave rise to inaccuracies in the assumed operational CFV of the system. Deviations of as high as $15 \text{ cm}\cdot\text{s}^{-1}$ were observed.

Upon evaluation of the bench-scale setup, it was found that the system can be used to investigate the operation of a typical FO membrane at various operating conditions, when accounting for the inaccuracies relating to the channel height and spacer porosity, by correcting for the operational CFV.

Chapter 4

Materials and Methods

Chapter 3 set out to identify the design requirements for the bench-scale setup design. The primary mechanical and process parameters were identified. Along with the identification of these parameters, the robustness of the system was investigated by evaluating the resulting performance indicators and their relationship specifically with the mechanical design parameters of the setup. In this chapter the procedures followed to evaluate the performance of a typical FO membrane critically, will be explained.

4.1. Experimental Problem Statement

An experimental setup was already constructed, evaluated and critically assessed. This setup will now be used to critically evaluate and characterise the mass transfer and membrane fouling of a typical FO membrane while considering:

- the effects of cross-flow velocity (CFV),
- the effects of operational configuration (whether the AL is facing the FS or the DS),
- the effects of intermittent switching of the flow path, as a combination of flushing and osmotic backwashing, and
- the practical realities related to flow-path switching when treating feed water saturated with gypsum.

4.2. Overall Approach

To achieve the objectives as set out by this study, the experimental planning phase was subdivided into three distinct phases.

Phase 1 entailed the validation of the bench-scale setup. It was indicated in the evaluation of the setup that the uncertainties relating to the mechanical design parameters influence the operational CFV of the system. The validation phase thus endeavoured to accurately characterise and validate the operability of the FO membrane, based on the performance indicators and in terms of various CFVs, as well as the operational configuration. The mass transport in terms of the occurrence and extent of CP, was also investigated.

Following on to Phase 2, the results of the 1st Phase then gave rise to the variations in CFV, to be tested via the implementation of intermittent flow-path switching. Refining and optimising the factors that mainly affected the operability of intermittent flow-path switching, led to the investigation of the

CHAPTER 4: Materials and Methods

commercial impact of the fouling control method, as per Phase 3. This was done by investigating the intermittent flow-path switching applied to a typical industrial saturated calcium stream, which translated to gypsum scaling within the FO train. The general approach-process followed, is outlined in Figure 4-1.

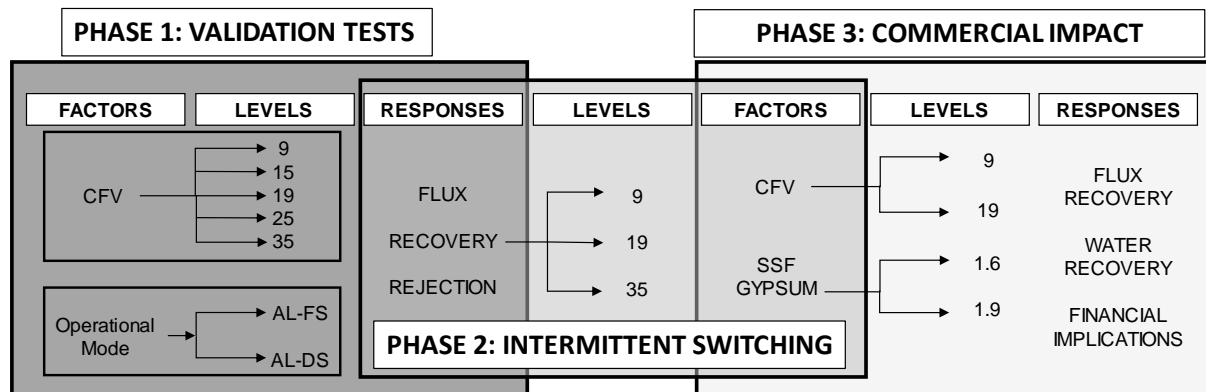


Figure 4-1. General approach process followed for the execution of the experimental work.

As per the general approach process, which is detailed in Figure 4-1, each phase was subdivided into the investigative factors, the variations of the factors (levels), and the expected responses which were specifically measured. Mainly five variations in the CFV were investigated at first in both operational configurations (AL-FS and AL-DS), in order to measure the (1) water flux, (2) water recovery and the (3) salt rejection. The primary aim of Phase 1 was then to (1) quantify the errors made with the operational and actual CFV by (2) evaluate the accuracy of the experimental and theoretical recovery at a certain experimental flux and (3) characterise the mass transfer occurring within the system in terms of CP and RSF.

The findings of Phase 1 then gave rise to the variations in the factors to investigate for Phase 2 of this study. The only factors which can mainly be tested, is the CFV, to confirm operational stabilisation times between the two operational configurations, when employing intermittent osmotic backwashing of the system. Three CFVs were selected, based on the recoveries attained at the respective operating conditions. According to the literature study, the system recovery is directly correlated with the concentration factor of the feed stream, thereby dictating the degree to which scaling ions will be concentrated in the feed stream. The characteristics associated with the factors identified in Phase 2 then dictate the levels of the factors for Phase 3.

The aim of Phase 3 was to investigate the implementation of the continuous osmotic backwashing principle with a typical gypsum scalant feed solution. The responses to be measured were (1) the extent of flux recovery possible with the implementation of the fouling control strategy, (2) how the system recovery is affected in comparison to the standardised conditions, and finally, (3) the financial implications of the method in terms of product water lost, due to contamination during the switching

from one configuration to the other, and *vice versa*, with the implementation of osmotic backwashing. The materials required and the methods followed to approach the above experimental process are detailed in the sections to follow.

4.3. Materials

The materials required to execute this study are listed in the sections to follow.

4.3.1. Chemicals

As stated in Section 2.2.2.2, thorough criteria have been developed in literature to select application-specific draw solutes to use. The three main draw solutes considered for this study were:

- (1) Sodium chloride (NaCl);
- (2) Magnesium chloride (MgCl₂) and;
- (3) Sodium Sulphate (Na₂SO₄).

These solutes were evaluated based on cost, availability and the ease with which high osmotic pressures can be attained. Furthermore, the effects of these ions on factors such as membrane scaling, CP and RSF, were also investigated. The main findings are listed in Figure 4-2 and Figure 4-3.

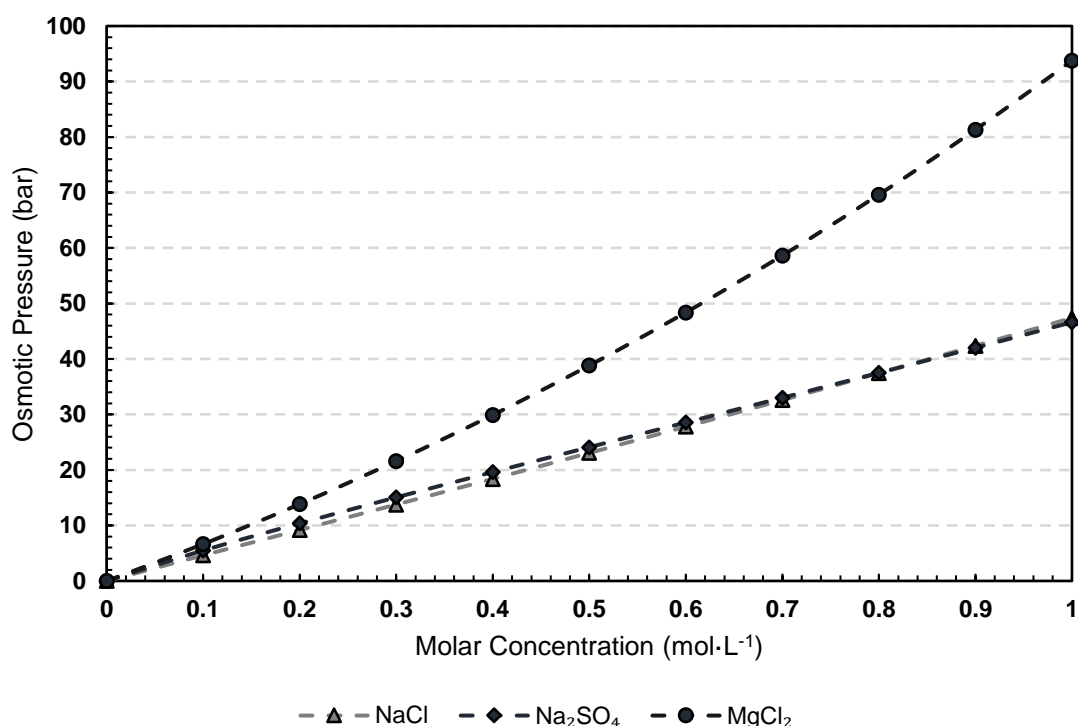


Figure 4-2. Osmotic pressure (bar) curves (generated in *OLI Stream Analyser*) for three of the most common inorganic solutes used for generating high osmotic pressures as draw solution solutes at 20°C.

CHAPTER 4: Materials and Methods

Although the composition and the concentration of the DS solutes dictate the solution osmotic pressure, the actual system driving force is also controlled by the diffusivity, and subsequently the viscosity of the solutes [26]. While the calculated osmotic pressure of MgCl_2 is much higher than NaCl , as depicted in Figure 4-2, its viscosity and diffusivity is lower, which in turn can result in subsequent CP effects, affecting the water fluxes attained detrimentally [17,34,42].

As indicated in Section 2.1.3.1, solute-solute interactions dictate the rate of ionic diffusivity through membranes. To investigate the ionic diffusion through the system, the dominant ions were identified and the rate of diffusion as a function of the molar concentration was modelled in *OLI Stream Analyser*. Recalling that, depending on the method of evaluation for ionic mobility (either via diffusion coefficients or via the change in conductivity), the rates of diffusion of ionic species will differ. As the DS systems were simulated, the method followed for the diffusion coefficients were used to identify the dominant ions. These results are detailed in Figure 4-3.

A trade-off exists between the rate of diffusivity, RSF and CP. The higher the diffusivity of the ion, the greater the RSF of the system will be, but the lower the effects of CP. The lower the rate of diffusivity, the more prominent the effects of CP, but the lower the effects of RSF. The ideal draw solute would then be required to only moderately affect the extent of RSF and CP within the system, whilst still generating an acceptable osmotic pressure. Due to the enhanced diffusivity of the monovalent sodium ions, and the fact that sodium does not act as a scaling precursor ion, NaCl was identified as a suitable draw solute for this investigation.

The findings of intermittent osmotic backwashing will be extrapolated to a typical scaling solution. The effectiveness of intermittent osmotic backwashing was then evaluated, based on the flux recovery of the system. Therefore, two feed solutions were utilised in this study. Firstly, deionised water was used as the feed solution for validating the membrane performance. With the conclusion of the baseline tests, typical scaling tests commenced to extrapolate the findings of intermittent flow path switching to industrial applications. The feed solution then comprised a host of scaling precursor ions, namely Na^+ , SO_4^{2-} , Ca^{2+} and Cl^- , and can be characterised as a quaternary ionic system.

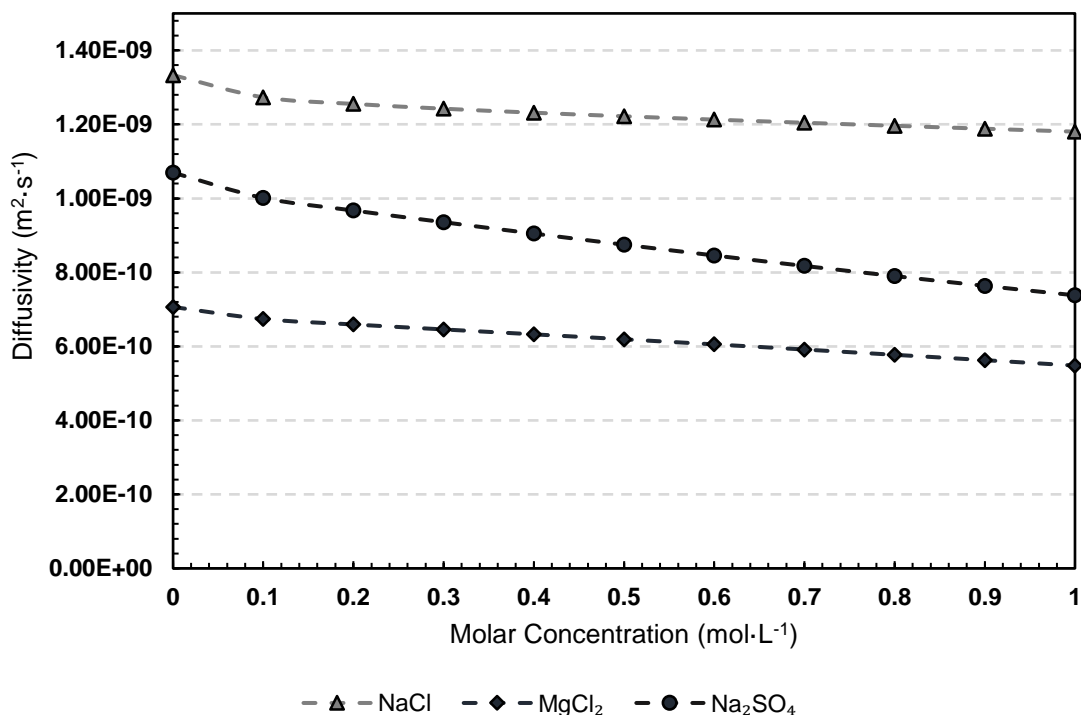


Figure 4-3. Ion diffusivity curves (generated in *OLI Stream Analyser*) for three of the most common inorganic solutes (Na^+ in NaCl , Mg^{2+} in MgCl_2 and SO_4^{2-} in Na_2SO_4), used for generating high osmotic pressures as draw solution solutes at 20°C .

Table 4-1 summarises the main chemicals used in this study, as well as the supplier and the purity of the respective chemicals. These chemicals were used as received and no further purification was done.

Table 4-1. Chemicals, chemical suppliers and purity of chemicals used for the FS and the DS.

Chemical	Supplier	Purity	Assay	Use
Na_2SO_4	Merck	UniVAR	98%	Gypsum FS simulation.
CaCl_2	Merck	UniVAR	98%	Gypsum FS solution.
SMBS	Sigma-Aldrich	Analytical Grade	98%	Membrane storage.
MgCl_2	Merck	UniVAR	98%	DS
NaCl	Makro	Food grade iodated salt	99.5%	DS

To investigate the amount of calcium required to reach certain levels of saturation, the saturation index (SI) was modelled using equilibrium speciation modelling programs, Minteq and Phreeqc. These programs are freely available online. The SI of a solution can be defined as an index, showing whether a particular mineral will dissolve or precipitate in water. The higher the SI of a solution the more oversaturated the solution. The simulation results are presented in Figure 4-4. Furthermore, a parameter named the supersaturation factor (SSF), was defined as the factor by which the saturation concentration of calcium (Ca^{2+}) was multiplied. Recall that the concentration of Ca^{2+} in a saturated gypsum solution is $\sim 630 \text{ mg}\cdot\text{L}^{-1}$. Gypsum saturation in the system was defined based on the

CHAPTER 4: Materials and Methods

oversaturation of Ca^{2+} ions in the system, as this is the divalent cation in the quaternary ionic system. Effectively, the saturation concentration along with the SSF were used to calculate the ionic quantities of the other ions (Na^+ , SO_4^{2-} and Cl^-). Sample calculations of this method are detailed in Appendix B.1.

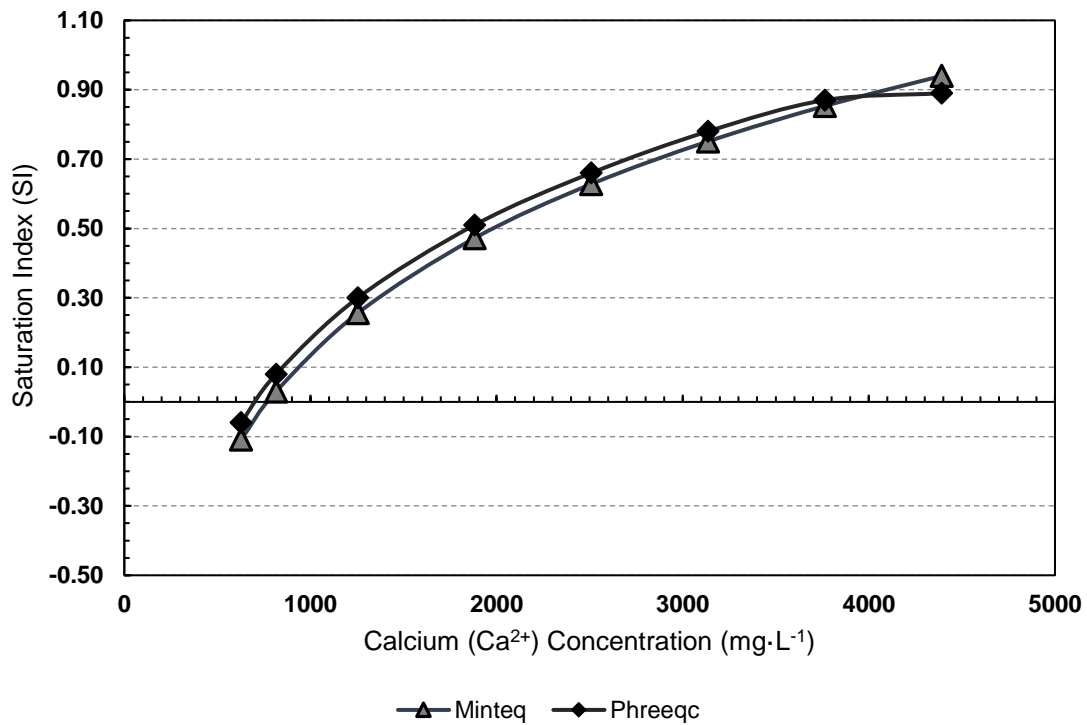


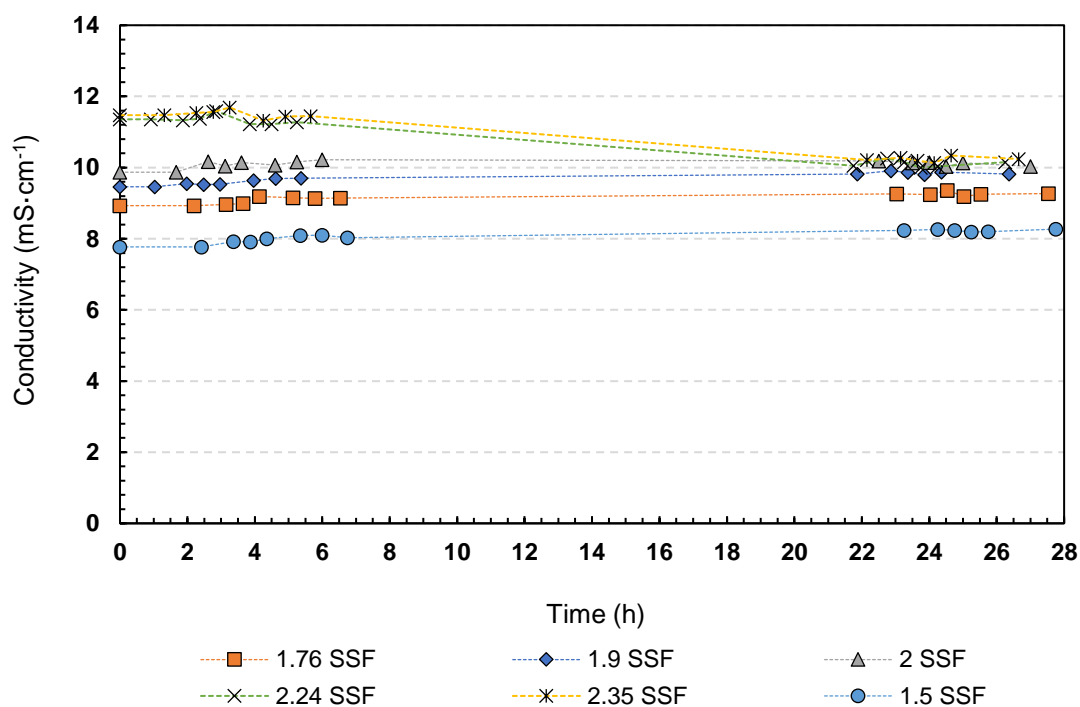
Figure 4-4. Calcium concentration corresponding to the various saturation indices as modelled in Minteq and Phreeqc.

In membrane systems, the rate at which gypsum crystals form is highly dependent on the concentration factor of the feed solution, which correlates directly to the recovery at which the system operates. The SI of the feed solution increases exponentially with the increase in the FS calcium concentration. It is expected that the SI index will reach a plateau at the same point, whereby the addition of calcium will be futile. Ensuring gypsum scaling in membrane systems via operating at a certain SI index, is strongly dependent on the system recovery. Hence, the system recovery at various CFVs requires quantification first. The effect of the system recovery and subsequently the concentration factor on the increase of the scaling potential (reflected in the SI of the solution) of a feed solution containing Ca^{2+} and SO_4^{2-} in equal molar parts, are presented in Table 4-2.

Table 4-2. Initial and final Ca^{2+} concentration at a 20% recovery, assuming no RSF in the system.

Initial Ca^{2+} Concentration ($\text{mg}\cdot\text{L}^{-1}$)	Initial SSF	System Recovery (%)	Concentration Factor	Final Ca^{2+} Concentration ($\text{mg}\cdot\text{L}^{-1}$)	Final SSF
940.88	1.5	20	1.25	1176.10	1.87
1103.96	1.76	20	1.25	1379.95	2.20
1191.78	1.9	20	1.25	1489.73	2.37
1254.50	2	20	1.25	1568.13	2.50
1405.04	2.24	20	1.25	1756.30	2.80
1474.04	2.35	20	1.25	1842.55	2.94

Jar tests were conducted to investigate the time for gypsum crystal formation at the initial SSF listed in Table 4-2. The conductivity of the solution was monitored to investigate if the mobility of the ions in solution will decrease, due to the formation of solid gypsum crystals, thereby decreasing the ionic activity in the solution. This also provided insight into how scale formation in membrane systems could potentially alleviate RSF, but detrimentally affect flux performance. The results of the jar tests are given in Figure 4-5.

**Figure 4-5.** Jar tests to investigate how gypsum precipitation will affect conductivity measurements. Experiments were conducted at a temperature of 20°C.

As per Figure 4-5, it is clear that after 22 hours at an SSF of 2.24 and 2.35, the formation of gypsum precipitation is evident from the decrease in conductivity, due to the ions in solution decreasing. Combining the effects of calcium (Ca^{2+}) oversaturation and increased recovery, would bring about gypsum scaling on the membrane surface in experimental runs of 30 hours or longer. Other factors

CHAPTER 4: Materials and Methods

which may contribute to the enhancement of gypsum scaling in the system is the vortex formation in the feed tanks, due to the continuous pump action from of the feed tank.

At a recovery of 20% an SSF of 2.37 is achieved with an initial gypsum feed solution having a Ca^{2+} SSF of only 1.9. Should the recovery achieved be higher (depending on the operating conditions such as the CFV), lower initial Ca^{2+} SSF would be required to attain gypsum scaling at the end of the FO process train. Therefore, gypsum feed solutions with an SSF of 1.6 and 1.9 were synthesised in this study to investigate the fouling control strategy. The feed solution is composed of the following two salts: $\text{CaCl}_2 \cdot 2\text{H}_2\text{O}$ and Na_2SO_4 . The ionic composition of the feed solution at a Ca^{2+} SSF of 1.6 and 1.9 is detailed in Table 4-3.

Table 4-3. Gypsum feed solution make-up at an SSF of 1.6 and 1.9 comprising $\text{CaCl}_2 \cdot \text{H}_2\text{O}$ and Na_2SO_4 .

SSF	Na^+ (mg·L ⁻¹)	Ca^{2+} (mg·L ⁻¹)	SO_4^{2-} (mg·L ⁻¹)	Cl^- (mg·L ⁻¹)	$\text{CaCl}_2 \cdot 2\text{H}_2\text{O}$ (mg·L ⁻¹)	Na_2SO_4 (mg·L ⁻¹)
1.6	1151.34	1003.60	2405.58	1775.57	7363.11	7113.69
1.9	1367.22	1191.78	2856.63	2108.49	8743.69	8447.51

4.3.2. FO Membrane

The spiral wound FO membrane used in this study was acquired by CSM, a subsidiary of the Toray Water group. As literature studies specifically related to FO do not explicitly list the exact membrane which was used, it was difficult to be sure that the membranes used in the listed studies were the same, even if stated that it is the same supplier. Only one known study has used a similar membrane as documented by Kim et al. [116].

The exact chemistry of this membrane is proprietary; however, certain characteristics are known and are listed in Table 4-4. Intrinsic morphological parameters inherent to the membrane were not determined via high pressure RO characterisation. These parameters are a function of the water flux measured, hence only flux evaluation was conducted.

Table 4-4. CSM spiral wound FO-8040 membrane characteristics.

Characteristic	Description
Membrane Thickness	100 μm
Membrane Type	TFC with polyamide coating
Water Flux ($\text{L} \cdot \text{m}^{-2} \cdot \text{h}^{-1}$)	35 ± 3
Specific Reverse Solute Flux of NaCl ($\text{g} \cdot \text{L}^{-1}$)	< 0.5
Operational Lifetime	Application and usage dependent
Shelf Life	Minimum 6 months
Operation pH Range	2 - 11

The membrane ordered was an 8" (20.32 cm) spiral wound membrane. Upon the reception of the membrane it was sealed in an air tight durable plastic bag and stored in an SMBS solution to prevent it from drying out and to minimise the occurrence of biological growth on the membrane surface. The membrane was disassembled in order to extract the actual membrane sheets from the rolled-up leaves inside the spiral wound membrane. Six 300 × 100 mm flat sheet membranes were cut from the respective membrane leaves, upon which the membrane was rolled-up into its spiral wound form and stored in the air tight plastic bag with a 1wt% SMBS solution away from direct sunlight.

The membrane was analysed via the use of a scanning electron microscope (SEM) analysis (Zeiss Electron Microscope) via the *Central Analytical Facility (CAF)* at Stellenbosch University. This was done to gain a better understanding of the morphological differences between the AL and the SL of the membrane. The cross-sectional area of the membrane, with surface photographs of the AL and the SL, are documented in Figure 4-6.

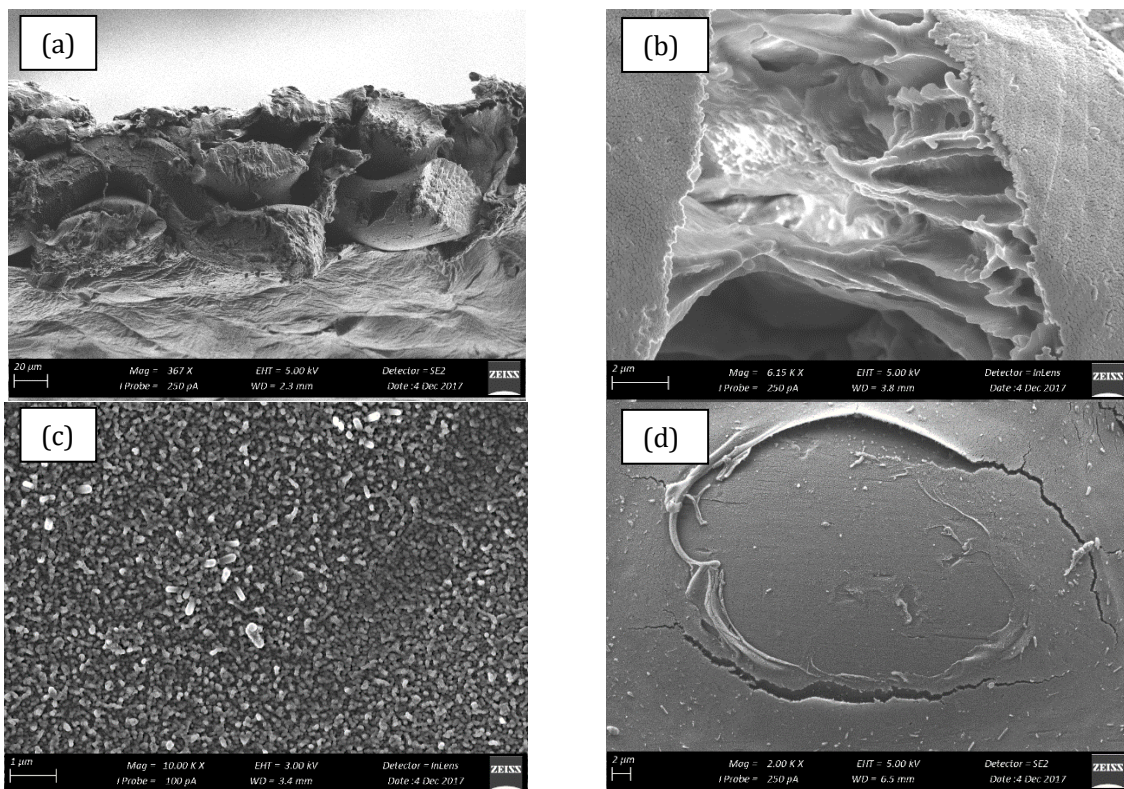


Figure 4-6. SEM images for the (a) cross section between the support layer (top) and the active layer (bottom) indicating the porosity of the support layer, (b) tortuosity of the support layer whereas (c) surface of the active layer and (d) surface of the support layer.

4.4. Experimental Procedures

The detailed approach-process followed to address the objectives as set out by this study, is provided in Figure 4-1. The experimental procedures were subdivided into three distinct phases. The experimental procedures followed to address each phase are detailed below.

4.4.1. Phase 1: Validation Tests

The primary aim of the validation tests was to characterise the operability of the system in terms of the operating CFVs, the performance parameters attained at these various CFVs, and the two operational configurations of the membrane. This subchapter is divided into two subsequent sections: (1) membrane standardisation and (2) FO characterisation tests.

4.4.1.1. Membrane Standardisation

Initial standardisation results showed that the system required 1–2 hours to stabilise and allow for the membrane to purge itself from the residual SMBS storage solution. Depending on the flow velocity, this allowed for a minimum of five system volume displacements for flushing. A set of standard operating conditions was only deduced in 2013 and is not even established in research communities at this point. Many research groups merely follow their own standardisation procedure, thereby making data comparison a challenging task. A list of standard operating conditions, mainly employed in literature, is recorded in Table 2-10.

It is clear from Table 2-10 that no clear standardisation protocol is in place for FO data standardisations. Standardisation tests were conducted with a 0.5 M NaCl solution as the DS (29 220 mg·L⁻¹), and deionised water as the FS. The respective feed tank temperatures were kept constant at 24°C.

4.4.1.2. FO Characterisation Tests

The first part of this study entailed investigating normal membrane operation with a high salinity 0.5 M DS (30 000 ± 2000 mg·L⁻¹ TDS) and normal RO permeate water (<10 mg·L⁻¹ TDS). This was done to evaluate the flux of a typical industrial scale FO membrane without the presence of foulants in the system. Furthermore, the extent of RSF could be established as various literature studies, detailed by Table 2-2, have shown that the membrane rejections attained by FO membranes are not comparable to typical RO membranes.

Although the experimental setup was verified as discussed in Chapter 3, the first set of baseline tests served as an experimental setup validation mechanism. The repeatability of flux curves, water recoveries and solute rejections attained, were evaluated with the first set of baseline tests. This was done specifically to account for factors such as the heterogeneity as well as the maturation of the membrane.

The parameters, levels and set-points for investigation for the validation part of the experimental work are listed in Table 4-5.

Table 4-5. Experimental design to investigate the effect of CFV and membrane orientation on membrane performance parameters such as flux, recovery and solute rejections. Secondary parameters that are evaluated are CP moduli and RSF.

Parameter	UOM	Levels	Set Point
Cross-Flow Velocity	cm·s ⁻¹	5	9
			15
			19
			25
			35
Membrane Orientation	-	2	AL-FS
			AL-DS

Certain conditions were kept constant during each experimental run to ensure that the data would not be skewed by experimental noise. These operating parameters are listed below:

- (1) Solution Temperature: Each feed tank was equipped with a thermostat where the solution temperature was kept constant at 24°C.
- (2) Solution pH: Neither acid nor base were added to the respective FS and DS, therefore the solution was kept at a natural neutral pH.
- (3) DS Concentration: It was not in the scope of this study to vary the driving force of the process; therefore, the draw solute concentration was kept constant throughout at 30 000 mg·L⁻¹ TDS.

The measurements that were taken, comprised of (1) the respective inlet and outlet flow rates, (2) the conductivity of the DS and FS inlet and outlet solutions and (3) noting the feed pressures to the FO process train.

4.4.2. Phase 2: Intermittent Flow-Path Switching

After characterising the membrane performance at various CFVs and per the two operational configurations, intermittent flow-path switching was investigated. Intermittent switching of the flow-path reverses the direction of water permeation for a said amount of time. In order to investigate the intermittent reversal of the direction of water permeation, two main factors require investigation. These factors also formed part of the identified design requirements of the experimental setup. The main factors were: (1) optimum time required for flushing and (2) the time required to attain stable operation. It is expected that the stable performance of the membrane after the flow-path switching be the same as for the membrane performance confirmed during the validation tests.

The mechanics underpinning the intermittent flow-path switching from the AL-FS configuration to the AL-DS configuration, and vice versa, were studied by conducting prolonged continuous switching experimental runs. The length of these runs was approximately 30+ hours, with operation in each configuration for approximately 8 ± 2 hours. Table 4-6 highlights the CFVs which were investigated.

CHAPTER 4: Materials and Methods

Table 4-6. Experimental design for investigation of the intermittent osmotic backwashing.

Parameter	UOM	Levels	Set Point		
Cross-Flow Velocity	cm·s ⁻¹	3	9	19	35

As per Table 4-6, three CFVs were investigated as opposed to the five in Phase 1 of the study. Mainly, the CFVs as per Table 4-6 were chosen as they provided a good representative sample of all the CFVs investigated. Again, the CFV was evaluated based on the errors and uncertainties associated with the system mechanical design.

4.4.3. Phase 3: Practical Implementation

The findings of Phases 1 and 2 were extrapolated to a FS which mimicked a typical industrial effluent stream, by being saturated with Ca²⁺ and SO₄²⁻ ions. The scaling potential of a FS is highly dependent on the recovery of the system, which in turn is a function of the system CFV, which in turn is a function of the feed flow rate (Q_F), as demonstrated in Chapter 3. Phase 3 investigated the efficiency of integrated flow-path switching when employed intermittently as a fouling control strategy. The efficiency of the strategy was monitored via flux recovery of the system, after flux declines were observed due to scaling. Mainly variations in the CFV and the SI of the feed solution were the manipulated variables.

The factors of investigation are tabulated in Table 4-7.

Table 4-7. Experimental design for the investigation of continuous osmotic backwashing for a typical industrial effluent stream.

Parameter	UOM	Levels	Set Point	
Cross-Flow Velocity	cm·s ⁻¹	3	9	19
			35	
			1.6	1.9
SFF	-	2		

It is important to note is that scaling typically occurs at the end of membrane process trains. Therefore, relatively high SIs were investigated to mimic the end of a typical process train.

4.5. Analytical Methods

The ionic diffusion of Na⁺ and Ca²⁺ across the membrane was evaluated by analysing for the concentration of these ions in the inlet and outlet solutions for the FS and the DS, respectively. Quantifying the ionic diffusion of these ions provided valuable insight into the transport phenomena of the FO membrane, specifically pertaining to CP and RSF.

4.5.1. Calcium Ions (Ca^{2+})

Ca^{2+} ions were analysed via ICP-MS (Inductively Coupled Plasma – Mass Spectrometry). Based on the concentration factor, which is a function of the water recovery of the system, supersaturation (SS) indices (SI) could be quantified and the calcium concentration at each of these indices could be estimated. This provided valuable insight to the dilution factor required for Ca^{2+} analyses.

Figure 4-7 visually represents the difference between the theoretical calculated calcium concentration at a certain degree of SS, and the actual calcium concentration observed when a gypsum solution at the same degree of SS was made up. Equimolar quantities of Ca^{2+} and SO_4^{2-} ions were present in solution at the respective SSFs. The theoretical and actual Ca^{2+} concentrations were compared to estimate the error associated with the experimental analysis of the Ca^{2+} ion concentration. It is evident from Figure 4-7 that the higher the degree of supersaturation, the greater the deviation between the theoretical predicted Ca^{2+} concentration and the actual solution calcium concentration. This clearly indicates the hygroscopic nature and the effects of calcium hydration when preparing any calcium dihydrate solution. It is of paramount importance to analyse for the actual concentration of Ca^{2+} ions in the stock solutions.

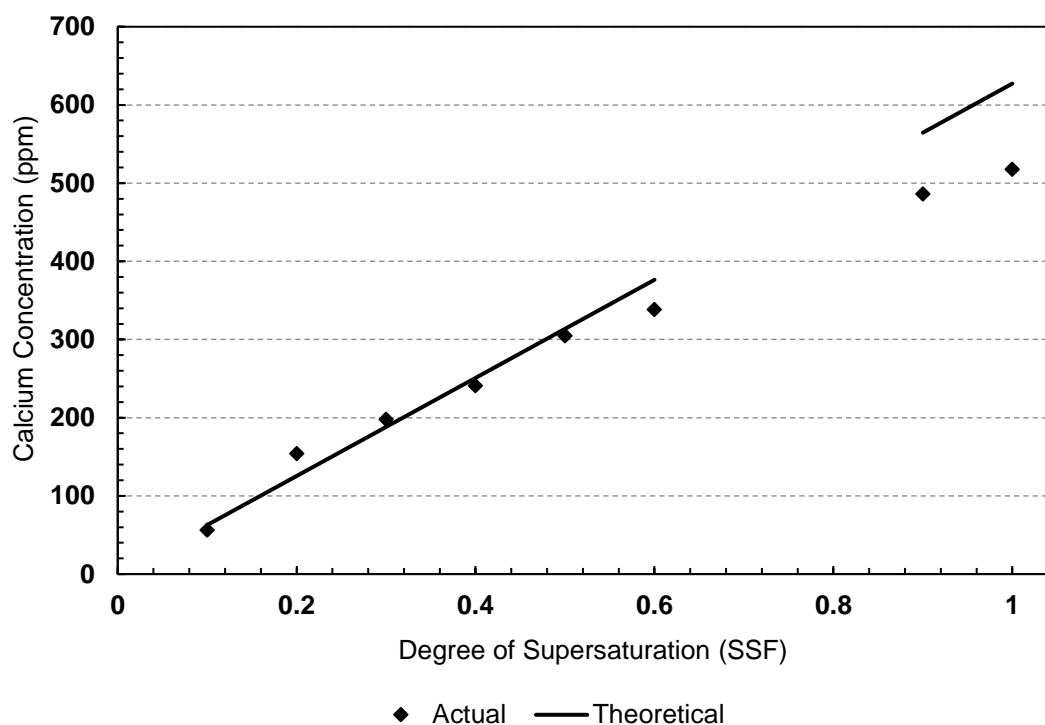


Figure 4-7. Typical Ca^{2+} concentrations for various degrees of supersaturation in gypsum solution.

4.5.2. Sodium Ions (Na^+)

For the analysis of the Na^+ ions in solution, atomic absorption spectroscopy (AAS) was used. The principle that was employed in this method was the introduction of the sample to a flame (with flame photometry). The light from the hollow cathode was then passed through the flame. The quantity of light absorbed at a selected wavelength is measured, and the analysis of the sample is then determined

CHAPTER 4: Materials and Methods

[118]. The dilution error in this method is automatically corrected via the sodium standards used for AAS calibration prior to analyses.

Chapter 5

Results and Discussion

This study endeavoured to expand our understanding of FO operation, with the **primary aim** to critically evaluate and characterise the mass transfer and membrane fouling behaviour, specifically considering:

- the effects of cross-flow velocity (CFV),
- the effects of operational configuration (whether the AL is facing the FS or the DS),
- the effects of intermittent switching of the flow path, as a combination of flushing and osmotic backwashing, and
- the practical realities related to flow-path switching when treating feed water saturated with gypsum.

The approach-process deduced in Chapter 4 provides the framework for this Chapter in which the experimental findings of the procedures in Chapter 4, are given.

5.1. System Validation & Characterisation

The operability and characterisation of an industrial FO membrane was investigated by evaluating and quantifying the mass transfer within the system. The mass transfer in a membrane system used for water purification is mainly quantified via the water flux. In broad terms this would be sufficient; however, the mass transfer of draw solutes also plays a pronounced role in the operability of the system. This is due to the transport effects of CP and RSF prevalent in FO systems. These transport phenomena are affected by mechanical parameters such as the CFV of the system, along with a host of other process parameters such as the solute mobility, DS concentration and operating temperature.

The system validation and characterisation endeavoured to quantify the performance indicators of the system. These indicators (water flux, water recovery and solute rejections) are evaluated based on changes in the system CFV and the operational configuration. The uncertainties associated with the mechanical design of the system have already been evaluated and quantified. Therefore, the effects of process parameters such as variations in the CFV and the operational configuration, can now be investigated while accounting for and incorporating the uncertainties in the mechanical design.

The validation experiments were conducted in duplicate and some in triplicate, in order to gain an overview of the error associated with readings, and to be able to construct a realistic error margin. A *baseline* curve was then constructed based on the average fluxes. This was used as an operational

CHAPTER 5: Results and Discussion

guideline at standard operating conditions. Furthermore, all of the data presented were normalised to the conditions stipulated in Table 5-1. This was done to compare data sets at the same standard conditions and to minimise data fluctuations, due to variances in the initial driving force of all the conducted experiments. It is important to note that the performance indicators can be evaluated either by considering the DS or the FS. Hence, water flux can be measured either by evaluating the water volume gained by the DS, or the water volume lost by the FS. Theoretically, the measured fluxes determined from the DS and the FS should be equal; however, as indicated in Table 3-3, measuring errors are made when measuring the respective volumetric flow rates of the solutions.

Table 5-1. Standard operating conditions to which measured data were normalised.

Operating Condition	Process Parameter	Value
Temperature (°C)	Draw Solution	20
Driving Force	Osmotic Pressure, $\Delta\pi$ (bar)	27
	Mechanical Over Pressure, ΔP (bar)	0

As detailed in Chapter 3 – Section 3.5.1.1 – the sensitivity analysis for the evaluation of the CFV indicated that uncertainties relating to the spacer porosity and the channel height has a significant impact on the assumed operation CFV. This, however, could be corrected for by evaluating the recovery of the system and using Equation (3.4) to calculate the actual operating CFV. Initially, the CFVs identified were 9, 15, 19, 25 and 35 $\text{cm}\cdot\text{s}^{-1}$. These velocities were chosen, based on the modal CFV of 25 $\text{cm}\cdot\text{s}^{-1}$ as established in the research community and also on the pump capacity. However, after correction by incorporating the mechanical uncertainties, these CFVs translated to 13, 21, 28, 37 and 52 $\text{cm}\cdot\text{s}^{-1}$. *Throughout, these were then the CFVs that were used to evaluate the operation of the FO system.* This translated to flow rates of 97 $\text{mL}\cdot\text{min}^{-1}$, 155 $\text{mL}\cdot\text{min}^{-1}$, 207 $\text{mL}\cdot\text{min}^{-1}$, 272 $\text{mL}\cdot\text{min}^{-1}$ and 382 $\text{mL}\cdot\text{min}^{-1}$. The Reynolds number for these flow rates are >2300 and therefore the system operates in the turbulent flow regime throughout. The flux versus time curves are presented in Figure 5-1 to Figure 5-6.

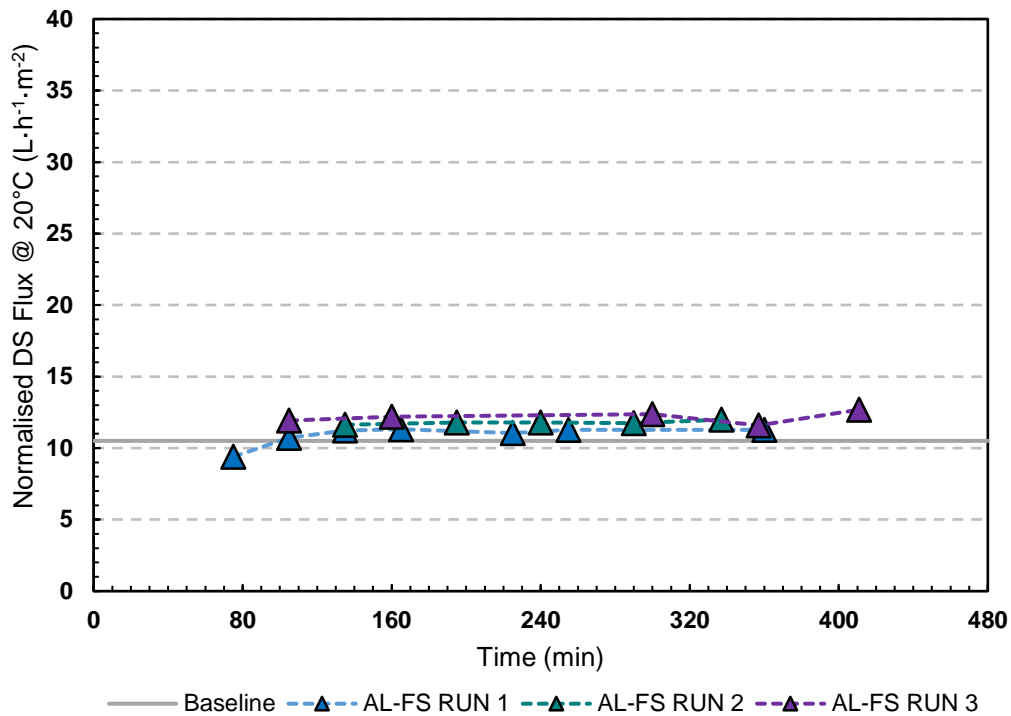


Figure 5-1. Experimental runs done in triplicate to determine the baseline flux curve at a CFV of 13 cm·s⁻¹ in the AL-FS configuration. The standard operating conditions were the same, with the FS being deionised water and the DS being a 0.5 M NaCl solution. Data normalised to a temperature of 20°C and a driving force of 27 bar.

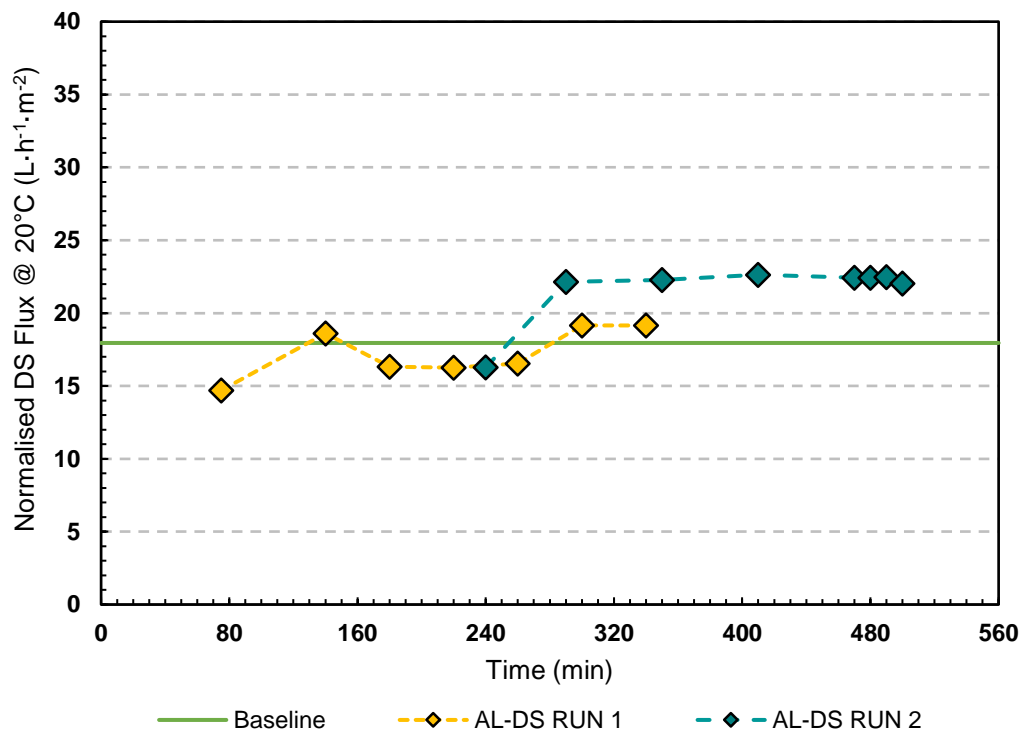


Figure 5-2. Experimental runs done in duplicate to determine the baseline flux curve at a CFV of 13 cm·s⁻¹ in the AL-DS configuration. The standard operating conditions were the same, with the FS being deionised water and the DS being a 0.5 M NaCl solution. Data normalised to a temperature of 20°C and a driving force of 27 bar.

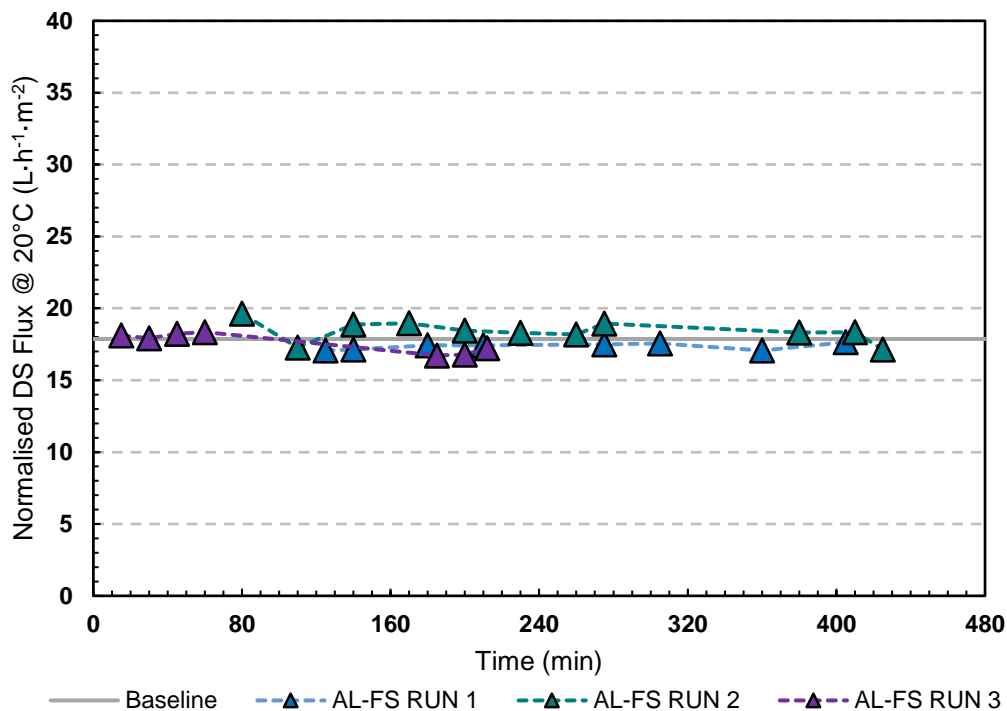


Figure 5-3. Experimental runs done in triplicate to determine the baseline flux curve at a CFV of 28 cm·s⁻¹ in the AL-FS configuration. The standard operating conditions were the same, with the FS being deionised water and the DS being a 0.5 M NaCl solution. Data normalised to a temperature of 20°C and a driving force of 27 bar.

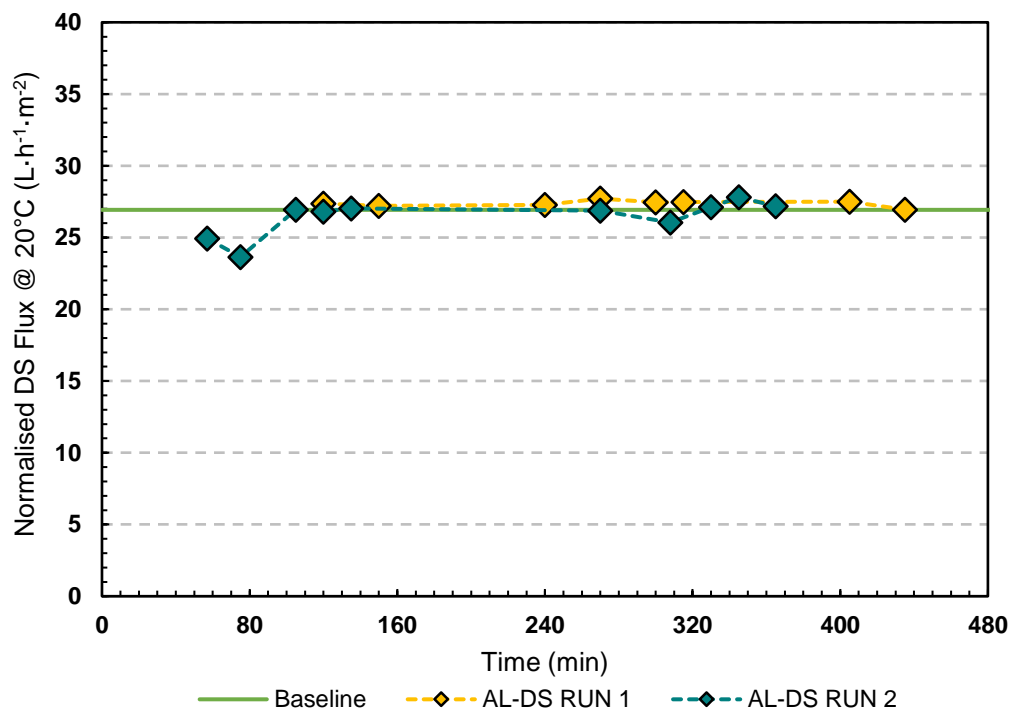


Figure 5-4. Experimental runs done in duplicate to determine the baseline flux curve at a CFV of 28 cm·s⁻¹ in the AL-DS configuration. The standard operating conditions were the same, with the FS being deionised water and the DS being a 0.5 M NaCl solution. Data normalised to a temperature of 20°C and a driving force of 27 bar.

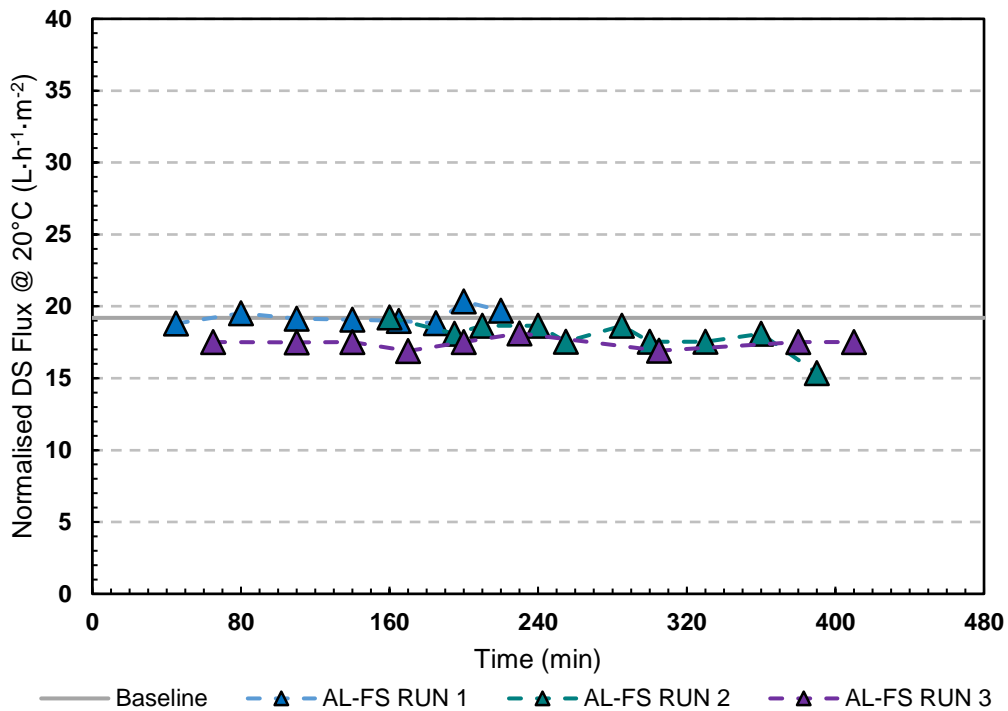


Figure 5-5. Experimental runs done in triplicate to determine the baseline flux curve at a CFV of 52 cm·s⁻¹ in the AL-FS configuration. The standard operating conditions were the same, with the FS being deionised water and the DS being a 0.5 M NaCl solution. Data normalised to a temperature of 20°C and a driving force of 27 bar.

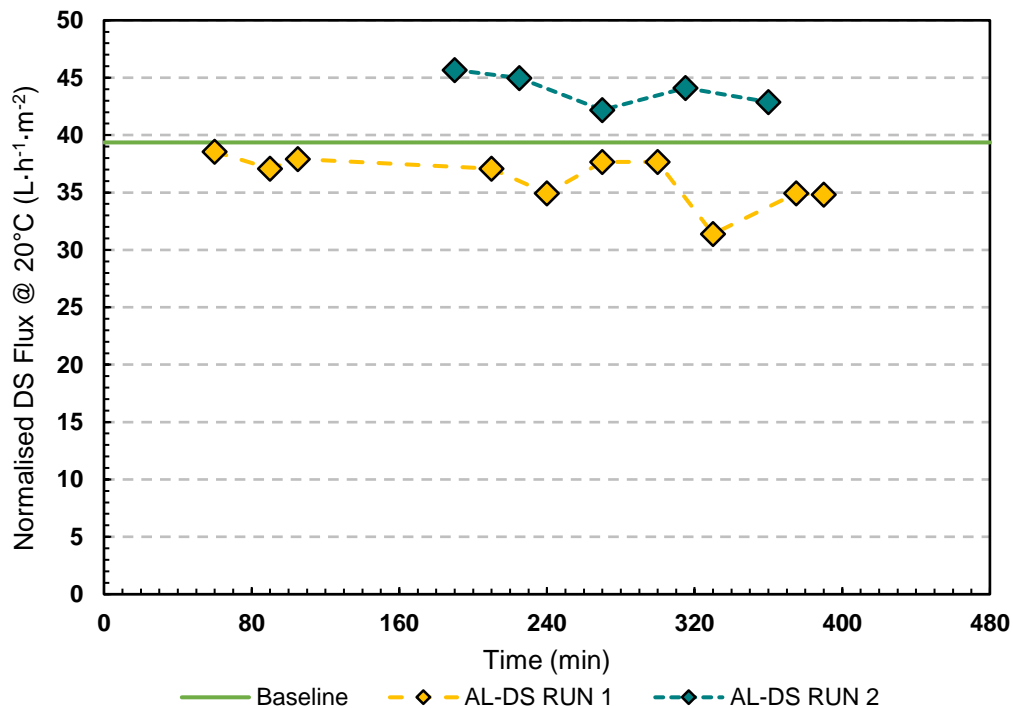


Figure 5-6. Experimental runs done in duplicate to determine the baseline flux curve at a CFV of 52 cm·s⁻¹ in the AL-DS configuration. The standard operating conditions were the same, with the FS being deionised water and the DS being a 0.5 M NaCl solution. Data normalised to a temperature of 20°C and a driving force of 27 bar.

CHAPTER 5: Results and Discussion

A summary of the average values of the verification data is presented in Table 5-2. The measured recoveries are indicated along with the absolute error associated. The absolute error was calculated based on what the theoretical recovery should be at the measured flux [see Equation (3.3)]. The measured recovery and the calculated recovery using Equation (3.3) should be the same – resulting in an absolute error of zero. This is indicated via manipulation of Equation (3.3) and substituting Equation (2.4) and Equation (3.5), resulting in Equation (5.1).

$$R = \frac{Q_F - Q_B}{Q_F} = \frac{\left(\frac{Q_F - Q_B}{A_m}\right) \times A_m}{Q_F} = \frac{J_w \times A_m}{Q_F} \quad (5.1)$$

The absolute error in the measured flux is attributed to the measuring errors associated with the respective feed and draw solution flow rates. The water flux measured was evaluated based on the DS flow rates, and the recovery was based on the FS flow rates. The absolute errors associated with the recovery then inherently represented the cumulative measurement errors made with the in-line flow rate measuring columns. The calculated recovery [based on the measured flux – see Equation (3.3)], incorporating the measurement error, was then used to evaluate the accuracy of the operating CFV of the system [see Equation (3.4)].

Table 5-2. Average water fluxes, recoveries and draw solute rejections attained for 0.5M NaCl DS and deionised water as the FS, with data normalised to 20°C and a driving force of 27 bar.

Experimental CFV (cm·s ⁻¹)	Operational Mode	Water Flux (L·m ⁻² ·h ⁻¹)	Water Recovery (%)		Draw Solute Rejections (%)
		Absolute Value	Absolute Measured Value	Absolute Error (%)	Absolute Value
13	AL-FS	11.23	31.53	5.60	98.93
	AL-DS	17.95	45.89	4.44	97.50
21	AL-FS	16.88	28.73	4.34	99.48
	AL-DS	23.27	40.57	6.94	97.72
28	AL-FS	17.88	21.76	2.41	99.42
	AL-DS	26.94	33.76	4.61	98.09
37	AL-FS	19.6	16.22	0.08	99.36
	AL-DS	31.24	30.54	4.81	98.34
52	AL-FS	19.2	13.29	2.03	99.81
	AL-DS	39.36	24.19	1.11	98.76

Uncertainties in the measured flux were quantified based on the fluctuations in the measured data. An error band was constructed based on these fluctuations for the maximum and minimum flux values, based on duplicate and triplicate experimental runs. The upper and lower uncertainty limits in the measurement of flux are shown in Figure 5-7 for the AL-FS configuration, and in Figure 5-8 for the AL-

DS configuration. These uncertainties are attributed heterogeneity in the membrane morphology, as new membrane coupons were installed for each experimental run. Furthermore, the mass transfer of solutes and water could also give rise to flux fluctuations. The exact quantification of the effects of CP and RSD will be elaborated on.

For the validation experimental runs, the first hour (60 minutes) of each run was regarded as the stabilisation time, and no measurements were taken in this time frame. The flux data indicates that the fluxes attained when operating in the AL-DS configuration are on average 40% higher than the fluxes attained in the AL-FS configuration. This finding corroborated extensive research which had similar results [4,5,25,33].

Figure 5-7 and Figure 5-8 illustrate that the water flux attained by the system is increased when the system is operated at increased CFVs. A limiting flux value of $20 \text{ L}\cdot\text{m}^{-2}\cdot\text{h}^{-1}$ was determined for the AL-FS configuration. Increasing the CFV beyond $37 \text{ cm}\cdot\text{s}^{-1}$ did not translate to increases in the water fluxes measured. The plateau of the measured flux values was also observed by Xu et al., as well as Wijmans et al.[119,120].

These results were consistent with the developed model as per Phuntsho et al. [38] which indicated that increasing the inlet flow rate increases the CFV as well as the cross flow shear at the membrane surface. This increases the mass transfer coefficient as well as the water flux. The equations can be viewed in [38]. In a study conducted by He et al. [121], similar results were found. It was reported that the effect of flow rate (i.e. CFV) on FO fluxes in the concentration of shale gas wastewater, when operated in AL-FS, did not have an effect on FO fluxes. However, when the system was operated with the DS facing the active layer (AL-DS), an increase in FO fluxes was observed.

In contrast to the experimental findings of this study and the study of Phuntsho et al. [38], He et al. [121] found that higher fluxes were attained in AL-FS mode. It was stated that the AL-FS mode provided a much steadier performance when compared to AL-DS, when operated with feed solutions with a tendency to scaling, due to its complex composition.

CHAPTER 5: Results and Discussion

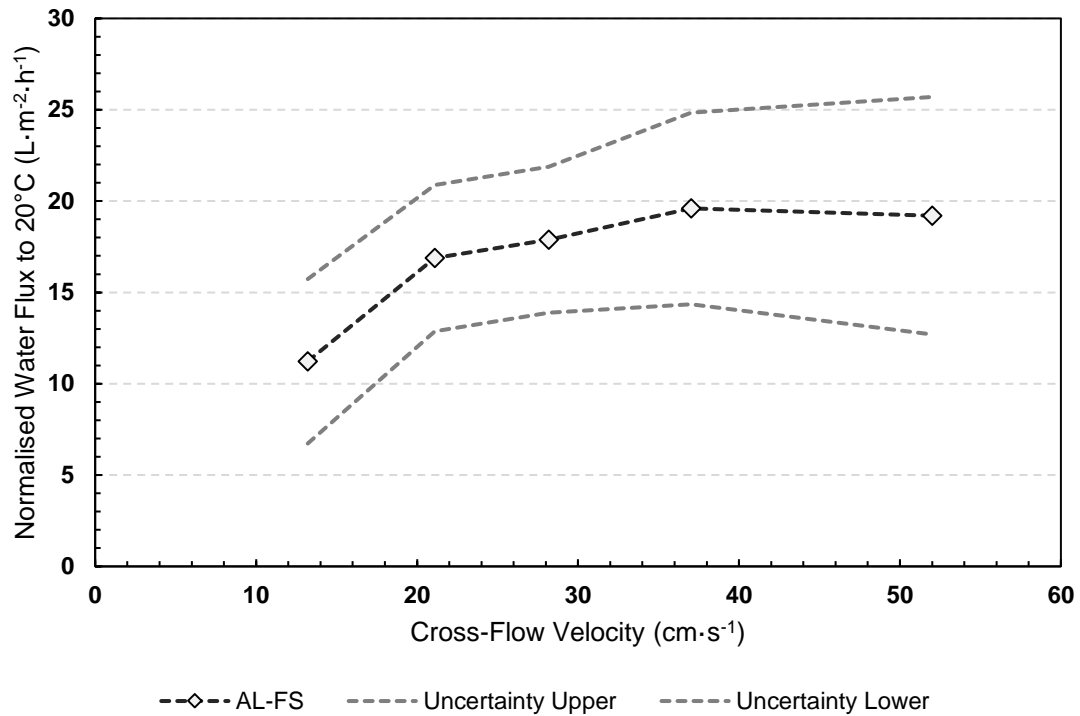


Figure 5-7. Variance in flux at different CFVs ranging from 13 – 52 cm·s⁻¹ when operating in the AL-FS configuration. The FS is deionized water and the DS is a 29 220 mg·L⁻¹ TDS NaCl solution. Data is normalised to 20°C and a driving force of 27 bar.

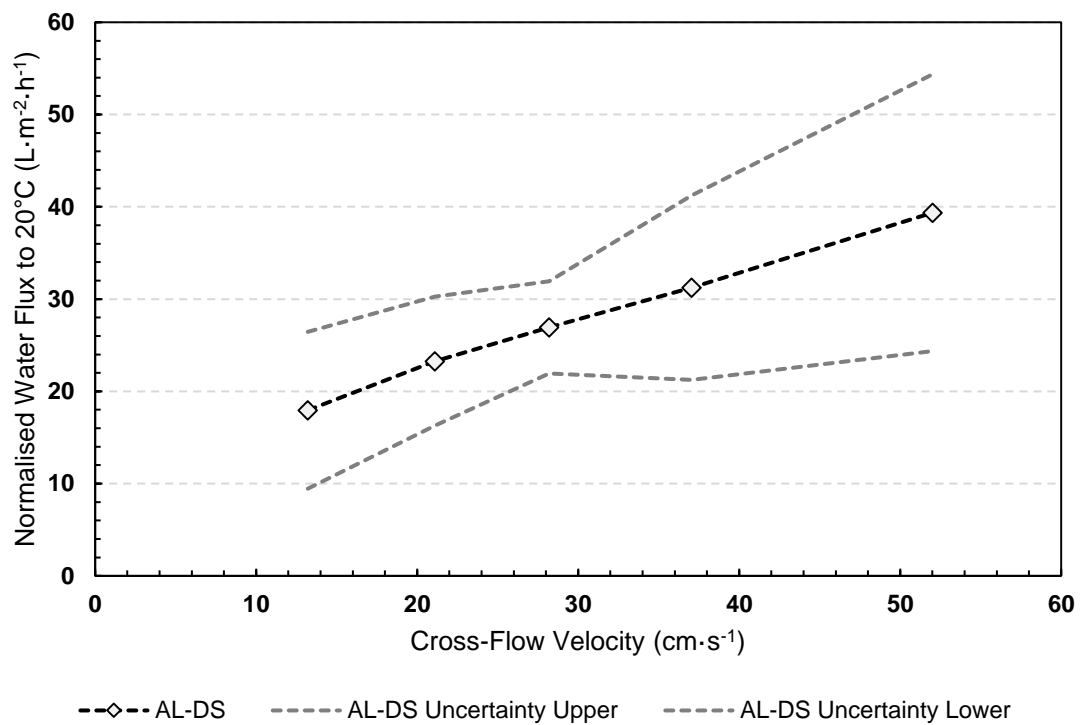


Figure 5-8. Variance in flux at different CFVs ranging from 13 – 52 cm·s⁻¹ when operating in the AL-DS configuration. The FS is deionized water and the DS is a 29 220 mg·L⁻¹ TDS NaCl solution. Data is normalised to 20°C and a driving force of 27 bar.

Two facts are evident from the above constructed flux curves:

- The water flux increases with an increase in CFV (exact reasons for this will be elaborated on below); and
- Increasing the CFV beyond a certain velocity brings about the limiting operating flux of the system, where after the increases in the CFV and the osmotic pressure become futile and will not translate to increases in water flux. For the AL-FS configuration the limiting flux was $20 \text{ L}\cdot\text{m}^{-2}\cdot\text{h}^{-1}$. Conversely, for the AL-DS configuration the limiting flux was not determined, and a linear increase in the water flux was observed when increasing the CFV.

According to the solution-diffusion model, permeates dissolve in the membrane material and then diffuse through the membrane along a concentration gradient [34]. Permeates are thus separated based on variances in the rates at which they diffuse through the membrane. The individual permeant molecules are in constant random molecular motion and have no particular preferred diffusion direction within the membrane material. The average displacement of molecules can be measured, but limited information is available as to which direction the individual molecule will move [34]. It was already determined that permeate molecules will diffuse through the membrane along a concentration gradient. The likelihood of this was proven by statistics.

An Equation was derived by Baker [34] predicting that the increases in the concentration gradient formed within the membrane will translate to an increase in the measured fluxes. This is mainly because the driving force at the membrane-liquid interface at the DS side is increased. At increased concentration gradients the increase in flux will be linear; however, as predicted by the derived equation, there is a certain concentration gradient at which the driving force, and hence the measured flux will plateau, thereby reaching its limiting value.

In FO membrane systems the mass transfer is quantified and evaluated based on the (1) water flux, (2) RSF and (3) CP, where water flux is a function of the mass-transfer coefficients of each channel, RSF is a function of solute mobility, and CP is a function of solute concentrations within the system.

As mass transfer within the FO system is dictated by the solution-diffusion model, the limiting flux can be brought about by two factors: (1) internal concentration polarisation (ICP) and (2) the dilution factor of the draw solution, thereby decreasing the osmotic pressure differential over the membrane. It is well documented that affecting ICP within the support layer by increasing the CFV, is less likely. Xu et al. [119] attributed this to the unstirred boundary layer forming within the support layer of the membrane, thereby resulting in a dilution of the effective salt concentration. In a study conducted by She et al. [48] it was documented that doubling the CFV, resulted in a marginal flux increase of 5%. The flux increases observed when increasing the CFV in this current study, can thus not be solely attributed to an increased mass-transfer coefficient at the membrane-liquid interface. The dilutive effect of the bulk DS was thus also considered.

CHAPTER 5: Results and Discussion

In both operating configurations it was evident that the water recovery decreased as the operating CFV increased. This was verified as per Figure 5-9 for the AL-FS configuration, and Figure 5-10 for the AL-DS configuration.

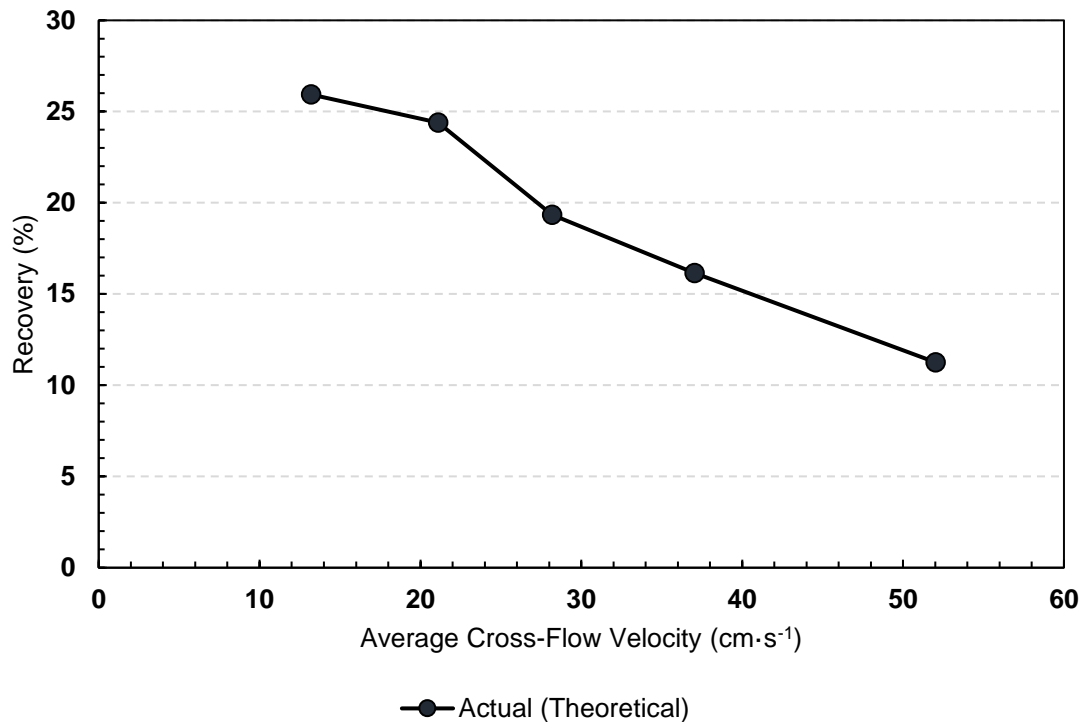


Figure 5-9. The experimentally-measured recovery along with the assumed operating CFV, compared to the calculated recovery and corrected CFV, as per the experimentally-measured water flux for the AL-FS operating configuration.

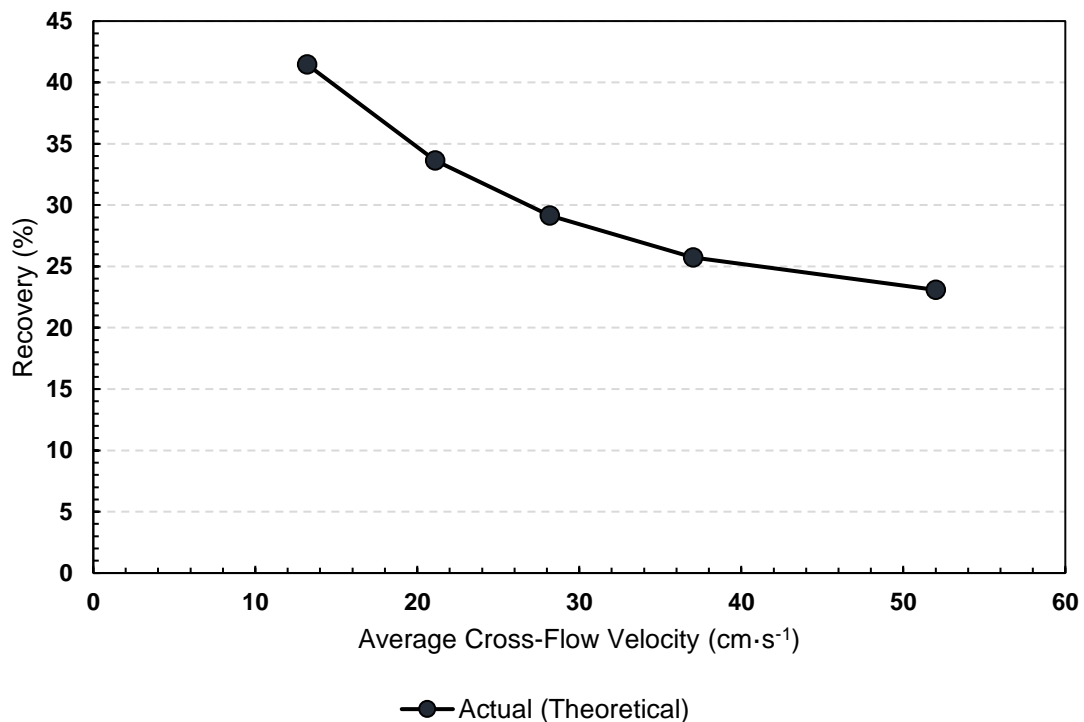


Figure 5-10. The experimentally-measured recovery along with the assumed operating CFV, compared to the calculated recovery and corrected CFV, as per the experimentally-measured water flux for the AL-DS operating configuration.

The permeate flux is enhanced at increased cross flow rates; however, as per Figure 5-9 and Figure 5-10, it is evident that the water recovery decreased at increased CFVs. The water recovery rate is highly dependent on the solution contact time on the membrane. As per the thin film theory, increasing the CFV rate of the solution, reduces the thickness of the mass transfer boundary layer on the membrane surface, thereby promoting mass transfer.

The fluid contact time on the membrane interface was calculated based on CFV and the total flow-path length. Intuitively, as the CFV increases, the fluid contact time on the membrane surface decreases. This is visually presented in Figure 5-11 for the assumed experimental CFVs and the actual operating CFVs as estimated by the recovery.

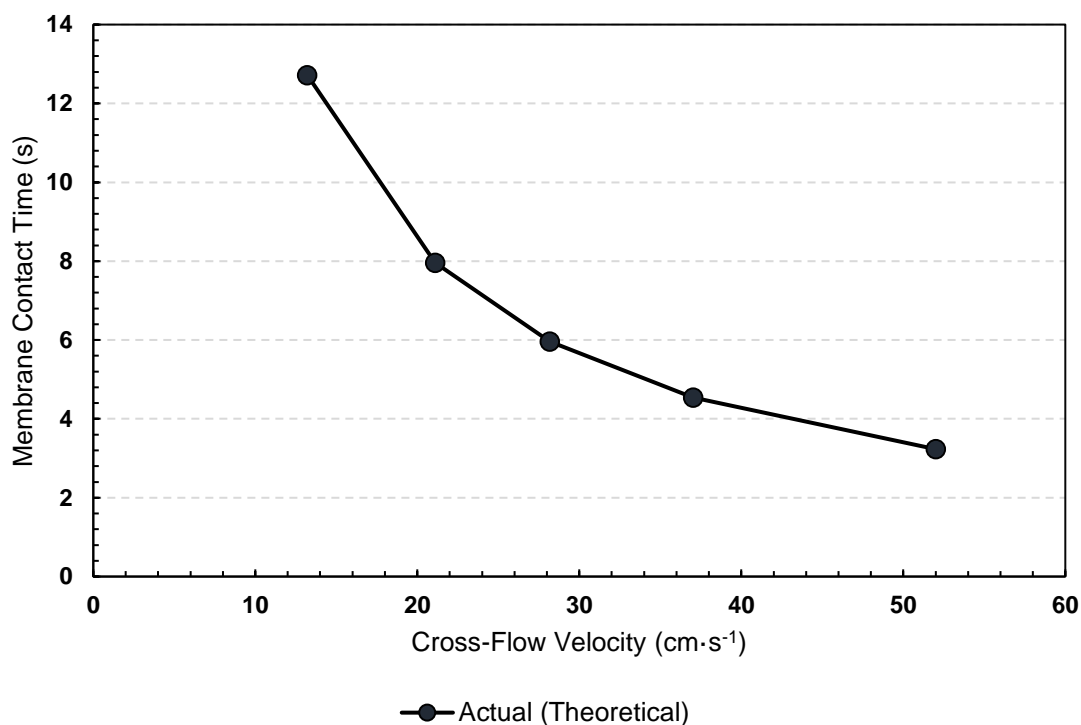


Figure 5-11. Fluid contact time with the membrane as a function of the operating CFV.

It was determined in the evaluation of the experimental setup that the CFV in the system is a function of the membrane train length (the total length of the channel). The total length of the channel was 1680 mm. Equation (5.2) indicates the recovery changes along the length of the channel due to changes in the CFV along the channel length.

$$R = \left(\frac{1}{\int_{l_{ch,1}}^{l_{ch,2}} CFV \, dl_{ch}} \right) \frac{J_w \times l_{ch}}{h_{ch} \times \Phi} \quad (5.2)$$

CHAPTER 5: Results and Discussion

Mathematically, in the absence of RSF, the measured flux is a function of the channel mass-transfer coefficients and the osmotic pressures of the respective DS and FS. This is described by Equation (1.2). Equation (1.2) is incorporated in Equation (5.2) to relate the factors affecting the measured water flux to the calculation of the water recovery. This is presented in Equation (5.3).

$$R = \left(\frac{1}{\int_{l_{ch,1}}^{l_{ch,2}} CFV dl_{ch}} \right) \frac{P_w [\pi_{D,b} \exp\left(\frac{-J_w}{k_D}\right) - \pi_{F,b} \exp\left(\frac{J_w}{k_F}\right)] \times l_{ch}}{h_{ch} \times \emptyset} \quad (5.3)$$

Mass-transfer coefficients are a function of: (1) fluid properties, (2) flow-channel geometry and (3) flow regime [43]. In addition, the estimation of the coefficients is complicated when fluid velocities change, due to the mass exchange between two fluids [43]. The following three points, relating to Equation (5.3), have proved to be true:

- The CFV changes along the length of the FO membrane train;
- Uncertainties in the mechanical design relating to the spacer porosity (flow restriction factor) and the channel height (h_{ch}), translate to inaccuracies with the assumed CFV of the system;
- The CFV can be corrected by calculating the actual recovery of the system, which is a function of the measured flux.

Changes in the CFV along the process train is brought about by the mass-exchange by two adjacent solutions. This implies that the concentration of the two solutions changes along the length of the process train. Furthermore, as indicated by the mathematical expression in Equation (2.1), the osmotic pressure of the solution is a function of the concentration of the solution. This is visually suggested by Figure 5-12. The data obtained was used to investigate the changes in the CFV per housing block, hence, along the length of the process train is the data that was then used to determine the effects of dilution of the DS.

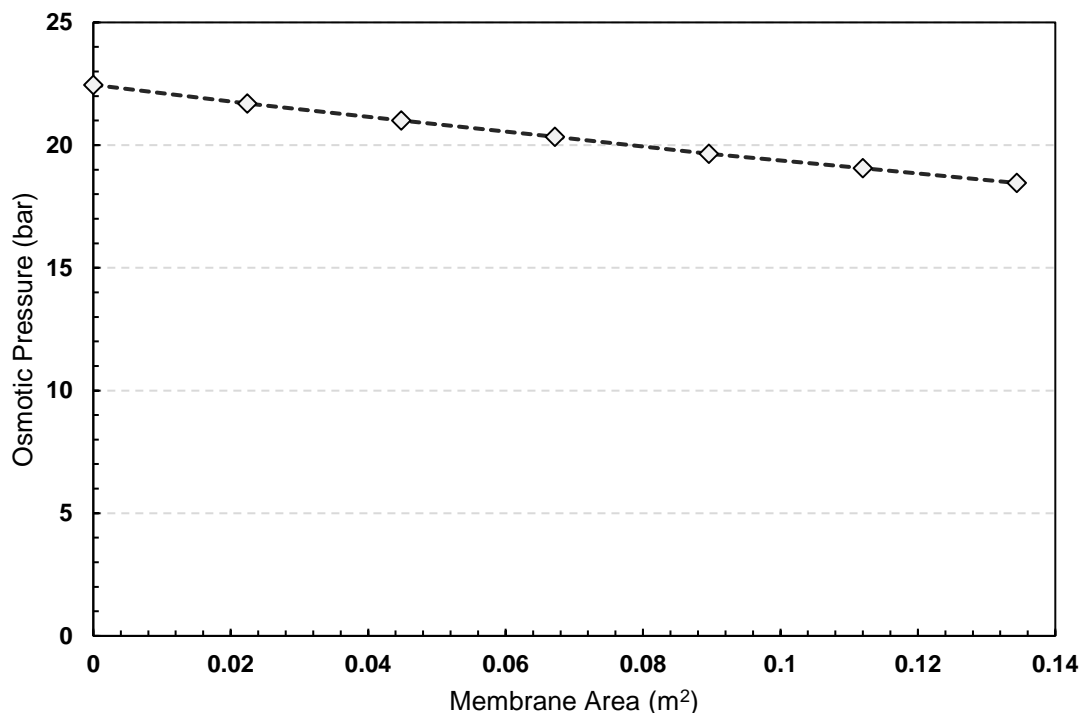


Figure 5-12. Effect of the DS dilution on decreasing the driving force of the process. The initial DS concentration was 29 220 mg·L⁻¹ and decreased to 23 835 mg·L⁻¹ along the length of the process train. Data obtained at a CFV of 19 cm·s⁻¹.

Figure 5-12 gives rise to the understanding that the process driving force is not constant along the process train, especially for an FS with a theoretical osmotic pressure of zero. For the validation experiments this is due to the fact that deionised water was used as the FS. No concentrative effects are evident although water extraction is prevalent, due to the lack of ions in solution. Therefore, the driving force for osmosis was not constant throughout the length of the process train. This is because the osmotic pressures of the solutions change along the length of the train. The dilution factor (DF) of the DS can be calculated via Equation (5.4) [119].

$$DF = \frac{Q_P + Q_{F,DS}}{Q_{F,DS}} \quad (5.4)$$

The average dilution factors of the DS for the AL-FS and the AL-DS, respectively, as a function of the actual operating CFV, are presented in Figure 5-13. In both operating configurations the dilution factor of the DS decreases with an increase in the CFV. Larger dilution factors are evident at lower CFVs, giving rise to lower water fluxes. Conversely, at higher operating CFVs a lower dilution factor of the bulk DS is achieved, thereby promoting water flux. Interestingly a plateau effect is also observed in the evaluation of the dilution factor of the AL-FS configuration. This suggests that beyond certain CFVs the dilution factor of the DSs is not decreased, thereby translating to a constant limiting flux achieved by the system.

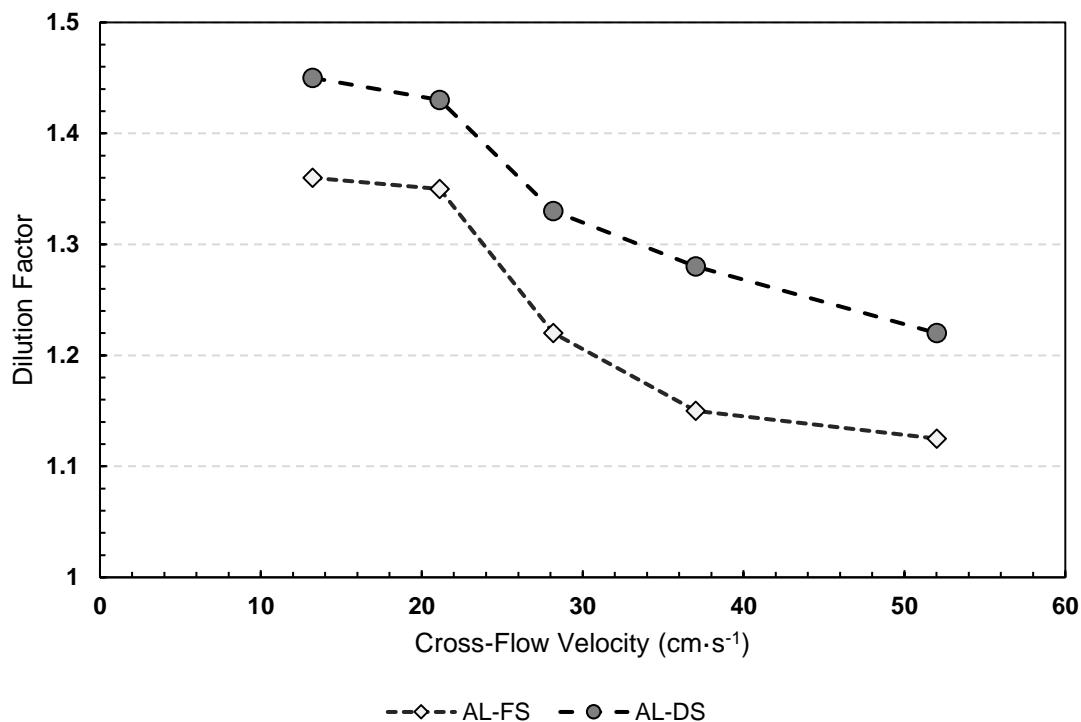


Figure 5-13. Dilution factors of the DS at the respective operating CFVs for the AL-FS and the AL-DS configuration.

The observed results are in agreement with the solution diffusion model, as applied to the process of osmosis. As stated, Baker [34] derived an equation relating the effects of an increased pressure gradient in the membrane to the water flux, achieved in RO membranes. Since the driving force in RO membranes is the applied hydraulic pressure, the same reasoning can be applied to FO membranes by considering the osmotic pressure differential, as this is the driving force in FO processes. Increasing the CFVs translates to increased water fluxes. It was also determined that at increased CFVs lower water recoveries are attained, thereby indicating lower dilution of the DS. This was corroborated with the calculating of the average dilution factor at the respective operating CFVs. Smaller dilution factors give rise to increased osmotic pressure differentials across the membrane, as opposed to larger dilution factors at lower operating CFVs. Then, as per the reasoning of Baker [34], the concentration of the DS at the membrane interface tends to zero (ICP) at higher differential osmotic pressures. This then gives rise to the observed limiting flux, as achieved by the AL-FS configuration.

For the AL-DS configuration it can then be assumed that the concentration gradient within the membrane was not large enough to bring about the limiting flux. This could be attributed to the increased dilution factors observed when operating in the AL-DS configuration. Counterintuitively to the increased dilution factor observed in the AL-DS configuration, the fluxes measured in this configuration were on average 40% higher than for the AL-FS configuration. This may be attributed to the inherent mass transfer occurring in each respective configuration.

The calculations to generate Figure 5-12, indicating the loss in osmotic pressure of the DS due to dilution, were based on the assumption that the only mass transfer occurring within the system, is water permeation. This is an invalid assumption as the mass transfer of solutes (of the DS) and the FS (should the FS contain any) also occurs within the system. The mass transfer of these solutes manifest as CP and RSF/RSD. To mathematically incorporate the solute mass transfer in the system, an additional term should be incorporated in Equation (5.3).

An equation to model water flux in membrane systems, has been developed by Field et al. [50]. Equation (5.5) presents the developed equation. Equation (5.5) is specifically developed for the AL-FS configuration, whereas Equation (5.6) presents the mathematical expression for flux for a system operating in the AL-DS configuration. These equations are similar and consistent to the equations for modelling flux in FO, as developed by She et al. [48].

$$J_w = P_w \left[\pi_{D,b} \exp\left(-\frac{J_w}{k_{SL}}\right) - \pi_{F,b} \exp\left(\frac{J_w}{k_{AL}}\right) \right] + B \left[\exp\left(-\frac{J_w}{k_{SL}}\right) - \exp\left(\frac{J_w}{k_{AL}}\right) \right] \quad (5.5)$$

$$J_w = P_w \left[\pi_{D,b} \exp\left(-\frac{J_w}{k_{AL}}\right) - \pi_{F,b} \exp\left(\frac{J_w}{k_{SL}}\right) \right] + B \left[\exp\left(-\frac{J_w}{k_{AL}}\right) - \exp\left(\frac{J_w}{k_{SL}}\right) \right] \quad (5.6)$$

Substituting the term for water flux in Equation (5.3) by either Equations (5.5) or (5.6) yields Equation (5.7). Equation (5.7) relates the recovery to the changes in CFV along the process train by linking the variable CFV to the mass transfer of water and solutes across the membrane.

$$R = \left(\frac{1}{\int_{l_{ch,1}}^{l_{ch,2}} CFV \, dl_{ch}} \right) \frac{P_w \left[\pi_{ds} \exp\left(-\frac{J_w}{k_{SL}}\right) - \pi_f \exp\left(\frac{J_w}{k_{AL}}\right) \right] + B \left[\exp\left(-\frac{J_w}{k_{SL}}\right) - \exp\left(\frac{J_w}{k_{AL}}\right) \right] \times l_{ch}}{h_{ch} \times \emptyset} \quad (5.7)$$

Moreover, the variability in the driving force, specifically the dilution of the DS, can be accounted for by rewriting Equation (5.7) to link the changes in the driving force of the process to the variability in the DS concentration. The rewritten form of Equation (5.7) is presented as Equation (5.8).

$$R = \left(\frac{1}{\int_{l_{ch,1}}^{l_{ch,2}} CFV \, dl_{ch}} \right) \frac{P_w \left[\int_{c_1}^{c_2} \pi_{ds} \, dC \exp\left(-\frac{J_w}{k_{SL}}\right) - \int_{c_1}^{c_2} \pi_f \exp\left(\frac{J_w}{k_{AL}}\right) \right] + B \left[\exp\left(-\frac{J_w}{k_{SL}}\right) - \exp\left(\frac{J_w}{k_{AL}}\right) \right] \times l_{ch}}{h_{ch} \times \emptyset} \quad (5.8)$$

The incorporation of the mass-transfer coefficient in Equations (5.8) along with the solute permeability coefficient (B), are to mathematically incorporate the effects of CP on water flux. CP can occur either externally or internally. Also, depending on the direction of water permeation, CP can be either dilutive or concentrative. It is known that the occurrence of CP is most significant when (1) the system is operating at high water fluxes and (2) low mass-transfer coefficients [43]. The degree of external CP within the system can be quantified, and hence, evaluated via the CP moduli. As per the

CHAPTER 5: Results and Discussion

thin film theory, increasing the inlet flow rate of the solution, decreases the thickness of the mass-transfer boundary layer, thereby promoting higher mass-transfer rates and lower ECP [122].

The Peclet number is a function of the CP moduli. The Peclet number describes the relationship between the convective flow through the membrane and the diffusion of solutes across the membrane. Moreover, the Peclet number is used to evaluate which transport phenomena is more dominant within the system. The Peclet number for the AL-FS and the AL-DS operating configuration, was estimated for the range of experimental CFVs that were investigated. The Peclet numbers are presented in Table 5-3 for the AL-FS configuration and in Table 5-4 for the AL-DS configuration. A boundary layer thickness of 20 μm was assumed, which is typically prevalent in spiral wound RO membranes [34]. Figure 5-14 indicates how the Peclet number will change as the boundary layer thickness increases or decreases.

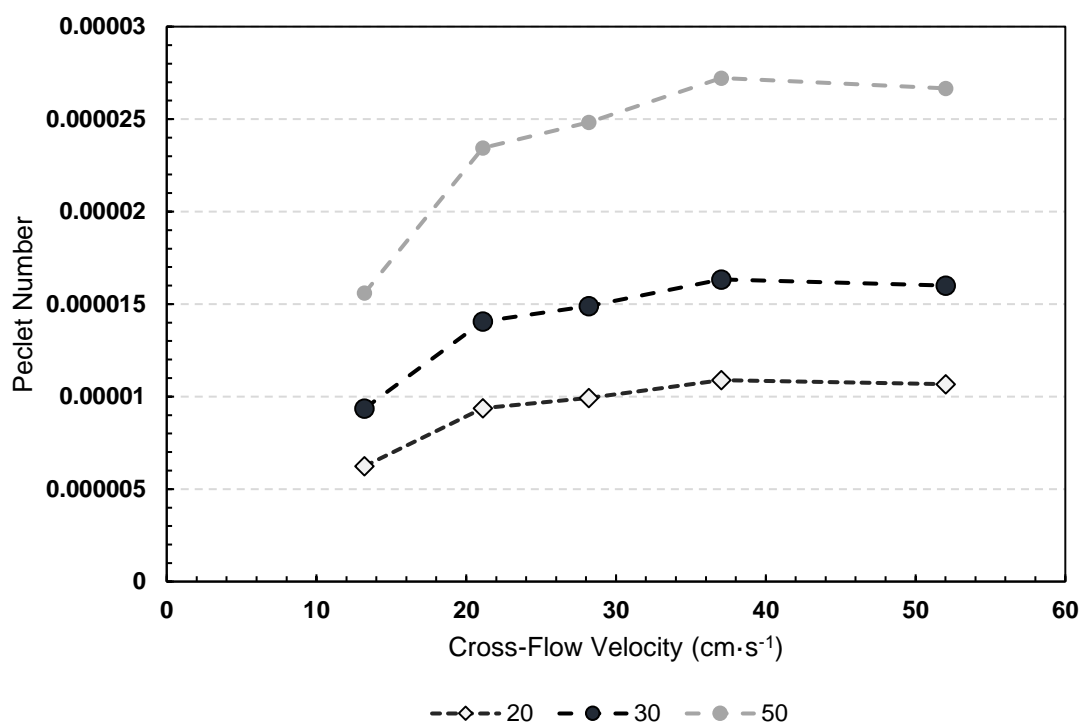
Table 5-3. Evaluation of ECP by calculating the Peclet number and the CP moduli at the actual operating CFV in the AL-FS configuration, with an assumed boundary layer thickness of 20 μm .

Designed CFV ($\text{cm}\cdot\text{s}^{-1}$)	AL-FS (Configuration 1)				
	Flux ($\text{L}\cdot\text{m}^{-2}\cdot\text{h}^{-1}$)	Recovery (%)	Actual CFV ($\text{cm}\cdot\text{s}^{-1}$)	Peclet Number	CP Moduli
9	11.23	25.93	13.21	0.0000058	0.9999996
15	16.88	24.39	21.11	0.0000094	1.0000045
19	17.88	19.35	28.19	0.0000099	1.0000042
25	19.60	16.14	37.04	0.0000109	1.0000039
35	19.20	11.26	52.02	0.0000107	1.0000086

A Peclet number less than unity, indicates that the convective flow of water through the membrane is dominant in the system when operating in the AL-FS configuration. Logically, the CP moduli then indicated that CP is not particularly significant in the system. This is expected in the AL-FS configuration as the feed water used for the validation tests were deionised water, thereby containing minimum ions. Interestingly enough, due to the significant number of ions in the DS, the CP number is less than unity. This indicates weaker rejections in the AL-DS configuration as the minor component permeates through the membrane. This finding is confirmed as per the rejections attained for the two configurations as detailed in Table 5-2. On average the solute rejections attained in the AL-FS configuration are 1.3% higher than for the AL-DS configuration.

Table 5-4. Evaluation of ECP by calculating the Peclet number and the CP moduli at the actual operating CFV in the AL-DS configuration, with an assumed boundary layer thickness of 20 μm .

Designed CFV ($\text{cm}\cdot\text{s}^{-1}$)	AL-DS (Configuration 2)				
	Flux ($\text{L}\cdot\text{m}^{-2}\cdot\text{h}^{-1}$)	Recovery (%)	Actual CFV ($\text{cm}\cdot\text{s}^{-1}$)	Peclet Number	CP Moduli
9	17.95	41.45	13.21	0.0000100	0.9999850
15	23.27	33.63	21.11	0.0000129	0.9999835
19	26.94	29.15	28.19	0.0000150	0.9999864
25	31.24	25.73	37.04	0.0000174	0.9999885
35	39.36	23.08	52.02	0.0000219	0.9999948

**Figure 5-14.** Effect of the boundary layer thickness (20, 30 and 50 μm) on the Peclet number for flux data attained in the AL-FS configuration, at various operating CFVs.

With the validation experiments of the membrane, ICP only occurs when the membrane operates with the AL facing the FS. The occurrence of ICP within the membrane support layer was confirmed by the validation experiments as the limiting flux of 20 $\text{L}\cdot\text{m}^{-2}\cdot\text{h}^{-1}$ was reached. However, the extent of ECP is yet to be determined, as the limiting flux was not evident for the AL-DS configuration. As mentioned before, it was also observed that a higher dilution factor of the DS is attained when operating in the AL-DS configuration.

To investigate the effect of ECP on the system performance and to characterise the effects thereof, the water flux was measured at different driving forces (varying the DS osmotic pressure). It is expected that the relationship between flux and the absolute osmotic process driving force would be linear.

Hence, an increase in the process driving force would translate to an incremental increase in the water flux. In reality this is not the case, due to the limiting effects of ECP, as mathematically expressed in Equation (5.5) with the positive exponential term, and in Equation (5.6) with the negative exponential term [123]. For the experimental data generated in Figure 5-15, dilutive ECP occurs when the system is operated with AL-DS. ECP is not significant when the system operates in the AL-FS as the FS utilised was deionised water.

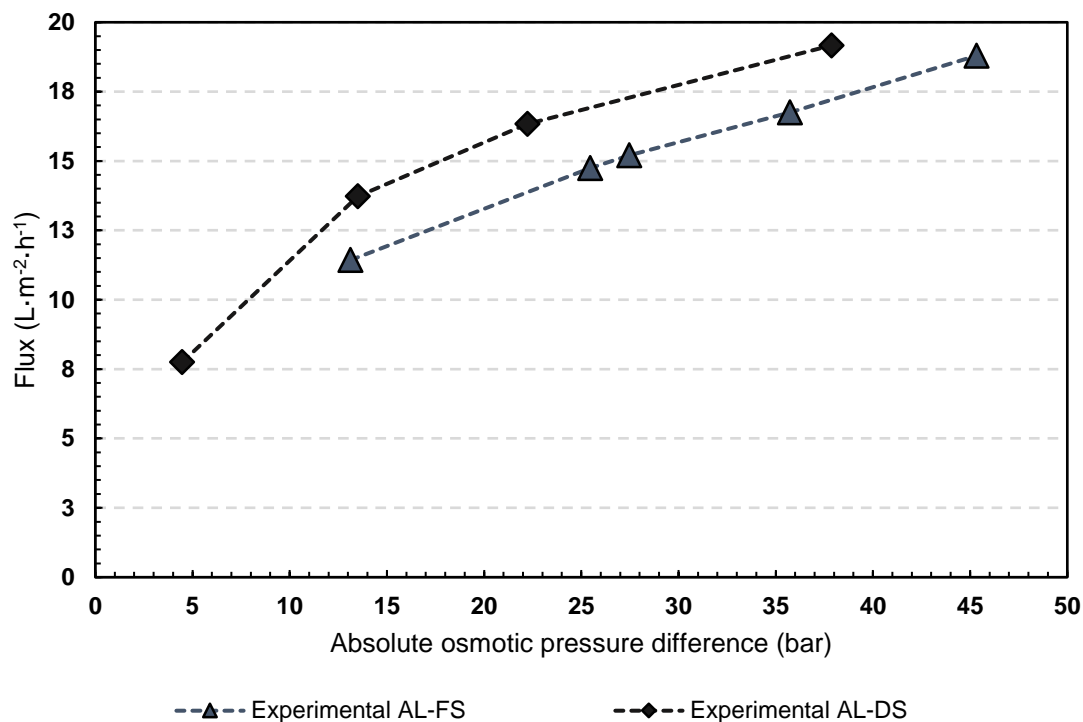


Figure 5-15. Relationship between flux and variable process driving force (variable transmembrane osmotic pressures) at a constant CFV of $37 \text{ cm}\cdot\text{s}^{-1}$ and a FS of deionised water.

In Figure 5-15 it is clear that when the system operates in the AL-DS configuration, higher fluxes are attained compared to the AL-FS configuration at corresponding transmembrane osmotic driving forces. On average the fluxes attained in the AL-DS configuration are $4 \pm 1 \text{ L}\cdot\text{m}^{-2}\cdot\text{h}^{-1}$ higher. Apart from the morphology of the two sides of the membrane being markedly different, the type of CP occurring in each operational configuration is also different. In the AL-FS configuration ICP is the predominant form of CP occurring within the system. Conversely, when the system operates in the AL-DS mode and the FS is deionised water, no ICP occurs within the system and dilutive ECP is the dominant form of CP.

Higher water fluxes are attained in the AL-DS configuration when increasing the osmotic driving force, as well as the CFVs of the system compared to the AL-FS configuration. CFV dictates the thickness of the mass-transfer boundary layer. At higher CFVs the mass-transfer boundary layer is decreased, thereby promoting mass transfer. Interestingly enough, the limiting flux was not achieved in the

AL-DS configuration when increasing the CFV, but the limiting flux of $20 \text{ L}\cdot\text{m}^{-2}\cdot\text{h}^{-1}$ was approached when increasing the osmotic pressure of the system. A stagnant region mainly exists in the support layer which is not affected by changes in the CFV. When operating in the AL-DS mode, the mass transfer of water from the FS (now facing the support layer) is marginally affected by increases in the CFV. Increasing the CFV on the DS side, diminishes the effects of ECP and the driving force can mainly be maintained, thereby relating increased CFVs to increased water fluxes.

However, when increasing the driving force of the process by altering osmotic pressure, the limiting flux in the AL-DS configuration is approached. This can be attributed to one of two reasons: (1) RSF is increased as the concentration of the DS is increased, or (2) as per the solution diffusion model, the dilutive ECP effects at increased osmotic driving forces, causes the concentration at the membrane interface on the DS side to tend to zero, thereby giving rise to the limiting flux.

In order to make a distinction between the two reasons, the RSF present in the system needs to be evaluated.

Figure 5-14 indicates that with an increase in the boundary layer thickness an increase in the Peclet number is observed, thereby indicating that solute diffusion plays a more dominant role. Intuitively, it is known that at increased CFVs the thickness of the boundary layer is said to decrease. Contrarywise, at lower CFVs the thickness of the boundary layer will increase. The RSF and specific RSF values obtained for the two operating configurations at increasing CFV, are documented in Figure 5-16.

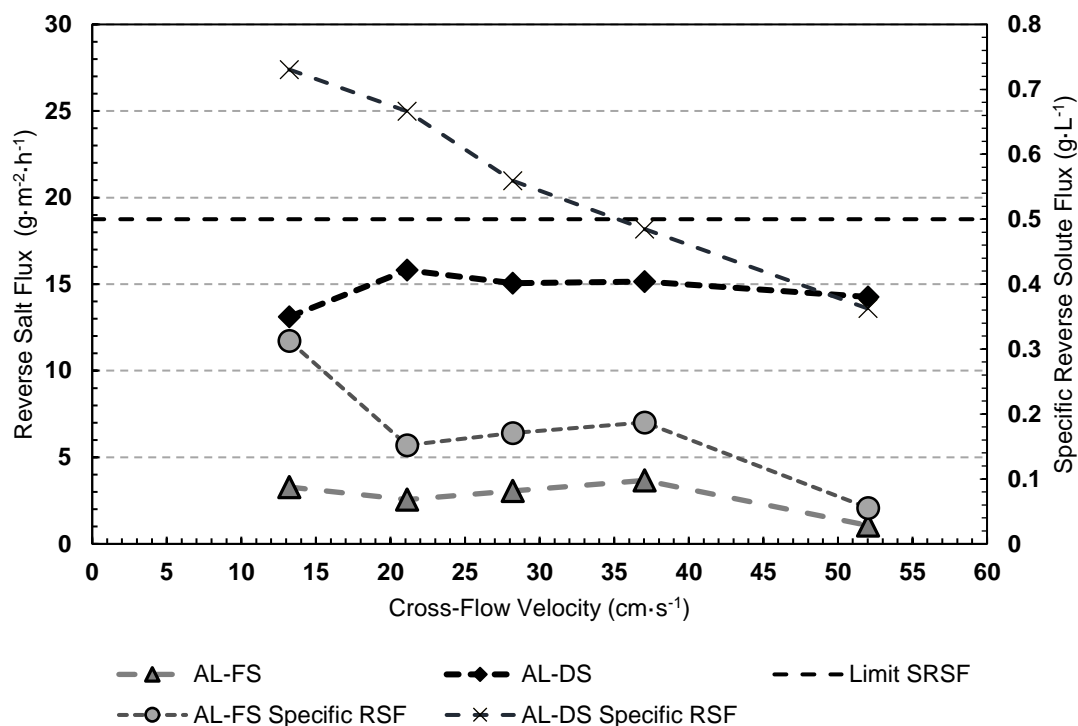


Figure 5-16. Reverse salt diffusion as a function of cross-flow velocity when the membrane AL is facing the FS and the DS. DS concentration was kept constant at 0.5 M, and normalised temperatures for both solutions were kept constant at 20°C.

The salt flux was calculated similarly to the study by Cath et al. [23] where the rate of change of the feed concentration was multiplied by the volume of the feed solution and then divided by the membrane active area. RSF values of up to 3 times higher than the AL-FS configuration were found to occur in the AL-DS configuration. The average RSF value for the AL-FS configuration was $4 \text{ g}\cdot\text{m}^{-2}\cdot\text{h}^{-1}$ as opposed to the $15 \text{ g}\cdot\text{m}^{-2}\cdot\text{h}^{-1}$ in the AL-DS configuration. The limit of the specific RSF as per the membrane supplier is $0.5 \text{ g}\cdot\text{L}^{-1}$. For the AL-FS configuration an overall decrease in the specific RSF value was found to be evident as the operating CFV increased. The specific RSF value for the AL-FS configuration was continually below the limit as per the membrane supplier. Conversely for the AL-DS configuration, at CFVs below $37 \text{ cm}\cdot\text{s}^{-1}$, the specific RSF value was above the limit of $0.5 \text{ g}\cdot\text{L}^{-1}$. A decrease was observed where the value decreased below the operational limit at CFVs above $37 \text{ cm}\cdot\text{s}^{-1}$.

The general trend for the decrease in the specific RSF as the CFVs increases, can be attributed to the fluid contact time with the membrane. As the CFV increases, the fluid contact time on the membrane surface decreases, thereby decreasing the effective time for diffusion from the DS to the FS. The enhanced turbulence on the membrane surface at higher CFVs relative to the lower CFVs, also enhances the ionic movement from the mass transfer boundary layer near the membrane surface to the bulk fluid, due to the formation of small fluid vortices on the membrane surface. This is done by

decreasing the hydrodynamic drag forces of the ions to the membrane surface due to the smaller boundary layer thickness at increased CFVs.

5.2. Intermittent Flow-Path Switching

Based on the validation and characterisation tests the following conclusions could be drawn:

- The mass-transfer phenomena limiting the operation of the system is different for the two operating configurations.
- RSF along with dilutive ECP was found to be the limiting mass-transfer phenomena when operating the AL-DS configuration;
- Conversely, dilutive ICP was found to be the dominant mass-transfer phenomena limiting the system when operating in the AL-FS configuration.

Based on the above findings it is integral to this study to evaluate the operability of the system when switching from the AL-FS configuration to the AL-DS configuration. Molecules are dissolved inside the membrane and diffuse along the concentration gradient. When operating in the AL-DS configuration, RSF is dominating the solute mass transfer in the system. Therefore, it is expected that salt molecules will be dissolved inside the membrane. At that point in time when the system is switched to the AL-FS configuration, dilutive ICP becomes the mass-transfer limiting factor. One of the design requirements of the system was to automate the switch over from one configuration to the other. Hence, the system switches over from mainly an RSF limiting system to a dilutive ICP limiting system. The following points then becomes evident:

- The stabilisation times when switching over from the one operating configuration to the other; and
- The CFV at which the most stable and predictable performance is achieved.

From the previous work conducted relating to the *baseline* tests, it was decided to select three CFVs to investigate the intermittent switching of the flow path to reverse the direction of water permeation. Based on the range CFV range investigated, it was decided on 13, 28 and 52 $\text{cm}\cdot\text{s}^{-1}$ to represent the CFV range. Experimental runs for a duration of 60 hours were conducted. The operational mode was changed twice during each run to investigate, *inter alia*, (1) how does the membrane mechanistically react to the sudden switch in permeate direction, (2) how long does it take for the residue solutions to be purged from the system, (3) what is the duration associated with stabilised conductivity measurements from samples taken from the outlet ports and (4) are the performance indicators the same as those determined during the validation tests for each configuration.

The points listed above were investigated by measuring the flux and the FS outlet conductivity continuously. The *baseline* fluxes for each CFV and operational configuration have been established, which were used as a point of reference to where the flux performance of the system ought to be. Imperative to this cleaning strategy is the predictability of the system. In industrial plants, when membrane cleaning is implemented, process upsets are undesirable. It is desired that a reliable and a predictable cleaning strategy be implemented to minimise any unforeseen process interruptions. This is then also the reason why the *baseline* fluxes were used as predictive system performance indicators.

The hypothetical performance of the system is already known. At this point the stabilisation times to the hypothetical performance, requires examination.

The results for continuous switching are presented in Figure 5-17 for $13 \text{ cm}\cdot\text{s}^{-1}$, Figure 5-18 for $28 \text{ cm}\cdot\text{s}^{-1}$ and Figure 5-19 for $52 \text{ cm}\cdot\text{s}^{-1}$. The DS flux attained and the FS outlet conductivity were evaluated. The spikes in the conductivity indicated the migration from one operational mode to the other.

The flux behaviour of the three CFVs clearly indicated that the most stable operation was achieved in terms of the membrane performance parameters, when operating at a CFV of $28 \text{ cm}\cdot\text{s}^{-1}$. The FS outlet conductivity was also evaluated. At a CFV of $13 \text{ cm}\cdot\text{s}^{-1}$ and $28 \text{ cm}\cdot\text{s}^{-1}$ the FS outlet conductivity was evaluated continuously, which is why the conductivity spikes are present. When the flow path is switched, residual solution is purged from each flow channel, presenting as increased conductivity via concentration in the FS outlet, and having a diluting effect in the DS outlet.

For the evaluation of the conductivity stabilisation at a CFV of $52 \text{ cm}\cdot\text{s}^{-1}$, the FS outlet conductivity was measured periodically. This was done as it was found that the continuous measurements skewed the data by indicating prolonged stabilisation times, due to the initial high conductivity DS exiting the flow channel. It was established that the FS outlet conductivity stabilised after approximately 5 minutes, whereby it was assumed that the system was stabilised in the new operating configuration. The stabilisation times were investigated further by introducing food colouring in the FS. Photographs of occurrence are documented in Table 5-5.

Initially, the system is flushed from the AL-FS configuration to the AL-DS configuration. The red food colorant particles represented various ions in the FS. After 30 minutes of operation in the AL-DS configuration, it became evident that the particles are present on the back-end active layer surface within the support layer. This was assumed to be true as the colour red became more prominent at a prolonged operational time. It should be noted that the photographs were taken from the AL side, and the DS exiting the process was clear. Therefore, it was assumed that no red food colorant particles diffused with the permeate convective flow.

When switching the operational configuration from the AL-DS to the AL-FS, the time was recorded that it took for the red food colorant particles to be purged from the system. After 2 minutes of operation the prominent red colour was seen to fade, and after approximately 12 minutes of operation it was clear that the system was purged from the red particles.

The following remarks and conclusions based on the above findings, are evident in going forward:

- The reversal of the membrane orientation from the AL-FS to the AL-DS configuration led to the occurrence of ICP within the system. The solute in the DS must penetrate the porous support layer to the interior surface of the active layer, before water flux can occur in order to generate an

CHAPTER 5: Results and Discussion

osmotic gradient as observed by the membrane. As water crosses the AL into the SL the DS is diluted at the interface of the AL, due to water convection and dilutive ICP is observed.

- The solute diffuses back to the interior surface to compensate for the concentration difference occurring within the boundary layer. It can be assumed that steady state is quickly reached, however the concentration of the bulk solution is still significantly higher than the concentration at the interior surface of the AL. It is thus evident that the concentration of the DS and the diffusivity of the ions in the solution, have an effect on the water fluxes attained as the average *baseline* fluxes are not achieved.
- The support layer acts as an entrapment area for particles and ions.
- Stabilisation times of up to 15 minutes are sufficient to purge the SL from entrapped particles and ions.

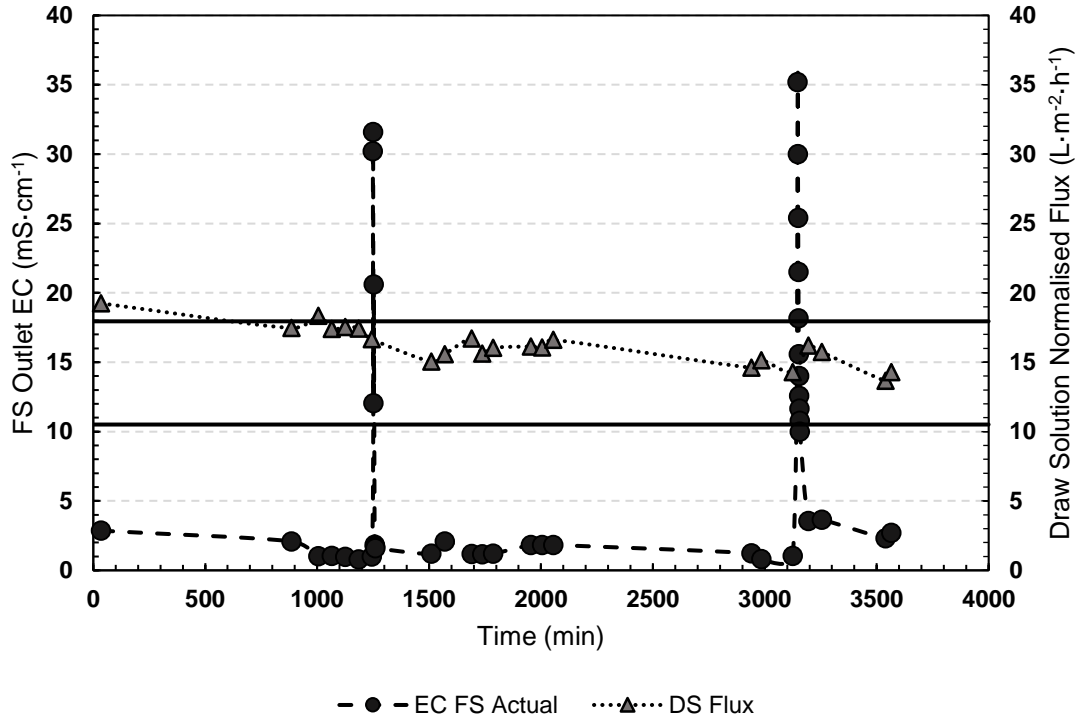


Figure 5-17. Continuous operational mode switching starting in the AL-DS configuration, switching to the AL-FS configuration at $t = 1250$ min and switching back to the AL-DS configuration at $t = 3125$ min. The operating conditions were $13 \text{ cm}\cdot\text{s}^{-1}$, deionised water as the FS, and 0.5 M NaCl DS, with the temperature maintained at 24°C .

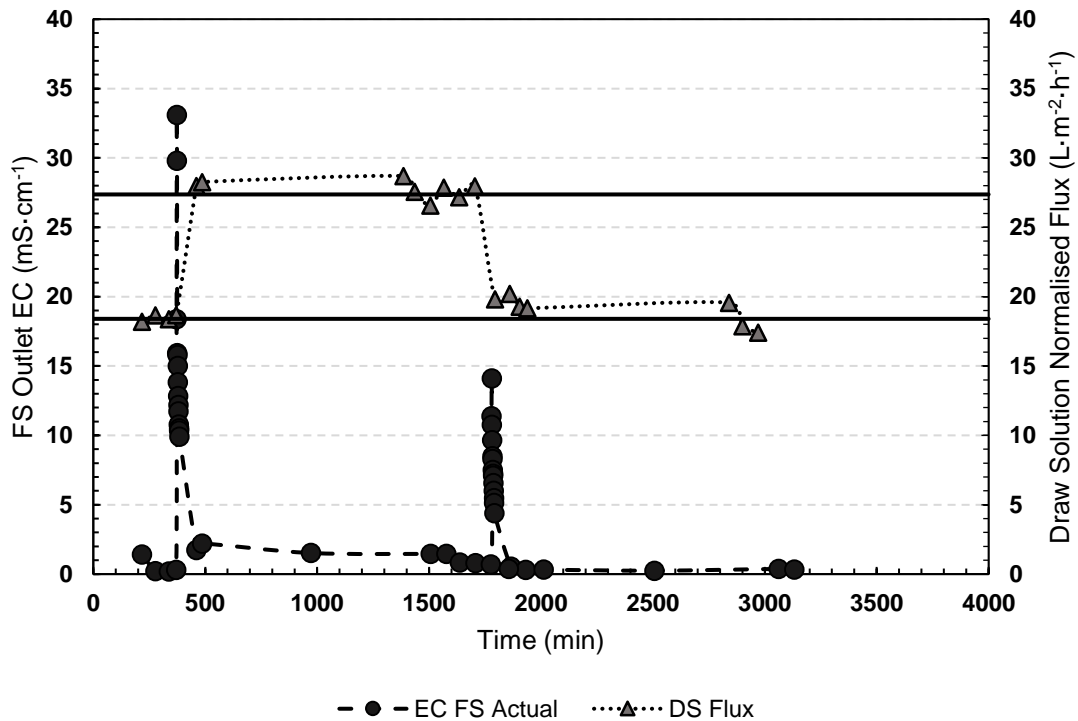


Figure 5-18. Continuous operational mode switching starting in the AL-DS configuration, switching to the AL-FS configuration at $t = 370$ min and switching back to the AL-DS configuration at $t = 1777$ min. The operating conditions were $28 \text{ cm}\cdot\text{s}^{-1}$, deionised water as the FS, and 0.5 M NaCl DS, with the temperature maintained at 24°C .

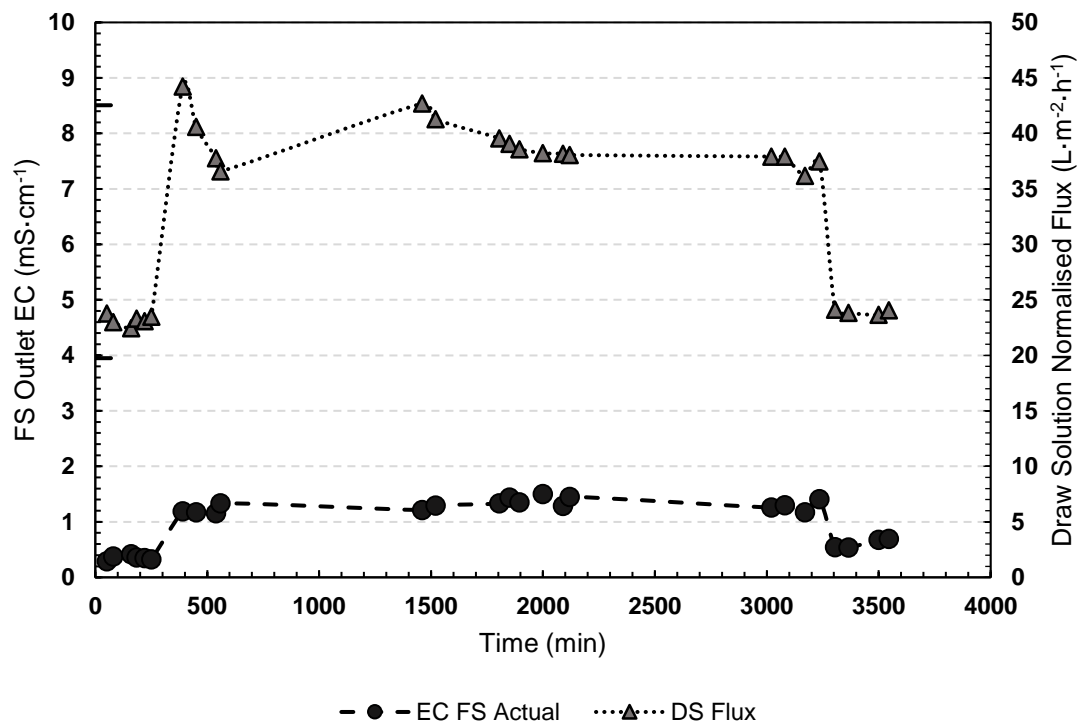
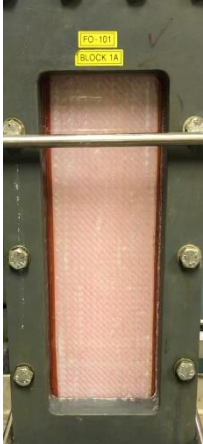
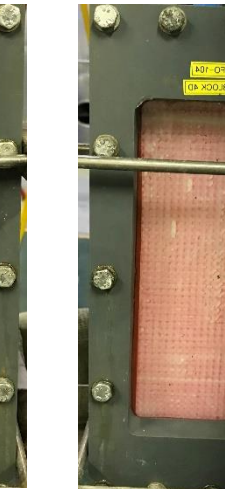
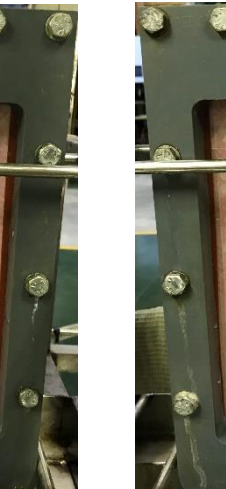
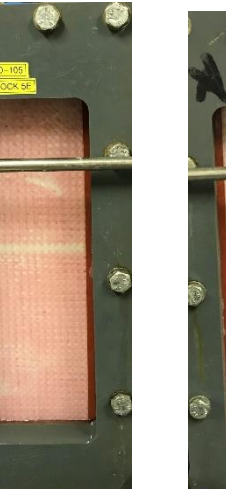
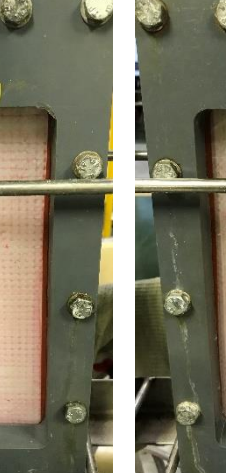


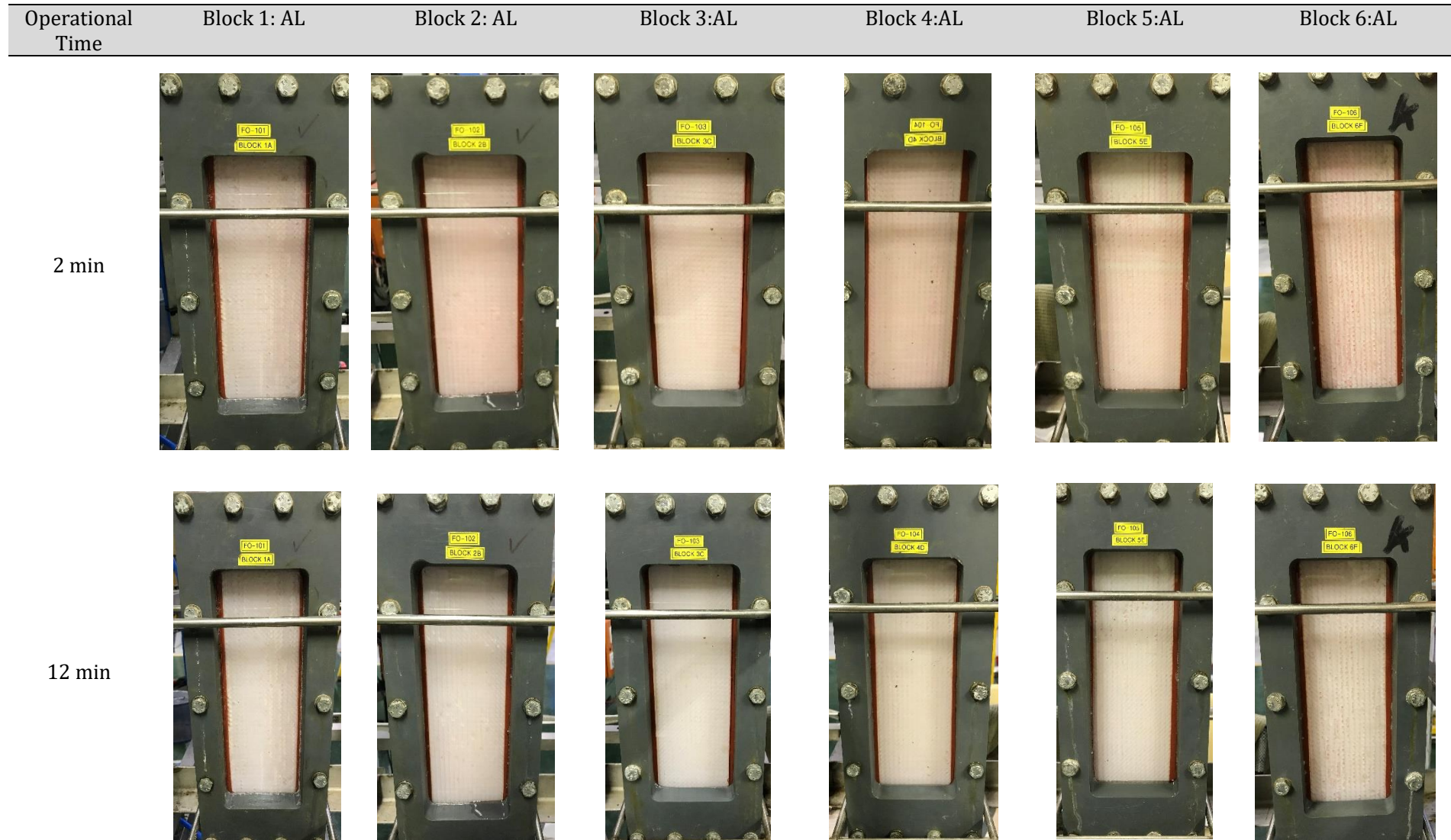
Figure 5-19. Continuous operational mode switching starting in the AL-DS configuration, switching to the AL-FS configuration at $t = 250$ min and switching back to the AL-DS configuration at $t = 3235$ min. The operating conditions were $52 \text{ cm}\cdot\text{s}^{-1}$, deionised water as the FS, and 0.5 M NaCl DS, with the temperature maintained at 24°C .

Table 5-5 The effects of ICP are demonstrated with red food colouring when operating with the active layer facing the feed solution (AL-FS) and the active layer facing the draw solution (AL-DS). With the AL facing the DS, ICP occurs within the SL with the FS (the red solution). These photographs were taken for $52 \text{ cm}\cdot\text{s}^{-1}$ CFV on both sides, with a 0.5 M DS, and a deionised water FS, both at 24°C .

Operational Time	Block 1: AL	Block 2: AL	Block 3:AL	Block 4:AL	Block 5:AL	Block 6:AL
Flushing: AL-FS to AL- DS						
30 min						

CHAPTER 5: Results and Discussion

Operational Time	Block 1: AL	Block 2: AL	Block 3:AL	Block 4:AL	Block 5:AL	Block 6:AL
105 min	 <p>FO-01 BLOCK 1A</p>	 <p>FO-102 BLOCK 2B</p>	 <p>FO-103 BLOCK 3C</p>	 <p>FO-01 BLOCK 4D</p>	 <p>FO-105 BLOCK 5E</p>	 <p>FO-101 BLOCK 6B</p>
Flushing: AL-DS to AL- FS	 <p>FO-101 BLOCK 1A</p>	 <p>FO-102 BLOCK 2B</p>	 <p>FO-103 BLOCK 3C</p>	 <p>FO-104 BLOCK 4D</p>	 <p>FO-105 BLOCK 5E</p>	 <p>FO-101 BLOCK 6B</p>



5.3. Practical Implementation

To investigate the practical implementation of the fouling control strategy, intermittent flow-path switching, the scaling potential of solutions required evaluation. This was mainly due to the transport phenomena limiting each operating configuration. In this section it was pertinent to investigate:

- How ECP manifests when the FS contains ions. It is known that operating in the AL-FS configuration is limited by dilutive ICP. This was established when the FS contained no ions. It is therefore required to clearly distinguish how ECP will affect flux declines in order to differentiate between ECP and scaling.
- ECP due to the feed solution ions that will manifest as concentrative ECP.
- The effects of gypsum scaling in the AL-FS configuration and the AL-DS configuration, respectively, on flux declines.

This was done by investigating a feed solution containing typical scaling ions such Ca^{2+} and SO_4^{2-} at a predetermined saturation concentration. Flux reductions due to the scaling solution were then compared to flux declines brought about by ECP in the FS, using NaCl and MgCl_2 as FS salts, which neither promote nor cause scaling. Typically, these salts would give a good indication of the flux declines observed due to ECP.

Figure 5-20 presents the flux declines brought about by a 1.64 M NaCl FS solution, compared to a solution having a Ca^{2+} SSF of 0.95 ($596 \text{ mg}\cdot\text{L}^{-1} \text{ Ca}^{2+}$ and $1428 \text{ mg}\cdot\text{L}^{-1} \text{ SO}_4^{2-}$). For comparative reasons the driving force of the two processes was kept constant at 24 bar. This was also done to investigate if flux declines can be attributed to ECP, or due to scaling being present on the membrane surface.

The NaCl FS showed an initial decrease in the normalised flux of 8%. This was attributed to the lower process driving force, when compared to the *baseline* driving force of 27 bar. After 2 hours the effects of ECP became prevalent in the system, where a flux decline of 40% from the normalised flux was viewed. Conversely, for the solution containing gypsum scaling ions at an SSF of 0.95, initial flux declines were 35% that is approximately five times more than the flux declines viewed for the non-scaling solution (NaCl as the FS). This was primarily attributed to the number of ions that were more with the scaling solution than it was a quaternary ionic system, compared to the NaCl FS, which comprised of only two ions. An overall flux decline for the SSF 0.95 solution of 39% was observed, thereby indicating that scaling was not present in the system and that flux declines could solely be ascribed to concentrative ECP.

The average recovery for the 0.95 SSF gypsum solution was 15.8%. This translated to a concentration factor of 1.2. The saturation concentration of Ca^{2+} is $627.3 \text{ mg}\cdot\text{L}^{-1}$, thereby indicating that the SSF of Ca^{2+} at the end of the process train was 1.14. Gypsum scaling was not observed, due to the induction time for crystal formation.

As per Figure 5-21 the effects of ECP from a divalent ion, specifically Mg^{2+} , was investigated and compared to the same SSF 0.95 scaling solution as per Figure 5-20. Initial flux declines of up to 22%

were found for the first 2 hours of operation with a final flux decline of 65% after 2.5 hours. When comparing Figure 5-20 to Figure 5-21, the following reasoning applies: The diffusivity of Mg^{2+} is approximately half of the diffusivity of the Na^+ ion. The smaller size and the enhanced diffusivity of the ion will cause the Na^+ ion to rather diffuse through the membrane, as opposed to enhancing CP. Conversely, the larger and slower Mg^{2+} ion will contribute to exacerbate the effects of CP. This can also be partly attributed to the enlarged hydrated radius of Mg^{2+} when compared to the hydrated radius of Na^+ . This reasoning is confirmed by various studies [16,17,26,69]. As indicated by Figure 2-4, severe CP can reduce RSF. However, the steep flux declines observed for the divalent Mg^{2+} solution, confirmed the occurrence of CP and that the declines of the SSF 0.95 solution did not cause scaling on the membrane surface.

Synthesis of a suitable scaling solution, where flux declines due to gypsum scaling on the membrane surface were present in the system, required investigation. From the results presented in Figure 5-20 and Figure 5-21, it is clear that a solution with a SSF of 0.95 did not bring about membrane scaling. As per Figure 5-22, SSF factors of 1.3 and 3 were also investigated.

An overall flux decline of 46% was brought about by a SSF 1.3 solution after an experimental duration of 30 hours. It was therefore concluded that scaling was present in the system, but that prolonged experimental time would be required for flux declines due to scaling.

For a SSF of 3, immediate flux declines of up to 65% were prevalent in the first 2 hours of the experimental duration. An overall flux decline of up to 85% was observed. The effects of gypsum scaling on the membrane immediately translated to the membrane performance indicators, with severe gypsum scaling that could visually be seen on the membrane surface. From the above data it was concluded that in order to investigate intermittent flow-path switching as a scaling control strategy, the effects of gypsum scaling needed to be prevalent in the system in a reasonable amount of time (5 – 10 hours). This translated to the initial FS SSF being between 1.3 and 3.

It was decided that an FS with an SSF of 3 would be too aggressive, adding the additional risk that gypsum scaling would form in the piping of the setup and act as seed crystals. Therefore, it was decided to report the flux declines observed in both operational configurations for an SSF 1.9 solution. The results from this testing are presented in Figure 5-23.

A flux decline of 62% in a 10-hour experimental run was established in the AL-FS operational configuration, whereas flux declines of 93% in a 4-hour experimental window were established for the AL-DS configurations. These results indicated that operation in the AL-DS configuration should be kept to a minimum as severe flux declines were prevalent.

CHAPTER 5: Results and Discussion

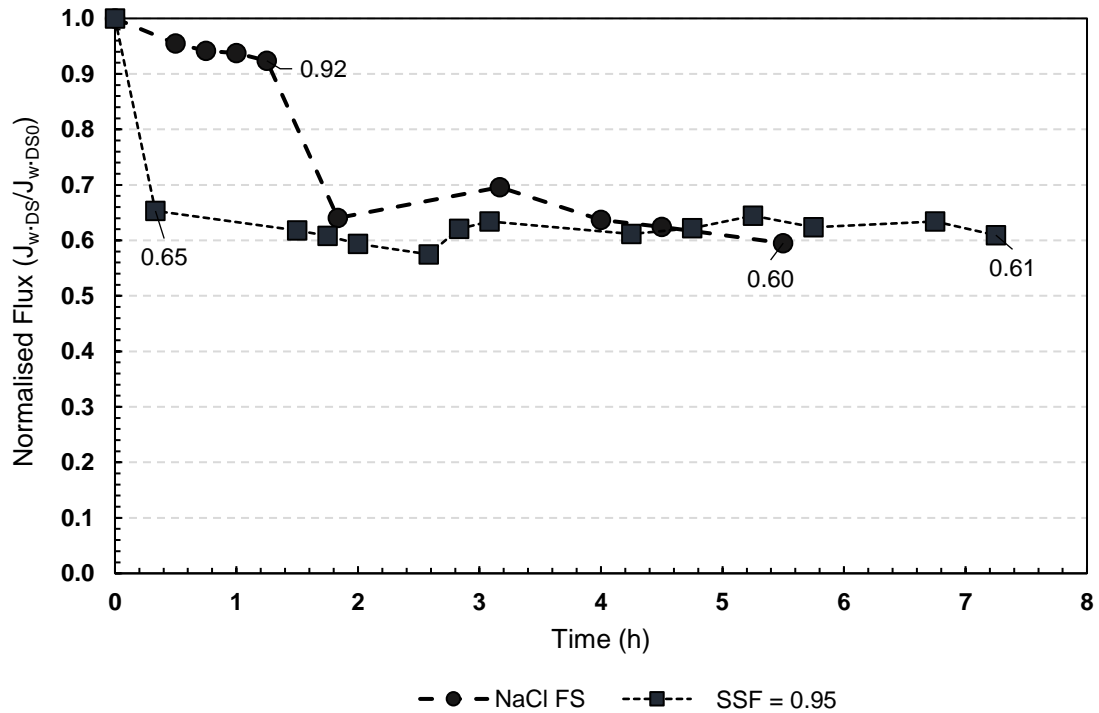


Figure 5-20. Normalised flux declines for a NaCl at an osmotic pressure of 3 bar and a gypsum scaling solution (containing) at an SSF of 0.95, at a CFV of $28 \text{ cm}\cdot\text{s}^{-1}$, with a normalised solution temperature at 20°C , and a DS concentration of 0.6 M NaCl, operating in the AL-FS configuration. The effective osmotic driving force between the two solutions is 24 bar.

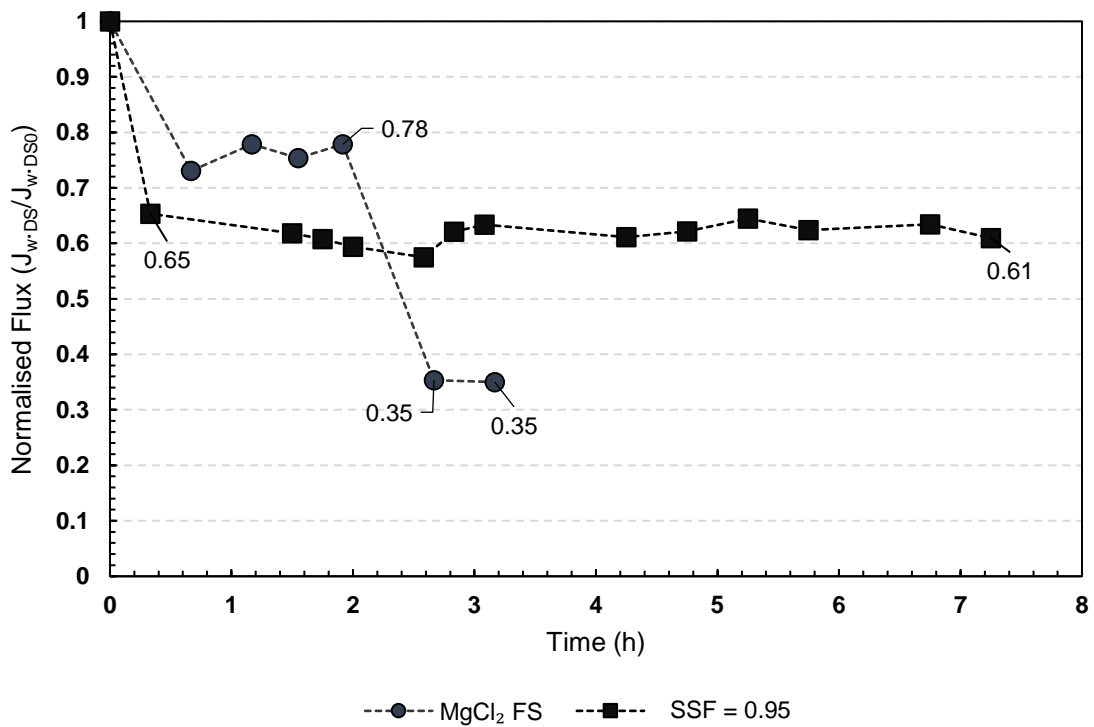


Figure 5-21. Normalised flux declines for a MgCl_2 at an osmotic pressure of 2 bar and a gypsum scaling solution (containing) at a SI of 0.95, at a CFV of $28 \text{ cm}\cdot\text{s}^{-1}$, with a normalised solution temperature at 20°C , and a DS concentration of 0.6 M NaCl, operating in the AL-FS configuration. The effective osmotic driving force between the two solutions is 24 bar.

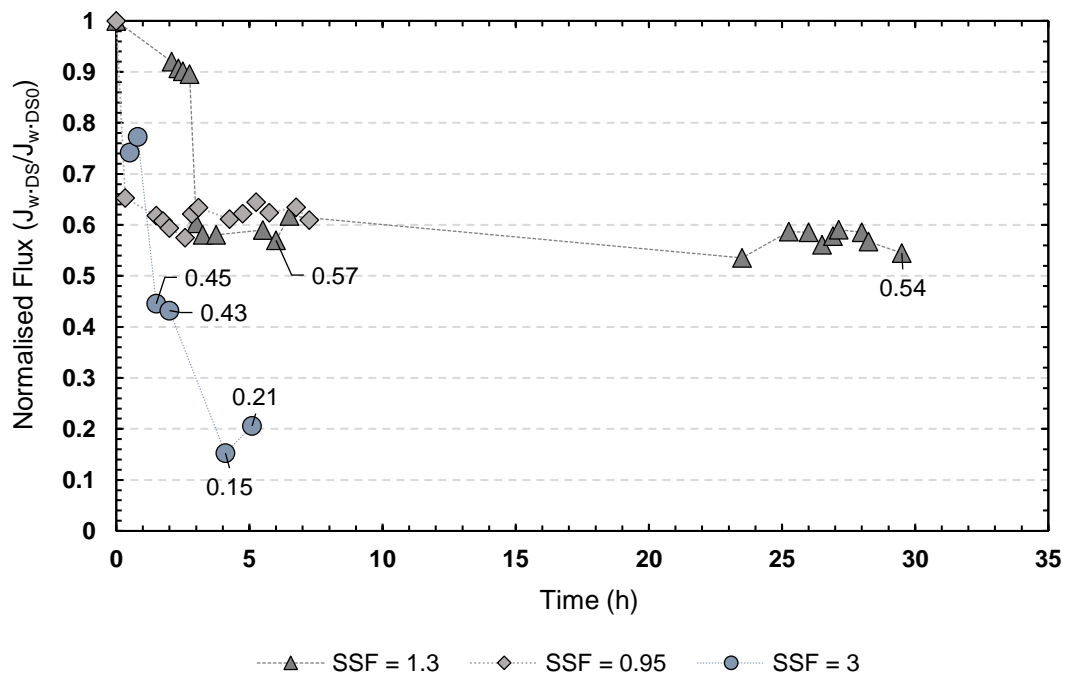


Figure 5-22. Normalised fluxes for three feed solutions and varying the calcium saturation factor by SSF of 0.95, 1.3 and 3 at a CFV of $28 \text{ cm}\cdot\text{s}^{-1}$, normalised solution temperatures of 20°C , and operating in the AL-FS configuration with a DS concentration of 0.6 M NaCl .

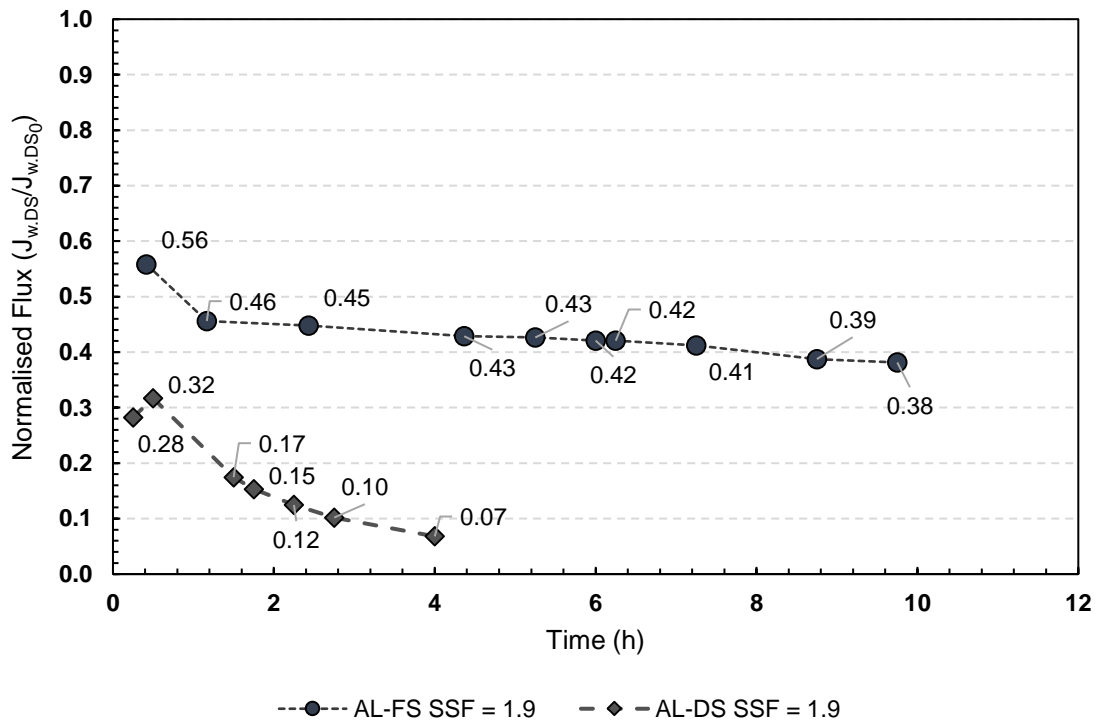


Figure 5-23. Normalised flux for a feed solution containing ($1191.78 \text{ mg}\cdot\text{L}^{-1} \text{ Ca}^{2+}$), translating to an SSF of 1.9 at a CFV of $28 \text{ cm}\cdot\text{s}^{-1}$, and normalised solution temperatures of 20°C for both the AL-FS and the AL-DS operational configuration, with a 0.6 M NaCl DS .

5.4. Evaluating Intermittent Flow-Path Switching

The implementation of intermittent flow-path switching was evaluated with a 1.9 SSF Ca²⁺ feed solution. This translated to a Ca²⁺ concentration of 1192 mg·L⁻¹ and a SO₄²⁻ concentration of 2857 mg·L⁻¹.

- The CFV was kept constant at a CFV of 28 cm·s⁻¹, because the best performance was achieved when investigating intermittent flow-path switching.
- It was prevalent from Figure 5-23 that scaling occurring within the support layer of the membrane, detrimentally affects the performance of the system via rapid flux declines (93% in 4 hours). Therefore, operation in the AL-DS configuration will be limited to the required 15 minutes for purging of the residual solutions.

5.4.1. Relevance to a Scaling Solution

Figure 5-24 represents the performance data of the membrane for a 12-hour experimental run, employing intermittent flow-path switching. Six flushing cycles with in-situ FS and DS switching were employed. The DS flux data is presented along with the DS flux attained for normal operation in AL-FS configuration, without employing intermittent flow-path switching.

A constant flux of 9 L·m⁻²·h⁻¹ was achieved over a 12-hour operating period. Flux recoveries of 22.67% below the baseline flux of 12.5 L·m⁻²·h⁻¹ were achieved, when operating at a CFV of 28 cm·s⁻¹ and reversing the permeate direction by switching from the normal AL-FS operation to 15 minutes in the AL-DS operation. This is on average *ca* 20.3% higher than the flux attained without employing backwashing. An overall flux decline of 38 % in the AL-DS configuration was achieved over a period of 12 hours. This emphasised the detrimental scaling effects in the AL-DS configuration. Furthermore, the process water from the flushing cycle had to be discarded as it was contaminated with scaling ions. This translated to a volume loss of 8 L·day⁻¹ for a 0.1344 m² system.

To evaluate the significance of the product water loss and the financial implications this has for the operating costs of an industrial plant, a high-level cost analysis was conducted. In industrial applications, feed waters containing a high scalant solution requiring treatment in a membrane process train, would be dosed with an antiscalant. The role of the antiscalant is to shift precipitation potential of the solution by impeding the formation crystals. Crystallisation can be impeded up to a concentration factor of 4. The high-level costs analysis comparing intermittent flow-path switching to antiscalant dosing, is presented in the following section.

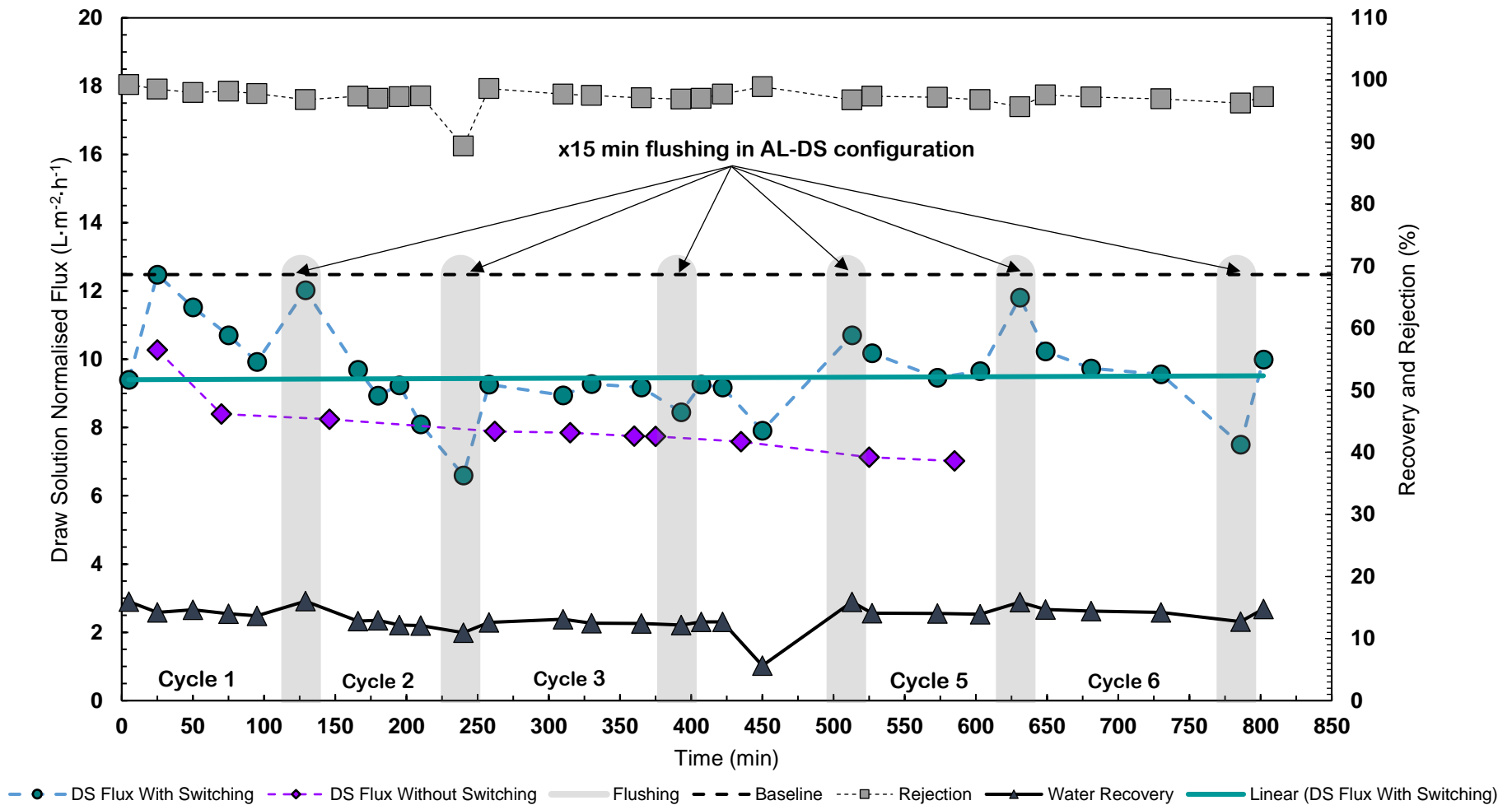


Figure 5-24. Water flux decline profile for a 1.9 SSF gypsum solution for accelerated fouling. Six flushing cycles with in-situ FS and DS switching at 15 minutes each at a CFV of $28 \text{ cm} \cdot \text{s}^{-1}$. Accelerated fouling conditions: Feed solution was $1.9 \times \text{Ca}^{2+}$ gypsum solution; NaCl DS maintained at 0.6 M ; the CFV of both the feed and the draw solution at $28 \text{ cm} \cdot \text{s}^{-1}$ (corresponding to $\pm 200 \text{ mL} \cdot \text{min}^{-1}$).

5.4.2. Product Water Contamination & Cost Trade-Off

Intermittent flow-path switching requires a flushing cycle to purge the system from residual solutions, before continuing normal operation in the other configuration. It has been established that a flushing cycle of 15 minutes is required to stabilise the system. This translated to 150 fluid volume displacements at a CFV of $28 \text{ cm} \cdot \text{s}^{-1}$.

In industry, gypsum scaling is inhibited by dosing with the appropriate antiscalant. Dosing with an antiscalant can have some adverse effects on the efficient operation of membrane processes, especially in the cases where there is some variability in the feed water to the membrane. Overdosing with the antiscalant can cause the deposition of the antiscalant on the membrane surface, which can lead to a fouling problem. With the dosing of antiscalant comes the added disadvantages that an auxiliary infrastructure should be accompanied with the membrane system, i.e. dosing pumps, feed tanks, mixers and chemical procurement. The system would also require regular flushing with deionised water (in this case valuable product water), to ensure that it does not settle on the membrane surface. It thus remains advantageous to impede scaling with a physical method rather than turning to chemical cleaning methods.

High-level cost analyses were conducted to investigate whether it would be less expensive to simply dose the feed water with the appropriate antiscalant, compared to employing the physical scaling control method proposed by this study, and losing some product water in the process. The most commonly-used antiscalant for impeding gypsum scaling is Vitec® 7000, a product of Avista Technologies. The properties of the product are listed in Table 5-6, as well as the applicable antiscalant dosage, depending on the degree of saturation of the feed solution.

Table 5-6. Properties of Vitec® 7000, a commercially used antiscalant

Product Property	Specification
Appearance	Clear, amber liquid
pH (10% solution)	5.0 – 7.0
Dosing range	2 – 5 $\text{mg} \cdot \text{L}^{-1}$
Specific gravity (@ 20°C)	1.15 – 1.25

Table 5-7 presents the results for the high-level costing analysis. The operational costs associated with the antiscalant dosage and the cost of product water loss, are compared over a plant lifetime of 20 years. The cost of the product water replacement, due to loss from the intermittent flow-path switching, was based on typical municipal water costs. However, in reality the purity of the product water used, will be even higher than that of typical municipal potable water, which would increase these costs even further.

Table 5-7. Cost comparison between continuous osmotic backwashing and the dosing of Vitec @ 7000 for impeding the effects of gypsum scaling on the membrane surface.

SUPERSATURATION FACTOR										
PROPERTY	UOM	1	1.3	1.4	1.5	1.75	2	2.5	3	
Ca ²⁺	mg·L ⁻¹	627	815	878	941	1098	1255	1568	1882	
SO ₄ ²⁻	mg·L ⁻¹	1503	1955	2105	2255	2631	3007	3759	4510	
Na ⁺	mg·L ⁻¹	720	935	1007	1079	1259	1439	1799	2159	
Cl ⁻	mg·L ⁻¹	1110	1443	1554	1665	1942	2219	2774	3329	
ANTISCALANT DOSAGE										
Antiscalant		Vitec 7000	Vitec 7000	Vitec 7000	Vitec 7000	Vitec 7000	Vitec 7000	Vitec 7000	Vitec 7000	Vitec 7000
	mg·L ⁻¹	2.9	3.77	4.06	4.35	5.29	6.02	7.46	8.91	
Dosage	mg·m ⁻³	2900	3770	4060	4350	5290	6020	7460	8910	
	mg·day ⁻¹	862	1121	1207	1294	1573	1790	2218	2649	
Maximum Limiting Recovery	%	80	74	72	70	66	61	51	41	
Antiscalant Cost**	R day ⁻¹	R 0.06	R 0.07	R 0.08	R 0.09	R 0.10	R 0.12	R 0.15	R 0.18	
20 Years Operational	R	R 416.80	R 541.84	R 583.52	R 625.20	R 760.30	R 865.22	R 1 072.18	R 1 280.58	
SWITCHING BETWEEN OPERATIONAL CONFIGURATION										
Switching /day	#	CFV	1	2	3	4	5	6	10	15
		9	1.94	3.88	5.82	7.76	9.70	11.64	19.40	29.09
Volume Lost/Switch*	L·day ⁻¹	19	4.13	8.26	12.39	16.52	20.65	24.78	41.30	61.95
		35	7.63	15.26	22.89	30.53	38.16	45.79	76.32	114.47
		9	R 0.09	R 0.17	R 0.26	R 0.34	R 0.43	R 0.51	R 0.86	R 1.29
Municipal Water Cost	R·day ⁻¹	19	R 0.18	R 0.36	R 0.55	R 0.73	R 0.91	R 1.09	R 1.82	R 2.74
		35	R 0.34	R 0.67	R 1.01	R 1.35	R 1.69	R 2.02	R 3.37	R 5.06
		9	R 625.55	R 1 251.10	R 1 876.64	R 2 502.19	R 3 127.74	R 3 753.29	R 6 255.48	R 9 383.22
20 Years Operational	R	19	R 1 331.98	R 2 663.97	R 3 995.95	R 5 327.93	R 6 659.91	R 7 991.90	R 13 319.83	R 19 979.74
		35	R 2 461.30	R 4 922.60	R 7 383.89	R 9 845.19	R 12 306.49	R 14 767.79	R 24 612.98	R 36 919.47

CHAPTER 5: Results and Discussion

For the experimental run conducted as showed in Figure 5-24, it would be 48 times less expensive over a 20-year operational period to rather dose with antiscalant than to replace the product water lost, due to employing intermittent flow-path switching for an average of 15 *switches* per day. These results provided valuable insight into the proposed fouling mitigation strategy.

Relating to this section, the following concluding remarks can be made:

- The main advantages of intermittent flow-path switching are (1) stable operating fluxes over a period of 12 hours and (2) no chemical requirements to control and limit gypsum scaling.
- The disadvantages include the volume loss during the flushing cycle, which translates to the loss of valuable product water. Furthermore, scaling in the support layer limits the implementation time of intermittent flow-path switching. Over a period of 12 hours a 38% decline in water fluxes achieved were observed when operating in the AL-DS configuration for 15 minutes every 2 hours.
- A high-level cost analysis indicated that it will be 48 times more expensive to replenish the product water loss than to dose with an appropriate antiscalant.

Chapter 6

Conclusions & Recommendations

The project summary, main conclusions and recommendations are detailed in this chapter.

6.1. Conclusions

While considering the study objectives defined in Section 1.3, as well as the various findings from the experimental and theoretical investigations, the following conclusions are drawn

6.1.1. Bench-Scale Setup

The first aim of this study was to design, construct and commission a FO system. Mainly, membrane housing blocks were designed along with flow measurement columns to evaluate the respective inlet and outlet flow rates of the feed solution and the draw solution. Uncertainties relating to the spacer porosity and the flow-channel height proved to be significant in the quantification of the operating cross-flow velocity.

The setup was evaluated experimentally. The measured flux was used as the basis for evaluation, from which the theoretical recovery could be calculated. The actual measured recovery deviated by $2 \pm 1\%$ from the theoretical recovery when using the measured flux. Since performance indicators can be evaluated from the feed solution or the draw solution side, water flux was evaluated from the draw solution side and recovery from the feed solution side. The 2% error then represents the measurement error associated with flux and recovery measurements. However, when calculating for the corrected CFV by using the theoretical recovery, deviations of up to $15 \text{ cm}\cdot\text{s}^{-1}$ in the calculated CFV and the assumed operating CFV were prevalent. After investigation it was found that the channel height was overestimated by 30%, assuming that the spacer porosity was accurate. This resulted in uncertainties in the mechanical design, relating to the flow channel height and the porosity of the spacer (i.e. the flow restriction factor). Nevertheless, the actual corrected operating CFV was calculated, based on the measured flux and calculated theoretical recovery.

6.1.2. Validation and Characterisation Tests

The primary aim of the validation tests was to evaluate the mass transfer over the FO membrane, by investigating the effects of CFV as well as the operational configuration of the membrane. Validation experiments were conducted with deionised water as the FS and a $29\,220 \text{ mg}\cdot\text{L}^{-1}$ TDS NaCl DS. The mass transfer present in the system was limited to water and NaCl.

CHAPTER 6: Conclusions & Recommendations

In the AL-FS configuration, the flux increased from $11.2 \text{ L}\cdot\text{m}^{-2}\cdot\text{h}^{-1}$ to $20 \text{ L}\cdot\text{m}^{-2}\cdot\text{h}^{-1}$ when the CFV was increased from $13 \text{ cm}\cdot\text{s}^{-1}$ to $37 \text{ cm}\cdot\text{s}^{-1}$. However, a further increase in CFV above $37 \text{ cm}\cdot\text{s}^{-1}$ did not result in higher fluxes and the limiting flux of $20 \text{ L}\cdot\text{m}^{-2}\cdot\text{h}^{-1}$ was reached. This is ascribed to the potential increase in dilutive internal concentration polarisation in the support layer of the membrane, thereby limiting the effective driving force (effective osmotic pressure difference) over the membrane.

In the AL-DS configuration, this limiting flux was not reached within the defined CFV range. However, it was found that operation in the AL-DS configuration tended to a limiting flux of $20 \text{ L}\cdot\text{m}^{-2}\cdot\text{h}^{-1}$ when operating at draw solution concentrations above $50\,000 \text{ mg}\cdot\text{L}^{-1}$ TDS. This is considered to be partly the result of an increased reverse solute flux (RSF) along with dilutive external concentration polarisation on the active layer side of the membrane. A 32% reduction in salt passage was observed for the AL-FS configuration, compared to the AL-DS configuration which was ascribed to the SL thickness and tortuosity, acting as an additional resistance for boundary layer penetration, thus serving as a barrier for salt diffusion for the draw solute from the DS to the FS. In the AL-DS configuration ECP becomes prevalent at CFVs $>13 \text{ cm}\cdot\text{s}^{-1}$. CP is more dominant at higher water fluxes which are attained at increased operating CFVs. At CFV $<13 \text{ cm}\cdot\text{s}^{-1}$, operation is limited by RSF. Based on the CP moduli, RSF is the limiting phenomenon at the range of CFVs investigated.

6.1.3. Intermittent Flow-Path Switching

Three variances in the CFV were investigated: $13 \text{ cm}\cdot\text{s}^{-1}$, $28 \text{ cm}\cdot\text{s}^{-1}$ and $52 \text{ cm}\cdot\text{s}^{-1}$. Experimental run lengths of 60 hours were conducted to determine at which CFV the most predictable performance is attained in alleviating RSF and ICP. This was found to be when operating at a CFV of $28 \text{ cm}\cdot\text{s}^{-1}$. Furthermore, a stabilisation or flushing time equal to 15 minutes, translated to 150 bed displacements at a CFV of $28 \text{ cm}\cdot\text{s}^{-1}$, which were sufficient to purge the system of residual solutions.

6.1.4. Practical Implementation

An overall flux decline of 38% in the AL-DS configuration was achieved over a period of 12 hours. This emphasised the detrimental scaling effects in the AL-DS configuration, irrespective of permeate reversal. Furthermore, the process water from the flushing cycle had to be discarded, as it was contaminated with scaling ions, and it could not be reclaimed via downstream processing units such as RO. This translated to a volume loss of $8 \text{ L}\cdot\text{day}^{-1}$ for a 0.1344 m^2 system. Therefore, it was clear that intermittent flow-path switching was effective in the AL-FS configuration, but was rendered ineffective in the AL-DS configuration. This is due to internal scaling in the support layer.

The main advantages of intermittent flow-path switching are (1) stable operating flux over a period of 12 hours and (2) no chemicals required to limit gypsum scaling. The disadvantages include the water volume lost due to the flushing cycle. In addition, a high-level cost comparison indicated that product water replacement due to the volume loss, would be approximately 48 times more expensive over a 20-year operational period as opposed to dosing with an antiscalant, Vitec ® 7000.

Therefore, a time constraint is placed on the implementation of intermittent flow-path switching. The severe scaling in the support layer limits the operation time. When the formation of gypsum crystals

starts forming in the support layer, pore clogging that severely limits membrane operation occurs, and this might leave the membrane to be ineffective.

6.2. Recommendations

As per the outcomes of this investigation, the following recommendations are made with regards to future work:

- The development of relationships and factors to correct and normalise water flux data to a standard set of operating conditions, taking the effects of the (1) draw solute, (2) ICP and ECP as well as RSD on the process driving force, into account. This can be done by incorporating the Peclet number and the concentration polarisation moduli in the normalisation correlations.
- The rate of flux decline due to gypsum scaling should be quantified. Thereby the critical or limiting flux can be determined under scaling conditions. The critical flux phenomenon aids in the prediction of a sharp decrease in the rate of membrane permeability decline due to scaling. It is suggested that experimental procedure be designed to: (1) investigate flux declines by keeping the level of supersaturation constant but to evaluate scaling at various initial fluxes, (2) changes in the membrane permeability can be evaluated to finally (3) quantify the rate of permeability decline due to scaling. Conducting these experiments will greatly aid in distinguishing between flux declines due to scaling or concentration polarisation as polarisation effects will not affect the membrane permeability.
- Based on the bench-scale system, a method should be developed to accurately quantify the channel height (h_{ch}), as well as the spacer porosity, in order to minimise deviations in the assumed and actual operating CFV. This will aid in experimental planning, especially when the system is designed to operate at a specific CFV. The spacer porosity can be determined by: (1) computed tomography, (2) volume displacement and (3) weight and density measurements.
- It is recommended that the test work relating to the practical implementation of the proposed fouling control strategy – intermittent flow-path switching – be extended over a prolonged period of a week (170 hours) at minimum. Prolonged experimentation will greatly aid in distinguishing between experimental noise and experimental trends observed.
- And finally, build and commission a more robust experimental setup, using a spiral wound industrial FO membrane to investigate the proposed method for fouling control in large scale membrane systems. It is suggested that the bench-scale setup be scaled to a pilot plant. The analytical equations [Equations (5.3) to (5.8)] derived in this study can be used to design the FO unit. Typically, FO systems are designed by quantifying and fixing (1) the product water production rate and (2) either the water flux of the recovery rate. Then, according to these parameters along with the derived equations, the system can be sized and performance predictions can be calculated.

References

- [1] Zhao S, Zou L, Mulcahy D. Effects of membrane orientation on process performance in forward osmosis applications. *J Membr Sci* 2011;382:308–15.
- [2] Arkhangelsky E, Wicaksana F, Chou S, Al-Rabiah AA, Al-Zahrani SM, Wang R. Effects of scaling and cleaning on the performance of forward osmosis hollow fiber membranes. *J Membr Sci* 2012;415:101–8.
- [3] Loeb S, Titelman L, Korngold E, Freiman J. Effect of porous support fabric on osmosis through a Loeb-Sourirajan type asymmetric membrane. *J Membr Sci* 1997;129:243–9.
- [4] McCutcheon JR, Elimelech M. Influence of concentrative and dilutive internal concentration polarization on flux behavior in forward osmosis. *J Membr Sci* 2006;284:237–47.
- [5] Tang CY, She Q, Lay WCL, Wang R, Fane AG. Coupled effects of internal concentration polarization and fouling on flux behavior of forward osmosis membranes during humic acid filtration. *J Membr Sci* 2010;354:123–33.
- [6] Phillip WA, Yong JS, Elimelech M. Reverse Draw Solute Permeation in Forward Osmosis: Modeling and Experiments. *Environ Sci Technol* 2010;44:5170–6.
- [7] Yip NY, Tiraferri A, Phillip WA, Schiffman JD, Elimelech M. High Performance Thin-Film Composite Forward Osmosis Membrane. *Environ Sci Technol* 2010;44:3812–8.
- [8] Zou S, Gu Y, Xiao D, Tang CY. The role of physical and chemical parameters on forward osmosis membrane fouling during algae separation. *J Membr Sci* 2011;366:356–62.
- [9] She Q, Jin X, Li Q, Tang CY. Relating reverse and forward solute diffusion to membrane fouling in osmotically driven membrane processes. *Water Res* 2012;46:2478–86.
- [10] Mi B, Elimelech M. Chemical and physical aspects of organic fouling of forward osmosis membranes. *J Membr Sci* 2008;320:292–302.
- [11] Lee S, Boo C, Elimelech M, Hong S. Comparison of fouling behavior in forward osmosis (FO) and reverse osmosis (RO). *J Membr Sci* 2010;365:34–9.
- [12] Liu Y, Mi B. Combined fouling of forward osmosis membranes: Synergistic foulant interaction and direct observation of fouling layer formation. *J Membr Sci* 2012;407–408:136–44.
- [13] Zhao S, Zou L. Effects of working temperature on separation performance, membrane scaling and cleaning in forward osmosis desalination. *Desalination* 2011;278:157–64.
- [14] Xie M, Price WE, Nghiem LD, Elimelech M. Effects of feed and draw solution temperature and transmembrane temperature difference on the rejection of trace organic contaminants by forward osmosis. *J Membr Sci* 2013;438:57–64.
- [15] Ge Q, Ling M, Chung T-S. Draw solutions for forward osmosis processes: Developments, challenges, and prospects for the future. *J Membr Sci* 2013;442:225–37.

References

- [16] Holloway RW, Maltos R, Vanneste J, Cath TY. Mixed draw solutions for improved forward osmosis performance. *J Membr Sci* 2015;491:121–31.
- [17] Achilli A, Cath TY, Childress AE. Selection of inorganic-based draw solutions for forward osmosis applications. *J Membr Sci* 2010;364:233–41.
- [18] Nicoll, P. (2013). Forward Osmosis as a Pre-treatment to Reverse Osmosis. The International Desalination Association World Congress on Desalination and Water Reuse, Tianjin, China 2013.
- [19] Phuntsho S, Shon HK, Zhang T, Surampalli R. Introduction: Role of Membrane Science and Technology and Forward Osmosis Processes. *Forw. Osmosis*, American Society of Civil Engineers; 2016.
- [20] Pendergast MM, Nowosielski-Slepowron MS, Tracy J. Going big with forward osmosis. *Desalination Water Treat* 2016;0:1–10.
- [21] Kim C, Lee S, Hong S. Application of osmotic backwashing in forward osmosis: mechanisms and factors involved. *Desalination Water Treat* 2012;43:314–22.
- [22] Ng HY, Tang W, Wong WS. Performance of Forward (Direct) Osmosis Process: Membrane Structure and Transport Phenomenon. *Environ Sci Technol* 2006;40:2408–13.
- [23] Cath TY, Elimelech M, McCutcheon JR, McGinnis RL, Achilli A, Anastasio D, et al. Standard Methodology for Evaluating Membrane Performance in Osmotically Driven Membrane Processes. *Desalination* 2013;312:31–8.
- [24] McCutcheon JR, Elimelech M. Modeling water flux in forward osmosis: implications for improved membrane design. *AIChE J* 2007;53:1736–1744.
- [25] Gray GT, McCutcheon JR, Elimelech M. Internal concentration polarization in forward osmosis: role of membrane orientation. *Desalination* 2006;197:1–8.
- [26] Hancock NT, Cath TY. Solute Coupled Diffusion in Osmotically Driven Membrane Processes. *Environ Sci Technol* 2009;43:6769–75.
- [27] Luttmiah K, Verliefe ARD, Roest K, Rietveld LC, Cornelissen ER. Forward osmosis for application in wastewater treatment: A review. *Water Res* 2014;58:179–97.
- [28] Blandin G, Vervoort H, Le-Clech P, Verliefe ARD. Fouling and cleaning of high permeability forward osmosis membranes. *J Water Process Eng* 2016;9:161–9.
- [29] She Q, Wong YKW, Zhao S, Tang CY. Organic fouling in pressure retarded osmosis: Experiments, mechanisms and implications. *J Membr Sci* 2013;428:181–9.
- [30] Zhao S, Zou L, Tang CY, Mulcahy D. Recent developments in forward osmosis: Opportunities and challenges. *J Membr Sci* 2012;396:1–21.
- [31] Jin X, Tang CY, Gu Y, She Q, Qi S. Boric Acid Permeation in Forward Osmosis Membrane Processes: Modeling, Experiments, and Implications. *Environ Sci Technol* 2011;45:2323–30.
- [32] Jin X, Shan J, Wang C, Wei J, Tang CY. Rejection of pharmaceuticals by forward osmosis membranes. *J Hazard Mater* 2012;227:55–61.

-
- [33] Zhang M, Hou D, She Q, Tang CY. Gypsum scaling in pressure retarded osmosis: Experiments, mechanisms and implications. *Water Res* 2014;48:387–95.
- [34] Baker RW. *Membrane Technology and Applications*. 3rd ed. Somerset: Wiley; 2012.
- [35] Mi B, Elimelech M. Gypsum Scaling and Cleaning in Forward Osmosis: Measurements and Mechanisms. *Environ Sci Technol* 2010;44:2022–8.
- [36] Shaffer DL, Werber JR, Jaramillo H, Lin S, Elimelech M. Forward osmosis: Where are we now? *Desalination* 2015;356:271–84.
- [37] Engel, T., & Reid, P. *Thermodynamics, statistical thermodynamics, & kinetics*. Boston: Pearson; 2013.
- [38] Phuntsho S, Hong S, Elimelech M, Shon HK. Osmotic equilibrium in the forward osmosis process: Modelling, experiments and implications for process performance. *J Membr Sci* 2014;453:240–52.
- [39] Benavides S, Oloriz AS, Phillip WA. Forward Osmosis Processes in the Limit of Osmotic Equilibrium. *Ind Eng Chem Res* 2015;54:480–90.
- [40] Kucera J. *Reverse osmosis: design, processes, and applications for engineers*. Salem, Mass.; Hoboken, N.J.: Scrivener Pub. ; Wiley; 2010.
- [41] Wang Z, Tang J, Zhu C, Dong Y, Wang Q, Wu Z. Chemical cleaning protocols for thin film composite (TFC) polyamide forward osmosis membranes used for municipal wastewater treatment. *ResearchGate* 2015;475.
- [42] Cussler EL. *Diffusion: Mass Transfer in Fluid Systems*. Cambridge University Press; 2009.
- [43] Seader, J. D., Henley, E. J., & Roper, D. K. *Separation process principles: Chemical and biochemical operations*. Hoboken, NJ: Wiley; 2011.
- [44] Walton NRG. Electrical Conductivity and Total Dissolved Solids—What is Their Precise Relationship? *Desalination* 1989;72:275–92.
- [45] Hancock NT, Phillip WA, Elimelech M, Cath TY. Bidirectional Permeation of Electrolytes in Osmotically Driven Membrane Processes. *Environ Sci Technol* 2011;45:10642–51.
- [46] Kim B, Gwak G, Hong S. Review on methodology for determining forward osmosis (FO) membrane characteristics: Water permeability (A), solute permeability (B), and structural parameter (S). *Desalination* 2017;422:5–16.
- [47] Lay WCL, Liu Y, Fane AG. Impacts of salinity on the performance of high retention membrane bioreactors for water reclamation: A review. *Water Res* 2010;44:21–40.
- [48] She Q, Wang R, Fane AG, Tang CY. Membrane fouling in osmotically driven membrane processes: A review. *J Membr Sci* 2016;499:201–33.
- [49] Shon HK, Phuntsho S, Zhang TC, Surampalli RY. *Forward osmosis: fundamentals and applications*. 2015.
-

References

- [50] Field RW, Wu JJ. On boundary layers and the attenuation of driving forces in forward osmosis and other membrane processes. *Desalination* 2018;429:167–74.
- [51] Wang Y, Zhang M, Liu Y, Xiao Q, Xu S. Quantitative evaluation of concentration polarization under different operating conditions for forward osmosis process. *Desalination* 2016;398:106–13.
- [52] Tang CY, Chong TH, Fane AG. Colloidal interactions and fouling of NF and RO membranes: A review. *Adv Colloid Interface Sci* 2011;164:126–43.
- [53] Cath TY, Childress AE, Elimelech M. Forward osmosis: Principles, applications, and recent developments. *J Membr Sci* 2006;281:70–87.
- [54] Yip NY, Elimelech M. Comparison of Energy Efficiency and Power Density in Pressure Retarded Osmosis and Reverse Electrodialysis. *Environ Sci Technol* 2014;48:11002–12.
- [55] Yip NY, Elimelech M. Influence of Natural Organic Matter Fouling and Osmotic Backwash on Pressure Retarded Osmosis Energy Production from Natural Salinity Gradients. *Environ Sci Technol* 2013;47:12607–16.
- [56] Lee Y-E, Jang A. Effect of forward osmosis (membrane) support layer fouling by organic matter in synthetic seawater solution. *Desalination Water Treat* 2016;57:24595–605.
- [57] Le-Clech P, Chen V, Fane TAG. Fouling in membrane bioreactors used in wastewater treatment. *J Membr Sci* 2006;284:17–53.
- [58] Wang Y, Wicaksana F, Tang CY, Fane AG. Direct Microscopic Observation of Forward Osmosis Membrane Fouling. *Environ Sci Technol* 2010;44:7102–9.
- [59] Cath TY, Hancock NT, Lundin CD, Hoppe-Jones C, Drewes JE. A multi-barrier osmotic dilution process for simultaneous desalination and purification of impaired water. *J Membr Sci* 2010;362:417–26.
- [60] Loeb S. Production of energy from concentrated brines by pressure-retarded osmosis. *J Membr Sci* 1976;1:49–63.
- [61] McCutcheon JR, McGinnis RL, Elimelech M. A novel ammonia—carbon dioxide forward (direct) osmosis desalination process. *Desalination* 2005;174:1–11.
- [62] Qin J-J, Kekre KA, Oo MH, Tao G, Lay CL, Lew CH, et al. Preliminary study of osmotic membrane bioreactor: effects of draw solution on water flux and air scouring on fouling. *Water Sci Technol J Int Assoc Water Pollut Res* 2010;62:1353–60.
- [63] Gao Y, Haavisto S, Li W, Tang CY, Salmela J, Fane AG. Novel Approach To Characterizing the Growth of a Fouling Layer during Membrane Filtration via Optical Coherence Tomography. *Environ Sci Technol* 2014;48:14273–81.
- [64] Boo C, Elimelech M, Hong S. Fouling control in a forward osmosis process integrating seawater desalination and wastewater reclamation. *J Membr Sci* 2013;444:148–56.
- [65] Hickenbottom KL, Hancock NT, Hutchings NR, Appleton EW, Beaudry EG, Xu P, et al. Forward osmosis treatment of drilling mud and fracturing wastewater from oil and gas operations. *Desalination* 2013;312:60–6.

-
- [66] Li Z-Y, Yangali-Quintanilla V, Valladares-Linares R, Li Q, Zhan T, Amy G. Flux patterns and membrane fouling propensity during desalination of seawater by forward osmosis. *Water Res* 2012;46:195–204.
- [67] Zhao Y, Ren Y, Wang X, Xiao P, Tian E, Wang X, et al. An initial study of EDTA complex based draw solutes in forward osmosis process. *Desalination* 2016;378:28–36.
- [68] Cussler, E. L. *Diffusion, mass transfer in fluid systems*. Cambridge University Press; 1984.
- [69] Bowden KS, Achilli A, Childress AE. Organic ionic salt draw solutions for osmotic membrane bioreactors. *Bioresour Technol* 2012;122:207–16.
- [70] Coday BD, Heil DM, Xu P, Cath TY. Effects of Transmembrane Hydraulic Pressure on Performance of Forward Osmosis Membranes. *Environ Sci Technol* 2013;47:2386–93.
- [71] Irvine GJ, Rajesh S, Georgiadis M, Phillip WA. Ion Selective Permeation Through Cellulose Acetate Membranes in Forward Osmosis. *Environ Sci Technol* 2013;47:13745–53.
- [72] Lu X, Boo C, Ma J, Elimelech M. Bidirectional Diffusion of Ammonium and Sodium Cations in Forward Osmosis: Role of Membrane Active Layer Surface Chemistry and Charge. *Environ Sci Technol* 2014;48:14369–76.
- [73] Xie M, Gray SR. Gypsum scaling in forward osmosis: Role of membrane surface chemistry. *J Membr Sci* 2016;513:250–9.
- [74] Elimelech M, O'Melia CR. Effect of electrolyte type on the electrophoretic mobility of polystyrene latex colloids. *Colloids Surf* 1990;44:165–78.
- [75] Childress AE, Elimelech M. Effect of solution chemistry on the surface charge of polymeric reverse osmosis and nanofiltration membranes. *J Membr Sci* 1996;119:253–68.
- [76] Mi B, Elimelech M. Silica scaling and scaling reversibility in forward osmosis. *Desalination* 2013;312:75–81.
- [77] Zou S, Wang Y-N, Wicaksana F, Aung T, Wong PCY, Fane AG, et al. Direct microscopic observation of forward osmosis membrane fouling by microalgae: Critical flux and the role of operational conditions. *J Membr Sci* 2013;436:174–85.
- [78] Parida V, Ng HY. Forward osmosis organic fouling: Effects of organic loading, calcium and membrane orientation. *Desalination* 2013;312:88–98.
- [79] Zhang J, Loong WLC, Chou S, Tang C, Wang R, Fane AG. Membrane biofouling and scaling in forward osmosis membrane bioreactor. *J Membr Sci* 2012;403–404:8–14.
- [80] Mi B, Elimelech M. Organic fouling of forward osmosis membranes: Fouling reversibility and cleaning without chemical reagents. *J Membr Sci* 2010;348:337–45.
- [81] Valladares Linares R, Yangali-Quintanilla V, Li Z, Amy G. NOM and TEP fouling of a forward osmosis (FO) membrane: Foulant identification and cleaning. *J Membr Sci* 2012;421–422:217–24.

References

- [82] She Q, Jin X, Tang CY. Osmotic power production from salinity gradient resource by pressure retarded osmosis: Effects of operating conditions and reverse solute diffusion. *J Membr Sci* 2012;401–402:262–73.
- [83] Tang CY, She Q, Lay WCL, Wang R, Field R, Fane AG. Modeling double-skinned FO membranes. *Desalination* 2011;283:178–86.
- [84] Qi S, Qiu CQ, Zhao Y, Tang CY. Double-skinned forward osmosis membranes based on layer-by-layer assembly—FO performance and fouling behavior. *J Membr Sci* 2012;405–406:20–9.
- [85] Chou S, Shi L, Wang R, Tang CY, Qiu C, Fane AG. Characteristics and potential applications of a novel forward osmosis hollow fiber membrane. *Desalination* 2010;261:365–72.
- [86] Shih W-Y, Rahardianto A, Lee R-W, Cohen Y. Morphometric characterization of calcium sulfate dihydrate (gypsum) scale on reverse osmosis membranes. *J Membr Sci* 2005;252:253–63.
- [87] Söhnle O, Mullin JW. A method for the determination of precipitation induction periods. *J Cryst Growth* 1978;44:377–82.
- [88] Innorta G, Rabbi E, Tomadin L. The gypsum-anhydrite equilibrium by solubility measurements. *Geochim Cosmochim Acta* 1980;44:1931–6.
- [89] Nancollas GH, Reddy MM, Tsai F. Calcium sulfate dihydrate crystal growth in aqueous solution at elevated temperatures. *J Cryst Growth* 1973;20:125–34.
- [90] Bock E. On the Solubility of Anhydrous Calcium Sulphate and of Gypsum in Concentrated Solutions of Sodium Chloride at 25 °c, 30 °c, 40 °c, and 50 °c. *Can J Chem* 1961;39:1746–51.
- [91] Power WH, Fabuss BM. Transient Solubilities in the Calcium Sulfate-Water System. *J Chem Eng Data* 1964;9:437–42.
- [92] Rahman F. Calcium sulfate precipitation studies with scale inhibitors for reverse osmosis desalination. *Desalination* 2013;319:79–84.
- [93] Bock H. The effect of humic substances on the crystallisation of gypsum. [Masters Dissertation]. University of Stellenbosch. Stellenbosch; 2017.
- [94] Abdel-Aal EA, Rashad MM, El-Shall H. Crystallization of calcium sulfate dihydrate at different supersaturation ratios and different free sulfate concentrations. *Cryst Res Technol* 2004;39:313–21.
- [95] Ramon G, Agnon Y, Dosoretz C. Dynamics of an osmotic backwash cycle. *J Membr Sci* 2010;364:157–66.
- [96] Boo C, Lee S, Elimelech M, Meng Z, Hong S. Colloidal fouling in forward osmosis: Role of reverse salt diffusion. *J Membr Sci* 2012;390–391:277–84.
- [97] Valladares Linares R, Li Z, Abu-Ghdaib M, Wei C-H, Amy G, Vrouwenvelder JS. Water harvesting from municipal wastewater via osmotic gradient: An evaluation of process performance. *J Membr Sci* 2013;447:50–6.
- [98] Bui N-N, Lind ML, Hoek EMV, McCutcheon JR. Electrospun nanofiber supported thin film composite membranes for engineered osmosis. *J Membr Sci* 2011;385–386:10–9.

-
- [99] Widjojo N, Chung T-S, Weber M, Maletzko C, Warzelhan V. The role of sulphonated polymer and macrovoid-free structure in the support layer for thin-film composite (TFC) forward osmosis (FO) membranes. *J Membr Sci* 2011;383:214–23. doi:10.1016/j.memsci.2011.08.041.
- [100] Shi L, Chou SR, Wang R, Fang WX, Tang CY, Fane AG. Effect of substrate structure on the performance of thin-film composite forward osmosis hollow fiber membranes. *J Membr Sci* 2011;382:116–23.
- [101] Qiu C, Qi S, Tang CY. Synthesis of high flux forward osmosis membranes by chemically crosslinked layer-by-layer polyelectrolytes. *J Membr Sci* 2011;381:74–80.
- [102] Wei J, Liu X, Qiu C, Wang R, Tang CY. Influence of monomer concentrations on the performance of polyamide-based thin film composite forward osmosis membranes. *J Membr Sci* 2011;381:110–7.
- [103] Qiu C, Setiawan L, Wang R, Tang CY, Fane AG. High performance flat sheet forward osmosis membrane with an NF-like selective layer on a woven fabric embedded substrate. *Desalination* 2012;287:266–70.
- [104] Sairam M, Sereewatthanawut E, Li K, Bismarck A, Livingston AG. Method for the preparation of cellulose acetate flat sheet composite membranes for forward osmosis—Desalination using MgSO₄ draw solution. *Desalination* 2011;273:299–307.
- [105] Yu Y, Seo S, Kim I-C, Lee S. Nanoporous polyethersulfone (PES) membrane with enhanced flux applied in forward osmosis process. *J Membr Sci* 2011;375:63–8.
- [106] Zhang S, Wang KY, Chung T-S, Jean YC, Chen H. Molecular design of the cellulose ester-based forward osmosis membranes for desalination. *Chem Eng Sci* 2011;66:2008–18.
- [107] Wei J, Qiu C, Tang CY, Wang R, Fane AG. Synthesis and characterization of flat-sheet thin film composite forward osmosis membranes. *J Membr Sci* 2011;372:292–302.
- [108] Saren Q, Qiu CQ, Tang CY. Synthesis and Characterization of Novel Forward Osmosis Membranes based on Layer-by-Layer Assembly. *Environ Sci Technol* 2011;45:5201–8.
- [109] Yang Q, Wang KY, Chung T-S. Dual-Layer Hollow Fibers with Enhanced Flux As Novel Forward Osmosis Membranes for Water Production. *Environ Sci Technol* 2009;43:2800–5.
- [110] Yip NY, Tiraferri A, Phillip WA, Schiffman JD, Hoover LA, Kim YC, et al. Thin-Film Composite Pressure Retarded Osmosis Membranes for Sustainable Power Generation from Salinity Gradients. *Environ Sci Technol* 2011;45:4360–9.
- [111] Ahmed M, Shayya WH, Hoey D, Al-Handaly J. Brine disposal from reverse osmosis desalination plants in Oman and the United Arab Emirates. *Desalination* 2001;133:135–47.
- [112] Morillo J, Usero J, Rosado D, El Bakouri H, Riaza A, Bernaola F-J. Comparative study of brine management technologies for desalination plants. *Desalination* 2014;336:32–49.
- [113] Tang W, Ng HY. Concentration of brine by forward osmosis: Performance and influence of membrane structure. *Desalination* 2008;224:143–53.
- [114] Martinetti CR, Childress AE, Cath TY. High recovery of concentrated RO brines using forward osmosis and membrane distillation. *J Membr Sci* 2009;331:31–9.
-

References

- [115] Siddiqui A, Lehmann S, Haaksman V, Ogier J, Schellenberg C, van Loosdrecht MCM, et al. Porosity of spacer-filled channels in spiral-wound membrane systems: Quantification methods and impact on hydraulic characterization. *Water Res* 2017;119:304–11.
- [116] Kim J, Blandin G, Phuntsho S, Verliefde A, Le-Clech P, Shon H. Practical considerations for operability of an 8" spiral wound forward osmosis module: Hydrodynamics, fouling behaviour and cleaning strategy. *Desalination* 2017;404:249–58.
- [117] Water Environment Federation. *Membrane systems for wastewater treatment*. New York: McGraw-Hill; 2006.
- [118] Robinson JW. Determination of sodium by atomic absorption spectroscopy. *Anal Chim Acta* 1960;23:458–61.
- [119] Xu Y, Peng X, Tang CY, Fu QS, Nie S. Effect of draw solution concentration and operating conditions on forward osmosis and pressure retarded osmosis performance in a spiral wound module. *J Membr Sci* 2010;348:298–309.
- [120] Wijmans JG, Athayde AL, Daniels R, Ly JH, Kamaruddin HD, Pinnau I. The role of boundary layers in the removal of volatile organic compounds from water by pervaporation. *J Membr Sci* 1996;109:135–46.
- [121] Li, X., Zhao, B., Wang, Z., Xie, M., Song, J., Nghiem, L. D., He, T., Yang, C., Li, C. & Chen, G. Water reclamation from shale gas drilling flow-back fluid using a novel forward osmosis-vacuum membrane distillation hybrid system. *Water Science and Technology*, 2014;69 (5), 1036-1044.
- [122] Phuntsho S, Sahebi S, Majeed T, Lotfi F, Kim JE, Shon HK. Assessing the major factors affecting the performances of forward osmosis and its implications on the desalination process. *Chem Eng J* 2013;231:484–96.
- [123] Lay WCL, Zhang J, Tang C, Wang R, Liu Y, Fane AG. Factors affecting flux performance of forward osmosis systems. *J Membr Sci* 2012;394–395:151–68.

Appendix A

Design

A.1. In-line Flow Meter Design

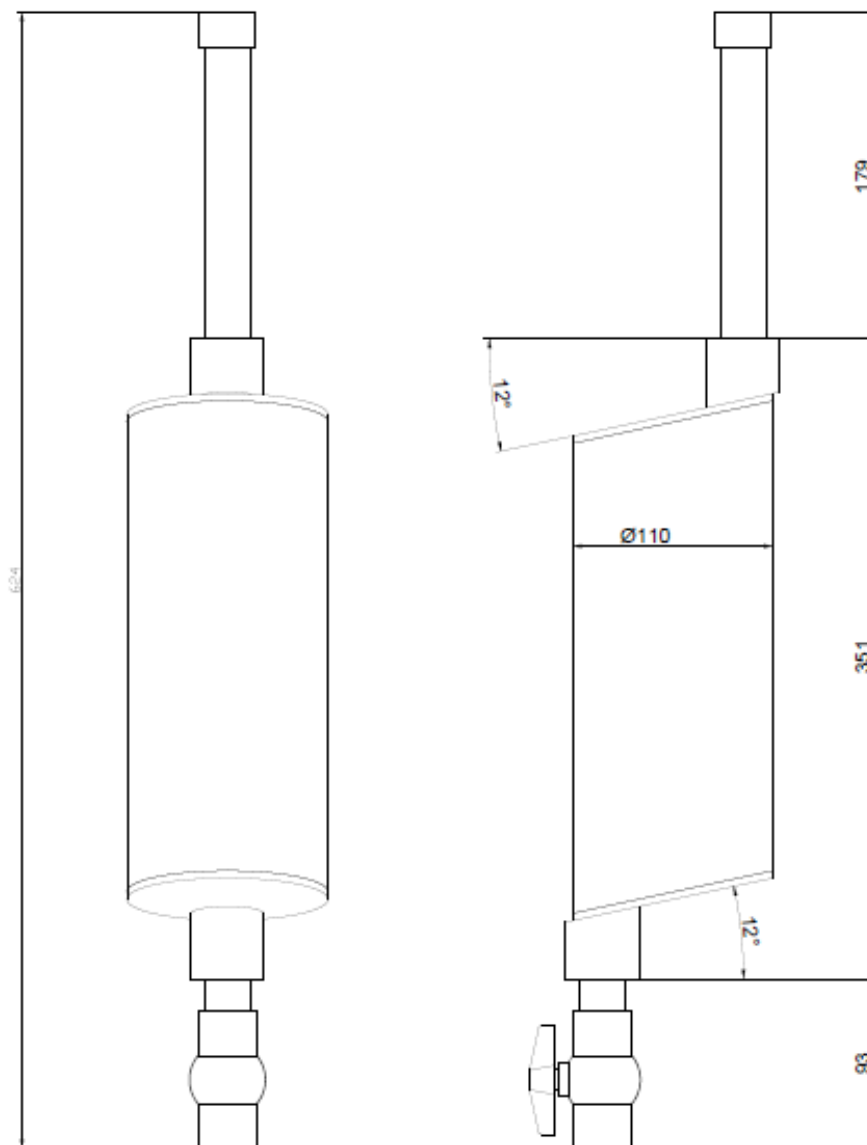


Figure A-1. Line drawing of the Perspex outlet inline flow meters.

APPENDIX A: Design

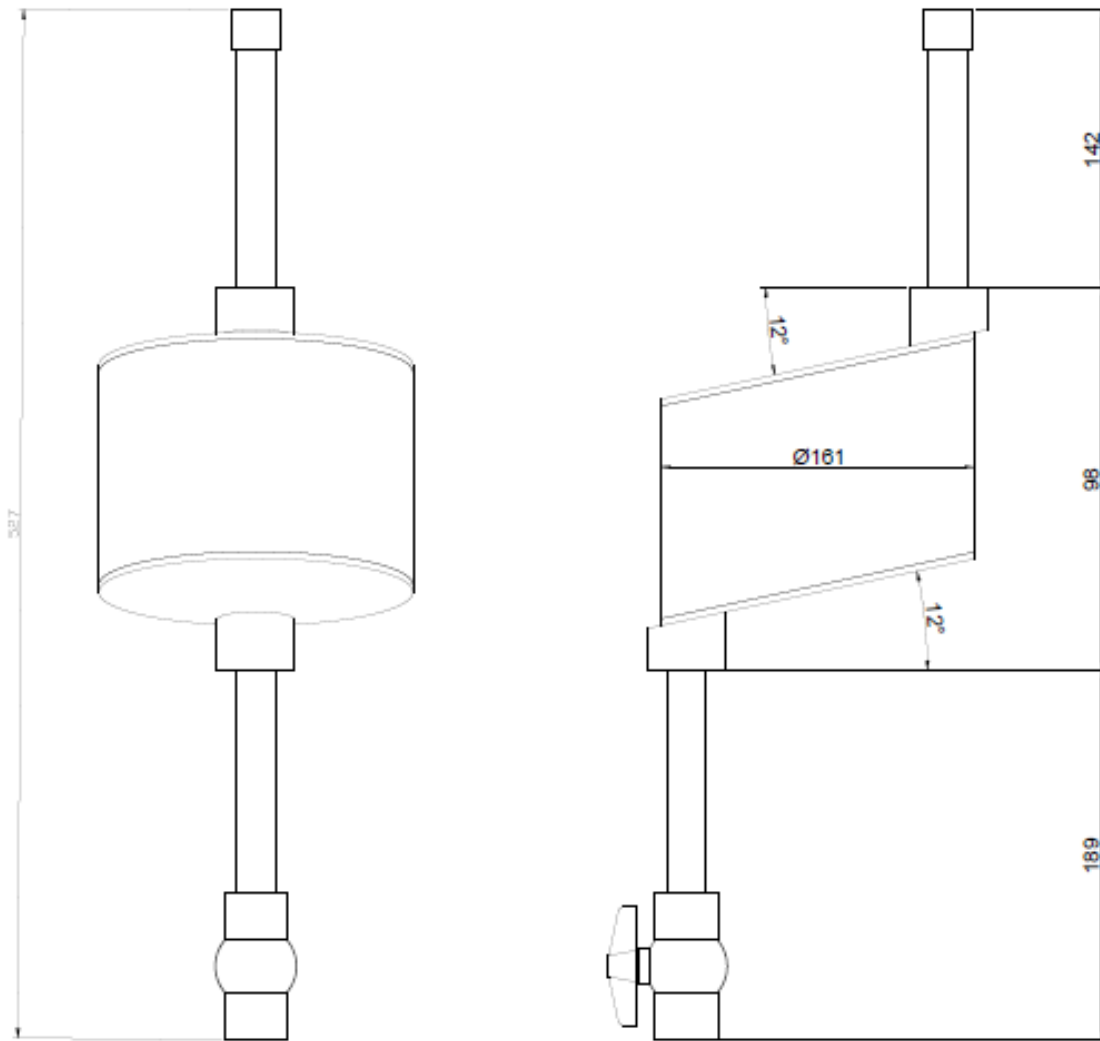


Figure A-2. Line drawing of the PVC inlet inline flow meters.

A.2. Hydraulic Design: Membrane Housing Blocks

Table A-1. Hydraulic characterisation of the flow channels in each housing block.

System Design Parameters							
Property	UOM	Block 1	Block 2	Block 3	Block 4	Block 5	Block 6
Maximum Flowrate	mL·min ⁻¹	272	264	256	248	241	234
Nominal Flowrate	mL·min ⁻¹	210	202	194	186	179	172
Minimum Flowrate	mL·min ⁻¹	93	85	78	70	63	55
Operating Temperature	°C	24	24	24	24	24	24
Operating Pressure: FS	bar _g	0.20000	0.19997	0.19995	0.19993	0.19991	0.19989
Operating Pressure: DS	bar _g	0.20000	0.19997	0.19995	0.19992	0.19989	0.19985
System Hydraulic Characterisation							
<u>Feed Solution</u>							
Nominal CFVs	m·s ⁻¹	0.20	0.20	0.19	0.18	0.17	0.17
Pressure Drop	m	0.0197	0.0182	0.0169	0.0156	0.0145	0.0134
	bar	2.55564E-05	2.37051E-05	2.19643E-05	2.03293E-05	1.87953E-05	1.73578E-05
Reynolds Number		24262	23345	22450	21577	20725	19895
Flow Regime		Turbulent	Turbulent	Turbulent	Turbulent	Turbulent	Turbulent
Friction Factor		0.0426	0.0426	0.0427	0.0428	0.0429	0.0430
<u>Draw Solution</u>							
Nominal CFVs	m·s ⁻¹	0.20	0.21	0.22	0.23	0.23	0.24
Pressure Drop	m	0.0197	0.0211	0.0226	0.0241	0.0257	0.0272
	bar	2.55564E-05	2.74771E-05	2.94195E-05	3.13789E-05	3.33506E-05	3.533E-05
Reynolds Number		24262	25178	26073	26947	27798	28629
Flow Regime		Turbulent	Turbulent	Turbulent	Turbulent	Turbulent	Turbulent
Friction Factor		0.0426	0.0425	0.0424	0.0424	0.0423	0.0423
Recovery	%	3.78	3.83	3.89	3.95	4.01	4.07

APPENDIX A: Design

A.3. Drawing: Membrane Housing Design

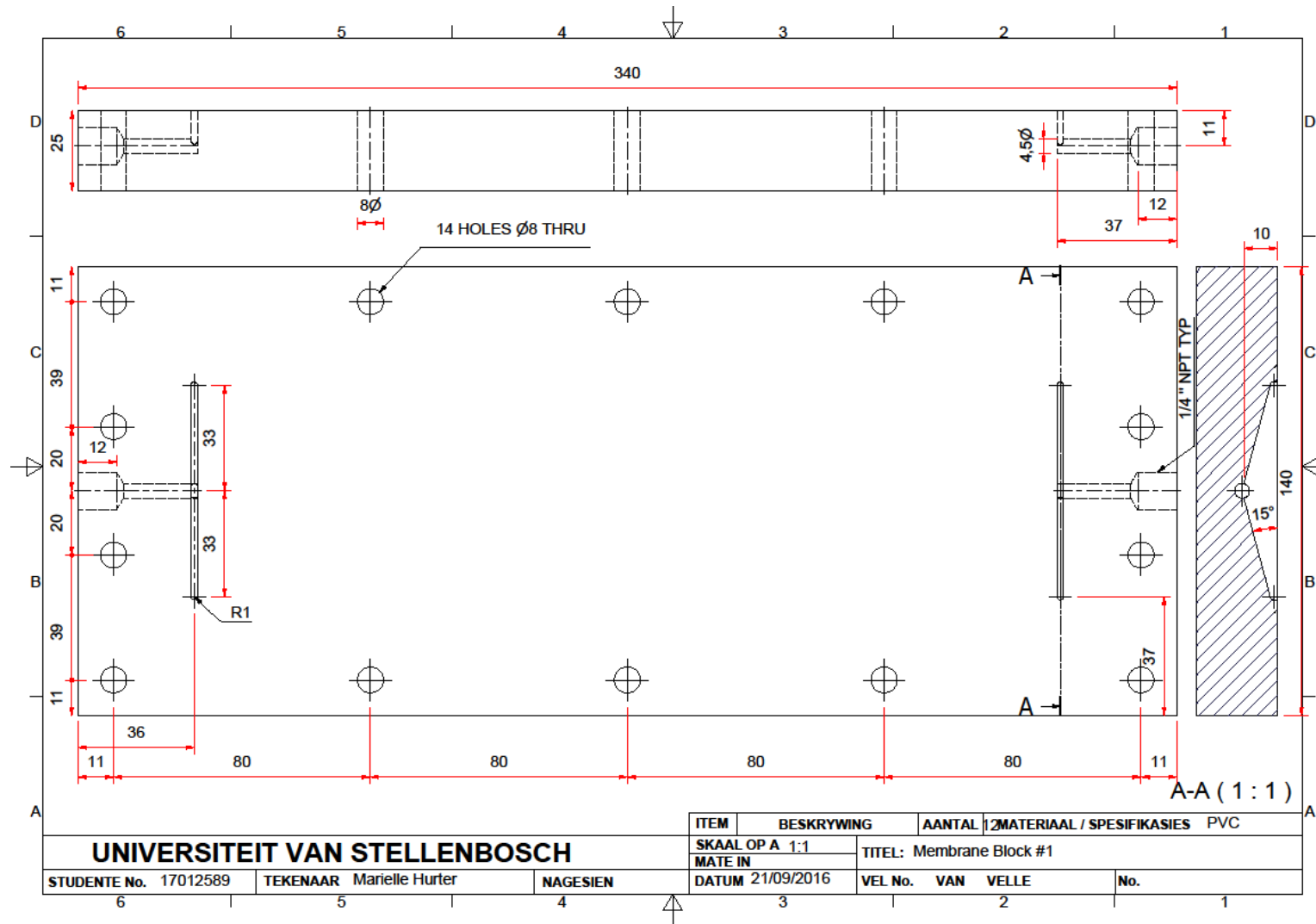


Figure A-3. Mechanical line drawing of the membrane housing block design.

Appendix B

Sample Calculations

B.1. Supersaturation Concentrations

The following molecular weights apply:

Table B-1. Molecular weights of species used to synthesise a saturated gypsum feed solution.

Specie		Molecular Weight	Units
Sodium	Na ⁺	22.989	g·mol ⁻¹
Sulphate	SO ₄ ²⁺	96.065	g·mol ⁻¹
Calcium	Ca ²⁺	40.078	g·mol ⁻¹
Chloride	Cl ⁻	35.453	g·mol ⁻¹
Sodium Chloride	NaCl	58.44	g·mol ⁻¹
Sodium Sulphate	Na ₂ SO ₄	142.04	g·mol ⁻¹
Gypsum	CaCl ₂ ·xH ₂ O	147.02	g·mol ⁻¹
Calcium Sulphate	CaSO ₄	136.14	g·mol ⁻¹

The supersaturation ratio was calculated using Equation (B.1):

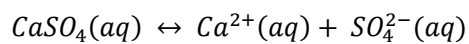
$$S = \frac{[Ca^{2+}]_i}{[Ca^{2+}]_s} \quad (\text{B.1})$$

Rearranging this formula [Equation (B.1)] by assuming a level of supersaturation, the initial calcium content present can be estimated in the initial solution:

$$[Ca^{2+}]_i = S \times [Ca^{2+}]_s$$

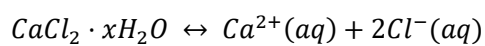
The calcium concentration corresponding to the equilibrium supersaturated concentration is 0.01565 mol·L⁻¹ as calculated by PHREEQC. Gypsum is insoluble in water, hence, for the formation of gypsum to occur, the following base compounds need to dissociate fully in water to form their constituent ions. In this study the base compounds utilised are equimolar amounts of CaCl₂ and Na₂SO₄. From the following dissociation reaction the concentration of the base compounds in the working fluid can be determined.

APPENDIX B: Sample Calculations

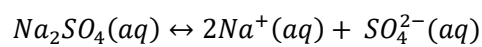


Compounds	Ratio
[CaSO ₄] : [Ca ²⁺]	1
[Ca ²⁺] : [SO ₄ ²⁻]	1

The saturation concentration calculated in PHREEQC of Ca²⁺ is 627.25 mg/L. The equilibrium concentration of Ca²⁺ on a molar basis is thus



Compounds	Ratio
[Ca ²⁺] : [CaCl ₂]	1



Compounds	Ratio
[SO ₄ ²⁻] : [Na ₂ SO ₄]	1
[Ca ²⁺] : [Na ⁺]	2
[Ca ²⁺] : [Cl ⁻]	2

B.2. Experimental Data Sample Calculations

Basic data sample calculations are detailed below to indicate to the reader how the data acquisition and data analysis were done. Specific details with regard to the data are given below:

- Data Set: Validation Experiment for AL-FS Configuration: 19 cm·s⁻¹
- Time On: 09h30
- Reading 1 @ 11h35

Table B-2. Data measurements from the baseline test in the AL-FS configuration at a CFV of 19 cm·s⁻¹

Solution	Time	Temperature	Conductivity
FS _{IN}	09:49.9	25.60	157.2 μS·cm ⁻¹
FS _{OUT}	14:18.5	25.50	0.64 mS·cm ⁻¹
DS _{IN}	09:18.5	26.30	47.80 mS·cm ⁻¹
DS _{OUT}	09:15.3	25.50	36.80 mS·cm ⁻¹

Fixed Variables included the membrane area of 0.1344 m²

B.2.1.1. Flux Calculation

As per Equation (3.5):

$$\begin{aligned}
 J_w &= \frac{\Delta \dot{Q}}{A_m} = \frac{\dot{Q}_{F,i} - \dot{Q}_B}{A_m} = \frac{\dot{Q}_P - \dot{Q}_{DS,F}}{A_m} & (B.2) \\
 &= \frac{\frac{2.3}{\left(\frac{(9)(60) + 15.3}{3600}\right)} - \frac{1.888}{\left(\frac{(9)(60) + (18.5)}{3600}\right)}}{0.1344 \text{ m}^2} \\
 &= \frac{2.741 \text{ L}}{0.1344 \text{ m}^2 \cdot \text{h}} \\
 &= 20.4 \text{ L} \cdot \text{m}^{-2} \cdot \text{h}^{-1}
 \end{aligned}$$

To normalise the flux by accounting for the changes in the viscosity of the solution along the process train, the average temperature across the DS channel needs to be quantified.

$$T_{\text{avg}} = \frac{(26.30 + 25.50)^\circ\text{C}}{2}$$

$$T_{\text{avg}} = 25.9 \text{ }^\circ\text{C}.$$

APPENDIX B: Sample Calculations

As per Equation (3.6):

$$\begin{aligned}
 J_{w,20^{\circ}C} &= J_{w,T}[1.784 - (0.0575 \cdot T) + (0.001 \cdot T^2) - (10^{-5} \cdot T^3)] & (B.3) \\
 &= 20.395[1.784 - (0.0575(25.9)) + (0.001(25.9)^2) - (10^{-5})(25.9^3)] \\
 &= 20.395(1.784 - 1.48925 + 0.67081 - 0.17373) \\
 &= 16.15 \text{ L} \cdot \text{m}^{-2} \cdot \text{h}^{-1}
 \end{aligned}$$

However, the driving force still needs to be normalised to the standard operating conditions, thus as per Equation (3.7):

$$\begin{aligned}
 J_{w,0} &= J_{w,a} \cdot (1.784 - (0.0575T) + (0.001T^2) - (10^{-5}T^3)) \cdot \frac{(\Delta\pi - \Delta P)_s}{(\Delta\pi - \Delta P)_a} & (B.4) \\
 &= 16.15 \times \frac{(27 - 0)}{(24.56 - 0.00225195)} \\
 &= 17.76 \text{ L} \cdot \text{m}^{-2} \cdot \text{h}^{-1}
 \end{aligned}$$

B.2.1.2. Recovery Calculation

As per Equation (2.4):

$$\begin{aligned}
 R &= \left(\frac{Q_F - Q_B}{Q_F} \right) \times 100 & (B.5) \\
 &= \frac{\left(\frac{1.854}{\frac{(9)(60) + 49.9}{3600}} - \frac{2.035}{\frac{(14)(60) + (18.5)}{3600}} \right)}{\frac{1.854}{\frac{(9)(60) + 49.9}{3600}}} \times 100\% \\
 &= 24.57\%
 \end{aligned}$$

B.2.1.3. Rejection Calculation

As per Equation (2.6):

$$\% \text{ Rejection} = 1 - \left[\frac{C_B - C_F}{C_{DS,F}} \right] \times 100 & (B.6)$$

B.2 Experimental Data Sample Calculations

$$= 1 - \left(\frac{0.64(0.55) - 0.1572(0.55)}{47.80(0.7)} \right) \times 100$$
$$= 99.21\%$$

Appendix C

Operational Procedures

C.1. Operational Procedure

Before operation of this setup can commence, the user should familiarise him/herself with the entire setup (valve locations, the working of the PLC, as well as how to take accurate measurements). In this section special safety considerations are mentioned, as well as risks associated with the operation of this setup. Procedures for setup operation as well as solution preparation are also detailed below.

C.1.1. Special Safety Considerations

- Safety

- The operational voltage of the valves is high (220V). Insulation of the electrical wiring as well as the electrical connections are required. The valves should be placed in a non-conductive housing.
- Water is contained within this setup; hence, special care should be taken to reduce exposure to the electrical wiring.

- Applicable Personal Protective Equipment

- A laboratory coat as well as closed shoes should be worn when operating this setup. Safety classes are required when measurements are being taken.

- Environmental Protection

- The flushing time should be long enough to flush out any residual solution contained in the membrane housing, to avoid contamination of the product water.

- Equipment Protection

- The valves associated with Configuration 2 should open before impeding the valves associated with Configuration 1. This is to avoid unnecessary abruptions and disturbances in the system which may lead to the disconnection of tubing, which will cause water spillage.

- Smooth & Easy Operation

- The valves associated with Configuration 2 should open before impeding the valves associated with Configuration 1. This is to avoid abruptions and disturbances within the system. Sufficient lag time of the valves should be provided for between each configuration.

- Product Quality

- The flushing time should be long enough to flush any residual solution contained within the membrane housing in a separate tank, to avoid contamination of the product water.

- **Efficiency & Optimisation**
- The time the process train operates in each configuration should be a process variable to allow for efficient operation and optimisations to the process at a later stage.
- **Monitoring & Diagnosis**
- No online monitoring and diagnostics are required for this process.

C.1.2. Process Risks & Precautionary Measures

Solenoid Valves

- The power used by the solenoid valves in setup is very high (220V). Appropriate housings and sealing mechanisms have been employed to avoid accidental contact with the valve, however, the user of the setup should still be vigilant not to spill water on or near the valves.

C.2. Pre-start-up Checklist

Membrane Housing

- Check that the blocks are placed in the correct orientation with regard to the orientation of the membrane inside the respective housing blocks.
- Check that the membrane did not move or shift from its original position when the housing was fastened with the 8 mm hexagonal bolts at a torque of 20 N·m.

Manual Valves

- Open the air trap valves: V-101, V-102, V-103, V-104, V-105 and V-106.
- Closed valves: VB-102, VB-104, VB-106 and VB-108, as well as VB-110 and VB-112.
- Ensure that valves VB-101, VB-103, VB-105, VB-107, VB-109 and VB-111 are open.

Tubing

- Check the configurations of the tubing connections to the blocks (tube configurations and tube fittings).
- Follow the respective process path and check tubing connections to the process train.

Solenoid Valves

- Check that the solenoid valves are all closed (normally closed) before system start-up. Blockages in the valves could lead to valve leakages, which would affect the measurement of data detrimentally.

C.2.1. Process Start-Up Procedure

1. Go through the pre startup checklist.
2. Switch the main power supply setup, to ON at the operating box.
3. All the 220V solenoid valves of the process should now be open.
4. Switch on P-101 and P-102. The pump speed can be adjusted manually by turning the black knob on the respective pumps.
5. Check if the flow rate specified at the pump (via adjusting the RPM on the pumps) is indeed what is indicated on the rotameters.
6. Continually check the levels of TK-101 and TK-102 to avoid the tanks running empty, thereby causing air suction to the FO process train.
7. Check the membrane housing blocks for any leakages.

APPENDIX C: Operational Procedures

C.2.2. Process Measurements**Flow Rate Measurement**

- The outlet flow rate of the respective solutions is measured with FM-103 and FM-104. The respective ball valves (VB-109 and VB-111) are closed and the time it takes for the column to fill up to the predetermined calibrated volume is measured.
- The inlet flow rate of the respective solutions is measured with FM-101 and FM-102. This is done by filling the column to the predetermined, calibrated volume. The time it takes for the respective columns to be pumped empty, is then measured with a stopwatch.

Conductivity Measurement

- The conductivity of the respective solutions can be measured by samples of the subsequent solutions and measuring the conductivity with the Eutech conductivity probe. It is important to note that calibration of the meter is required bi-weekly.

C.2.3. Process Shut-Down Procedure

1. Manually switch off the pumps.
2. Shut down the main power supply to the system.
3. Open the following drain valves: VB-102 and VB-106.
4. Remove the membranes from their respective housing blocks.
5. Flush the system with RO water by following the start-up procedure.

C.3. Preparation of Various Solutions**C.3.1. Sodium Chloride Draw Solution****Product Information**

- Iodated table salt.

Solution Preparation

- The salt was stored in an airtight container, once the subsequent bags were opened. This was done to prevent salt hydration, due to its hygroscopic nature.

C.3.2. Sodium Sulphate**Product Information**

- Anhydrous sodium sulphate.

Solution Preparation

- The salt was dried overnight to dehydrate in a vacuum oven at approximately 60–80 °C.
- Sodium sulphate is very soluble in water, however, since the dissolution reactions between sodium sulphate and water is endothermic, the addition of heat will aid in dissolving the salt in water.

C.3.3. Calcium Chloride**Product Information**

- Calcium Chloride

Solution Preparation

- Calcium chloride is very hygroscopic. Hence, the salt was dissolved in water as quickly as possible. Furthermore, to ensure that the subsequent Ca^{2+} concentration is known, the Ca^{2+} content in the solution was analysed for using ICP-MS analyses.

C.4. System Operation**C.4.1.1. Pre start-up procedure**

1. Switch off the power source inside the electrical box to the (1) pumps, (2) configuration 1, (3) configuration 2 and (4) the flushing cycle.
2. Ensure that the thermostat of the two respective heaters in the feed tanks are set at 24°C.
3. Switch on the heaters at the switch located on the setup-frame. A red light on the submersible heaters indicates that the heaters are on.
4. Wait for the feed solutions to reach the set temperature.
5. Switch the heaters off at the switch located on the frame. Open the electrical box and switch on the power source to the (1) pumps, (2) configuration 1, (3) configuration 2 and (4) the flushing cycle.
6. Switch on the heaters at the switch located on the frame. A red light on the submersible heaters indicates that the heaters are on.

C.4.1.2. Start-up procedure

1. At the electrical box switch on the setup by turning the red knob to the ON position. All of the 220V solenoid valves are now open.
2. Switch on the setup by pressing the green button on the electrical box.
3. Configuration times can be altered by accessing the timer on the Phoenix Nanoline screen.
4. Switch on the respective pumps.
5. The pump speed can be adjusted by turning the black knob on the pump to the required rotations per minute.

C.4.1.3. Shut-down procedure

1. Switch the flow from the feed tanks to the tank pumping deionized water to the process. This would flush the system and prevent excessive CP occurring when the FS and the DS are adjacent to the membrane for a prolonged period.
2. Switch off the pumps at the respective pumps by pressing down the green button.
3. Turn off the operational cycle by pressing the red button located on the electrical box.
4. Switch off the heaters at the switch located on the frame.
5. Switch off the entire setup by turning the red knob on the electrical box to the OFF position.